Nramp Metal Transporters:
Insights into their structure, function, and subcellular targeting

Steven Lam-Yuk-Tseung

Department of Biochemistry
McGill University
Montréal, Québec, Canada

June 2006

A thesis submitted to the Faculty of Graduate Studies and Research in partial fulfillment of the requirements of the degree of Doctor of Philosophy.

Your file Votre référence
ISBN: 978-0-494-27804-8
Our file Notre référence
ISBN: 978-0-494-27804-8

Abstract

This thesis examines the molecular properties of Nramp proteins by centering on the two mammalian orthologs. Nramp1 (Slc11a1) is expressed in phagocytic cells and restricts replication of intracellular pathogens by removing divalent metals from the phagolysosome. Nramp2 (DMT1, Slc11a2) mediates uptake of dietary iron in the duodenum and aids in the acquisition of transferrin-associated iron in many cell types. The first half of this thesis explores structure-function relationships. In Chapter 2, the role of charged amino acids within the membrane-spanning segments of Nramp2 was examined by site-specific mutagenesis. These studies identified several invariant charged residues essential for metal transport and pH regulation of activity. In Chapters 3 and 4, the effects of two *NRAMP2* mutations found in human patients suffering from severe congenital hypochromic microcytic anemia and iron overload were characterized in vitro. The first mutation was an E399D substitution in a region known as the "conserved transport motif" of the protein. The second mutation was an R416C substitution at an invariant residue in TM9. The effects of both mutations on expression, activity, and subcellular targeting were characterized. In both cases, a quantitative reduction in Nramp2 expression was found to be the cause of microcytic anemia and iron overload in the patients. The second half of this thesis focuses on the subcellular targeting of Nramp1 and 2. In Chapter 5, cytoplasmic signal(s) in Nramp2 responsible for its subcellular targeting/internalization from the plasma membrane were studied. This work led to the identification of a tyrosine-based motif in the carboxyl terminus of Nramp2 ($YLLNT^{555-559}$) critical for the transporter's internalization from the cell surface and its recycling back to the plasma membrane. Chapter 6 explored differences in trafficking between two splicing isoforms of Nramp2 and found that one isoform (isoform I) possessed differences in internalization/recycling which enabeled it to become enriched at the plasma membrane. In Chapter 7, the subcellular trafficking properties of Nramp1, including cytoplasmic sequences responsible for targeting to lysosomes, were investigated by using chimeric Nramp1/Nramp2 proteins. This work led to the identification of a tyrosine-based motif ($YGSI^{15-18}$) in the amino terminus of Nramp1 that functions as a lysosomal targeting signal.

Abrégé

Cette thèse examine les propriétés moléculaires des protéines Nramp, en particulier celles des deux orthologues de mammifère. Nramp1 (Slc11a1) est exprimé par les cellules phagocytaires et bloque la réplication intracellulaire d'agents pathogènes en diminuant la concentration phagosomale de métaux divalent. Nramp2 (DMT1, Slc11a2) est responsable de l'absorption de fer par le duodenum provenant de l'alimentation et aide à l'acquisition fer associé à la transferrine par plusieurs types cellulaires. La première moitié de cette thèse explore les relations structure-fonction. Au chapitre 2, le rôle des acides aminés chargés des segments transmembranaires de Nramp2 a été examiné par mutagenèse de sites spécifiques. Ces études ont identifié plusieurs résidus chargés conservés comme étant essentiels au transport de métaux et à l'activité de régulation du pH. Aux chapitres 3 et 4, les effets de deux mutations de la protéine *NRAMP2* trouvées chez des patients souffrant d'une anémie hypochromique microcytique congénitale grave et d'un surplus de fer ont été caractérisées *in vitro*. La première mutation, la substitution E399D, se situe dans une région de la protéine nommée "motif de transport conservé". La seconde mutation, la substitution R416C, modifie un résidu invariant du domaine transmembranaire 9. Les effets des deux mutations sur l'expression, l'activité et la localisation intracellulaire ont été caractérisés. Dans les deux cas, une réduction significative de l'expression de Nramp2 s'est avérée la cause de l'anémie microcytique et de la surcharge de fer observées chez les patients. La seconde moitié de cette thèse se concentre sur la localisation intracellulaire des protéines Nramp1 et 2. Au chapitre 5, les signaux cytoplasmiques de la protéine Nramp2 responsables de sa localisation et de son internalisation à partir de la membrane plasmique ont été étudiés. Cette étude a mené à l'identification d'un motif à base de tyrosine situé en carboxy terminal de Nramp2 ($YLLNT^{555-559}$) essentiel à l'internalisation du transporteur de la surface cellulaire et à son recyclage vers la membrane plasmique. Le chapitre 6 explore les différences de localisation entre deux isoformes de Nramp2 issues d'épissage alternatif. Il a été trouvé que l'isoforme I présente des différences d'internalisation et de recyclage, ce qui provoque son enrichissement à la membrane plasmique. Au chapitre 7, les propriétés de localisation intracellulaire de la protéine Nramp1, incluant les séquences cytoplasmiques responsables de sa localisation aux lysosomes, ont été examinées à l'aide de protéines chimères Nramp1/Nramp2. Cette étude a mené à l'identification d'un motif à base de tyrosine ($YGSI^{15-18}$) dans la portion amino terminal de la protéine Nramp1 qui fonctionne en tant que signal de localisation aux lysosomes.

Preface

The work described in Chapters 2, 3, 4, 5, 6, and 7 of this thesis are published as follows:

Chapter 2: Lam-Yuk-Tseung S., G. Govoni, J. Forbes, and P. Gros. 2003. "Iron transport by Nramp2/DMT1: pH regulation of transport by 2 histidines in transmembrane domain 6." *Blood.* **101(9)**:3699-707. Reprinted with permission, © the American Society of Hematology 2003.

Chapter 3: Lam-Yuk-Tseung S., M. Mathieu, and P. Gros. 2005. "Functional characterization of the E399D DMT1/NRAMP2/SLC11A2 protein produced by an exon 12 mutation in a patient with microcytic anemia and iron overload." *Blood Cells, Molecules and Diseases.* **35(2)**:212-6. Reprinted with permission, © Elsevier 2005.

Chapter 4: Lam-Yuk-Tseung S., C. Camaschella, A. Iolascon, and P. Gros. 2006. "A Novel R416C Mutation in Human DMT1 (Slc11a2) Displays Pleiotropic Effects on Function and Causes Microcytic Anemia and Hepatic Iron Overload." *Blood Cells, Molecules and Diseases.* Reprinted with permission, © Elsevier 2005.

Chapter 5: Lam-Yuk-Tseung S., N. Touret, S. Grinstein, and P. Gros. 2005. "Carboxyl-terminus determinants of the iron transporter DMT1/SLC11A2 isoform II (-IRE/1B) mediate internalization from the plasma membrane into recycling endosomes." *Biochemistry.* **44(36)**:12149-59. Reprinted with permission, © American Chemical Society, 2005.

Chapter 6: Lam-Yuk-Tseung S. and P. Gros. 2006. "Distinct targeting and recycling properties of two isoforms of the iron transporter DMT1 (Nramp2, Slc11a2)." *Biochemistry.* **45(7)**:2294-301. Reprinted with permission, © American Chemical Society, 2006.

Chapter 7: Lam-Yuk-Tseung S., V. Picard, and P. Gros. 2006. "Identification of a tyrosine-based motif (YGSI) in the amino terminus of Nramp1 (Slc11a1) responsible for lysosomal targeting." *Journal of Biological Chemistry.* (Submitted)

Contribution of Authors

Chapter 2. The work in this chapter is essentially my own. Gregory Govoni, who began the project prior to my arrival, created 12 of the 21 mutations studied in the manuscript and provided me with valuable advice at the start of my graduate studies. I constructed the remaining mutants, expressed and functionally characterized them in yeast as well as stably transfected Chinese hamster ovary cells. All the figures that appear in Chapter 2 are based on experiments I performed. John Forbes performed an additional radioisotopic metal transport experiment that was requested by one of our reviewers at the time of publication. However, the data from this experiment was not included in the final published manuscript.

Chapter 3. In this chapter, all the figures are based on experiments I performed. I constructed, expressed and characterized all the mutations in stably transfected LLC-PK_1 cells. I optimized the conditions for the immunofluorescence microscopy images and set-up and optimized an ELISA-based technique to quantify the fraction of DMT1-HA expressed at the cell surface. Two undergraduate students I supervised, Lauren Hamlin-Douglas and Rachel Beckerman, helped me create the E399D and E399Q mutants for their undergraduate research projects. I am also indebted to Melissa Mathieu for her help in culturing and screening the LLC-PK_1 cells for DMT1 expression.

Chapter 4. All the figures in this chapter are based on experiments I performed. Clara Camaschella and Achille Iolascon identified the original *DMT1/SLC11A2* human mutation and approached us to characterize the effects on expression, function, and subcellular localization of the R416C human mutation *in vitro*.

Chapter 5. All the figures in this chapter are based on experiments I performed. I created the mutants, stably expressed them in LLC-PK_1 cells, and characterized them for proper expression, activity, cell surface targeting, subcellular localization, and fate upon internalization. I also set-up and optimized the cell surface biotinylation technique to measure the rate of endocytosis of the variants from the plasma membrane. Nicolas

Touret provided me with valuable technical advice and helped me acquire the images in Figures 3A and 5A, which I performed at the Hospital for Sick Children (Toronto) in the laboratory of Sergio Grinstein. I am also indebted to Dr. Grinstein for his critical reading of the manuscript and for his scientific guidance.

Chapter 6. The work described in this chapter is entirely my own. I expressed both DMT1 isoforms in stably transfected LLC-PK_1 cells, and characterized them for differences in function, subcellular localization, endocytosis kinetics, and fate upon internalization.

Chapter 7. The work described in this chapter is essentially my own. Virginie Picard created two of the constructs I used in the study. I created the remaining constructs, expressed all the variants in transfected LLC-PK_1 and studied them for expression, stability, cell surface targeting, transport activity, and subcellular localization.

My supervisor, Dr. Philippe Gros, provided supervision and advice throughout all of the studies.

Table of Contents

List of Figures

Chapter 7

List of Tables

Acknowledgements

Foremost, I would like to thank Philippe Gros for providing me with much needed guidance and support, especially during the first few years of my graduate studies. He provided clarity and direction when I needed it, but at the same time allowed me enough room to make mistakes and grow stronger both as a person and as a scientist – and for that, I will always be grateful. I would like to thank Sergio Grinstein and other members of his group for not only welcoming me into their lab on two separate occasions, but also for providing a tremendously positive working environment during my stay. I am especially indebted to Nicolas Touret for helping me with the fluorescence microscopy work for Chapter 5. I would like to thank Gregory Govoni, from whom I took over the Nramp project. He was a great help at the beginning of my studies, providing me with both personal and professional advice that I value still today. I would also like to thank several former post-doctoral fellows from our lab. I am grateful to François Canonne-Hergaux for his advice regarding the use of the anti-Nramp polycolonal antibodies, and also for his enthusiasm and willingness for scientific discussion. I would like to thank Virginie Picard for setting-up and teaching me the fluorescence quenching assay to measure Nramp metal transport activity. I also thank Jie Cai and John Forbes, whose advice helped guide me through the "rough patches". My thanks also goes to Anne Fortier, who is responsible for the French translation of the abstract and whose friendship is greatly valued. I would also like to thank all the other past and present members of the Gros laboratory who have provided a pleasurable working environment over the years. I was financially supported during my studies by studentships from the Fonds de la recherche en santé Quebec (FRSQ), the Canadian Institutes of Health Research (CIHR), and the McGill University Faculty of Medicine. I would like to thank my friends for their support, especially my Loyola brethren. Most importantly, I would like to thank my family for their love and support, without whom I could not have finished this degree and without whom, it would not even matter.

Objectives of the Presented Work

The first member of the Nramp family (*Nramp1*) was identified in 1993 as the gene responsible for natural resistance in mice to infection by certain intracellular parasites [1]. Since Nramp1 was isolated by a positional cloning approach and represented the first member of a novel family of proteins, its molecular function was unknown and remained debated for several years. This debate virtually ended in 1997 when a second member of the Nramp family (Nramp2) was shown to function as a pH-dependent transporter of divalent metals important for intestinal iron absorption [2;3]. Because of the high degree of conservation of among Nramp family members, it was believed that all Nramp orthologs shared similar metal transport characteristics. At the start of my thesis work in September 1999, the molecular basis of proton-coupled metal transport by Nramp proteins was not well understood. At this time, structure-function studies became essential to understanding the molecular basis for both metal transport and pH-dependence by Nramp proteins. Also unclear were the molecular mechanisms of subcellular trafficking of mammalian Nramp1 and Nramp2. Therefore, the objective of my thesis project was to use biochemical and molecular biological techniques to provide a greater understanding of the structure, function, and subcellular trafficking of Nramp proteins.

To accomplish this, the work described in the first three chapters of my thesis focus on the importance of conserved amino acid residues in the function of Nramp2. Chapter 2 addresses the role of charged amino acids within the membrane-spanning segments of Nramp2 and identifies several negatively-charged residues that are essential for metal transport as well as two invariant histidines necessary for the pH dependence of activity. Chapters 3 and 4 study the importance of conserved residues in Nramp2 that were found to be mutated in human patients suffering from severe congenital hypochromic microcytic anemia and iron overload. These studies were essential to understanding the cause of disease in the patients and also provided insight into the role of Nramp2 in human iron homeostasis.

The last three chapters of my thesis were aimed at better understanding the subcellular distribution of Nramp1 and Nramp2. Chapter 5 addresses the importance of

cytoplasmic sequence motifs in the subcellular targeting and trafficking of Nramp2. This work led to the identification of a novel tyrosine-based motif in the carboxyl terminus of Nramp2 (isoform II) that is critical for the transporter's internalization from the cell surface and its recycling back to the plasma membrane. Work described in Chapter 6 was aimed at comparing the distinct targeting and recycling properties of two naturally-occurring splice isoforms of Nramp2. This work ultimately showed that alternate splicing of Nramp2 critically regulates the subcellular localization and site of iron transport. Finally, Chapter 7 of this thesis was aimed at better understanding the subcellular targeting of Nramp1. It was known for some time that Nramp1 is expressed in the lysosomes of phagocytic cells however, specific signals responsible for targeting to lysosomes remained unclear. Work described in Chapter 7 showed for the first time that a tyrosine-based motif of the form YXXΦ in the amino terminus Nramp1 is responsible for the transporter's lysosomal targeting.

Chapter 1:

Introduction and Literature Review

1.1 The Nramp family

Nramp proteins represent a growing family of membrane metal transporters that perform a variety of functions in organisms ranging from bacteria to humans [1]. The sequence conservation among members of the Nramp family is astoundingly high, even among phylogenically distant species (supplementary figure 1). In many organisms, Nramp proteins are critical for the absorption of divalent metals and the maintenance of normal divalent metal homeostasis. More specialized roles for Nramp proteins have also been reported. In *Drosophila*, Nramp orthologs play a role in taste discrimination [2] and in some mammals, *Nramp1* is critical for host-resistance to infection by intracellular pathogens [3]. In humans, polymorphisms in *NRAMP1* have been associated with increased susceptibility to a number of infectious and inflammatory diseases while mutations at *NRAMP2* disrupt normal iron homeostasis [4-6].

Tremendous advances have been made in understanding Nramp protein function since the first member of this family was cloned in 1993 [7]. Much of the current knowledge on Nramp proteins originates from genetic studies performed in mouse models of diseases. The usage of mouse models provides many advantages over studies in humans. Whereas genetic and environmental factors are heterogeneous and complex in humans, these factors can be controlled for in inbred mouse strains. Furthermore, the breeding of mice is relatively fast and biological samples are easier to obtain from mice than from human patients. Finally, candidate genes can be individually targeted in mice by germ line inactivation through homologous recombination and gain-of-function alleles can be re-introduced by BAC clones.

1.2 Nramp1: Discovery of the first *Nramp* gene

1.2.1 The *Bcg/Ity/Lsh* Locus and the *Nramp1* gene

Thirty years ago, there were reports of a mouse locus that possibly controlled the intracellular replication of a number of diverse intracellular pathogens. In 1976, studies performed on several inbred mouse strains showed that resistance or susceptibility to infection by *Salmonella typhimurium* was controlled by a single locus, which was called *Ity* [8]. At the same time, similar experiments demonstrated that another locus, called *Lsh*,

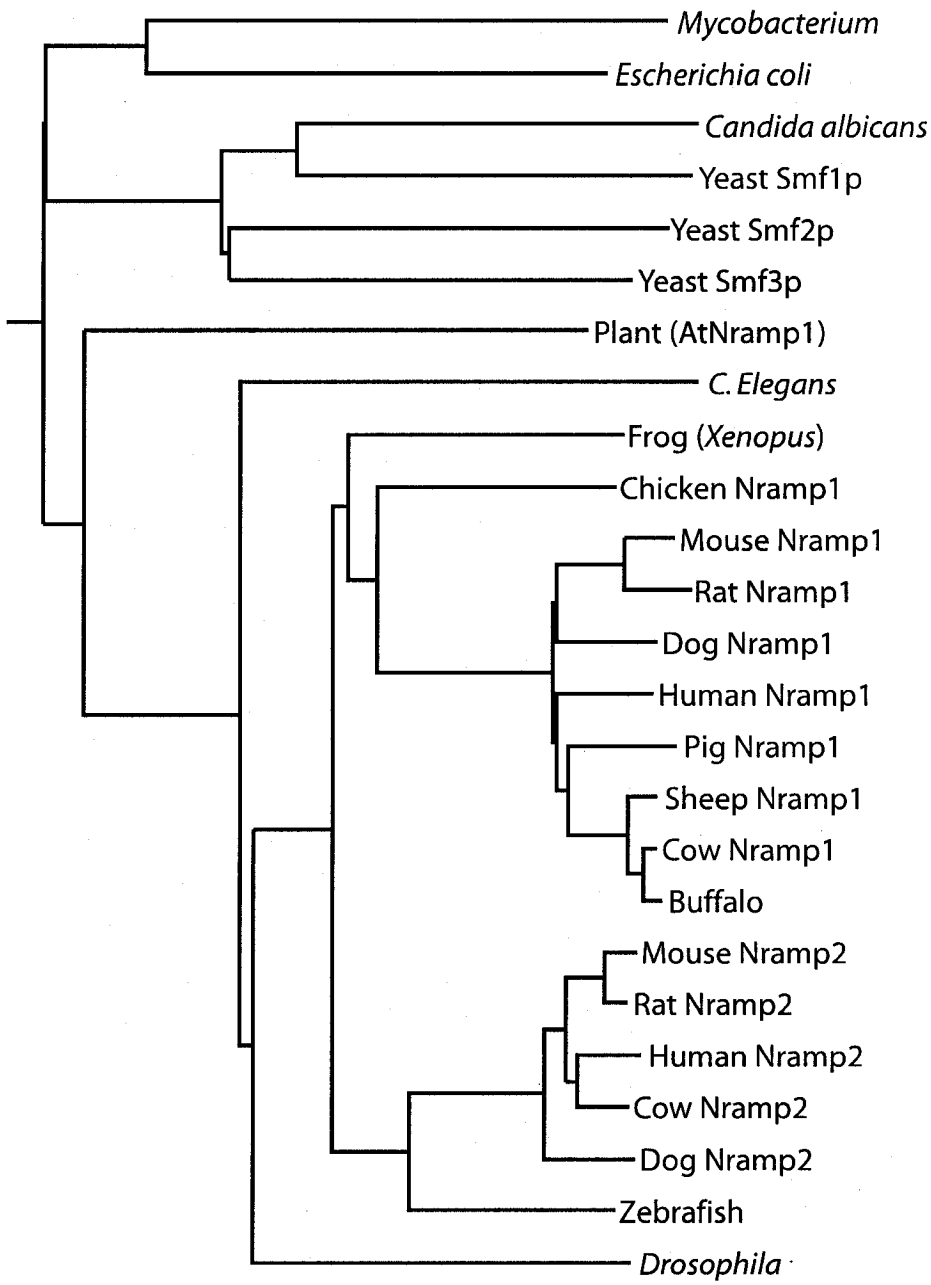

Supplementary figure 1. Dendogram of some of the members of the Nramp family of metal transporters. The sequence conservation among members of the Nramp family is astoundingly high, even among phylogenically distant species.

controlled intracellular replication of the protozoan parasite *Leishmania donovani* and that *Lsh* was either identical or tightly linked to *Ity* [9]. A third locus, *Bcg*, which controlled intracellular replication of several mycobacteria was also mapped to the same region [7]. The *Bcg/Ity/Lsh* locus that gave resistance to these pathogens in a dominant fashion was traced back to a region on the proximal portion of mouse chromosome 1. Subsequent *in vitro* and *in vivo* studies demonstrated that the cells affected by *Bcg/Ity/Lsh* were mature macrophages residing especially in the reticuloendothelial organs (spleen and liver) [10-12].

In 1993, without the benefit of a known gene product or a practical way to measure gene function, our group used a positional cloning approach to isolate the *Bcg/Ity/Lsh* locus [7]. The minimal genetic and physical intervals for the gene were defined and transcriptional units were isolated from the interval by exon amplification. Of the six genes present in the region, one emerged as a likely candidate since it encoded mRNA that was highly expressed in the reticuloendothelial organs and almost exclusively in macrophages and neutrophils. The candidate gene was named *Natural resistance associated macrophage protein 1* or *Nramp1* (OMIM # 600266, now re-classified as *Slc11a1* but will be referred to as *Nramp1* in this thesis).

1.2.2 Validation of *Nramp1* as a candidate gene

Following the identification of *Nramp1* as a candidate gene for *Bcg/Ity/Lsh*, several subsequent experiments confirmed *Nramp1* as the gene responsible for host resistance to infections. First, the sequencing of *Nramp1* mRNA from 27 inbred mouse strains showed that susceptibility to infection could be traced back to a single nucleotide point mutation. The result of this mutation was a non-conservative glycine to aspartate substitution (G169D) in the fourth membrane-spanning segment (TM4) of the Nramp1 protein [7]. This mutation was later shown to cause a complete loss of Nramp1 protein expression in macrophages [7;13] and result in a protein that is misfolded and retained in the endoplasmic reticulum for eventual degradation [14]. Second, a null mutation at *Nramp1* (*Nramp1*$^{-/-}$) introduced into embryonic stem cells by homologous recombination caused normally resistant 129sv mice to be susceptible to infection by *Mycobacterium*, *Salmonella*, and *Leishmania* [15]. Finally, introducing a transgene containing the *Nramp1*

resistance allele (G169) into a naturally susceptible mouse strain (D169) granted resistance to infection by *Mycobacterium* and *Salmonella* [16]. The broad effect of *Nramp1* mutations on susceptibility to infection with antigenically diverse pathogens suggested a critical role for this protein in innate immunity.

In mice, the *Nramp1* gene is made up of 15 exons that span an 11.5 kb region and is transcribed from one major and several minor transcription start sites. Using primer extension and S1 nuclease mapping experiments, Govoni and colleagues showed that the upstream region of *Nramp1* contains a TATA box-less promoter, with consensus SP1 binding sites and initiator sequences linked to RNA polymerase II transcription [17]. Also in the promoter region are consensus binding sites for several ubiquitous and tissue-specific transcription factors. Among them are sites for a macrophage and B-cell specific transcription factor (PU.1), general transcription factors (AP-1, AP-2, AP-3, and SP1), as well as response elements for lipopolysaccharide (NF-IL6) and interferon-γ [17]. *Nramp1* mRNA is found in primary macrophages and granulocytes [7;18] and its expression is increased in response to infection with *mycobacterium*, exposure to LPS, interferon-γ, or by other inflammatory stimuli [17-23]. In addition, studies by Lafuse and colleagues suggest that *Nramp1* mRNA levels can be controlled at the level of stability by MAP kinase signaling cascades in activated macrophages [24;25]. By comparing RAW264.7 cells stably transfected with either resistant (G169) or susceptible (D169) Nramp1, they showed that inhibition of ERK1,2 and p38 MAP kinase activities decreases Nramp1 mRNA stability in cells infected with *M. avium*. Furthermore, phosphorylation of ERK1,2 and p38 MAP kinases was higher in infected cells expressing resistant Nramp1^{G169} compared to susceptible Nramp1^{D169} [24].

1.2.3 The Nramp1 protein

In 1996, Vidal and colleagues generated a polyclonal anti-Nramp1 antisera and used it to demonstrate that *Nramp1* encodes a 90-100 kDa integral membrane protein that is highly glycosylated (up to 50% of its mass) and phosphorylated in peritoneal macrophages obtained after thioglycolate stimulation [13]. They also showed that susceptible (*Nramp1*^{D169}) macrophages fail to express mature Nramp1 protein. The

topology of Nramp1 in the membrane was initially predicted from hydropathy plots and has been partially confirmed by epitope accessibility studies in intact cells [1;26;27]. Nramp1 contains 12 putative transmembrane domains and a large extracellular loop flanked by TM7/8, which is heavily glycosylated at two neighboring N-linked glycosylation signals [1]. Complex glycosylation of Nramp1 seems to be the end result of a stable and properly folded transporter but glycosylation itself does not appear to be critical for subcellular targeting [14]. Nramp1 contains a number of highly conserved yet thermodynamically disfavored charged amino acids within its transmembrane domains. These charged residues have been shown to be critical for the proper structure/function of Nramp proteins [28;29]. Nramp1 also possesses several phosphorylation sites including putative sites for protein kinase C phosphorylation and a Src homology3 domain (SH3) binding region in the amino terminus of the protein [1;30]. Little is known about the role of phosphorylation or the binding of SH3 domain-containing proteins in the function of Nramp1, however, the fact that these regions are not conserved in Nramp orthologs suggests their lack of functional importance. Alternatively, these regions may be critical for the unique regulation of Nramp1. Finally, the fourth intra-cytoplasmic loop of Nramp1 flanked by TM8/9 is a region of extremely high conservation that contains a sequence motif known as the "binding-protein-dependent transport system inner membrane component signature" or simply "conserved transport motif" (CTM). This motif was originally discovered on the cytoplasmic face of the membrane anchor subunits of bacterial periplasmic permeases, where it is believed to participate in the interaction of membrane components with peripheral ATP binding subunits of these transporters [31;32]. This motif in Nramp1 also shows similarity to a sequence motif identified in the K^+ channel superfamily and other ion channels and transporters as a key structural determinant of the ion permeation pathway [33]. The exact function of the CTM in the context of Nramp proteins is not currently known, however, mutations at key residues within this region are known to abrogate function [34].

At steady-state, Nramp1 is not expressed at the plasma membrane but is almost exclusively found in the membranes of Lamp1-positive late endosomes/lysosomes of macrophages and other phagocytic cells [35]. The sorting machinery and specific proteins

involved in the subcellular trafficking of Nramp1 are currently not well understood. In Chapter 7 of this thesis, experiments performed on Nramp1/Nramp2 chimeric proteins expressed in transfected LLC-PK_1 kidney cells demonstrated that a tyrosine-based motif of the form YXXΦ in the amino terminal region of Nramp1 ($YGSI^{15-18}$) can function as a lysosomal targeting signal. Using subcellular fractionation and immunofluorescence microscopy, Gruenheid and colleagues demonstrated that Nramp1 is recruited to the membrane of the phagosome and remains associated with this structure during its maturation to phagolysosome. After phagocytosis, Nramp1 is acquired by the phagosomal membrane with kinetics similar to Lamp1 [35] where it controls the replication of intracellular parasites by altering the luminal environment of the microbe-containing phagosome. In addition to macrophages, Nramp1 is expressed in polymorphonuclear (PMN) leukocytes such as neutrophils and other granulocytes. Using subcellular fractionation of granule populations together with immunoblotting with granule-specific markers as well as immunogold electron microscopy, Canonne-Hergaux *et al* demonstrated that Nramp1 is expressed primarily in the tertiary gelatinase-positive granules of neutrophils [36]. They also showed that Nramp1 is recruited from tertiary granules to the membrane of *Candida albicans*-containing phagosomes in human neutrophils [36].

1.2.4 The function of Nramp1 at the phagosomal membrane

Nramp1 is rapidly recruited to the phagosomal membrane upon phagocytosis of live bacteria (*Salmonella, Leishmania, Mycobacterium, Yersinia*) or inert particles (latex or zymosan beads) where it is proposed to exercise its antimicrobial activity [37-39]. The molecular basis for Nramp1's function remained unclear for several years after its cloning. However, the polypeptide sequence of Nramp1 showed structural features that suggested it was a membrane transporter [7]. In 1997, the identification and characterization of a second Nramp protein in mammals, Nramp2, provided strong evidence that Nramp proteins were pH-dependent divalent metal transporters. Gunshin and colleagues identified *Nramp2* (DMT1/Slc11a2, OMIM # 600523) as a novel intestinal iron transporter in a screen for duodenal genes up-regulated in rats fed a low-

iron diet [40]. They showed evidence that Nramp2 behaved as a proton-coupled divalent metal transporter with an unusually broad substrate specify, including Fe^{2+} and Mn^{2+}. The cloning and characterization of *Nramp2* is described in detail in Chapter 1.3 of this thesis. Indeed, the identification and characterization of numerous Nramp orthologs in species ranging from bacteria to humans suggested a potential function for Nramp1 at the phagosomal membrane as a pH-dependent divalent metal transporter. By analogy to the known substrates, membrane organization, and direction of transport established for Nramp2, we and others proposed a model whereby Nramp1 would act as an efflux pump at the membrane of pathogen-containing phagosomes, restricting microbial access to essential metals such as Mn^{2+} and Fe^{2+} [41;42]. However, early studies suggested that Nramp1 would act as a metal influx pump at the phagosomal membrane to facilitate the production of oxygen radicals via the Haber-Weiss reaction [43;44]. These studies reported an Nramp1-dependant increase in the accumulation/binding of radiolabeled Fe^{2+} into isolated phagosomes containing either Latex beads or *Myocobacterium avium* [43-45]. The phagosomal Fe^{2+} accumulation was blocked by the addition of anti-Nramp1 antibodies suggesting that Nramp1 might transport cytoplasmic Fe^{2+} into phagosomes. However, a potential limitation of these studies was the lack of distinction between phagosomal metal binding (whether Nramp1-dependent or independent) and actual metal transport across the phagosomal membrane. A later study using *Nramp1* mRNA injected into *Xenopus laevis* oocytes found an increase in Zn^{2+}-dependent inward currents when the cells were exposed to alkaline extracellular pH, which suggested metal uptake against the experimental proton gradient [46]. Based on additional pH-dependent transport studies using radioabeled Zn^{2+}, these authors concluded that Nramp1 might transport metals from the cytoplasm into phagosomes by a proton/divalent-metal antiport mechanism. They proposed that increased phagosomal Fe^{2+} could stimulate oxygen radical production via the Fenton reaction for increased bactericidal activity [43-47]. However, for Nramp1 to function as proton/divalent-metal antiporter at the phagosomal membrane it would dictate a transport mechanism distinct from other Nramp orthologs as well as Nramp2, both with respect to the direction of transport and utilization of the transmembrane pH gradient.

This was very unlikely considering the high amino acid conservation in the polypeptide sequences of Nramp1 and Nramp2 (64% identify and 78% similarity) [1].

Recent experiments have provided strong evidence that Nramp1 indeed functions as a pH-dependent divalent metal efflux pump at the phagosomal membrane, consistent with the biochemical transport data reported in studies of Nramp orthologs [26;27;40;48-51]. First, a metal-sensitive fluorescent dye was covalently coupled to zymosan particles, which were then fed to peritoneal macrophages isolated from Nramp1-expressing (+/+) and Nramp1-deficient (-/-) mice. The transport of divalent metals across the phagosomal membrane was monitored by tracking fluorescence quenching. *Nramp1*$^{+/+}$ phagosomes showed reduced accumulation and increased efflux of Mn^{2+} compared to *Nramp1*$^{-/-}$ phagosomes. This difference was lost when phagosomal acidification was blocked with the V-type ATPase inhibitor bafilomycin, suggesting that divalent metal transport by Nramp1 was H^{+}-dependent, like Nramp2 [52]. Second, another consequence of the functional similarity between Nramp1 and Nramp2 is that should Nramp1 be expressed at the plasma membrane, it would function comparably to Nramp2 and transport divalent metals into the cell in a pH-dependent manner. Such an Nramp1 variant was created by inserting a hemaglutinin epitope tag in the fourth predicted extracytoplasmic loop of the protein delineated by TM7 and TM8 [27]. At the cell surface, the Nramp1 variant indeed caused pH-dependent uptake of Fe^{2+} and Mn^{2+}, as measured by both fluorescence quenching and radioisotopic metals [27]. Interestingly, Nramp1 was found to be a more efficient transporter for Mn^{2+} than Fe^{2+}, suggesting that Mn^{2+} is the natural substrate for Nramp1 at the phagosomal membrane [27]. These results give strong credence to the model that Nramp1 controls the intracellular replication of mycobacteria and other pathogens by acting as an efflux pump at the phagosomal membrane, restricting microbial access to essential metals (Figure 1).

1.2.5 Pathogens under *Nramp1* control

In addition to *Salmonella typhimurium, Leishmania donovani*, and several species of Mycobacteria *(M. bovis* [53], *M. avium* [54], *M. lepraemurium* [55], *M. intracellulare* [56]), there are a number of other pathogens to which different levels of resistance or

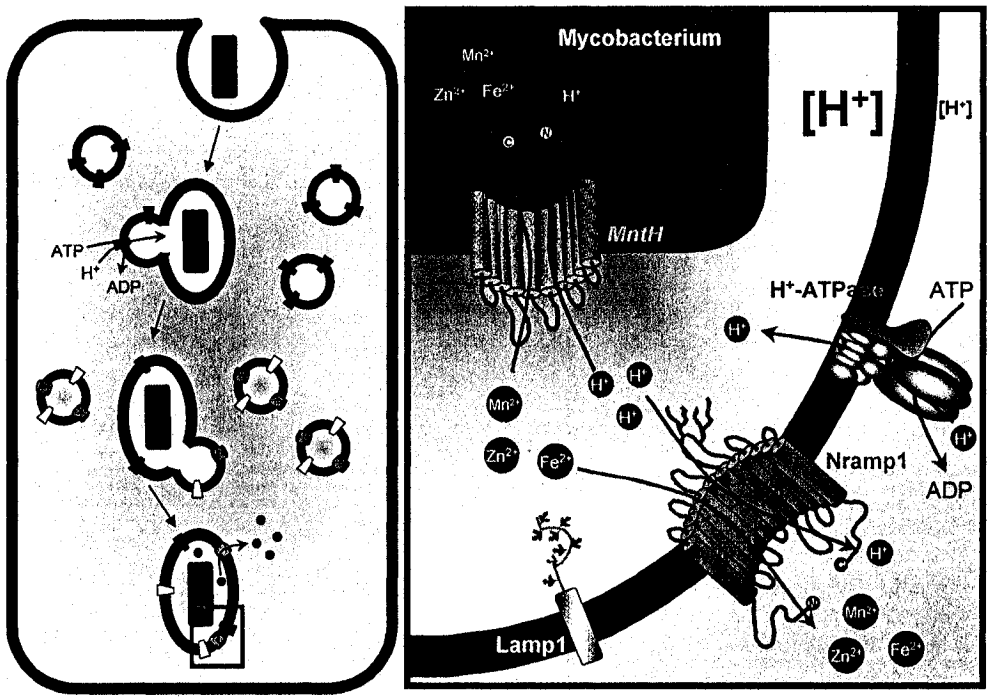

Figure 1. Metal transport by Nramp proteins at the interface of host–pathogen interaction. In the two diagrams, Nramp1 (green), lysosomal associated membrane protein Lamp (yellow), vacuolar H^+-ATPase (red), and metal ions (blue) are colour coded (left) and identified (right). In macrophages, bacterium-containing phagosomes mature by fusion to vacuolar H^+-ATPase positive vesicles, and Lamp-1/Nramp1 positive lysosomes. ATP-dependent acidification of the phagosome is required for Nramp1-mediated efflux of divalent metals (Fe^{2+}, Mn^{2+}, Zn^{2+}). At the phagosomal membrane (right panel), the vacuolar H^+-ATPase creates a proton gradient ($[H^+]$ versus $_{[H^+]}$), which is necessary for Nramp1-mediated metal efflux from the phagosomal lumen. Bacteria present in the phagosome express Nramp homologues (e.g. MntH) that may import divalent metals from the phagosomal space by a similar pH-dependent mechanism. The membrane topology of Nramp proteins is shown with respect to the amino (N) and carboxyl (C) terminus. *(From: Lam-Yuk-Tseung, S. and Gros, P. "Genetic control of susceptibility to bacterial infections in mouse models". Cellular Microbiology. 2003 May;5(5):299-313.)*

susceptibility have been associated with polymorphic variations in *Nramp1*. These include a variety of ovine [57] and avian [58] strains of *Salmonella*, as well as *Brucella abortus* [59], *Pasteurella pneumotropica* [60], *Candida albicans* [47], *Toxoplasma gondii* [61;62], and *Francisella tularensis* [63;64]. Surprisingly, *Nramp1* is not critical for resistance in mice to *in vivo* infection with H37rv *Mycobacterium tuberculosis*, the cause of pulmonary tuberculosis in humans [65-67]. These reports are in contrast to the situation in humans where polymorphic variants at *NRAMP1* have been associated with tuberculosis [68-74]. However, this apparent paradox may be explained by differences between the experimental model of tuberculosis in the mouse (low or high doses, *i.v.*), and the natural human situation (low doses, aerosol). The next sections of this thesis will describe the effects of Nramp1 on controlling the intracellular replication of *Mycobacterium* and *Salmonella*, since the role of Nramp1 in infection by these parasites have been relatively well characterized.

1.2.6 Effect of Nramp1 on intracellular *Mycobacterium*

Nramp1-mediated metal efflux from the phagosome has pleiotropic effects on the engulfed pathogen. It has long been established that mycobacteria survive within macrophages by preventing the maturation of phagosomes into fully bactericidal phagolysosomes [75-81]. Mycobacteria present in Nramp1-deficient phagosomes are able to inhibit luminal acidification by blocking recruitment of vacuolar H^+-ATPase pumps to the phagosomal membrane, as well as reducing the acquisition of lysosomal markers such as Lamp1 and Cathepsin D [78-81]. Rather, these phagosomes retain sorting/early endosome markers such as transferrin receptor (an important source of Tf-iron) and Rab5 (required for early endosome fusion). This inhibition of phagosomal maturation appears to be an active process from the live pathogen since it does not occur when macrophages engulf latex beads or dead mycobacteria. In the presence of Nramp1 (*Nramp1*$^{+/+}$), mycobacteria are unable to block phagosomal maturation, resulting in increased luminal acidification, increased fusion with lysosomes, enhanced bacterial damage, and diminished mycobacterial replication compared to *Nramp1*$^{-/-}$ phagosomes [82;83] (Figure 2). *Nramp1*$^{+/+}$ macrophages also produce more nitric oxide (NO) in response to mycobacterial infection

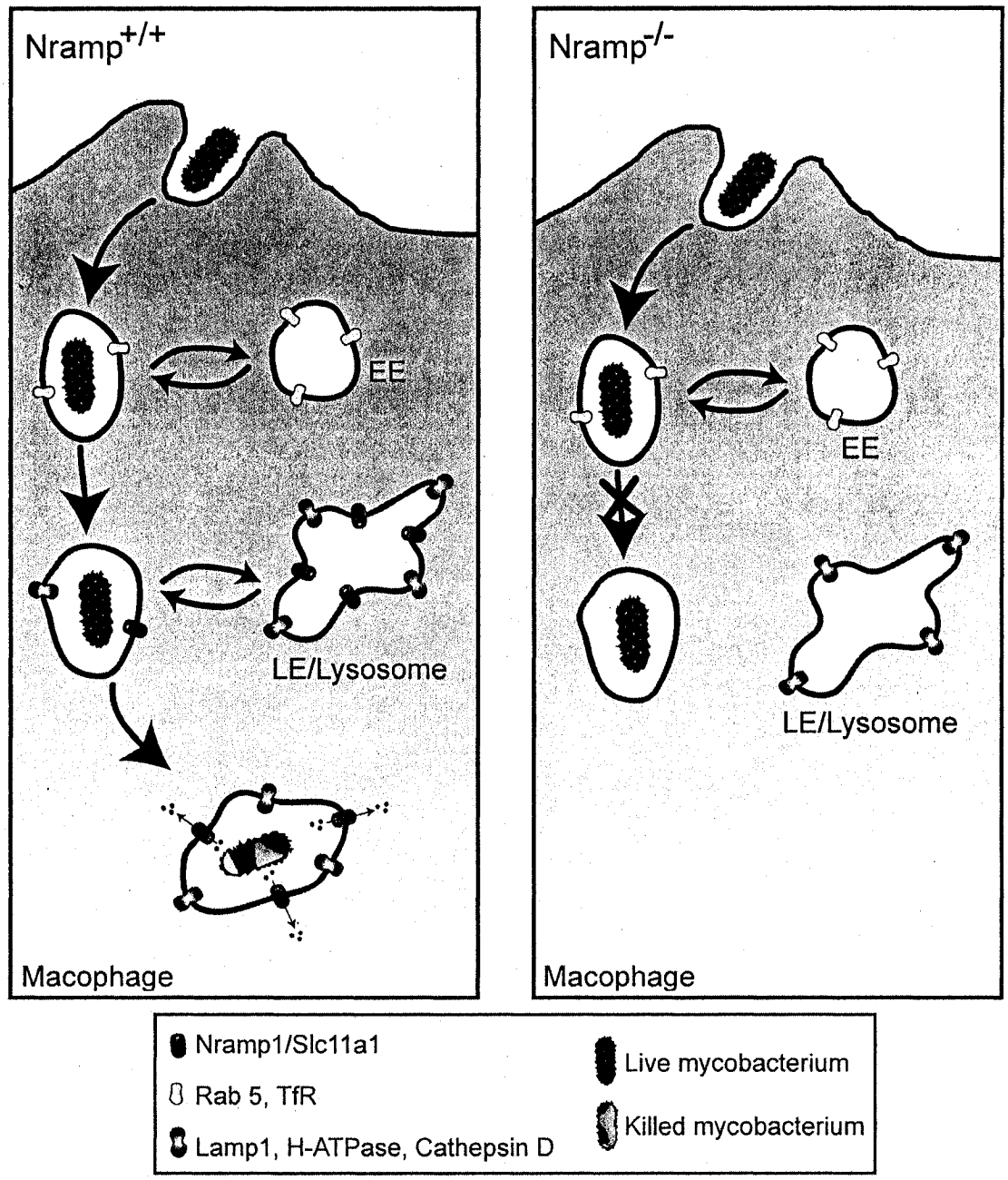

Figure 2. The effect of Nramp1 on intracellular Mycobacterium. In the presence of Nramp1 (Nramp1+/+, left panel), mycobacteria are unable to block phagosomal maturation, resulting in increased luminal acidification, increased fusion with lysosomes, enhanced bacterial damage, and diminished mycobacterial replication. Mycobacteria survive within macrophages by preventing the maturation of phagosomes into fully bactericidal phagolysosomes. Mycobacteria present in Nramp1-deficient phagosomes (right panel) inhibit luminal acidification by blocking recruitment of V-ATPase pumps to the phagosomal membrane, as well as reducing the acquisition of lysosomal markers such as Lamp1 and Cathepsin D. Rather, these phagosomes retain sorting/early endosome markers such as transferrin receptor and Rab5.

and/or interferon-γ stimulation than *Nramp1*$^{-/-}$ controls, possibly contributing to bacteriostasis [84-86].

The mechanism by which mycobacteria can inhibit phagosomal maturation is poorly understood. However, Nramp1 clearly plays a role in antagonizing this process. One possible explanation is that inhibition of phagosomal maturation by mycobacteria is a metal-dependant process that can be countered by Nramp1-mediated metal efflux. Indeed, a number of studies have demonstrated the importance of iron in mycobacteria-mediated inhibition of phagosomal maturation as well as in the virulence of the intracellular pathogens [87-90]. In addition, microarray gene expression analysis of *M. tuberculosis* isolated from activated macrophages, showed up-regulation of mycobacterial genes involved in metal uptake, accounting for over half of the activated genes [89]. Iron promotes mycobacterial growth in *Nramp1*$^{+/+}$ mice and promotes the development of active tuberculosis in humans [90;91]. Likewise, extracellular iron can stimulate intracellular growth of *M. avium* in both *Nramp1*$^{+/+}$ and *Nramp1*$^{-/-}$ macrophages [92], suggesting that excess cellular iron may overwhelm the function of Nramp1 [90;92]. Collectively, these results suggest that iron is required by mycobacteria to arrest phagosomal maturation and survive intracellularly.

1.2.7 Effect of Nramp1 on intracellular *Salmonella*

Unlike mycobacteria, *Salmonella* do not survive intracellularly by inhibiting phagosomal acidification. Rather, they sequester themselves inside specialized *Salmonella*-containing vacuoles (SCVs) that become acidified and are able to fuse with Lamp1-positive lysosomes [93]. In permissive *Nramp1*$^{-/-}$ macrophages, *Salmonella* survive by blocking recruitment of mannose-6-phosphate receptor (M6PR) positive vesicles and isolate themselves from the endosomal pathway [37]. In non-permissive Nramp1-expressing macrophages, SCVs fuse with M6PR-positive vesicles and maintain access to the endosomal pathway, expressing endosomal markers such as EEA1 and fluid phase FITC-dextran [37]. These effects could be mimicked in Nramp1-negative macrophages

by using membrane-permeant iron chelators [94]. These results suggest a model in which Nramp1 counteracts the ability of *Salmonella* to sequester itself from the degradative phagosomal pathway by restricting its access to divalent metals.

Divalent metals, such as Fe^{2+} and Mn^{2+}, have been shown to be essential in *Salmonella* for virulence *in vivo* and replication in cultured macrophages [91;95]. *Salmonella* possess several high and low affinity iron and manganese transporters [96-99] and several of these transporters have been shown to contribute to virulence *in vivo* [98;100-102]. In fact, mutations at a number of these transporters (such as *feoB*, *sitA-D*, or *MntH*) or divalent metal chelation have been shown to reduce or abrogate virulence of *Salmonella* [101]. Thus, Nramp1-mediated depletion of metals from the intra-phagosomal space appears to have a major impact on intracellular survival and replication of *Salmonella*. The pathogen, in turn, reacts to the metal depletion by upregulating expression of metal transporters such as *MntH* and *sitA* [103] and increasing expression of their *Pathogenicity Island 2* (*SPI2*) virulence genes [104].

1.2.8 *NRAMP1* and its role in resistance to infection in humans

In humans, *NRAMP1* has been mapped to chromosomal region 2q35 and consists of 15 exons that span a 13 kb region [105;106]. Two transcriptional start sites have been mapped and regulatory motifs in the *NRAMP1* promoter region have been identified. These include a TATA box element, interferon-γ response elements, and binding sites for the transcriptional factors NFκB, AP-1, and PU.1 [105-108]. Results obtained in murine models have raised the possibility that *NRAMP* genes could be important determinants of susceptibility to common human diseases. A number of studies conducted on ethnically and geographically diverse populations are in general agreement that *NRAMP1* alleles are risk factors for tuberculosis [74;109-116]. Indeed, a number of genomic DNA polymorphisms have been identified in or near *NRAMP1* that have been associated with several infectious and inflammatory diseases such as leprosy [117-119], non-tuberculous mycobacterial (NTM) lung disease [120], human immunodeficiency virus (HIV) [121], rheumatoid arthritis [122-125], inflammatory bowel diseases [126;127], multiple sclerosis [128], and type 1 diabetes [129;130]. The numerous illnesses affected by *NRAMP1* polymorphisms reflect the pleiotropic effects of

Nramp1 function and the importance of divalent metals in disease and infection. Recently, Kissler *et al* used lentiviral transgenesis and RNA interference to knock-down expression of Nramp1 in a nonobese diabetic (NOD) mouse model, and showed that Nramp1-silencing reduced the frequency of type 1 diabetes in these animals [130]. Their results provided strong evidence that the insulin-dependent diabetes locus 5.2 (*idd5.2*), which has been implicated in the NOD mouse model, is indeed *Nramp1*.

1.3 Nramp2 and its role in iron homeostasis

1.3.1 Cloning of the *Nramp2* gene

Two years after the positional cloning of *Nramp1*, a second mouse *Nramp* gene was identified by cDNA cross-hybridization studies based on its high sequence homology with *Nramp1* [131]. The novel gene was named *Nramp2*, and was mapped to the distal part of mouse chromosome 15. The murine *Nramp2* gene consists of 18 exons spread over more than a 30 kb region. Analysis of the nucleotide and predicted amino acid sequence of *Nramp2*, indicated that it was a novel protein closely homologous to *Nramp1* and that the two proteins defined a new family of proteins [1]. The two Nramp proteins identified share a high 63% sequence identity and 78% similarity [1;131]. However, in contrast to the macrophage-specific *Nramp1*, *Nramp2* mRNA expression is detected almost ubiquitously [40;131].

1.3.2 *Nramp2* encodes a divalent metal transporter

Although the polypeptide sequences of Nramp1 and Nramp2 suggested that both proteins functioned as membrane transporters, the substrate and mechanism of transport of Nramp proteins remained elusive. Perhaps the first indication of the function of Nramp proteins occurred in 1996 when Supek and colleagues reported the identification a novel *Saccharomyces cerevisiae* mutant that was unable to grow in the presence of the metal chelator EGTA [132]. The mutant could be suppressed by overexpression of the yeast gene *SMF1*, a gene originally cloned as a multicopy suppressor of a temperature-sensitive mutant (*mif1-1*) defective in the function of mitochondrial processing peptidase [133]. However, the ability of Smf1p to complement growth in the presence of EGTA suggested

that *SMF1* played a direct role in metal homeostasis in yeast. Consistent with this hypothesis, Supek *et al.* showed that a *smf1* null mutant exhibited reduced Mn^{2+} uptake. Interestingly, Smf1p showed significant resemblance (46% similarity) to both Nramp1 and Nramp2 proteins [1].

Further insight into the function of Nramp proteins occurred in 1997, when two simultaneous independent studies showed by different methods that Nramp2 functions as a transporter of divalent cations, including iron. In the first study, *Nramp2* was isolated by expression cloning from a rat cDNA library in *Xenopus* oocytes by Gunshin and colleagues in a search for iron transport proteins [40]. The goal of this study was to identify the intestinal transporter responsible for absorption of non-heme dietary iron. To accomplish this, they prepared a cDNA library using duodenal mRNA from rats that were kept on a low-iron diet. The proximal duodenum had been previously identified as the main site of non-heme iron absorption by physiological iron uptake measurements [134;135]. A single cDNA clone caused a 200-fold increase in iron uptake compared to control uninjected oocytes. The clone was found to contain rat *Nramp2*, although it was re-named *DCT1* (*Divalent Cation Transporter 1*) in this report, and was later re-named again to *DMT1* for *Divalent Metal Transporter 1.* Although *DMT1* is the most commonly used term for *Nramp2* today, it has been recently re-named once again to Slc11a2 (solute carrier family 11 member 2). For clarity, I will use the *Nramp2/DMT1* nomenclature in the remainder of this thesis.

Expression of *Nramp2* in oocytes was demonstrated to mediate uptake of a broad range of divalent metals including Fe^{2+}, Mn^{2+}, Zn^{2+}, Co^{2+}, Cu^{2+}, Ni^{2+}, Pb^{2+}, and Cd^{2+} but not Ca^{2+} or Mg^{2+} [40]. Metal transport was shown to be dependent on extracellular pH and the cell membrane potential. Furthermore, mRNA expression studies confirmed the ubiquitous expression of *Nramp2* but also demonstrated a striking tissue-specific upregulation of *Nramp2* mRNA upon chronic iron depletion. This upregulation was strongest in the proximal intestine but was also seen to a lower extent in the kidney, liver, brain, heart, lung, and testis [40].

1.3.3 A mutation at *Nramp2* causes iron deficiency in rats and mice

In a parallel study to Gunshin *et al.* [40], Fleming and colleagues used a positional cloning approach to identify *Nramp2* as the causative mutation in mice with microcytic anemia (*mk*) [136]. Homozygous *mk/mk* mice suffer from severe hypochromic, microcytic anemia due to impaired intestinal iron absorption and defective erythroid iron utilization [137-140]. The *mk* mutation arose spontaneously in the breeding stocks of the Jackson Laboratory over thirty years ago and is inherited as an autosomal recessive trait with full penetrance [137]. Newborn mice homozygous for the mutation (*mk/mk*) were readily distinguishable at birth by their small size and pale coloration, and were subsequently maintained by breeding onto several genetic backgrounds [137]. The study by Fleming *et al.* traced the *mk* phenotype to a mutation in *Nramp2* that results in a non-conservative glycine to arginine substitution (G185R) in the predicted TM4 of the protein [136]. Strikingly, it was later discovered that the identical mutation in Nramp2 (G185R) was the cause of disease in a radiation-induced rat mutant that exhibited an *mk*-like phenotype, the *Belgrade* (*b*) rat [141]. Like *mk*, *b* is inherited as an autosomal recessive trait that results in hypochromic, microcytic anemia associated with impaired reticulocyte iron uptake and gastrointestinal iron absorption [142-145]. Together, these results provided strong evidence that Nramp2 functions as a pH-dependent iron transporter essential for both normal intestinal iron absorption and erythroid iron usage.

In vitro studies have shown that the Nramp2^{G185R} protein expressed in both *mk* mice and *Belgrade* rats displays multiple biosynthetic and functional defects that combine to cause iron deficiency in rodents. Su and colleagues have shown that the G185R mutation reduces the ability of Nramp to transport iron in transfected HEK293 kidney cells [146]. In contrast, protein expression studies in wild-type and mutant animals led Canonne-Hergaux *et al* to conclude that Nramp2^{G185R} is inadequately targeted or retained by the plasma membrane of enterocytes and reticulocytes from *mk* mice [147]. Experiments performed by Touret *et al* in transfected LLC-PK$_1$ epithelial cells showed that Nramp2^{G185R} is functionally impaired, less stable, and inefficiently processed resulting in defective glycosylation and reduced plasma membrane expression [148]. Consequently,

Nramp2^{G185R} was also shown to accumulate in the endoplasmic reticulum where it is rapidly degraded by a proteosome-dependent mechanism [148].

The fact that the G185R mutation has occurred spontaneously on two occasions in *mk* mice [136] and once in *Belgrade* [141] rats is striking and suggests that either the codon containing G185 is hypermutable or that G185R represents a gain of function that confers some survival advantage to the organism. Work by Xu and colleagues support the latter hypothesis. They showed that Nramp2^{G185R}, despite presenting multiple biosynthetic and function deficiencies, confers a novel Ca^{2+}-selective permeability pathway [149]. They argue that the influx of Ca^{2+} might potentiate the residual Nramp2 iron-transport activity. The transferrin cycle is essential for iron uptake by erythroid precursor cells [150] and Nramp2 mediates transfer of iron from transferrin cycle endosomes to the cytoplasm [42;51;141]. Elevated intracellular Ca^{2+} has been reported to accelerate iron uptake through the transferrin cycle, apparently through activation of protein kinase C [151].

Recently, mutations in *NRAMP2* have been identified in three human patients suffering from severe microcytic anemia and hepatic iron overload [4-6]. The effects of these mutations at both the physiological and molecular levels are discussed further in section 1.3.9.3 of this chapter.

1.3.4 Alternate splicing of *Nramp2* mRNA

The amino acid sequence predicted from the rat cDNA isolated by Gunshin *et al.* was almost identical to the sequence reported for mouse *Nramp2*, except at the extreme C terminus, where the two sequences diverged [40;131]. However, the rat Nramp2 sequence was homologous to the published C-terminal sequence of human *NRAMP2* [152]. The discrepancy in the C-terminal sequences was explained in subsequent studies reporting the existence of two isoforms of *Nramp2*, generated by alterative splicing at two 3' exons in mice, rats and humans [40;131;136;152;153]. This alternate splicing generates two Nramp2 proteins with different C-terminal segments. Interestingly, one of the two *Nramp2* splice isoforms, named isoform I or +IRE, contains an iron responsive element (IRE) in its 3' untranslated region (UTR) and produces a 561 amino acid protein in rats and mice. The other splice isoform, named isoform II or –IRE, lacks an IRE in its 3' UTR and produces

a 568 amino acid protein. IREs are known to play regulatory roles in cellular iron metabolism through interactions with iron regulatory proteins (IRPs). The role IRPs in regulating cellular iron homeostasis is described further in section 1.3.8.4 of this Chapter. Recently, a novel 5' upstream exon has been identified in the human, mouse, and rat *Nramp2* genes [154]. This novel exon (exon 1A) is generated by the usage of an alternate transcription initiation site, and is predicted to produce an Nramp2 protein bearing an additional 29-31 amino acids (exon 1A) upstream of the previously identified start codon of Nramp2 isoforms I and II (exon 1B). The usage of exon 1A also appears to be highly tissue-specific, with enhanced usage in the kidney and duodenum [154]. Thus, a theoretical total of four *Nramp2* mRNAs and proteins can be produced by the gene, depending on alternate 5' (exon 1A vs. 1B) and 3' (I/+IRE vs. II/–IRE) splicing, giving rise to four Nramp isoforms: I(A), I(B), II(A), and II(B) (Figure 3). However, most *in vitro* studies on Nramp2, including all the studies described in this thesis, have been performed using the originally identified isoforms I(B) and II(B). Little is currently known about the importance of exon 1A or the extra 29-31 N-terminal residues in the regulation, function, or targeting of Nramp2.

1.3.5 Structural features of the Nramp2 protein

Like *Nramp1*, *Nramp2* is expressed as a 90-100 kDa integral membrane phosphoglycoprotein in transfected CHO or LLC-PK_1 cells that is predicted to have twelve membrane-spanning domains. The predicted topology of Nramp2 in the membrane has been supported by several epitope accessibility studies in intact cells [26;27;51]. Picard and colleagues used immunofluorecence experiments on intact CHO cells expressing an epitope-tagged Nramp2 variant to show that the region connecting TM7 and 8 is indeed exofacial. Similar experiments with Nramp1 and Nramp2 variants possessing N or C terminal epitope tags have demonstrated that the amino and carboxyl terminal segments of both transporters face the cytosol [26;27]. Glycosylation in Nramp2 is extensive, with the transporter owing ~50% of its molecular mass to sugar moieties added at two consensus N-linked glycosylation signals present in the fourth extra-cytoplasmic loop [42]. Extensive glycosylation of Nramp2 may help protect the protein against

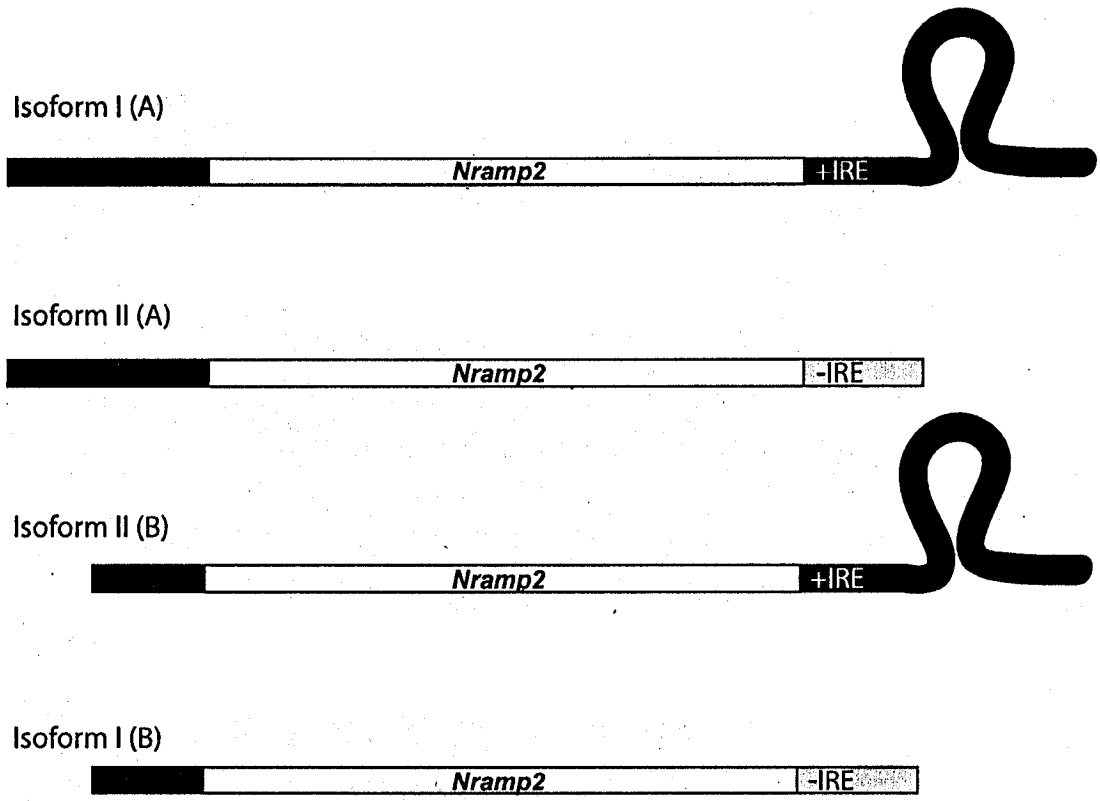

Figure 3. Alternative splicing of *Nramp2* pre-mRNA generates four theoretical isoforms. The use of alternate transcription initiation sites at the 5' exon (exon 1A vs. 1B), generates diversity at the 5' end of the message. Alternate splicing at the 3' terminal exon generates further diversity, causing the inclusion (+IRE) or not (-IRE) an iron resonpive element (IRE) in the 3'untranslated region.

degradation or may be important for proper maturation and targeting of the transporter to it site of action. Tabuchi and colleagues have shown that disruption of the N-linked glycosylation sites in Nramp2 affect the transporter's polarized distribution to the apical membrane of confluent MDCK kidney cells [155]. As in Nramp1, the fourth intra-cytoplasmic loop of Nramp2 contains a conserved transport motif (CTM) of unknown function [1;131].

Consistent with other members of the Nramp family, Nramp2 possesses nine highly conserved, yet thermodynamically disfavored, charged amino acids within its TM domains [1]. Also present are two highly conserved histidine residues in TM6 of the protein. Because of their high conservation, these charged residues likely play a critical role in the structure and/or function of Nramp2. The work described in Chapter 2 of this thesis identifies three negatively charged residues (D86, D192, E299) within transmembrane domains 1, 4, and 7 of Nramp2 that are essential for metal transport activity [28]. These negative residues are thought to form part of a metal binding site or line a hydrophilic pore or transport path. These results have been supported by similar subsequent mutagenesis studies of the charged TM residues in the bacterial Nramp ortholog, *MntH* [156]. Several studies have been aimed at better understanding the pH-dependence of metal transport by Nramp proteins. Sacher and colleagues have provided evidence from electrophysiological measurements that Nramp2, and other Nramp proteins, may exhibit a proton clutch mechanism, allowing multiple protons to "slip" through the transporter at acidic pH [50]. The advantage of such a proton slippage mechanism is not currently known, however, it has been postulated to protect the organism against the overloading of metals in the presence of excess protons. At the molecular level, experiments described in Chapter 2 identify two conserved histidines (H267, H272) in TM6 of Nramp2 that are critical for regulating the pH dependence of metal transport [28]. Subsequent studies on rat Nramp2 expressed in *Xenopus* ooctyes using electrophysiological and radioisotopic techniques have shown that H267 and H272 are critical for the H^+-coupling required for metal transport [157]. Finally, electrophysiological studies have shown that a single amino acid substitution (F227I) in TM4 of Nramp2 can increase the ratio of metals to protons transported by 14-fold [158].

Studies involving the yeast Nramp orthologs (*Smf1-3*) have also provided valuable insight into the molecular structure and function of Nramp2. A mutant yeast strain with two of its *Nramp* orthologs inactivated (*Smf1Δ/Smf2Δ*) is unable to grow in the presence of the metal chelator EGTA [34;132]. Expression of Nramp2 in *Smf1Δ/Smf2Δ* yeast is known to suppress this phenotype and restore growth in the presence of EGTA [34]. Pinner *et al* took advantage of this to demonstrate that mutations (Q384E, G394V) at highly conserved residues within the CTM of Nramp2 abrogate the function of the protein [34]. Cohen and colleagues used complementation assays in yeast in conjunction with electrophysiological measurements in oocytes to analyze the structural and functional importance of the first extra-cytoplasmic loop (EC1) of Nramp2 [159]. They showed that critical single mutations in EC1, G119A and Q126D, resulted in a complete loss of metal uptake activity by Nramp2. However, the non-functional Q126D mutant could be partially restored by the introduction of a second mutation at two amino acids upstream of Q126 (D124A). The double mutant D124A/Q126D also appeared to alter the metal ion specificity of the transporter in favor of Fe^{2+} while a triple mutant (G119A/D124A/Q126D) displayed no transport activity yet possessed altered pre-steady-state currents [159]. These results suggest that the first extra-cytoplasmic loop of Nramp2 may be involved in metal ion binding and proton-coupling of transport.

1.3.6 Nramp2 expression

Nramp2 expression has been detected at high levels in epithelial cells as well as peripheral tissues. In general, isoform I of Nramp2 appears to be predominantly expressed in epithelial cells while isoform II appears to be expressed mostly in non-epithelial cells. However, preferential expression of Nramp2 isoforms I and II is not necessarily mutually exclusive: simultaneous expression of both isoforms at the mRNAs level has been observed in several tissues including kidney, thymus, and liver [40;155;160].

Isoform I is expressed at the apical membrane of duodenal brush border enterocytes [161], where it is responsible for the uptake of dietary inorganic iron (Figure 4). Immunostaining experiments of tissue sections show that Nramp2 expression is limited to the villi and absent in the crypts cells [161-165]. Nramp2 expression appears to be strongest

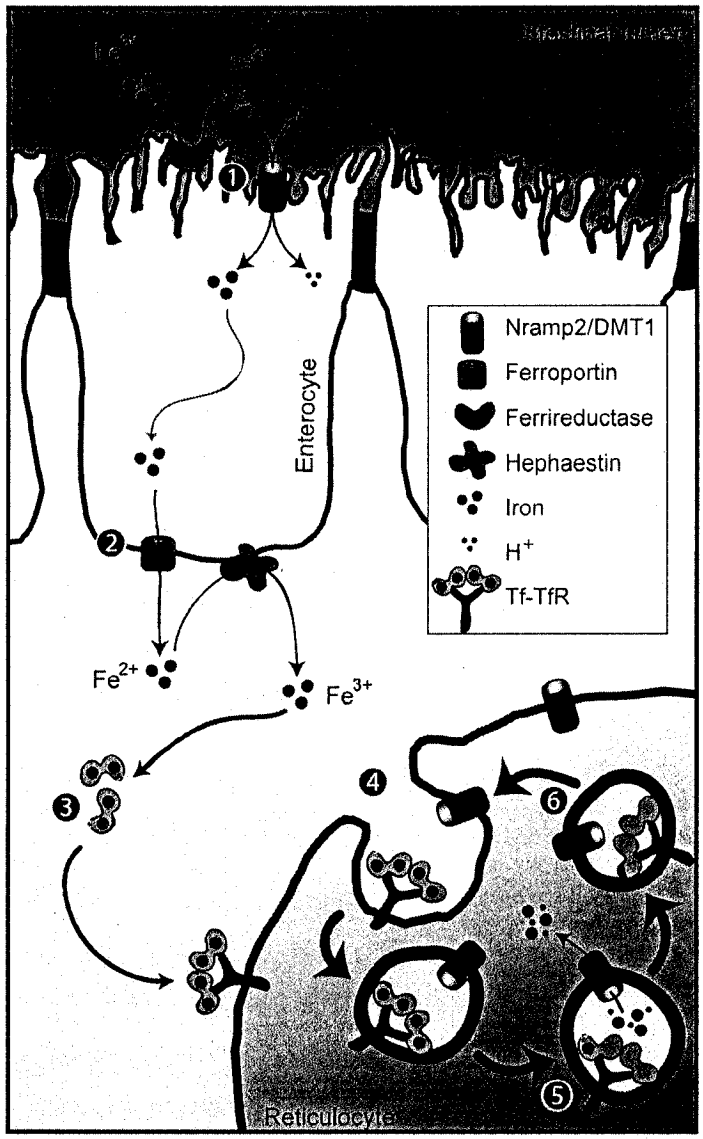

Figure 4. Absorption of non-heme iron at the intestinal brush border and in reticulocytes. DMT1/Nramp2 isoform I is expressed at the apical membrane of intestinal enterocytes, where it mediates the absorption of non-heme divalent iron that has first been reduced by a putative ferrireductase (1). At the basolateral membrane, Ferroportin (Fpn) is responsible for the export of iron from the enterocyte into circulation (2). Following oxidation at the basolateral membrane by the ferroxidase Hephaestin, iron is rapidly bound to transferrin (3). Non-epithelial cells such as erythroid precursors uptake iron primarily through internalization of the transferrin-transferrin receptor complex (4). Endosomal acidification facilitates the release of iron from transferrin and creates the proton gradient required for iron transport by Nramp2 isoform II across the endosomal membrane and into the cytosol (5). Iron is then transported into the mitochondria for heme synthesis or stored bound to ferritin. Apotransferrin-transferrin receptor and Nramp2 isoform II are subsequently recycled back to the cell surface.

in the apical two-thirds of the villi where it is limited to enterocytes that make up the columnar absorptive epithelium of the mucosa. In these cells, Nramp2 localizes primarily to the apical plasma membrane known as the brush border. This pattern of expression was also observed in the human intestinal cell line Caco-2 [163;166-168]. In the intestine, Nramp2 isoform I expression is up-regulated in response to dietary iron depravation and seems repressed under iron overload conditions [161]. Immunohistochemical studies by Canonne-Hergaux and colleagues showed that in *mk/mk* enterocytes, Nramp2 expression is upregulated but is not properly targeted to the brush border [147].

In contrast, isoform II of Nramp2 is predominantly expressed in peripheral or non-epithelial cells such as in erythroid cells. Studies in primary as well as transfected cell lines have shown that isoform II is not only expressed at the plasma membrane of these cells but also in transferrin receptor positive recycling endosomes [42;51;146]. In mice, reticulocytes and reticulocyte precursors cells (which give rise to mature oxygen-carrying red blood cells) are the major physiological site of isoform II expression, where the transporter is detected as a 70 kDa species and has been shown to colocalize with transferrin receptor [169]. During erythropoiesis, precursor red blood cells have a large requirement for iron for heme biosynthesis and the production of hemoglobin. The high level of expression of isoform II in these cells permits the coordinated uptake of iron into recycling endosomes via the transferrin cycle and the transport of iron across the endosomal membrane into the cytosol by Nramp2 (Figure 4). Although Nramp2 expression in reticulocytes does not seem to be regulated by body iron status, treatment of mice with phenylhydrazine or erythropoietin (to boost erythropoiesis) induces the production of Nramp2-expressing reticulocytes [170]. However, reticulocytes from *mk/mk* mice express no detectable Nramp2 protein.

Macrophages are another source of significant Nramp2 isoform II expression [42]. These phagocytic cells play a critical role in the recycling of heme iron through phagocytosis of senescent red blood cells. Nramp2 may indeed transport phagosomal iron into the cytosol after hemoglobin degradation. Immunoblotting experiments have shown that Nramp2 is expressed as a glycosylated 70-90 kDa protein in macrophages [42]. Immunofluorescence experiments revealed that Nramp2 is localized primarily to the early

endosome compartment with some presence in Lamp1-positive late endosomes/lysosomes in transfected RAW264.7 macropages and two murine Seroli cell lines of the testis (TM4 and 15P-1) [171]. Immunofluorescence studies have also shown that Nramp2 can be associated with phagosomal membranes during phagocytosis [42]. More recently, Jabado *et al* showed that Nramp2 can associate with erythrocyte-containing phagosomes in transfected RAW264.7 macrophages [171].

In the kidney, Nramp2 protein has been detected in microsomal membrane fractions as a 70-75 kDa membrane protein [161]. In mouse kidneys, Canonne-Hergaux and colleagues used immunohistochemical staining with an affinity purified anti-Nramp2 antibody to detect Nramp2 in the cortex but not the medulla, and at the brush border and apical poles of epithelial cells of the proximal tubule [172] . In rat kidneys, Ferguson and colleagues detected Nramp2 expression in the intracellular vesicles of proximal tubule cells of S3 segment, collecting ducts, thick ascending limbs of Henle's loop and, more intensely, at the apical membrane of distal convoluted tubules [173]. Recently, Abouhamed *et al* reported the detection of Nramp2 in Lamp1-positive late endosomes and lysosomes within rat proximal tubule cells [174]. Because these studies used polyclonal antibodies recognizing the N terminus of Nramp2, the exact isoform (I or II) expressed in the kidney could not be determined. Although the fact Canonne-Hergaux *et al* could not detect any significant expression in the kidney using an antibody specifically recognizing isoform II strongly suggests that the majority of Nramp2 present in the kidney is indeed isoform I [172]. In sharp contrast to the intestine, Nramp2 mRNA and protein expression appears to be only modestly affected by dietary iron deprevation and is not affected by stimulation of erythropoiesis [172;175]. Furthermore, while anemic *mk* and *Belgrade* mutants show strong upregulation of Nramp2 in the intestine, they show very low Nramp2 expression in the kidney [172;176].

In the brain, work by Gunshin and colleagues showed Nramp2 mRNA is expressed in most neurons at low levels but not in glial or ependymal cells [40]. Stronger Nramp2 expression was detected in densely packed cell groups, such as the hippocampal pyramidal and granule cells, cerebellar granule cells, the preoptic nucleus and pyramidal cells of the piriform cortex [40]. Strong Nramp2 mRNA expression was also seen in the

ventral portion of the anterior olfactory nucleus and in the epithelial cells of the choroid plexus [40]. At the protein level, Burdo and colleagues detected Nramp2 in neurons of striatum, cerebellum, thalamus and in the ependymal and vascular cells throughout the rat brain [177]. Immunohistochemical studies by Moos and Morgan in rats confirmed that Nramp2 protein is expressed in neurons and the choroid plexus, but not in brain capillary endothelial cells or in macro- or microglial cells [178]. Some studies have suggested that Nramp2 expression in neuronal cells is regulated by the hypoxia regulator. Recent studies by Lis and colleagues have shown that hypoxia selectively increases expression of Nramp2, particularly the exon 1A containing isoforms of the transporter, in rat pheochromocytoma (PC12) cells [179].

In the liver, the main site of body iron storage, Nramp2 mRNA expression has been detected in a number of cells types. Using *in situ hybridization* and quantitative real-time PCR, Zhang and colleagues detected Nramp2 mRNA expression in rat liver hepatocytes, Kupffer cells, sinusoidal endothelial cells (SECs), and hepatic stellate cells (HSCs) [180]. At the protein level, immunohistochemical studies by Trinder and colleagues detected Nramp2 on the plasma membranes of rat hepatocytes and this expression appeared to increase and decrease in response to iron overload or iron deficiency, respectively [162]. Trinder *et al* suggested that upregulation of Nramp2 in the liver during iron overload could reduce the risk of increased iron intake and cell damage elsewhere in the body.

Nramp2 has also been detected in several other tissues, although the distribution of the transporter at these sites has been less extensively characterized. In the thymus, Nramp2 mRNA was detected in the cortical, but not medullary, thymocytes [40]. In the testis, Nramp2 mRNA [40] and protein [171] expression has been detected in the Sertoli cells of seminiferous tubules. Nramp2 protein has also been detected in the placenta, both in the cytoplasm at the junction of fetal membrane and fetal vessels [181]. In this study, Georgieff and colleagues suggested that Nramp2 may transport endosomal ferrous iron into the cytoplasm of the human syncytiotrophoblast to supply the fetus [181].

1.3.7 Subcellular targeting of Nramp2

Although both Nramp2 isoforms I and II are expressed at the plasma membrane, immunolocalization studies in transfected cells have shown that isoforms I and II exhibit different subcellular endosomal targeting at steady-state. In transfected LLC-PK_1, CHO and RAW264.7 cells, isoform II is mostly expressed in early and recycling endosomes [42;51]. Studies using an exofacially-tagged Nramp2 molecule have shown that isoform II molecules present at the cell surface and in recycling endosomes are in dynamic equilibrium, with surface transporters being continuously internalized via a clathrin and dynamin-dependent process [51]. In contrast, isoform I has been detected in Lamp1-positive late endosomes and lysosomes in transfected HEp-2 and LLC-PK_1 cells [155;182]. Lysosomal expression of isoform I in phagocytic cells such as macrophages may be required for the recycling of iron from senescent red blood cells. Work described in Chapter 6 of this thesis compares Nramp2 isoforms I and II with respect to function, subcellular localization, endocytosis kinetics, and fate upon internalization in transfected LLC-PK_1 cells. This work shows that isoform I is expressed at higher levels at the cell surface compared to isoform II due to a slower rate of internalized from the plasma membrane. In addition, isoform I is not efficiently recycled upon endocytosis and is targeted to late endosomes and lysosomes [182]. Higher surface expression is advantageous for isoform I-expressing epithelial cells, which must absorb Fe^{2+} and possibly other divalent metals across their plasma membranes. Thus, alternative splicing of Nramp2 critically regulates the subcellular localization and site of metal transport.

Cytoplasmic motifs such as tyrosine-based (NPXY, YXXΦ) and dileucine-based motifs (LL) signals have been shown to dictate the subcellular targeting and trafficking of membrane proteins (reviewed in [183]). Experiments by Tabuchi and colleagues in transfected HEp-2 larynx carcinoma cells showed that the 36 carboxy terminal residues of Nramp2 isoform II are important for targeting to early endosomes. Truncation and mutagenesis experiments subsequently revealed that a novel $YXLXX^{555\text{-}559}$ motif in the C terminus of isoform II is responsible for the early endosome targeting of the protein, with mutations in this motif resulting in accumulation of the transporter in Lamp2-positive late endosomes/lysosomes [155]. In addition, experiments described in Chapter 5 of this thesis

show that critical residues in the C terminus of isoform II, including the $YXLXX^{555-559}$ signal, are required for the transporter's internalization from the cell surface and its recycling back to the plasma membrane [184]. Furthermore, removal of an intact $YXLXX^{555-559}$ motif appears to cause lysosomal targeting by default. Targeting motifs in the N terminus of Nramp2, including putative NPXY and YXXΦ signals, were shown to have an additional but less determinate effect on subcellular targeting of the transporter [184].

1.3.8 Nramp2 and cellular iron homeostasis

Iron is an essential element for life, playing a variety of roles in organisms ranging from the transportation of oxygen to the generation of anti-microbial reactive oxygen species. One of the key properties of iron is its ability to mediate oxidation-reduction reactions by altering between its Fe^{3+} and Fe^{2+} oxidative states. However, it is this highly reactive nature that makes an excess of "free" iron very toxic to organisms and necessitates strict mechanisms of regulation.

1.3.8.1 Mechanisms of cellular iron absorption

Highly reactive iron in its ionic form is not normally found at high levels in normal organisms. Rather, the majority of circulating iron (Fe^{3+}) exists in an inert form bound to the abundant plasma glycoprotein transferrin (Tf). Most cells gain access to iron by internalizing the entire diferric-Tf complex through the ubiquitously-expressed transferrin receptor 1 (TfR1), which resides in clathrin-coated pits on the surface of cells. Diferric Tf binds TfR1 at the plasma membrane and entire complex is internalized by clathrin-dependent receptor-mediated endocytosis into early endosomes. Endosomal acidification (pH 5.5-6.0) by vacuolar H^+-ATPase strengthens the interaction between Tf and TfR1 but weakens the binding of iron to Tf, causing the release of Fe^{3+} in the endosomal lumen. A recently identified ferrireductase, *Steap3*, reduces Fe^{3+} to Fe^{2+} in the endosomal lumen [185;186]. The acidic environment in the endosome also provides the proton gradient for Nramp2 to transport Fe^{2+} across the endosomal membrane into the cytosol [141;169]. Apo-Tf/TfR1 as well as Nramp2 are then recycled back to the cell surface,

where they can be used in further cycles of iron uptake [51] (Figure 4). Although most cells are thought to uptake iron via the Tf-TfR1 cycle, this process is of particular importance for developing erythrocytes which have an enormous need of iron for hemoglobin synthesis. A homolog of TfR1, transferrin receptor 2 (TfR2), is expressed exclusively in erythroid cells, hepatocytes, and duodenal crypt cells [187]. TfR2 also functions in the uptake of Tf-iron, although it binds Tf with less affinity compared to TfR1 and is not regulated by the IRP/IRE regulatory system. TfR2 clearly plays a critical role in iron homeostasis as mutations at the human *TfR2* gene result in systemic iron overload [188]. Polarized epithelial cells of the kidney are able to uptake Tf-iron by a megalin-dependent mechanism using the Tf-binding endocytic receptor cubilin [189].

There are several Tf-independent cellular mechanisms of iron uptake. Brush border intestinal enterocytes uptake dietary non-heme iron directly across their apical membranes through the action of Nramp2 (Figure 4). Non-heme iron is found in vegetables and grain products and exists in its insoluble Fe^{3+} form, which must first be converted to Fe^{2+} before it can be transported by Nramp2. This is thought to occur through the action of a cytochrome b-like ferrireductase called Dcytb (*Cybrd1*), which is expressed at the apical enterocyte membrane [190]. Other redundant ferrireductases may also exist since studies involving targeted disruption of the *Cybrd1* gene in mice suggest Dcytb is not essential for intestinal iron absorption in mice fed a normal iron diet [191]. Gastric acid secretion by the stomach promotes the solubility of iron complexes and also provides the proton gradient required for Nramp2-mediated Fe^{2+} uptake.

Iron is required to maintain proper neuronal cell function, however, an excess of iron causes neurodegeneration. Early immunohistochemical studies by Moos clearly showed a diverse expression of transferrin receptor throughout the central nervous system (CNS) [192]. More recently, several independent groups have shown that Nramp2 is also expressed in neuronal cells [40;177;193], suggesting that TfR and Nramp2 work in conjunction in these cells to uptake transferrin-bound iron. Iron transported through the blood-brain barrier may exist in the brain interstitial fluid in a low molecular weight form, such as iron-citrate. The presence of nontransferrin-bound iron in brain

extracellular fluids suggests that neurons can also take up iron in a transferrin-free form [194-197]. This may be mediated by Nramp2 expression at the neuronal plasma membrane.

Iron re-absorption in the kidney is not completely understood yet studies by Canonne-Hergaux *et al* [172] and Ferguson *et al* [173] suggest that apically expressed Nramp2 may function as part of an iron re-absorption system in the kidney, possibly to prevent the loss of precious iron in the urine. This idea is supported by the observation that Nramp2 expression in the kidney increases approximately two-fold in mice fed a low-iron diet [172]. Furthermore, Wareing and colleagues have shown using microinjection and microperfusion techniques that increased Nramp2 expression in rat kidney was accompanied by a decrease in urinary iron excretion rate and vice versa [198]. Interestingly, *mk/mk* mice and *b/b* rats suffering from severe mycrocytic anemia show almost a complete loss of Nramp2 expression in the kidney [172;176]. However, another study by Ferguson *et al* showed that although *b/b* rats exhibit higher serum iron levels than *+/b* rats, both animals display similar urinary iron excretion rates, suggesting that Nramp2 is not play a critical role in iron re-absorption by the kidney [176].

Dietary heme iron is an important nutritional source of iron in carnivores and omnivores that is more readily absorbed than non-heme iron. Iron is released from heme through the breakdown of hemoglobin and myoglobin present in red meat. In mammals, it has been known for some time that proximal duodenal enterocytes and hepatocytes are the major sites of heme transport [199;200]. The mechanism of heme transport across the plasma membrane remained elusive until Shayeghi and colleagues recently identified a duodenal membrane protein, heme carrier protein 1 (HCP1), that mediates cellular heme uptake [201]. HCP1 shows sequence similarity to several bacterial metal-tetracyclin transporters, is upregulated is response to hypoxia, and appears to be recruited to the plasma membrane from the cytoplasm upon iron deficiency [201]. Upon translocation across the plasma membrane, heme appears to localize in membrane bound vesicles within the cytoplasm [199;200;202;203;203] before it is degraded by the enzyme heme oxygenase (HO-1 and HO-2) to yield ferrous iron [204].

Small peptide siderophores are secreted by micro-organisms to trap and import iron across the cell membrane. Like this bacterial iron-uptake system, mammalian neural

gelatinase-associated lipocalin (NGAL/24p3) has been reported to complex with iron and be internalized and trafficked to late endosomes [205]. Recombinant NGAL/24p3 loaded with iron has been shown to deliver the metal into cultured cells and affect the expression of iron-regulated genes. This NGAL/24p3 delivery pathway appears to be important for differentiating epithelial cells during early embryonic development [205;206].

Finally, tissue macrophages absorb iron indirectly through the phagocytosis of old or damaged erythrocytes. Engulfed red cells are lysed, hemoglobin is degraded (with the help of heme oxygenase), and the released iron is either stored bound to ferritin or exported to reload circulating apo-Tf. The recycling of iron by macrophages is a highly efficient process that represents the major source of iron for cellular processes such as erythropoesis.

1.3.8.2 Mechanisms of cellular iron storage and usage

Once imported into the cell, excess iron that will not be immediately used is stored bound to the ubiquitous protein ferritin [207]. Ferritin is a highly conserved multimeric protein that is able to sequester inorganic Fe^{2+} by first converting it to Fe^{3+} before storing it as the chemically less reactive ferrihydrite [208]. Mammalian ferritin consists of 24 light (L) and heavy (H) chain subunits that can accommodate up to 4500 atoms of iron [209]. When cells experience a greater requirement for iron, ferritin is degraded and iron is released, however this process is not currently well understood.

Most of the iron within cells is directed to the mitochondria for either heme biosynthesis or maturation of iron-sulfur (Fe-S) clusters. Heme is synthesized by an enzyme called ferrochelatase, which catalyzes the insertion of ferrous ions into protoporphyrin IX (reviewed in [210]). Heme synthesis is of particular importance in oxygen-carrying erythroid cells, however the mechanism by which iron is delivered to mitochondria is not currently known. Recently, Zhang and colleagues proposed that a transient interaction between iron-rich endosomes and mitochondria is responsible for the transfer of iron acquired from transferrin to ferrochelatase [211]. Newly synthesized heme is rapidly exported outside the mitochondria into the cytosol and endoplasmic reticulum, and associates with apo-hemoproteins [212;213]. Fe-S clusters are ubiquitous and participate

in a number of processes including electron transfer, substrate binding/activation, and iron/sulfur storage [214]. The mitochondrial matrix protein frataxin is required for biogenesis of Fe-S proteins and is thought to play roles in mitochondrial iron export and storage [215-217]. Mutations at the *frataxin* gene cause the neurodegenerative disorder Friedreich's ataxia. Patients with Friedreich's ataxia possess a deficiency in Fe-S containing proteins and display mitochondrial iron overload [218].

1.3.8.3 Mechanisms of iron export

Because iron is such a precious element, the current dogma is that there is no excretion mechanism for iron, with loss from the body normally resulting from desquamation or the loss of biological fluids (especially blood). At the cellular level, in contrast to the numerous mechanisms identified for cellular iron import, much less is known about the mechanisms underlying cellular iron export. In fact, the only putative mammalian iron exporter identified to date is ferroportin (MTP, Ireg1) [219-221]. Ferroportin is expressed at the basolateral membrane of duodenal enterocytes where it mediates iron (Fe^{2+}) export into the bloodstream in conjunction with the ferroxidase hephaestin, which converts Fe^{2+} to Fe^{3+} before it can be bound by circulating apo-Tf [222]. Mutation of *hephaestin* in sex-linked anemia (*Sla*) mice leads to iron accumulation in the epithelia and results in *Sla* mice having a systemic iron deficiency [222]. In non-intestinal cells, iron export requires oxidation by the plasma protein ceruloplasmin [223]. Ferroportin is also highly expressed in intracellular vesicles of tissue macrophages, where it is thought to play a role in the export of iron recycled from engulfed red blood cells. When ferroportin expression is upregulated through iron treatment or erythropagocytosis, ferroportin expression is strongly enhanced at the plasma membrane of macrophages [224]. In contrast, treatment with the iron regulatory protein hepcidin (see below) causes rapid internalization and degradation of the macrophage iron exporter [224;225].

1.3.8.4 Regulation of cellular iron homeostasis

Proteins involved in iron uptake, usage, storage and export require tight regulation. The best characterized form of iron-dependent regulation is at the level of

mRNA stability. Iron responsive elements (IREs) are conserved hairpin structures approximately 30 nucleotides in length found in either the 5' or 3' untranslated regions (UTRs) of mRNAs encoding proteins involved in iron homeostasis such as Nramp2, TfR, ferroportin, and ferritin. Specialized iron regulatory proteins (IRP1, IRP2) interact with the IREs based on cellular labile iron pool levels. Iron levels regulate the binding of IRP1 and IRP2 to IREs by distinct mechanisms [226]. When cellular iron levels are high, iron (as Fe-S clusters) binds IRP1 and inhibits its binding to IREs by converting it to an aconitase, which interaconverts citrate and isocitrate. When cellular iron stores are low, IRP1 is able to freely bind IREs. IRP/IRE interactions are also controlled by other factors including the presence of reactive oxygen species, nitric oxide, and hypoxia. The mechanism by which iron regulates IRP2 is less well understood. Unlike IRP1, IRP2 does not bind Fe-S clusters but has been shown to accumulate in iron-starved cells and is targeted for degradation when iron levels are high [227]. IRP2 is also sensitive to degradation in the presence of nitric oxide (NO), whereas IRP1 is activated by NO [228;229]. Recent studies have suggested that IRP2 is the predominant regulator of iron homeostasis in mammalian cells. Indeed, mice deficient in IRP1 appear normal yet mice deficient in IRP2 show pronounced mis-regulation of iron metabolism and nerve damage [230;231].

Single IREs are found in the 5' UTRs of mRNAs encoding ferritin, erythroid 5-aminolevulinic acid synthase (required for heme biosynthesis), mitochondrial aconitase (a citrate cycle enzyme), and ferroportin [220;221;227;232]. The formation of IRP/IRE complexes on the 5' UTR of these transcripts inhibits their translation, leading to down-regulation of the protein [233]. The opposite result occurs when IREs are located in the 3' UTR of transcripts. Multiple IREs are present in the 3' UTR of mRNA encoding TfR1 and binding of IRP serves to stabilize the transcript, leading to increased translation and up-regulation of the protein [227]. The 3' UTR of mRNA encoding Nramp2 isoform I contains a single IRE that has been shown to bind IRP1 *in vitro* [234]. However, this IRE has been shown to only marginally regulate Nramp2 expression in cultured cells [234]. The recently identified 5' promoter/exon 1A region of *Nramp2* appears to work in conjunction with the 3' UTR IRE modulate Nramp2 expression in response to the cellular and systemic iron levels [154].

Genes involved in iron homeostasis are also regulated at the transcriptional level. For example, cytokine production has been reported to modulate expression of various iron-related genes. Interferon-γ (INF-γ), tumor necrosis factor-α, interleukin-1 (IL-1), and IL-6 have all been reported to stimulate ferritin expression but down-regulate TfR1 [207]. INF-γ and lipopolysaccharide (LPS) have been reported to induce Nramp2 expression but inhibit ferroportin expression in activated monocytes [235;236]. The response of ferroportin to LPS appears to require signaling through the LPS receptor, Toll-like receptor 4 (TLR-4) [236], and may contribute to the iron sequestration by phagocytic cells observed during inflammation.

1.3.9 Nramp2 and systemic iron homeostasis

Over 65 years ago, studies on iron balance in humans showed that virtually no iron is excreted and that stable iron levels are maintained by modulating absorption of iron from the gut. Insufficient or excessive accumulation of iron can be problematic, especially coupled with the fact that mammals lack a natural physiological excretion system for iron. Therefore, organisms have developed sophisticated mechanisms to sense and regulate body iron levels in response to the demanding needs of systemic processes such as erythropoesis. The maintenance of healthy iron homeostasis requires efficient communication between the cells that use the most iron (erythroid precursors) and the cells that obtain and store iron (duodenal enterocytes, tissue macrophages, hepatocytes).

1.3.9.1 Systemic iron regulators

The primary iron storage sites are tissue macrophages and hepatocytes. Iron is stored bound to ferritin in these cells and the level of these stores is monitored and maintained by a so-called "stores regulator" [237;238]. The stores regulator can, in part, alter intestinal iron absorption in response to body stores. Erythroid cells are by far the major consumers of iron and the amount the iron present in the bone marrow, erythroid precursors, and circulating red blood cells is normally greater than the amount of iron present in the stores. When systemic iron demand for erythropoeisis exceeds what is available in the storage pools, an "erythroid regulator" up-regulates intestinal iron uptake

to compensate and replenish the stores [238]. A "hypoxia regulator" is also believed to exist, altering iron homeostasis in response to insufficient blood and tissue oxygen levels. Meanwhile, an "inflammatory regulator" is thought to mediate the retention of iron within tissue macrophages as well as the reduction of intestinal iron absorption, as a host response to infection or inflammation. This action is believed to promote host resistance by restricting the amount of iron available to pathogens.

It is clear that a hierarchy exists among the regulators. This is especially evident in diseases where erythropoesis is iron-deficient yet the body iron stores are overfilled. Hypotransferrinemic mice (*Trf*^{hpx}), which possess a mutation disrupting a splice donor site in the *transferrin* gene, have a near total deficiency in circulating serum transferrin [239]. Erythroid precursors uptake the majority of their iron as diferric-Tf via TfR1 and therefore erythropoesis is severely impaired in *Trf*^{hpx} mice [150]. However, since a number of non-erythroid cells and tissues readily uptake non-transferrin bound iron, iron overload develops in various organs such as the liver and pancreas. In this case, signals from the erythroid regulator seem to override signals from the stores regulator, up-regulating the absorption of dietary iron in the duodenum. The body appears to prioritize (and rightfully so) iron needed for erythropoesis over the need to avoid iron overload. An analogous scenario occurs in two other mouse models of iron overload generated by targeted disruption of the *Hfe* and *β-2 microglobulin* genes [240;241].

The search for regulatory effectors that can modulate intestinal iron absorption, iron recycling by macrophages, and iron storage by hepatocytes has been extensive. This search led to the recent identification of hepcidin (HAMP, LEAP-1), a small cysteine-rich peptide hormone that is produced by hepatocytes and excreted through the kidneys [242-244]. Produced from the cleavage of a larger precursor protein, hepcidin shows sequence similarity to peptides (defensins) involved in innate immunity and possesses itself anti-microbial properties [242;243]. Hepcidin controls extracellular iron levels by regulating its intestinal absorption, placental transport, recycling by macrophages, and release from stores. Hepcidin-deficient (*USF2*$^{-/-}$) mice develop elevated body iron stores while transgenic mice constitutively-expressing hepcidin eventually die from severe iron deficiency anemia [245;246]. Hepcidin also appears to be an acute phase response peptide

induced directly by various inflammatory stimuli including bacterial lipopolysaccharide [247-250]. Several studies have linked hepcidin to the erythroid, stores, hypoxia, and inflammatory regulators (reviewed in [251]). Although the signaling pathways of these mechanisms are not completely understood, most studies are in agreement that when iron is scarce, decreased serum hepcidin expression is associated with enhanced iron release from intestinal cells and macrophages [248;252;253]. Conversely, in a state of iron overload, increased serum hepcidin expression is associated with decreased iron release from intestinal cells and macrophages [244;254;255]. Recently, hepcidin was found to inhibit cellular iron efflux by binding to the iron exporter ferroportin and inducing its internalization from the cell surface and degradation [224;256]. Mutagenesis studies have revealed that the N terminus of hepcidin is responsible for its interaction with ferroportin [257].

1.3.9.2 Importance of Nramp2 in systemic iron homeostasis

Because of its dual role in intestinal iron absorption as well as in acquisition of transferrin-iron, mutations in *Nramp2* severely affect systemic iron homeostasis. Both *mk* mice and *Belgrade* rats, which possess the identical mutation (G185R) in *Nramp2*, suffer from severe microcytic anemia [136;141]. The need for increased erythropoesis in these rodents prompts the erythroid regulator to increase intestinal iron absorption by up-regulating Nramp2 expression at the duodenal brush border [147]. However, because the G185R mutation attenuates Nramp2 function, the anemia persists [146;148].

Recent work by Gunshin and colleagues has furthered our understanding of the role of Nramp2 *in vivo*. They showed that global inactivation of *Nramp2* in mice results in a similar but more severe phenotype than that seen for animals homozygous for the G185R mutation [258]. Although *Nramp2*$^{-/-}$ mice were born alive with no apparent anatomical abnormalities, they were noticeably paler at birth and later displayed progressive post-natal growth retardation, with no mice surviving more than 7 days [258]. The relatively normal development of the *Nramp2*$^{-/-}$ mice *in utero* suggested that fetal Nramp2 is not essential for materno-fetal iron transfer. Transplanting hematopoetic stem cells from *Nramp2*$^{-/-}$ mice into irradiated WT mice resulted in abnormal erythrocyte

morphology and decreased hemoglobin levels, confirming the importance of Nramp2 in erythroid iron utilization [258]. Furthermore, studies involving selective inactivation of *Nramp2* in the intestine confirmed the importance of Nramp2 in the absorption of dietary non-heme iron [258].

1.3.9.3 Diseases associated with NRAMP2 *mutations in humans*

Currently, there are three reported cases of mutations in human *NRAMP2* associated with iron-related disorders. The first case was identified in 2004, when Priwitzerova and colleagues reported a 20-year-old female patient of Czech origin, the product of a consanguineous union, who suffered from liver hemosiderosis and severe congenital hypochromic microcytic anemia due to defective erythroid iron use [259]. A year later, Mims *et al* reported that this patient was in fact homozygous for a G to C substitution at the last nucleotide of exon 12 of *NRAMP2* (*NRAMP2*^{G1285C}) [4]. This mutation had a dual effect, impairing normal splicing of exon 12 by an estimated 90% and introducing an amino acid substitution (E399D) in the remaining (~10%) properly spliced transcript found in the patient. The impaired splicing is thought to result from alteration of the consensus sequence for binding of the U1snRNP at the exon 12/intron 12 boundary and translates into a truncated, non-functional Nramp2 protein [4;260;261]. Although E399D represents a conservative mutation, E399 resides in the highly conserved fourth intra-cytoplasmic loop of Nramp2 defined as the conserved transport motif. Work described in Chapter 3 of this thesis examined the effects of the E399D mutation as well as other mutations at that position in transfected LLC-PK$_1$ cells. These results showed that the E399D mutation does not in itself affect expression, function, or targeting of the Nramp2 protein, and that the reduced Nramp2 function in the patient is likely caused by a quantitative reduction in *NRAMP2* mRNA levels due to improper splicing [262]. This result was confirmed by studies from other groups [260;261].

In early 2006, Iolascon and colleagues reported a second human patient who is compound heterozygous for two novel mutations in *NRAMP2* [263]. The patient is a 5-year-old male of Italian origin suffering from severe hypochromic microcytic anemia with hepatic iron overload. The patient possessed two novel mutations in *NRAMP2*: a 3 base

pair deletion (del CTT) in intron 4 and a C to T transition (*NRAMP2*^{C1246T}) in exon 13 resulting in an Arg to Cys substitution at position 416 (R416C) of Nramp2. The CTT deletion was shown to disrupt normal splicing of *NRAMP2* pre-mRNA, causing a partial (30-35%) skipping of exon 5 [263]. This skipping results in a truncated, non-functional Nramp2 protein that is inherited in a fully recessive manner. R416 represents a highly conserved residue located in TM9. Work described in Chapter 4 of this thesis examined the effects of conservative and non-conservative mutations at R416. These results showed that non-conservative substitutions at R416 (C, A, E) cause multiple functional deficiencies including defective protein processing, loss of transport activity, impaired cell surface targeting and recycling through endosomes, concomitant with retention of the transporter in the endoplasmic reticulum [264]. These findings demonstrated that the R416C mutation represents a complete loss-of-function and that a quantitative reduction in Nramp2 expression is the cause of the microcytic anemia and iron overload in the patient.

Recently, Beaumont and colleagues reported a third human patient compound heterozygote for two novel *NRAMP2* mutations, associated with microcytic anemia and progressive liver iron overload [265]. In the first mutation, a GTG deletion in exon 5 causes the in-frame deletion of V114 in TM2. The second mutation, a G >T transition in exon 8, causes a G212V substitution in TM5. The effects of these recently identified mutations on Nramp2 function are not currently known and need to be studied. Although V114 is not a highly conserved among Nramp2 orthologs, its in-frame deletion may still affect Nramp2 function. On the other hand, G212 in TM5 is significantly conserved and it is likely that the non-conservative G212V substitution affects Nramp2 function.

Together, these three reported cases define a new syndrome of congenital microcytic hypochromic anemia with liver iron overload. In the first two reports, a quantitative reduction in Nramp2 expression was the cause of disease, indicating the presence of a minimum threshold of Nramp2 expression required for normal physiological function. This minimum threshold appears to be between the low level of activity observed in both *NRAMP2* mutant patients and the 50% activity retained in their phenotypically normal heterozygote relatives [4;263]. Results from studies with *Nramp2*$^{-/-}$ mice suggest that complete loss of Nramp2 activity may not be compatible with life [258].

1.3.9.4 Other iron-overload disorders in humans

Hereditary hemochromatosis (HH) is an autosomal recessive inherited iron overload disorder characterized by increased intestinal iron absorption and iron accumulation in vital organs, eventually leading to organ failure (reviewed in [266]). When identified before severe organ damage has occurred, hemochromatosis can be treated by phlebotomy (bleeding) to remove iron-rich red blood cells. Mutations in four genes have been linked to HH: *HFE*, *TFR2*, hemojuvelin, and hepcidin.

The first gene shown to be associated with HH was *HFE*, an atypical major histocompatibility class I protein that heterodimerizes with β-2 microglobulin but does not bind a small peptide [267;268]. Most patients (80%) with *HFE*-linked hemochromatosis are homozygous for a missense mutation (C282Y) that partially disrupts HFE function [267]. The C282Y mutation is particularly common in individuals of Northern European descent. Other mutations at *HFE* are rare and their contributions to clinical disease have not been well established. Only a fraction of patients with a hemochromatosis genotype develop clinical iron overload symptoms and environmental factors play a significant role in disease penetrance. Despite vast efforts, the precise molecular function of the HFE protein has remained elusive and experiments expressing HFE in transfected cells has yielded conflicting results [268-271]. However, it is clear that HFE is linked to the transferrin cycle and can form a high-affinity complex with TfR1, competing with transferrin to bind the receptor [268;272;273]. Recent studies in *Hfe*$^{-/-}$ mice have linked HFE to hepcidin levels and suggested the two proteins are part of the same signaling pathway [274-276].

Although less common than *HFE* mutations, homozygous mutations in TfR2 have also been identified in patients with hemochromatosis [188;277-282]. The clinical symptoms of *TFR2* hemochromatosis are similar but more severe than the *HFE*-related disease [283]. A defining characteristic of *TFR2* hemochromatosis is the persistence of high transferrin saturation, even following phlebotomy.

Some patients with juvenile hemochromatosis are homozygous for mutations at *HAMP*, the gene encoding hepcidin [284]. Mutations identified thus far cause either a complete inactivation of the protein [285] or substitute one of the invariant cysteines of the

peptide [286-288]. However, most juvenile hemochromatosis patients possess mutations in the gene hemojuvelin (*HFE2* or *HJV*) [289]. Hemojuvelin encodes a glycosylphosphatidylinositol (GPI)–linked protein, characterized by an RGD motif and a von Willebrand type D domain that is highly expressed in the liver, skeletal muscle, and heart. Over 30 different mutations have been identified in the *HJV* gene in patients with juvenile hemochromatosis (reviewed in [290]). *HJV* hemochromatosis shares numerous features with *HFE* hemochromatosis, but all the clinical manifestations develop earlier due to greater intestinal iron absorption and faster rate of iron accumulation. The fact that patients with critical mutations in *HJV* display low or unmeasurable hepcidin levels [289] suggest that the protein is a component of the hepcidin regulatory pathway.

A distinct type of iron overload inherited in an autosomal dominant fashion is found in patients with critical mutations in *ferroportin* [291;292]. These patients present variable clinical phenotypes depending on the specific mutation they harbor. *Ferroportin* mutations essentially fall into two main classes: (1) mutations that disrupt cell surface expression and inhibit iron export [293]; and (2) mutations that localize to the cell surface but are unable to respond the regulatory peptide hepcidin [294]. Patients with the first type of mutation show typical ferroportin disease with low transferrin saturation and iron accumulation in macrophages. Patients with the second type of mutation show high transferrin saturation and early hepatocyte iron loading similar to classic hereditary hemochromatosis. The dominant inheritance of ferroportin-linked hemochromatosis may be explained by *in vitro* experiments that suggest ferroportin functions as a multimer and that mutants act as dominant negatives, affecting the behavior of the wild type protein [295]. However, this still remains controversial since other studies have shown that WT and mutant ferroporins do not form oligomers in transfected HEK293 cells [293;296].

Preface to Chapter 2

The identification of Nramp2 as a transporter of divalent metals in 1997 provided new insight into the function of Nramp proteins *in vivo* [40;136]. Electrophysiological measurements indirectly identified Fe^{2+}, Mn^{2+}, Co^{2+}, Cd^{2+}, Cu^{2+}, Ni^{2+}, Pb^{2+}, and Zn^{2+} as substrates for Nramp2 and showed that transport occurred by a pH-dependent mechanism [40]. The demonstration of divalent metal transport by numerous distant Nramp orthologs highlighted functional conservation in the Nramp super-family [1;2;297;298]. At this time, structure-function studies became essential to understanding the molecular basis for both metal transport and pH-dependence by Nramp proteins.

Chapter 2 of this thesis describes one of the first systematic attempts to explore structure-function relationships in Nramp proteins by site-specific mutagenesis. Through multiple sequence alignments of various prokaryotic and eukaryotic Nramp sequences, we identified a number of highly conserved yet thermodynamically disfavored charged amino acids residing within the hydrophobic TM domains of Nramp2. Our mutagenesis studies revealed several charged residues that are essential for Nramp2-mediated metal transport, as well as two invariant histidines (H267 and H272) that are critical for pH-dependence. Later, similar mutagenesis studies performed in a bacterial Nramp ortholog, MntH, confirmed the importance of TM charged residues in metal transport by Nramp proteins [299]. Furthermore, our identification of H267 and H272 as critical for pH-dependence was later supported by electrophysiological experiments in *Xenopus* oocytes [300].

Chapter 2:

Iron transport by Nramp2/DMT1: pH regulation of transport by two histidines in transmembrane domain 6

ABSTRACT

Mutations at *Nramp1* impair phagocyte function and cause susceptibility to infections while mutations at *Nramp2* (DMT1) affect iron homeostasis and cause severe microcytic anemia. Structure-function relationships in the Nramp super family were studied by mutagenesis, followed by functional characterization in yeast and in mammalian cells. These studies identify three negatively charged and highly conserved residues in transmembrane domains (TM) 1, 4, and 7 as essential for cation transport by Nramp2/DMT1. The introduction of a charged residue (G185R) in TM4 found in the naturally-occurring microcytic anemia *mk* (mouse) and *Belgrade* (rat) mutants is shown to cause a partial or complete loss of function in mammalian and yeast cells, respectively. A pair of mutation-sensitive and highly conserved histidines (H267, H272) was identified in TM6. Surprisingly, inactive H267 and H272 mutants could be rescued by lowering the pH of the transport assay. This indicates that H267/H272 are not directly involved in metal binding but rather they play an important role in pH regulation of metal transport by Nramp proteins.

INTRODUCTION

Nramp2 (DMT1, DCT1) is essential for nutritional iron (Fe^{2+}) uptake by the duodenum brush border [40;136;141] and for iron transport across the endosomal membrane in peripheral tissues [42;141;301]. Nramp2 is an integral membrane protein composed of 12 predicted transmembrane (TM) domains [1]. The *Nramp2* gene produces 2 mRNAs by alternative splicing of the terminal 3' exon that show different 3' untranslated regions containing (isoform I, +IRE) or not (isoform II, -IRE) an iron response element (IRE), as well as distinct C-terminal protein sequences [153;302]. In normal tissues, *Nramp2* protein (isoform I) is expressed at the brush border of the proximal portion of the duodenum, where it is regulated by dietary iron deprivation [161]. Nramp2 (isoform II) is also present in the Tf receptor positive recycling endosome compartment of erythroid precursors that can be recruited *in vivo* by treatment with phenylhydrazine or erythropoietin [169]. *Nramp2* mRNA expression was also detected in the kidney (Isoforms I and II) [175] and Nramp2 protein expression (isoform I) was detected at the brush border of the kidney proximal tubule [172]. Direct transport studies in *Xenopus laevis* oocytes suggest that Nramp2 is a pH-dependent divalent metal transporter with broad substrate specificity including Fe^{2+}, Mn^{2+}, Co^{2+}, Cd^{2+}, Cu^{2+}, Ni^{2+}, Pb^{2+}, and possibly Zn^{2+} and that may function by a H^+ co-transport mechanism [40]. Parallel studies with metal-sensitive dyes have shown similar transport properties for Nramp2 expressed at the plasma membrane [26;168]. An independently arising natural mutation in TM4 of *Nramp2* (G185R) is responsible for microcytic anemia of the *mk* mouse [136] and the *Belgrade* rat [141], both associated with a severe defect in intestinal iron absorption and impaired use by erythroid cells [138]. Transport experiments *in vitro* in transfected HEK293 cells, as well as subcellular localization studies *in vivo* in target tissues from *mk/mk* mice have shown that the $Nramp2^{G185R}$ mutation causes a severe loss of function characterized by reduced activity and possibly impaired maturation/targeting [146;147]. Together, these studies suggest a dual role for Nramp2 as the Tf-independent iron acquisition system of the duodenum, and as transporting reduced Tf-iron across the endosomal membrane [251 303].

The *Nramp2* homolog, *Nramp1* [1;7] is expressed in the lysosomal compartment of macrophages and neutrophils [18] and is recruited to the membrane of pathogen containing

phagosomes formed in these cells [35;304], where it may function as a Mn^{2+} efflux pump [52]. A naturally-occurring mutation in predicted TM4 of Nramp1 (G169D) impairs maturation and membrane targeting of the protein, and causes susceptibility to infection with unrelated intracellular pathogens [7;15]. *Nramp1* and *Nramp2* define a large super-family of membrane transporters highly conserved from bacteria to humans [1;41;305]. Demonstration of divalent cation transport by distant Nramp homologs from bacteria (*MntH*, *Mramp*), yeast (*Smf1*, *Smf2*, *Smf3*), fly (*Mlv*), and plant (*AtNramp*) has highlighted functional conservation in this family [1;2;297;298]. In addition, expression of mouse Nramp2 protein in a double *smf1/smf2* mutant can restore the ability of this mutant to grow at alkaline pH and on medium containing metal chelators [34;306]. Likewise, expression of human *NRAMP1* in the fly mutant *malvolio* corrects the taste discrimination defect of this mutant [2], in a manner similar to that produced by increasing dietary Fe^{2+} or Mn^{2+} [307].

In the present study, we have used multiple sequence alignments to identify highly conserved residues in the Nramp super-family. We have studied the functional role of conserved charged TM domain residues in substrate selectivity and pH regulation of Nramp2.

MATERIALS AND METHODS

Materials

Calcein acetoxymethylester (calcein-AM; 500 μM stock solution prepared in DMSO) was obtained from Molecular Probes (Eugene, OR). Stock Fe^{2+} (2 mM) aqueous solutions of ferrous ammonium sulfate (FAS; Sigma) were always prepared fresh in degassed, de-ionized water. $CoCl_2$ (Sigma) was prepared as a stock solution (2 mM) in water. The membrane-permeable iron chelator salicylaldehyde isocotinoyl hydrazone (SIH, 25 mM stock solution) was prepared in DMSO, and the membrane-impermeable iron chelator HES-DFO (6 desferroxamine/M_r 50,000 starch molecule; 38 mM stock) was prepared in water and stored at -20°C. SIH and HES-DFO were generous gifts from Dr. P. Ponka (McGill University, Lady Davis Institute, Montreal, Canada).

Plasmids and Constructs

A full length mouse *Nramp2* (*DMT1*) cDNA Isoform II lacking the IRE (GenBank™ Accession Number L33415) was modified by the in-frame addition of 2 antigenic cMyc epitope tags at the carboxy terminus of the protein (N2-2Myc) [34]. Mutations at specific amino acid positions were created by site-directed mutagenesis using a recombinant PCR protocol [308], and using oligonucleotide primers listed in Table 1. The mutants were cloned into the mammalian expression vector pCB6. For complementation studies in yeast, mutants were introduced in the yeast expression vector pVT.

Yeast Transformation and smf1/smf2 Complementation Assays

The *S. cerevisiae smf1/smf2* double mutant, is a mutant in which the *SMF1* and *SMF2* genes have been insertionally inactivated (*MAT*a *ura*3-52 *leu*2-3 –112 *gal*2 *SMF1::LEU2*, *SMF2::LEU2*) [34]. This mutant cannot grow on alkaline medium or on medium containing metal chelators [34;306]. Yeast cells were transformed with pVT/*Nramp2* constructs [309] and *ura*+ transformants were grown as mass populations, and crude membrane fractions [310] were prepared for *Nramp2* protein expression by immunoblotting using the mouse anti-cMyc monoclonal antibody 9E10 (Babco, Berkeley, CA) [161]. To test

Table 1. Primers used for mutagenesis.

Primer	Nucleotide sequence (5' to 3')	Position in N*ramp2*
pCB6 F	aatgggcggtaggcgtgta	848-866 of pCB6
pCB6 R	aggccaggagaggcactgg	1006-1034 of pCB6
N2 D86A F	cctacctagCccccaggaaac	248-267
N2 R119A F	ctgctgctccagGCccttgcag	346-367
N2 R146A F	caaggtcccaGCgatcatcctgtg	426-449
N2 E154A F	ctgatggtggCgttggcaatca	451-472
N2 D161A F	cattggttctgCcatgcaggaagtc	471-495
N2 G184D F	ccctgtgggAcggagtcctca	542-563
N2 G185R F	gggtccccctgtggggcaGagtcctcatcaccatc	536-570
N2 D192A F	caccatcgcagCcacttttgtg	564-585
N2 E225A F	gtttggatatgCgtacattac	663-684
N2 H267A F	atcatgccgGCCaacatgtacct	790-825
N2 H267C F	atcatgccgTGcaacatgtacct	790-825
N2 H267R F	atcatgccgcGGaacatgtacct	790-825
N2 H272A F	aacatgtacctgGCttctgcctta	802-825
N2 H272C F	aacatgtacctgTGttctgcctta	802-825
N2 H272R F	atgtacctgcGttctgcctta	805-825
N2 H267/272A F	atcatgccgGCCaacatgtacctgGCttctgcgtta	790-825
N2 H267/272C F	atcatgccgTGcaacatgtacctgTGttctgcgtta	790-825
N2 H267/272R F	ctgtgatcatgccgcGGaacatgtacctgcGttctgc cttagtc	785-828
N2 E299A F	acttcttcatcgCgtcctgcatcg	883-907
N2 R416A F	gtgatcctgaccGCgtctatcgc	1234-1256

F indicates forward; R, reverse. Codons of mutated amino acids are underlined. Uppercase letters in nucleotide sequences indicate bases that differ from the *Nramp2* sequence.

for possible complementation of the growth defects of the *smf1/smf2* mutant by *Nramp2* variants, duplicate aliquots (1 mL) of *ura+* transformants were resuspended in either YPD medium or in alkaline YPD medium (pH 7.9, OD_{595} = 0.02) in 96-well plates (100 μL/well). Growth was measured after 24 h incubation at 30°C using an ELISA microplate reader (Bio-Rad model 450). Sensitivity to alkaline pH was measured as relative growth of each transformant (expressed as a %) in alkaline YPD 7.9 compared to growth of the same transformant in normal YPD medium (pH 5.5-6.0). For complementation studies on alkaline agar, cells grown to saturation in normal YPD were diluted to OD_{595} = 0.2, 0.02, 0.002, 0.0002, and 0.00002 in YPD 7.9, and 20 μL of each dilution was spotted on alkaline YPD agar plates and grown for 36 to 48 hours at 30°C before photography.

Cell Culture and Transfection

LR-73 Chinese Hamster Ovary (CHO) cells were routinely grown in α-minimum essential medium (MEM) supplemented with 10% fetal bovine serum, 50 units/mL penicillin, and 50 μg/mL streptomycin (Invitrogen). All pCB6 (*neo*) plasmid constructs were transfected into cells as calcium phosphate co-precipitates, according to a procedure we have previously described [311]. Clones of stable transfectants were selected in medium containing geneticin (G418; 770 μg/mL; Invitrogen) and were picked after 8-13 days of selection.

Crude Membrane Preparation from CHO Transfectants

Cell pellets were resuspended in 250 μL of TNE Buffer (100 mM NaCl; 10 mM Tris-Cl, pH 7.0; 10 mM EDTA) containing protease inhibitors (1mM PMSF, 1 μM pepstatin, 0.3 μM aprotinin, 1 μM leupeptin). Cells were homogenized by 20 passages through a 25 gauge × 5/8 in needle, followed by centrifugation (4°C, 2000 × *g*, 10 minutes) to eliminate nuclei and unbroken cells. Membranes were then pelleted from the supernatant by ultracentrifugation (75 000 rpm, TLA-100 rotor (Beckman), 4°C), and were resuspended in TNE containing 30% glycerol and protease inhibitors. Recombinant Nramp2 protein variants were detected using the mouse monoclonal anti-c-Myc antibody 9E10 (1:1000, Babco) as previously described [26].

Calcein Loading of the Cells and Divalent Metal Transport Assay

CHO *Nramp2* transfectants were loaded with the metal sensitive fluorescent dye calcein-AM, as we have previously described [26]. Briefly, CHO transfectants (1×10^6 cells) were incubated with 0.250 μM calcein-AM for 10 minutes at 37°C in 1 mL of loading medium (α-minimum essential medium, 1 mg/mL BSA, 20 mM HEPES, pH 7.4). The cells were washed twice in and resuspended in 500 μL of transport buffer (150 mM NaCl, 20 mM MES, pH 5.0-6.5). The cell suspension was transferred to a stirred thermostated (37°C) semi-micro cuvette, and fluorescence was recorded using an LS-50B fluorescence spectrometer (PerkinElmer, Inc.; excitation, 488 nm; emission, 517 nm; excitation and emission bandpass, 5 nm; response time, 6 s; data interval, 0.5 s). Divalent metals (20 μM final concentration of Fe^{2+} or Co^{2+}) were added to the cell suspension after allowing fluorescence to stabilize for 60 s. For assays using iron, a combination of membrane-permeable (SIH) and membrane-impermeable (HES-DFO) iron chelators were used at various time points (Fig. 5A) to distinguish intracellular from cell-associated quenchable fluorescence: After fluorescence was allowed to stabilize for 60 s, 20 μM Fe^{2+} was added to the cell suspension (Fig. 5A, *arrow 1*). After 240 s, the membrane-impermeable iron chelator HES-DFO was added (Fig. 5A, *arrow 2*) to release metal-induced quenching of extracellular cell-associated complexed calcein. At 300 s, a membrane-permeable iron chelator SIH was added (Fig. 5A, *arrow 3*), to release metal-induced quenching of intracellular calcein fluorescence. Initial rates were calculated from quenching curves, and the size of the intracellular labile iron pool was extracted from data obtained with the 2 metal chelators.

Cell Surface Protein Biotinylation

CHO Nramp2 transfectants were washed thoroughly with cold PBS (supplemented with 1 mM $MgCl_2$, 0.1 mM $CaCl_2$) and then with cold borate buffer (10 mM boric acid, 154 mM NaCl, 7.2 mM KCl, 1.8 mM $CaCl_2$, pH 9.0). Cells were labeled for 15 min on ice with 0.5 mg/mL Sulfo-NHS-SS-Biotin (Pierce) in cold borate buffer. After washing three times with cold quenching buffer (PBS, 200 mM glycine), cells were

scraped, collected and resuspended in 1 mL lysis buffer (1% Triton X-100, 150 mM NaCl, 2 mM EDTA, 10 mM Tris-Cl pH 7.4, 30% glycerol) plus protease inhibitors. Lysates were incubated on ice for 20 min and pelleted (10 min, 10 000×*g*, 4°C). Supernatants were collected and protein levels were quantified by Bradford assay. 500 μg of total protein lysate were incubated overnight at 4°C with 50 μL of immobilized streptavidin beads (Pierce) in a final volume of 500 μL (with lysis buffer and protease inhibitors). Streptavidin beads were washed three times with lysis buffer then once with PBS. Labeled cell surface proteins were eluted with 50 μL 1× SDS-PAGE loading buffer and separated by SDS-PAGE.

RESULTS

Mutagenesis Strategy

Alignment of 28 eukaryotic and prokaryotic Nramp sequences identify a common and conserved hydrophobic core of 10 TM domains (~30% identity between bacteria and man) [1] that contain four absolutely invariant (D86, E154, E299, R416) and 5 highly conserved (R119, R146, D161, D192, E225) charged residues (6 negative, 3 positive) in TM domains (Fig. 1; dark blue residues). Another unique feature of the Nramp family is the presence of two invariant Histidine residues (H267, H272) in the predicted TM domain 6 (Fig. 1; red residues). In mice, naturally occurring mutations at adjacent residues in TM4 of *Nramp1* and *Nramp2* cause susceptibility to infection and microcytic anemia, respectively, and the loss-of-function phenotype of the microcytic anemia *Nramp2* variant (G185R) was studied. Mutant cDNAs were expressed in yeast *S. cerevisiae*, and tested for their ability to complement 2 phenotypes of a *smf1/smf2* mutant: (a) impaired growth on metal chelators [306] and (b) impaired growth at alkaline pH.[34] Mutants showing partial or complete loss-of-function were subsequently expressed in CHO cells, and tested for Fe^{2+} and Co^{2+} transport at the plasma membrane.[26]

Conserved Charged Residues in Membrane Domains

Immunoblotting indicated that all mutants could be stably expressed as 60-65kDa immunoreactive proteins in yeast membrane fractions (Fig. 2A, *left panel*). These results suggest that none of the mutations had a major effect on protein expression or stability in yeast. The ability of each mutant to complement the null *smf1/smf2* yeast mutant was tested in parallel by plating serial dilutions of each transformant on YPD agar pH 7.9 (Fig. 2B, *left panel*), and using a growth inhibition assay in liquid YPD (pH 7.9). Routinely, yeast WT *Nramp2* transformants showed a 9-fold stimulation for growth on alkaline medium over negative controls (pVT, *smf-/-*; Fig. 3, *left panel*). Two *Nramp2* mutants previously shown to either abrogate (G394V) or to have no effect (Q395E) on Nramp2 function in yeast [34] were used as additional controls (Fig. 3, *left panel*).

In both assays, mutants R119A, R146A, D161A, E225A showed full complementation of the *smf1/smf2* growth defect, while mutants D86A, E154A, D192A,

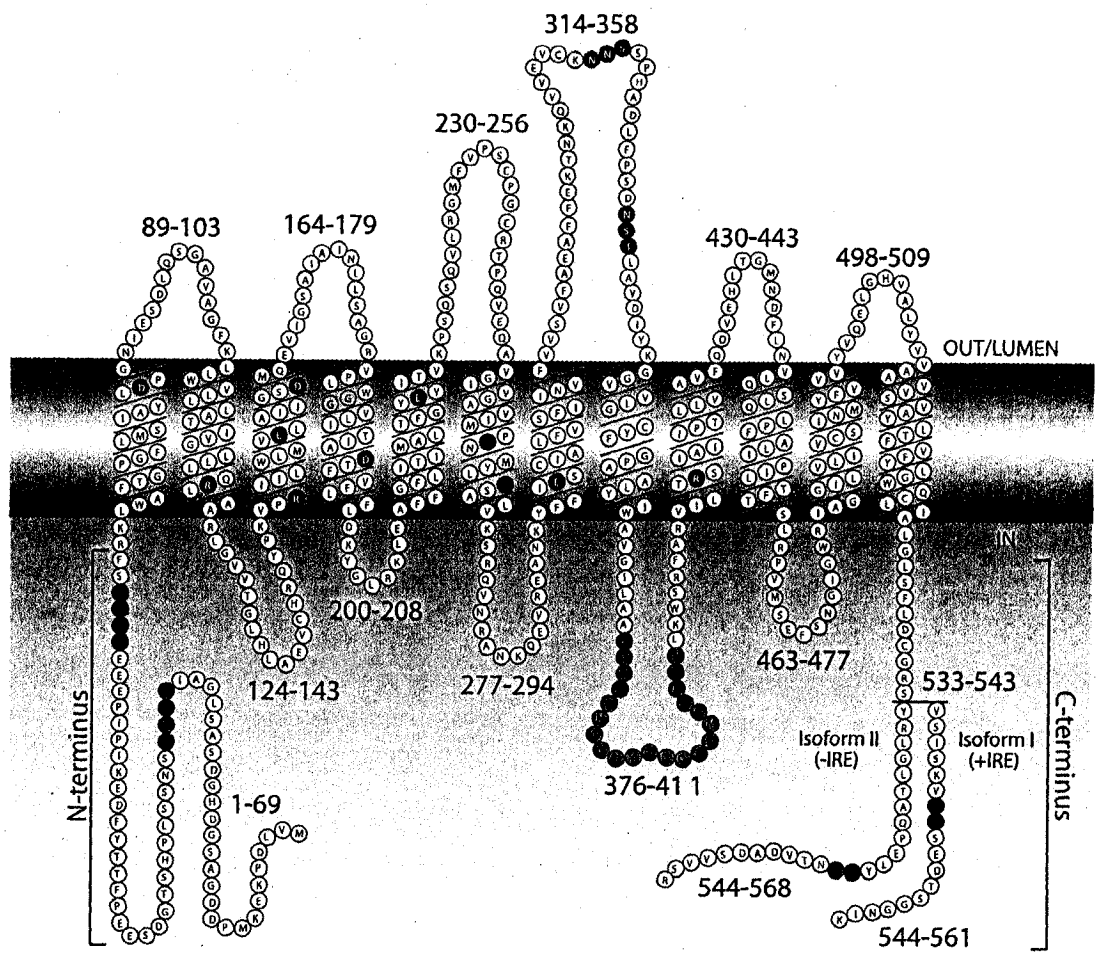

Figure 1. Schematic representation of mouse Nramp2 (DMT1) isoform II (-IRE) and isoform I (+IRE). The twelve transmembrane domains are predicted from hydropathy profiling, calculations of hydrophobic moment and other computer-assisted analyses6 and from direct epitope mapping studies.13 Individual predicted intracellular and extracellular segments are identified and their position within the primary sequence is shown. Amino acid residues defining sequence landmarks and signature motifs are depicted in different colors, including negatively and positively charged residues within predicted TM domains (dark blue), conserved histidine residues in TM6 (red), glycine residues in TM4 altered in anemic mk/Belgrade mutants (G185R), and mutated (in Nramp1) in mice susceptible to infections (G185D)(yellow). Also identified are Asn-linked glycosylation signals in the TM7-TM8 extracytoplasmic loop (black), predicted membrane targeting/sorting motifs (tyrosine-based, and di-leucine)(green), and consensus transport signature common to Nramp orthologs and present in the cytoplasmic face of membrane anchors of bacterial periplasmic permeases (orange). The 2 different C-termini of the protein generated by alternative mRNA splicing containing or not an iron-response element (isoform I, +IRE; isoform II, -IRE) in the 3' untranslated region are identified, with corresponding numbering. Finally, the polarity of the protein and membrane domains with respect to the membrane (light blue) is indicated (in, out, lumen).

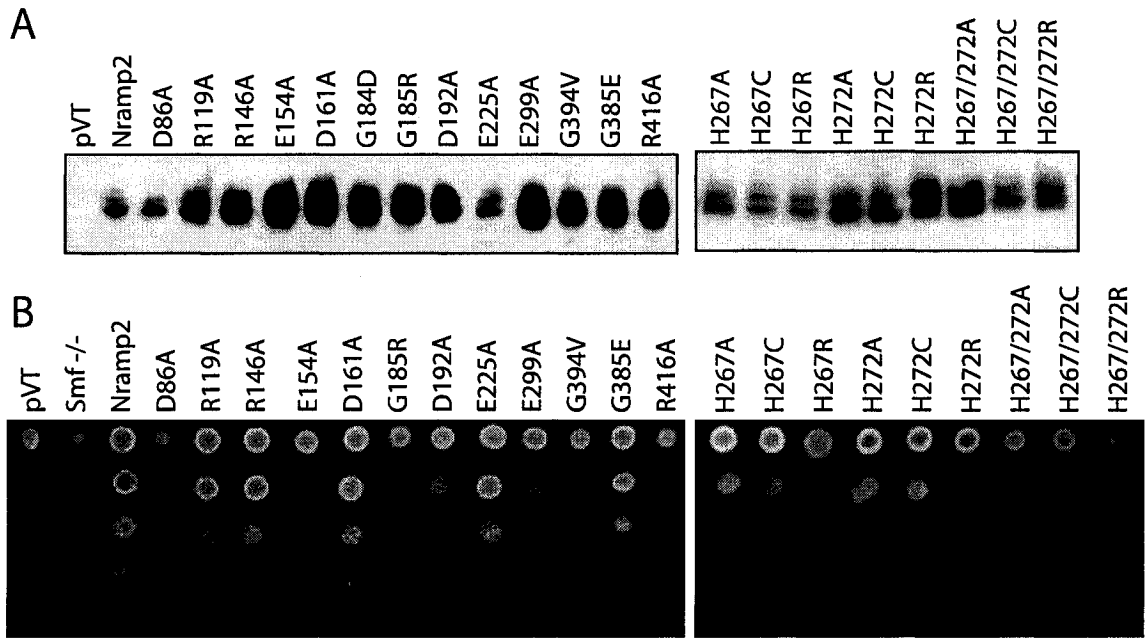

Figure 2. Nramp2 protein expression in smf1/smf2 mutant yeast and functional complementation of growth at alkaline pH. (A). Crude membrane fractions from smf1/smf2 yeast cells (pVT) expressing either wild type (Nramp2) or individual mutant variants of Nramp2 (indicated on top) were separated by SDS-polyacrylamide gel electrophoresis. Immunoblotting was performed using an affinity purified rabbit anti-mouse polyclonal anti-Nramp2 antibody. Apparent electrophoretic mobility of the immunoreactive species is consistent with a molecular mass of 60-65 kDa. (B). Functional complementation of the growth defect of the smf1/smf2 mutant was tested on solid YPD agar adjusted at alkaline pH (pH 7.9). Serial ten-fold dilutions of cultures corresponding to individual Nramp2 mutants (identified) were spotted (from top to bottom) on YPD-agar plates (pH 7.9), followed by incubation for 48 h at 30?C and photography.

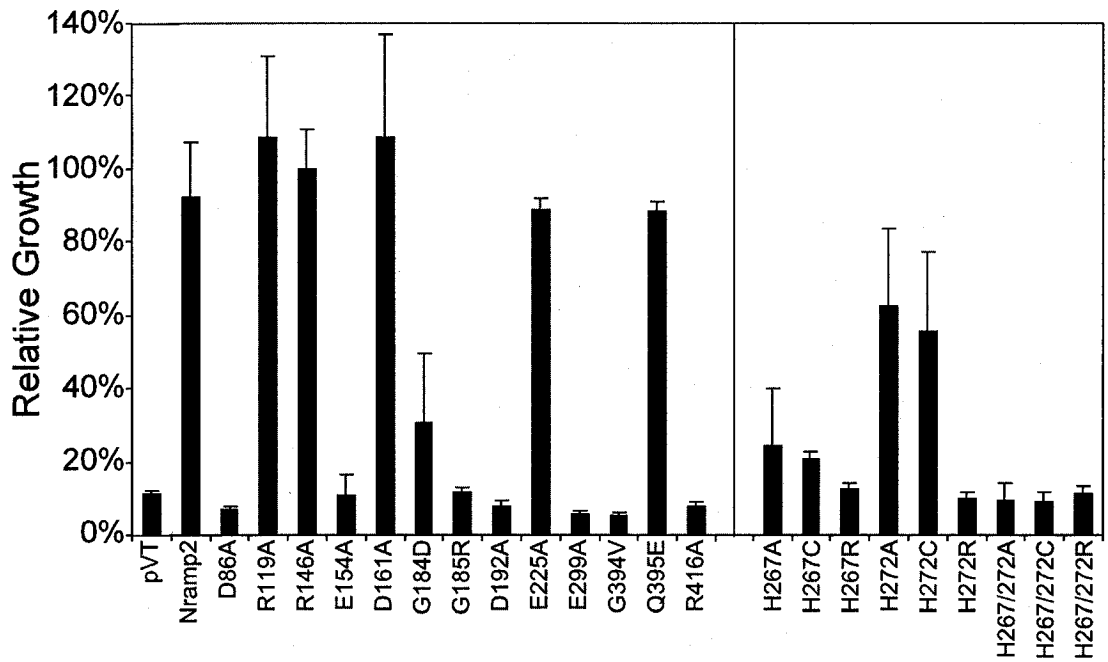

Figure 3. Quantitation of complementation of the Smf1/Smf2 yeast mutant by Nramp2 variants. Individual Nramp2 mutants (identified), together with positive (Nramp2) and negative (pVT) controls were grown to saturation and diluted to OD595 = 0.02 in either YPD or YPD pH 7.9. Cells were seeded in 96-well plates and growth was measured after 24 h incubation at 30 C by measuring OD595. Results represent relative growth (expressed as a percentage) of individual mutant grown at pH 7.9 vs. normal YPD. Error bars represent standard deviations of the means.

E299A, R416A failed to do so. In addition, testing these 11 mutants for their ability to complement susceptibility of *smf1/smf2* mutant to metal chelator (growth in EGTA-containing liquid medium) showed relative activities similar to that seen for growth at alkaline pH (data not shown). These results identify 5 of the 9 charged residues in TM domains as essential for Nramp2 function and *smf1/smf2* complementation in yeast.

The D86A, E154A, D161A, D192A, E299A, R416A mutants were analyzed for metal transport after transfection in CHO cells (Fig. 4A, *left panel*). Transfectants were screened by immunoblotting for expression of the corresponding *Nramp2* variants at the cell membrane. Membranes from cells transfected with the pCB6 empty vector were used as negative controls, while two previously characterized transfectants [26] expressing either low (N2GG) or high (N2.3) levels of Nramp2 protein were used as positive controls. CHO cell clones stably expressing mutants E154A and R416A, could not be obtained in 4 independent transfections (141 clones screened) for E154A and 3 independent transfections (75 clones screened) for R416A, suggesting possible effect of these mutations on protein folding/processing and/or toxicity for the cells. Stable CHO transfectants expressing D86A, D192A and E299A could be readily isolated. In these clones the level of expression varied but was in the range of levels seen in positive controls expressing WT (N2.3, N2GG) or D161A proteins (Fig. 4A, *left panel*). The variability in expression can be attributed to a combination of the site of integration of the vector and the effect of the introduced mutation. In addition, biotin labeling experiments in intact cells identified cell surface reactivity of all expressed mutants (D86A, D161A, D192A, E299A), with levels approximately proportionate to total expression levels detected in membrane fractions by immunoblotting (Fig. 4B, *left panel*). These results indicate that mutations at D86, D161, D192, and E299 do not have a major effect on Nramp2 protein maturation or membrane targeting.

Transport properties of the mutants were investigated in intact cells using a calcein quenching assay [26]. Metal transport by Nramp2 using the calcein quenching assay and transport of isotopic ^{55}Fe has been shown to be comparable in the identical control Nramp2 CHO transfectants [26] as well as some Nramp2 mutant variants (data not shown).

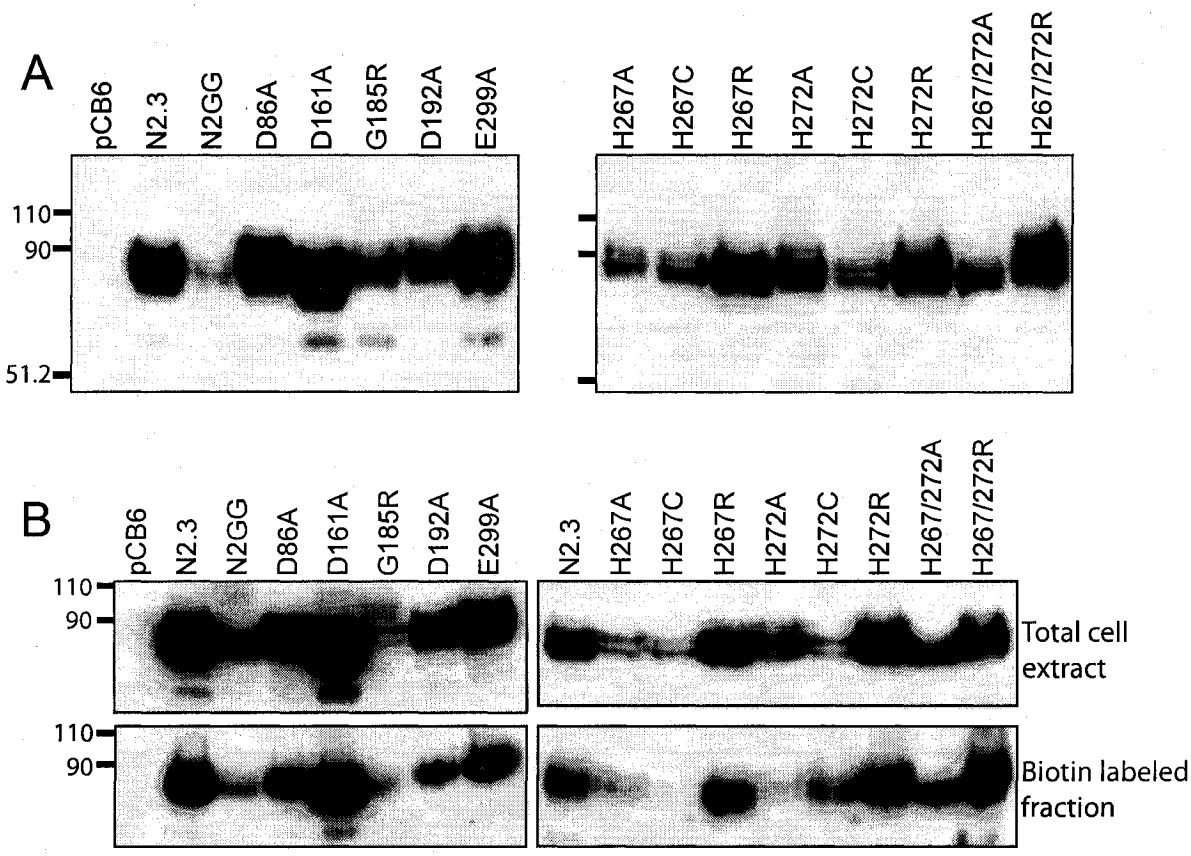

Figure 4. Expression of Nramp2 variants in stably transfected CHO cells. Left panels, mutants at conserved charged residues in TM domains; Right panels, multiple mutants at the conserved histidines in TM6. Crude membrane fractions (A) or total cell lysates (B) were prepared from various transfected cell clones (identified) and separated by SDS-polyacrylamide gel electrophoresis. Immunoblotting was performed using a mouse monoclonal anti-cMyc antibody directed against a corresponding epitope tag inserted in-frame in the Nramp2 constructs. Controls include cells transfected with the plasmid alone (pCB6), and cells expressing low (N2GG) or high amounts (N2.3) of wild type Nramp2.13 Molecular mass markers are identified in kDa to the left of the immunoblots. (B) Prior to electrophoresis, intact cells were labeled with biotin and disrupted with lysis buffer (upper panels). Labeled cell surface proteins were then isolated with strepavidin beads (lower panels).

For the calcein quenching assay, CHO transfectants were loaded with the metal-sensitive fluorescent dye calcein, and the effect of externally added divalent cations Fe^{2+} or Co^{2+} on the rate of quenching of fluorescence was monitored (at optimal pH 6.0), and the slope of the initial quenching curve was calculated (initial rate; [26]). Results shown in Fig. 5A show a typical set of fluorescence quenching traces for positive and negative controls. Transport activity of mutants are shown in Fig. 5B and are expressed as a relative transport activity (%). Mutants were classified as having either low (less than 33% of WT), intermediate (between 34% and 67%) or WT activity (above 67%). Expression of WT Nramp2 in clones N2.3 and N2GG caused a 10-fold and 5-fold stimulation of calcein quenching, and hence Co^{2+} and Fe^{2+} transport respectively, compared to controls. Likewise, cells expressing mutant D161A showed transport rates similar to WT (Fig. 5B). On the other hand, mutant D192A in TM4 showed intermediate transport activity when compared to WT and this both for Fe^{2+} and Co^{2+}. Finally, mutants D86A and E299A were completely inactive for the two substrates tested. These results identify residues D86 and E299 in corresponding TM1 and TM7 as playing key roles in metal transport by Nramp2.

G185R Mutation of mk *Mice*

A naturally occurring mutation at Gly185 in TM4 (G185R) is associated with severe iron deficiency and microcytic anemia of the *mk* mouse [136] and of the *Belgrade* rat [141]. When expressed in the yeast *smf1/smf2* mutant, the G185R variant of Nramp2 can be expressed in the membrane fraction of these cells at levels similar to those seen for either the WT protein and for the other mutants (Fig. 2A). Complementation studies indicated that G185R could not restore growth in alkaline medium (Fig. 3) nor in medium containing metal chelators (data not shown). These results suggest that in yeast cells, G185R is either transport-incompetent or is active but mis-targeted to an inappropriate transport site. CHO transfectants expressing robust levels of G185R mutant could be readily isolated (Fig. 4). Interestingly, transport experiments in these cells (Fig. 5B) indicated that the G185R mutant retains significant and intermediate transport activity, with 50% (Co^{2+}) and 30% activity (Fe^{2+}) of the WT protein. These results in CHO cells

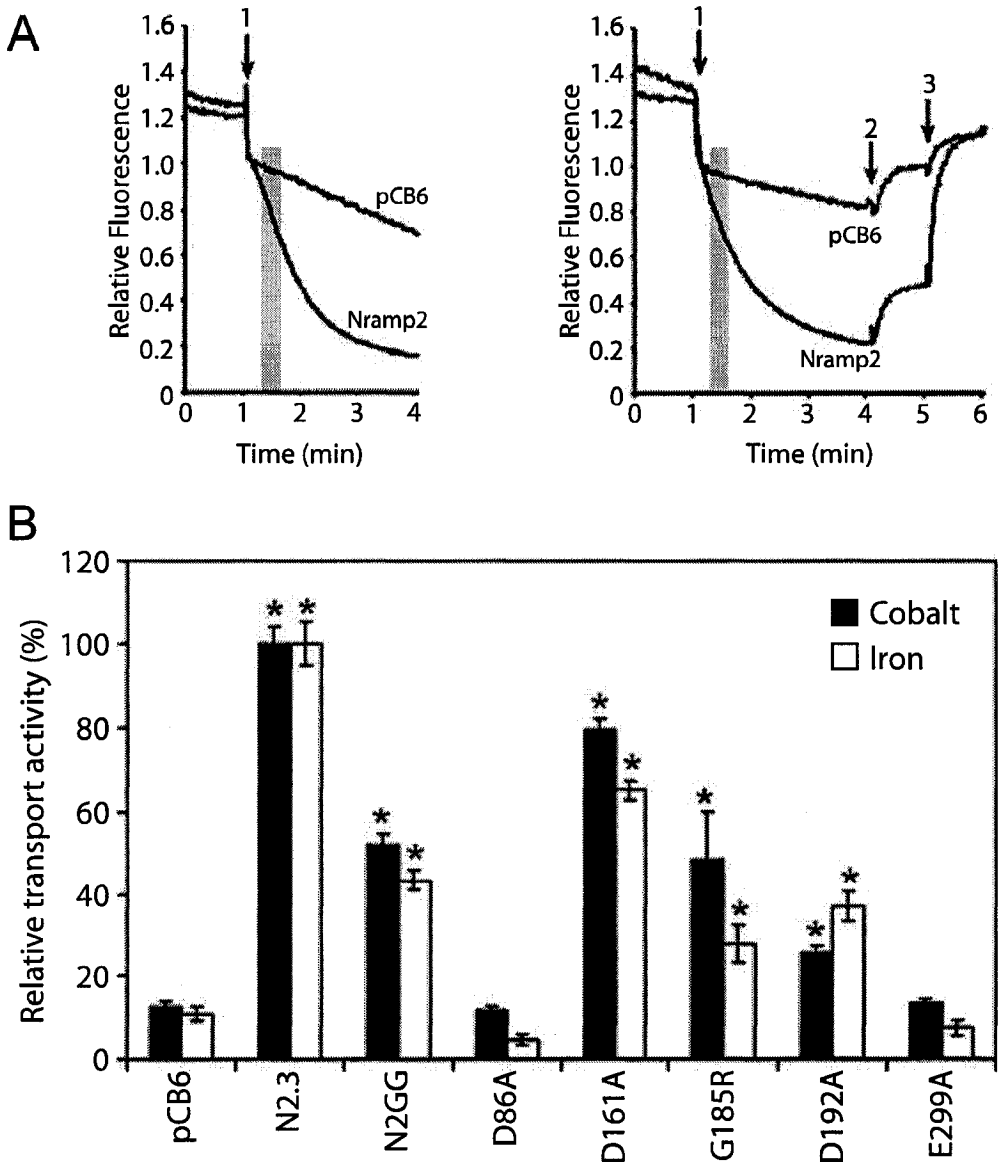

Figure 5. Relative iron and cobalt transport activity of Nramp2 mutations affecting conserved charged residues in TM domains. (A) Control CHO cells (pCB6), as well as CHO transfectants expressing wild type Nramp2 (N2.3) were loaded with the metal sensitive fluorescent dye calcein . Cells were washed, resuspended transport buffer (pH 6.0), and fluorescence was recorded with a fluorescence spectrometer. When fluorescence stabilized, divalent metals (20 μM final concentration of Fe2+ or Co2+) were added to the cell suspension (arrow 1), and fluorescence was continuously monitored for an additional 3 minutes. For iron transport studies (right panel), the membrane-impermeable iron chelator HES-DFO (200 μM) was added at 4 min (arrow 2) to reveal cell associated extracellular Fe-calcein complexes. At 5 min, the membrane-permeant iron chelator SIH (250 μM) was added (arrow 3), and revealed intracellular Fe-calcein complexes (see Materials and Methods). The transport activity of Nramp2 was measured as an initial rate (slope) during the early portion of the calcein quenching curve, and is shown as a shaded area (slope interval). (B). Relative transport activities of wild type (N2.3, N2GG) and mutant Nramp2 variants (identified) were calculated from the initial slope of calcein quenching curves as shown in (A), and are expressed as a relative transport activity with transport in the positive control N2.3 set at 100%. Error bars represent standard errors on the means of 3 or more independent experiments. Asterisks (*) mark transport activities significantly different (i.e. more than 2 standard deviations) from those detected in the negative control, vector-transfected (pCB6) cells.

clearly suggest that the G185R mutation only attenuates but does not eliminate transport function of Nramp2 protein in mammalian cells.

Conserved Histidine Pair in TM6.

Histidine pairs can form metal binding sites in soluble [312] or in membrane proteins [313;314]. The highly conserved Histidine pair found in TM6 (H267, H272) of the Nramp super-family was initially studied in Nramp2 by mutagenesis to the small neutral residue Alanine in mutants H267A, H272A and in the double mutant H267A/H272A. Metal binding by His residues involves donating imidazole nitrogen lone-pair electrons to the unfilled orbitals of the metal, and Cysteines can substitute for His in this process [312;315-317]. Thus, mutants H267C, H272C and H267C/H272C were created. The imidazole proton of His has a pK_a of 6.6 and can mediate pH-dependent effects in proteins. Thus, a last set of mutants were created in which His was replaced by the positively charged Arg (pK_a ~12) which may functionally mimmic the protonated His, albeit with a much larger bulk. Mutants were transformed in yeast cells, and immunoblotting analyses show that all 9 single and double mutants could be stably expressed in the membrane fraction of the *smf1/smf2* mutant (Fig. 2A, *right panel*). Complementation studies for growth at alkaline pH (Fig. 3) and in the presence of metal chelators (data not shown) indicate that H267 is highly mutation-sensitive with replacements to Ala, Cys and Arg causing severe or complete loss-of-function. H272 was less mutation sensitive than H267, with H272A and H272C retaining near WT activity, and only substitution to the bulkier Arg (H272R) abrogated complementation. Finally, the three double mutants (H267A/H272A; H267C/H272C; H267R/H272R) were completely inactive in yeast.

Immunoblotting analysis (Fig. 4A, *right panel*) revealed that all mutants could be stably expressed after transfection in CHO cells, with the exception of the double H267/H272C mutant (3 independent transfections, 119 clones screened). The other 8 *Nramp2* mutants were expressed at varying levels, but that generally fell between those seen in the positive controls expressing low (N2GG) and high (N2.3) amounts of Nramp2. Biotin labeling experiments in intact cells identified cell surface reactivity of all expressed mutants, with levels approximately proportionate to total expression levels

detected in membrane fractions by immunoblotting (Fig. 4B, *right panel*). However, some reduced trafficking of protein to the plasma membrane may have occurred in H267C and H272A. Metal transport activity of the mutants was tested in the calcein quenching assay for Fe^{2+} and Co^{2+} at pH 6.0. Mutants bearing either single mutations to Arg at either position (H267R, H272R), or double mutations (H267A/H272A, H267R/H272R) were completely inactive for transport (Fig. 6). Likewise, mutant H272A was also inactive in these conditions, and mutant H267C only retained low transport activity but for Co^{2+} only (Fig. 6). In fact only H267A and H272C retained modest but significant transport activity towards both metal cations analyzed in the assay, with H267A possibly having a higher selectivity for cobalt (see below). These results indicate that H267 and H272 play an important role in Nramp2 metal transport, both in yeast and mammalian cells.

The apparent change is substrate selectivity (cobalt over iron) in the H267A mutant was investigated further through radioisotopic ^{55}Fe transport measurements. Competition experiments with cold iron and cobalt failed to reveal a significant preference for cobalt in H267A compared to the wild-type Nramp2. Therefore, the change in substrate selectivity in H267A observed in the calcein quenching assay, while statistically significant, could not be confirmed by radioactivity and remains unclear.

Possible pH effects on transport activity of the mutants were investigated (Fig. 7). Fe^{2+} (Fig. 7A, *top row*) and Co^{2+} (data not shown) transport by Nramp2 in clones N2.3 and N2GG approached maximum at pH ~6.0, and decreasing the pH to 5.0 had little effect on transport. Likewise, background uptake of metal in negative controls was not affected by lowering pH. However, the low level of transport activity detected at pH 6.0 in mutants H267A, H267C, and H272C (Fig. 6) could be significantly enhanced by progressively lowering pH (Fig. 7A, 7B). This increase occurred gradually over background, pH-insensitive levels detected in control pCB6 cells. Surprisingly, mutants 272A and 267A/272A which showed complete loss-of-function at pH 6.0 (Fig. 6) could be rescued by lowering the pH. Interestingly however, lowering the pH of the extracellular medium had no effect on Co^{2+} (not shown) or Fe^{2+} transport (Fig. 7B) of any of the histidine to arginine mutants (H267R, H272R, H267/272R). The pH effect seen in

the Cys/Ala mutants was specific for the conserved His pair of TM6 and was not observed in any of the other inactivating mutations studied (e.g. D86A, E299A or G185R) (data not shown). Therefore, mutations at the two conserved His in TMD6 clearly affect pH sensitivity of Nramp2 transport, and suggest that these residues may be involved in pH regulation of transport.

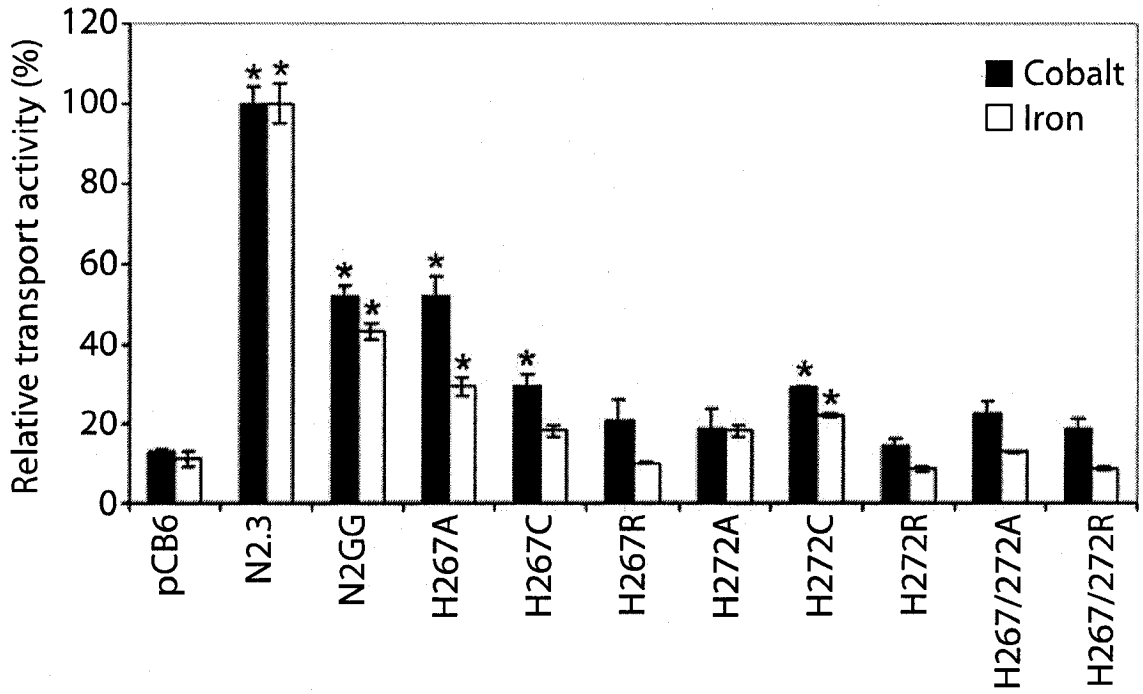

Figure 6. Relative iron and cobalt transport activity of Nramp2 mutations affecting conserved histidine residues in TM6. Transport studies were conducted at pH 6.5. Results are presented for different mutants at H267 and H272, as described in the legend to Figure 5.

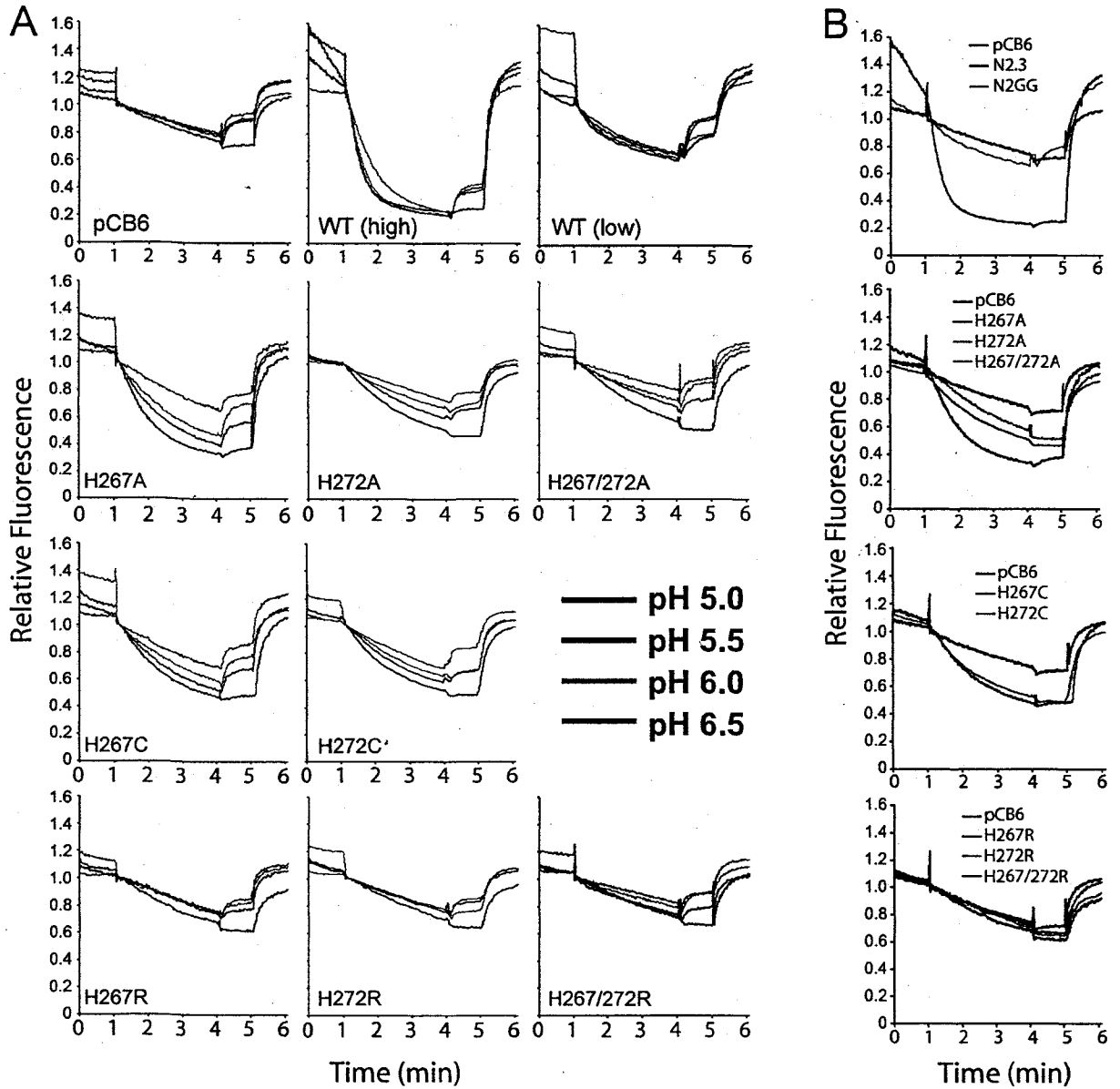

Figure 7. Effect of pH on transport activity of Nramp2 mutants at conserved histidine residues in TM6. (A) Iron transport in the various negative (pCB6), and positive controls (N2.3, N2GG) as well as in CHO clones expressing Nramp2 mutants at the plasma membrane (H267A, H272A, H267/272A, H267C, H272C, H267R, H272R, H267/272R) was studied by the calcein quenching assay as described in the legend to Figure 5A, with the following modifications. After loading with calcein-AM at pH 7.4, cells were washed and resuspended in transport buffer at different pH (indicated). Fluorescence was allowed to stabilize for 1 min, followed by addition of 20 μM Fe2+. (B) Summary of transport results obtained for the histidine mutants at pH 5.0.

DISCUSSION

We aimed to study the functional role of highly conserved charged residues in the TM domains of Nramp proteins on substrate transport and pH regulation. Such residues were mutated in the backbone of Nramp2 and corresponding mutants were tested in yeast and mammalian cells. With few exceptions, there was good general agreement between *smf1/smf2* complementation results in yeast and transport data in mammalian cells. Interestingly, although all mutants could be expressed in the membrane fractions of yeast cells (Fig. 2A), several could not be expressed in CHO cell membranes. These results suggest that such TM mutations 1) affected normal protein folding, maturation and processing, possibly leading to protein instability and/or degradation or 2) that overexpression of the corresponding mutant protein was somehow toxic for the cells. These results highlight possible differences in protein sorting, maturation and targeting mechanisms in both cell systems, but also stress the importance of maturation and membrane targeting for proper Nramp2 function.

Gly185 is invariant in all Nramp orthologs from bacteria to man. Strikingly, its mutation to Arg arose independently in 2 rodent models of iron deficiency, the microcytic anemia mouse *mk*[136], and the anemic *Belgrade* (*b*) rat [141]. The G185R mutation showed a complex phenotype. In yeast, G185R could be expressed in yeast membranes, but could not complement the *smf1/smf2* mutant, suggesting a loss of transport activity, in agreement with results from Su et al [146], and Worthington et al [318] who reported a 95% and 85% reduction in $^{55}Fe^{2+}$ transport activity of G185R in HEK293 cells and COS-7 cells, respectively. G185R could also be expressed in the membrane fraction of CHO cells (Fig. 4), where it retained significant transport activity for both Co^{2+} (50% of WT) and Fe^{2+} (35% of WT). Similar transport activity of G185R has also been observed in stable transfectants in the LLC-PK1 porcine kidney cells (data not shown). This significant transport activity suggests that loss of transport function may not be the sole defect responsible for the *mk* phenotype *in vivo*. Rather, the mutation may affect membrane targeting in a cell-specific fashion, perhaps including targeting to a transport incompetent compartment in yeast cells. Recent studies *in vivo* support such a tissue or cell-specific effect. Indeed, immunoblotting studies show robust expression of the G185R

isoform in duodenum membrane fractions of *mk/mk* mice, but immunohistochemistry studies revealed absence of protein targeting to the brush border, the site of active transport [147]. Likewise, *mk/mk* mice show a strong reduction of Nramp2 (G185R) protein expression in the kidney [172], while *mk/mk* reticulocytes are completely devoid of Nramp2 expression [169]. Parallel analysis of the disease susceptibility G169D mutation in TM4 of *Nramp1* (reconstructed in Nramp2; data not shown) associated with susceptibility to infections also indicated absence of *smf1/smf2* complementation in yeast. Also, we could not isolate CHO clones stably expressing this mutant, a situation similar to that seen *in vivo* in macrophages from *Nramp1*^{G169D} mouse strains, where no mature protein is detected [13]. Together, these results suggest an important role for this residue and TM segment for transport activity, but also suggest that its integrity is required for proper maturation, folding and/or targeting of the Nramp proteins.

Helical wheel projections in the conserved hydrophobic core of Nramp proteins reveal strong amphipathic character for several TM domains, including TM 3, 5 and 9 [1]. Sequence conservation expressed as a variability moment [1], indicates periodicity with strong conservation of the polar face, with the apolar "lipid-accessible" face of the helix being heavily substituted. Several highly charged residues map to the polar side of TM helices. Such an arrangement is characteristic of familes of ion transporters and ion channels [1]. Mutations at the 9 conserved charges in TM domains had either no effect (R119, R146, D161, E225), or caused partial (D192) or complete loss-of-function (D86, E154, E299, R416). D86, E154, E299, and R416 are the most highly conserved being invariant in multiple sequence alignments performed (appended). It is striking that 3 of them have negatively charged side chains, raising the possibility that they may mediate interaction with the positively charged divalent cation substrates of Nramp transporters. Alternatively, such residues may be involved in hydrogen bonding, salt bridge formation (dipole), or other interactions in the formation of a water-filled pore or transport path.

The absolute conservation of the Histidine pair H267/H272 in TM6 in eukaryotic and prokaryotic Nramp sequences suggests an important role. In addition, studies by us (data not shown) and others [318] show that Nramp2-mediated transport in transfected cells is sensitive to the action of the histidine-specific reagent diethyl pyrocarbonate (DEPC).

Here, we show that both residues are mutation-sensitive (in particular H267), with independent substitutions at either or both residues causing loss-of-function. Strikingly, several poorly active (H267A, H267C, H272C) or completely inactive His mutants (H272A, H272C, H267A/H272A) at pH 6.0 could be rescued by lowering the pH of the transport assay (Fig. 7). The observed pH effect was incremental, with maximal transport attained at or below pH 5.0. However, completely inactive histidine to arginine mutants (H267R, H272R, H267/272R) could not be rescued by lowering the pH of the transport assay. This may be a result of increased steric hindrance associated with replacement of histidine to bulky arginine. Thus, mutations at either His residues in TM6 shifted the pH required to achieve maximal transport to a more acidic value.

Several explanations can be put forward to account for the unique effect of pH on transport properties of the Nramp2 His mutants. Firstly, H267 and H272 may be involved in direct binding of the metal substrate in a pH-dependent fashion. Metal binding by His pairs has been documented in soluble proteins such as transcription factors [312], and has also been used in membrane proteins where they have been engineered to study proximity relationships between individual TM domains by electroparamagnetic resonance [314]. Although H267 and H272 may indeed form part of a binding site for metals in the membrane portion of Nramp2, it appears unlikely. Indeed, an *Nramp2* mutant lacking both Histidines (H267A/H272A) is still transport active at pH 5.0 (Fig. 7B). A second possibility is that H267, H272 or both participate in H^+ movement across the membrane in a H^+ co-transport mechanism possibly by a proton relay system [40]. Such a relay system has been described for the lactose permease of *E. coli*, and involves TM residues R302/H322/E325 [319]. Such a proton relay system may exist in Nramp2 and may involve conserved residues such as H267/H272 as well as other negatively and positively charged residues in TM domains. Partial or complete inactivation of this system would be predicted to have a major effect on the pH dependence of transport. A third explanation for the observed pH effect on transport properties of single or double His mutants, is that H267/H272 may be implicated in pH regulation of the transporter through gain or loss of the imidazole proton (pK 5.5 to 6.5). In this favored model, protonation of H267/H272 would be required to maintain the protein in a functional, transport-competent

conformation. This effect could be either general and involve additional residues, resulting in a pH-dependent global conformational change from an inactive state (neutral pH) to an active state (acidic pH). In this model, loss of the key His residues would shift the pH for maximal transport to a more acidic value, requiring protonation of other groups or side chains to create the same overall conformational change. Alternatively, either or both H267/H272 could play a more specific role in creating a pH-dependent transport path in the transporter. For example, an interaction with adjacent and highly conserved negatively charged residues in other TM domains could be necessary to open an ion transport path. Loss of H267/H272 would require formation of compensatory interactions of conserved negatively charged residues with other protonated side chains and/or water molecules in the transport path. Although highly speculative, such a mechanism appears to account for the pH-dependence of anion transport by the Band 3 transporter [320;321].

ACKNOWLEDGMENTS

The authors are indebted to Drs. S. Grinstein (University of Toronto, Toronto) and H.R. Kaback (University of California, Los Angeles) for helpful discussions and suggestions during this work, and Dr. P. Ponka (McGill University, Montreal) for the generous preparation and gift of iron chelators.

Preface to Chapters 3 and 4

Following its initial functional cloning in 1997, mounting evidence made it increasingly clear that Nramp2 played a dual role in iron homeostasis [40;136]. We now know that Nramp2 is the transporter responsible for not only the intestinal absorption of nutritional non-heme iron but is also the protein responsible for the transfer of transferrin-iron from endosomes to the cytosol. Before 2005, much of what was known about the role of Nramp2 in systemic iron homeostasis came from studies in rodent models of iron deficiency. Both *mk* mice and *Belgrade* rats possess identical mutations in *Nramp2* (G185R) leading to severe hypochromic microcytic anemia [136;141]. Critical mutations in human *NRAMP2* were thought to cause a similar phenotype in people.

In 2004, Priwitzerova and colleagues reported a first human patient suffering from an iron-related disorder linked to a mutation in *NRAMP2*. The patient, a young female of Czech origin, suffered from severe congenital hypochromic microcytic anemia and iron overload [4;259]. The phenotype was similar to that of the *mk/Belgrade* rodent models except for the elevated hepatic iron stores that were specific to the human patient. Recently, a second human patient compound heterozygote for two novel mutations in *NRAMP2* was identified [263]. The patient, a 5-year-old male of Italian origin, suffered from severe hypochromic microcytic anemia and hepatic iron overload similar to the first patient. In both human cases, mutations in *NRAMP2* resulted in amino acid substitution mutations at conserved residues in the Nramp2 protein. The effects of these mutations on the expression, function, and subcellular targeting of Nramp2 were unclear and needed to be studied in order to explain the phenotypes of the patients at the molecular level. The following two chapters of this thesis (Chapters 3 and 4) describe the functional properties and possible contribution to disease of the two human mutations expressed in transfected LLC-PK_1 kidney cells.

Chapter 3:

Functional characterization of the E399D DMT1/NRAMP2/SLC11A2 protein produced by an exon 12 mutation in a patient with microcytic anemia and iron overload

ABSTRACT

DMT1 (Nramp2, Slc11a2) mediates iron uptake at the intestinal brush border and across the membrane of acidified endosomes. A single patient with severe microcytic anemia and iron overload was recently reported to carry a mutation in exon 12 of *DMT1* (1285G>C). The mutation has two effects: it severely impairs splicing causing skipping of exon 12, and introduces an amino acid polymorphism (E399D) in the protein encoded by the remaining properly spliced transcript found in the patient. The functional properties and possible contribution to disease of the DMT1 E399D mutation are unknown and have been studied in independent mutants at that position (E399D, E399Q, E399A) expressed in LLC-PK_1 kidney cells. The 3 mutants are shown to be fully functional with respect to stability, targeting and trafficking to the membrane, and are transport competent. This indicates that $DMT1^{G1285C}$ is not a complete loss of function but rather that a modest amount of active DMT1 is produced in this patient. This activity may explain the distinguishing iron overload seen in this patient in addition to microcytic anemia, that is absent in parallel rodent models of *DMT1* deficiency.

INTRODUCTION

Studies in mouse models of disorders in iron metabolism have identified some of the key transporters (*DMT1/NRAMP2/SLC11A2* and *ferroportin*), enzymes (*hephaestin*), and regulatory peptides (*hepcidin*) that play a critical role in iron homeostasis [251]. *DMT1/NRAMP2/SLC11A2* (herein referred to as DMT1) is expressed at the brush border of the duodenum where it mediates uptake of dietary iron [161], but is also expressed at the plasma membrane and in recycling endosomes of peripheral tissues and cells, including erythroid precursors, where it is required for transport of transferrin-associated iron into the cytoplasm [169]. DMT1 transports several divalent cations (Fe^{2+}, Mn^{2+}, Co^{2+}, Zn^{2+}) in a pH-dependent fashion, and down a proton gradient [40]. A mutation (G185R) in *DMT1* causes microcytic anemia and iron deficiency in the *mk* mouse and in the *Belgrade* rat [136;141]. This G185R mutation maps in transmembrane domain 4 (TM-4) of DMT1 and causes multiple biosynthetic and functional defects, affecting stability, maturation, targeting and transport [148]. Recently, Priwitzerova *et al* identified a first human patient homozygous for a mutation in *DMT1* [259]. The patient, a product of consanguineous union, presented severe congenital hypochromic microcytic anemia, high serum iron and serum transferrin receptor (TfR) levels, and required several blood transfusions after birth and during infancy. She also shows erythroid hyperplasia with defective hemoglobinization, and developed liver hemosiderosis by the age of 19. Erythroid progenitors isolated from the patient were small, poorly hemoglobinized, and grew less efficiently in the presence of erythropoietin compared to healthy controls. Erythroid growth, morphology and hemoglobinization were rescued in this patient by treatment with Fe-SIH, an iron delivery strategy that by-passes the DMT1/TfR iron pathway [259]. Intriguingly, and despite obvious similarity in phenotypes, the liver iron overload noted in this patient is not seen in DMT1-deficient (G185R) *mk* mice or in *Belgrade* rats.

The patient has intact *Ferroportin* and *Transferrin Receptor* (*Tfr1*) genes but is homozygous for a G to C substitution at the last nucleotide of exon 12 of *DMT1* (*DMT1*^{G1285C}) [4]. *DMT1*^{G1285C} disrupts normal splicing of *DMT1* pre-mRNA leading to skipping of exon 12, and concomitant production of a truncated DMT1 protein which lacks predicted TM-8, and is unlikely to be functional. This truncated DMT1 variant

(ΔTM-8) appears to represent a loss-of function and is unlikely to act as a dominant negative since the defect in iron metabolism caused by *DMT1*^{G1285C} is inherited in a fully recessive manner [4]. Although skipping of exon 12 normally occurs at low levels (~10% of mRNA) in certain tissues of healthy individuals, the *DMT1*^{G1285C} mutation greatly exaggerates this process (~90% mRNA) [4]. Conversely, a small amount of full length, properly spliced, and exon 12-containing *DMT1* RNA is expressed in the patient. In this full length transcript, however, the *DMT1*^{G1285C} mutation causes a Glu to Asp substitution at position 399 (E399D) in the 4th predicted intracellular loop of DMT1.

The consequence of the E399D mutation on protein function, including a possible contribution to the iron metabolism disorder seen in this patient (alone or in combination with exon 12 skipping) remain unknown. Here, we have created independent mutations at E399 and analyzed the effect on protein stability, targeting and function in transfected LLC-PK$_1$ cells.

MATERIALS AND METHODS

Construction and Expression of DMT1 Mutants

A mouse *DMT1* (*Nramp2, Slc11a2*) isoform II (non-IRE) cDNA modified by insertion of a hemagglutinin epitope (HA) tag in predicted TM7-TM8 extracytoplasmic loop was used for mutagenesis [26], using a recombinant polymerase chain reaction strategy[28] and primers 5'-gtttgtcatggacggattcctga-3' (E399D), 5'-tcaggaatccctgcatgacaaac-3' (E399Q), and 5'-gtttgtcatggcgggattcctga-3' (E399A). Mutants were introduced in plasmid vector pCB6 as *Sac* I/*EcoR* I fragments followed by transfection and expression in porcine LLC-PK_1 kidney cells as previously described.[28] DMT1 transport of Fe^{2+} and Co^{2+} was measured using a calcein fluorescence quenching assay (pH 5.0, 20 μM final metal concentration) [26-28]. Initial rates of metal transport were calculated from the fluorescence quenching curves.

Immunofluorescence

LLC-PK_1 cells grown on coverslips were transfected with GFP-Syntaxin 13 [51], fixed with 4% paraformaldehyde, permeabilized (5% non-fat milk, 0.2% saponin in PBS), and incubated (16hrs, 4°C) with anti-Nramp2 NT polyclonal antibody [42] (1:300). Coverslips were then washed, incubated with goat anti-rabbit-Cy3 (1:2000) for 1h, and mounted on glass slides.

Cell surface Quantification

Cells were grown to confluency in 48-well plates and fixed in 4% paraformaldehyde (30'). Cells were washed (PBS containing 1 mM $MgCl_2$, 0.1 mM $CaCl_2$), blocked (5% nonfat milk in PBS), and incubated first with anti-HA Ab (1:500, 90 min) and then with donkey anti-mouse-HRP secondary antibody (1:4000, 1 h). For total DMT1-HA expression, cells were permeabilized (5% nonfat milk, 0.2% saponin in PBS) prior to incubation with anti-HA antibody. Peroxidase activity was measured with an HRP substrate (0.4 mg/mL o-phenylenediamine dihydrochloride), according to conditions from the commercial supplier (Sigma). Background absorbance readings from non-specific binding of secondary antibody, and non-specific binding of primary antibody to untransfected cells were subtracted for each sample. Cell surface readings were normalized to total DMT1-HA values for each clone expressed as a percentage.

RESULTS

The *DMT1*^{G1285C} mutation causes a Glu to Asp substitution at position 399 (E399D) in the 4th predicted intracellular loop of DMT1 (Figure 1A). E399 forms part of a highly conserved transport signature that defines the *Nramp* family. E399 is invariant in mouse, zebrafish (*cdy*), and yeast (*Smf1p*) relatives of human DMT1 (Figure 1B), suggesting an important structural or functional role [1]. A mouse *DMT1-HA* isoform II (non-IRE) cDNA template was used to create mutants E399D (from *DMT1*^{G1285C} mutation), E399Q (loss of charge, side chain size retained), and E399A (loss of charge, smaller side chain). Wild type (WT) and mutant *DMT1* variants were transfected in LLC-PK_1 porcine kidney cells, and cell clones stably expressing individual proteins were selected for analysis. LLC-PK_1 was chosen since is derived from proximal tubule, a site of abundant DMT1 protein expression *in vivo*, and the maturation, targeting and transport function of DMT1 have been extensively characterized in these cells [51;148]. Immunoblot analysis of whole cell extracts prepared from either WT or mutant-expressing cells (Figure 2A) using an antibody directed against an epitope tag introduced in all constructs identified robust expression of E399D and E399Q similar to WT, while E399A was expressed at a lower level. WT and mutant DMT1 variants were detected as 2 immunoreactive species of sizes ~60 and ~90 kDa. Previous studies have shown that the 90 kDa species corresponds to the fully processed, "complex glycosylated" form of DMT1, while the 60 kDa species corresponds to the full-length unprocessed or "core glycosylated" protein [51]. Studies with the translation inhibitor cyloheximide failed to detect a major effect of any of the 3 mutations on protein stability in LLC-PK_1 cells (data not shown). These results suggest that mutations at E399 (including E399D) do not affect expression, stability or maturation of DMT1.

Previous studies from our laboratory have shown that DMT1 mutations can affect stability, maturation, targeting, and transport activity [28;148]. Thus, we investigated a possible effect of E399 mutations on these parameters. The transport activity of WT and mutant DMT1 variants for Fe^{2+} and Co^{2+} was tested in intact LLC-PK_1 transfectants, using a fluorescence quenching assay [26;28]. Transport, measured as initial rates from calcein quenching curves, was very similar for the 3 mutants and within the range of that

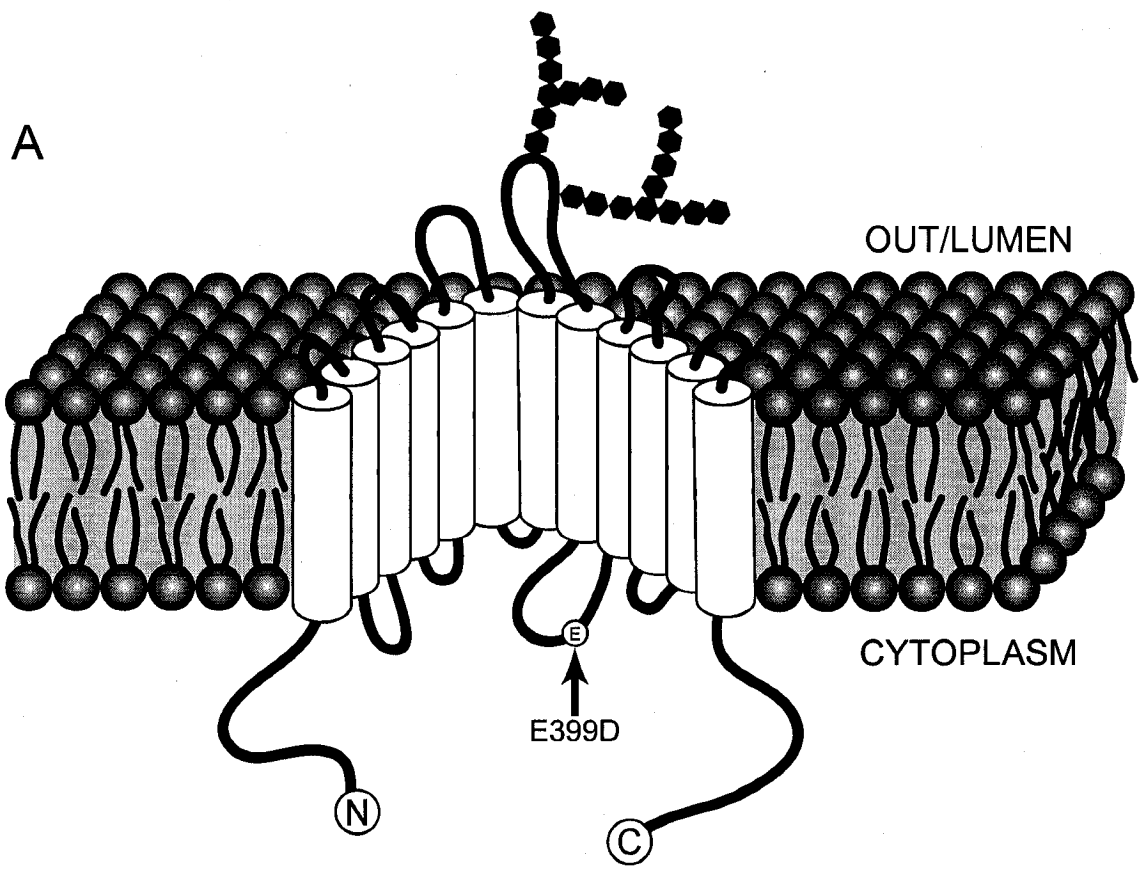

B

```
Mouse Nramp2      WAVGILAAGQ SSTMTGTYSG QFVMEGFLNL KWSRFAR
Human Nramp2      WAVGILAAGQ SSTMTGTYSG QFVMEGFLNL KWSRFAR
Zebrafish         WAVGILAAGQ SSTMTGTYSG QFVMEGFLNL RWSRFAR
Human Nramp1      WAIGLLAAGQ SSTMTGTYAG QFVMEGFLRL RWSRFAR
Mouse Nramp1      WAVGLLAAGQ SSTMTGTYAG QFVMEGFLKL RWSRFAR
Drosophila (Mvl)  WGVGILAAGQ SSTMTGTYAG QFSMEGFLNL QWPRWCR
Yeast (Smf1p)     FMLALLLSGQ SAGVVCTMSG QIVSEGHINW KLQPWQR
Salmonella (MntH) FGLSLVAAGL SSTVVGTLAG QVVMQGFVRF HIPLWVR
```

Figure 1. Position and conservation of E399 residue in DMT1. (A) A schematic representation of DMT1-HA showing the position of the E399D mutation in the fourth predicted intracellular loop of the protein. (B) Multiple sequence alignments of DMT1 orthologs for residues forming the fourth predicted intracellular loop. The position of E399 is highlighted (black) along with residues defining the highly conserved consensus transport motif (grey).

measured in independent cell clones expressing WT DMT1 (Figure 2B). The mutations did not have a major effect of either preference for Fe^{2+} and Co^{2+} ions (Figure 2B), or on the pH-dependence of transport (data not shown) [28]. These results demonstrate that residue E399 is not critical for transport activity of DMT1. The sub-cellular localization of WT and E399D, E399Q and E399A variants expressed in LLC-PK_1 cells was next analyzed by double immunofluorescence labeling using an anti-DMT1 antibody, and additional markers of endomembrane compartments [42]. Having previously shown that DMT1-HA isoform II is expressed in syntaxin 13-positive recycling endosomes [51], we examined the effect of the mutations on targeting to this compartment. All three mutations at E399 showed strong co-localization with GFP-syntaxin 13 (Figure 3A; introduced by co-transfection), and little if any overlap with the lysosomal marker GFP-Lamp1 or the ER-marker GFP-Sec 61 (not shown). These findings suggest that E399 is not critical for proper targeting of DMT1 to recycling endosomes.

Finally, we used an ELISA-based surface labeling method to quantify the amount of WT or mutant DMT1 targeted to the surface of transfected LLC-PK_1 cells. Two independent clones of WT DMT1-HA analyzed in this manner were found to express 22.9 ± 1.5% and 33.1± 4.4% of total DMT1-HA at the cell surface (Figure 3B). Mutants E399D (26.7 ± 2.5%) and E399A (28.2 ± 6.9%) showed similar cell surface expression levels compared to the WT protein (Figure 3B). Mutant E399Q (49.2 ± 7.0%) showed slightly higher cell surface expression compared to WT. These results clearly show that the E399D mutation does not affect cell surface targeting of DMT1.

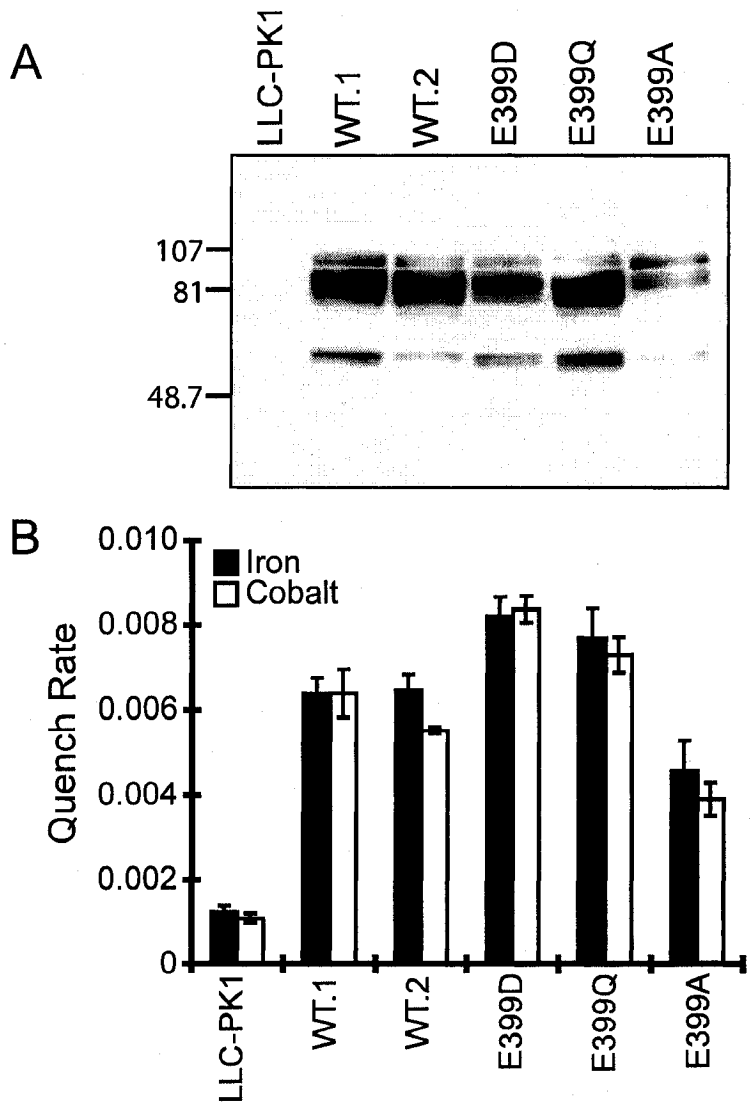

Figure 2. Stable expression and metal transport activity of E399 mutants. (A) Equivalent amounts of total cell extracts from LLC-PK1 cells stably expressing either WT DMT-HA or mutant constructs (identified) were separated by SDS-PAGE followed by immunoblotting with an anti-HA monoclonal antibody. Size of molecular weight markers (in kDa) are identified to the left of the blot. (B) Cells loaded with the metal-sensitive fluorescent dye calcein, were incubated with Fe2+ or Co2+ in acidic buffer (pH 5.0), and the rate of fluorescence quenching was measured over time. The results are expressed as the initial rate of fluorescence quenching. Error bars represent standard error of the means of three or more independent experiments.

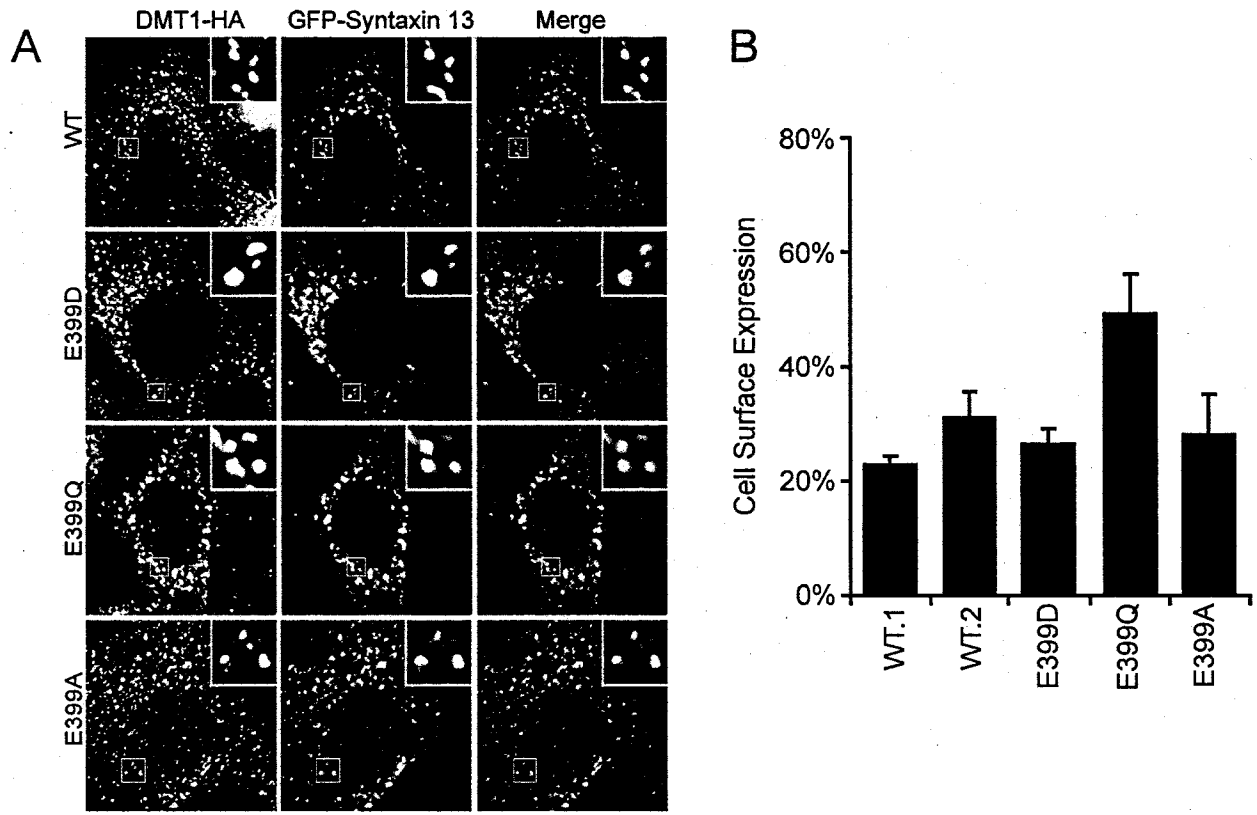

Figure 3. Subcellular and cell surface expression of E399 mutants at steady-state. (A) LLC-PK1 cells stably expressing WT or mutant DMT1-HA were transiently transfected with GFP-syntaxin 13 to label recycling endosomes. Seven hours later, cells were fixed, permeabilized and stained with a polyclonal anti-DMT1 antibody. DMT1 molecules were visualized using a secondary anti-rabbit antibody coupled to fluorescent Cy3. Images were acquired by epifluorescence microscopy. Insets show magnifications of the area boxed in the figure. (B) Fixed LLC-PK1 cells were incubated with anti-HA primary antibody with or without prior detergent permeabilization as described in Materials and Methods. Cells were then incubated with an HRP-coupled secondary anti-mouse antibody, and the amount of bound primary antibody present was determined for both conditions by a colorimetric reaction using o-phenylenediamine dihydrochloride (OPD) followed by spectrometry. The amount of DMT1-HA expressed at the cell surface (in non-permeabilized cells) is shown as a fraction (%) of total protein expression (in permeabilized cells).

DISCUSSION

Taken together, our results strongly suggest that the E399D variant created by the *DMT1*^{G1285C} mutation is functional. This indicates that *DMT1*^{G1285C} mutation is not a complete, but rather constitutes a partial loss-of-function, and therefore the patient indeed expresses a small amount of functional E399D. This protein is produced in addition to the loss-of-function ΔTM-8 variant generated by exon 12 skipping. This small level of activity is clearly insufficient to maintain minimum physiological function in the erythroid compartment, and causes microcytic anemia. This minimum threshold activity is presumed to be between the ~10% level of full length transcript (E399D) seen in the *DMT1*^{G1285C} patient, and the ~50% levels observed in her heterozygote phenotypically normal sibling [4].

These findings also help explain the apparent phenotypic differences between rodents (microcytic anemia) and humans (microcytic anemia plus iron overload) with mutations at *DMT1*. The small amount of functional E399D produced in the *DMT1*^{G1285C} patient may be sufficient for acquisition of nutritional iron at the brush border and storage in liver (hemosiderosis), but not sufficient enough for efficient use and recycling in the erythroid compartment (microcytic anemia). This proposal would suggest that the minimum DMT1 activity required for physiological "sufficiency" in the erythroid compartment for hemoglobin production is higher than for acquisition of nutritional iron at the brush border in the form of inorganic metal (Fe^{2+}) or of heme-iron. This situation may be exacerbated in rodents where the laboratory diet is free of heme iron.

Finally, the combined findings that the *DMT1*^{G1285C} patient is the only human known to carry an alteration in *DMT1*, but yet that this mutation behaves as a partial but not complete loss-of-function, indirectly suggests that true null mutations at *DMT1* may not be compatible with life.

ACKNOWLEDGEMENTS

We would like to thank Lauren Hamlin-Douglas and Rachel Beckerman for valuable technical assistance.

Chapter 4:

A novel R416C mutation in human DMT1 (Slc11a2) displays pleiotropic effects on function and causes microcytic anemia and hepatic iron overload

ABSTRACT

A patient suffering from microcytic anemia and hepatic iron overload was found to be compound heterozygote for polymorphisms in the iron transporter *DMT1* (*Nramp2, SLC11A2*), including a 3 base pair deletion ($DMT1^{delCTT}$) in intron 4 that partially impairs splicing, and an amino acid substitution ($DMT1^{C1246T}$, R416C) at a conserved residue in transmembrane domain 9 of the protein. The functional properties and possible contribution to disease of the DMT1 R416C mutation were studied in independent mutants at that position (R416C, R416A, R416K, R416E) expressed in LLC-PK_1 kidney cells. Non-conservative substitutions at R416 (C, A, E) cause multiple functional deficiencies including defective protein processing, loss of transport activity, impaired cell surface targeting and recycling through endosomes, concomitant with retention of the transporter in the endoplasmic reticulum. Conversely, a conservative isoelectric substitution (R416K) was less vulnerable, resulting in a functional transporter that was properly processed and targeted to the cell surface and to recycling endosomes. We propose that $DMT1^{C1246T}$ (R416C) represents a complete loss-of-function and that a quantitative reduction in DMT1 expression is the cause of the microcytic anemia and iron overload in the patient.

INTRODUCTION

The mechanisms by which nutritional iron is acquired, re-distributed and recycled involve a number of structurally and functionally distinct membrane transporters including the *Divalent Metal Transporter 1* (*DMT1*, also known as *Nramp2* or *SLC11A2*) [251]. DMT1 is an integral membrane phosphoglycoprotein expressed at the brush border of the duodenum, where it imports dietary iron in absorptive epithelial cells [161]. DMT1 is also ubiquitously expressed in recycling endosomes of many cell types and is abundant in erythroid precursors, where it is required for transport of transferrin-associated iron into the cytoplasm [169]. DMT1 requires a proton gradient to transport Fe^{2+} as well other divalent cations (Mn^{2+}, Co^{2+}, Zn^{2+}) in a pH-dependent manner [40]. Much of our knowledge of the function of DMT1 *in vivo* comes from studies of rodent models of microcytic anemia and iron deficiency such as *mk* in mice and *Belgrade* in rats, that are both caused by the same naturally-occuring mis-sense mutation in DMT1 (G185R) [136;141]. A similar but more severe phenotype has recently been reported for a mouse mutant with a complete inactivation of *DMT1* (*DMT1*$^{-/-}$) [258]. Furthermore, studies involving tissue-specific inactivation of *DMT1* have demonstrated the critical role of the transporter in intestinal iron absorption and in erythroid iron utilization, but suggested a less critical role of DMT1 in liver iron uptake [258].

In humans, Priwitzerova *et al* first reported a human patient homozygote for a mutation in DMT1 (*DMT1*^{G1285C}). The young female patient is the product of a consanguineous union who suffered from severe congenital hypochromic microcytic anemia and iron overload [4;259]. The phenotype is similar to that of *DMT1* mouse mutants with the notable exception of elevated hepatic iron stores that are specific to the human patient. The mutation has a dual effect, partially impairing splicing of exon 12 of *DMT1* (1285G>C) and introducing an amino acid substitution (E399D) in the remaining properly spliced transcript found in the patient. We recently showed that the E399D mutation does not in itself affect expression, function, or targeting of the DMT1 protein [260-262], and thus reduced DMT1 function in this patient is likely caused by a quantitative reduction in *DMT1* mRNA levels due to improper splicing.

Recently, some of us reported a second human patient who was compound heterozygote for two novel mutations in *DMT1* [263]. The patient is a 5-year-old male who suffers from severe hypochromic microcytic anemia and who has developed hepatic iron overload shortly after birth. Hematological values and iron metabolism indices for this patient and for the patient reported by Priwitzerova *et al* were similar: both had low hemoglobin, low mean corpuscular volume, low mean corpuscular hemeoglobin, high serum iron and serum ferritin, and elevated transferrin saturation. However, the degree of anemia was more severe in the child patient who required blood transfusions until erythropoietin treatment sufficiently ameliorated the anemia to allow transfusion independence. The patient possessed two novel mutations in *DMT1*: a 3 base pair deletion (del CTT) in intron 4 and a C to T transition at nucleotide 1246 ($DMT1^{C1246T}$) in exon 13 that results in an Arg to Cys substitution at position 416 (R416C) of DMT1. The CTT deletion disrupts normal splicing of *DMT1* pre-mRNA by affecting the consensus splicing acceptor site of intron 4, causing a partial (30-35%) skipping of exon 5 [263]. This truncated DMT1 variant lacks 40 amino acids, including an entire transmembrane domain (TM2), and appears to represent a loss-of-function that is inherited in a fully recessive manner. In contrast, the effects of the R416C mutation on DMT1 expression, targeting, and function is unknown. Previous studies by our group have suggested that R416 may be critical for DMT1 function [28]. An alanine substitution mutant at R416 (R416A) failed to restore growth under metal limiting conditions to a yeast mutant deleted for two of the three endogenous *DMT1* homologs (*smf1/smf2*) despite robust membrane expression of this mutant. The R416A variant may not be stably expressed in transfected CHO cells precluding its functional analysis.

The effects of the R416C mutation on DMT1 function, including a possible contribution to the iron metabolism disorder seen in this patient remain unknown and were studied. We have created independent mutations at R416 and analyzed the effect on protein expression, glycosylation, targeting and function in transfected LLC-PK_1 cells.

MATERIALS AND METHODS

Construction, expression, and functional characterization of DMT1 Mutants

A mouse *DMT1* isoform II (non-IRE) cDNA backbone modified by insertion of a hemagglutinin epitope (HA) tag in the predicted extracytoplasmic loop defined by the TM7-TM8 interval (DMT1-HA) was used for mutagenesis [26]. Mutations at R416 were constructed using a recombinant polymerase chain reaction (PCR) strategy [28], utilizing primers 5'-GTGATCCTGACATGTTCTATCGCCATC-3' (R416C), 5'-GATCCTGACCAAGTCTATCGCCATC-3' (R416K), and 5'-GATCCTGACCGAGTCTATCGCCATC-3' (R416E). Mutants were introduced into the plasmid vector pCB6 as *Sac I/EcoR I* fragments. Construction of the R416A mutation in a DMT1 construct bearing two c-Myc epitope tags at the carboxyl terminus has been described earlier (R416A-myc) [28]. R416A-myc was introduced into DMT1-HA as a *Sac I/EcoR I* fragment. All mutants were transfected and stably expressed in porcine LLC-PK_1 kidney cells as previously described [28]. DMT1 transport of Co^{2+} was measured using a calcein fluorescence quenching assay (pH 5.0, 20 μM final metal concentration) [262]. Initial rates of metal transport were calculated from the initial slopes of the fluorescence quenching curves.

Quantification of cell surface expression by ELISA

Quantification of the proportion of DMT1-HA molecules expressed at the cell surface was by an ELISA we have previously described [184]. Briefly, cells were grown to confluency in 48-well plates and fixed with 4% paraformaldehyde (30'). Cells were washed (PBS containing 1 mM $MgCl_2$, 0.1 mM $CaCl_2$), blocked (5% nonfat milk in PBS), and incubated first with anti-HA Ab (1:500, 90 min) and then with donkey anti-mouse-HRP secondary antibody (1:4000, 1 h). For total DMT1-HA expression, cells were permeabilized (0.1% Triton X-100 in PBS, 30') prior to blocking and incubation with anti-HA antibody. Peroxidase activity was measured with an HRP substrate (0.4 mg/mL o-phenylenediamine dihydrochloride), according to conditions from the commercial supplier (Sigma).

Background absorbance readings from non-specific binding of secondary antibody, and non-specific binding of primary antibody to untransfected cells were subtracted for each sample. Cell surface readings were normalized to total DMT1-HA values for each clone expressed as a percentage.

Immunofluorescence

GFP plasmids were kind gifts of Dr. D. Williams (University of Toronto; GFP-Syntaxin 13) and Dr. S. High (University of Manchester, Manchester, United Kingdom; GFP-Sec61). LLC-PK_1 cells grown on coverslips were transfected with GFP plasmids, fixed with 4% paraformaldehyde, permeabilized (5% non-fat milk, 0.2% saponin in PBS), and incubated (1 h, 20°C) with anti-DMT1 NT polyclonal antibody (1:300) [42]. Coverslips were then washed, incubated with goat anti-rabbit-Cy3 (1:2000) for 1h, and mounted on glass slides.

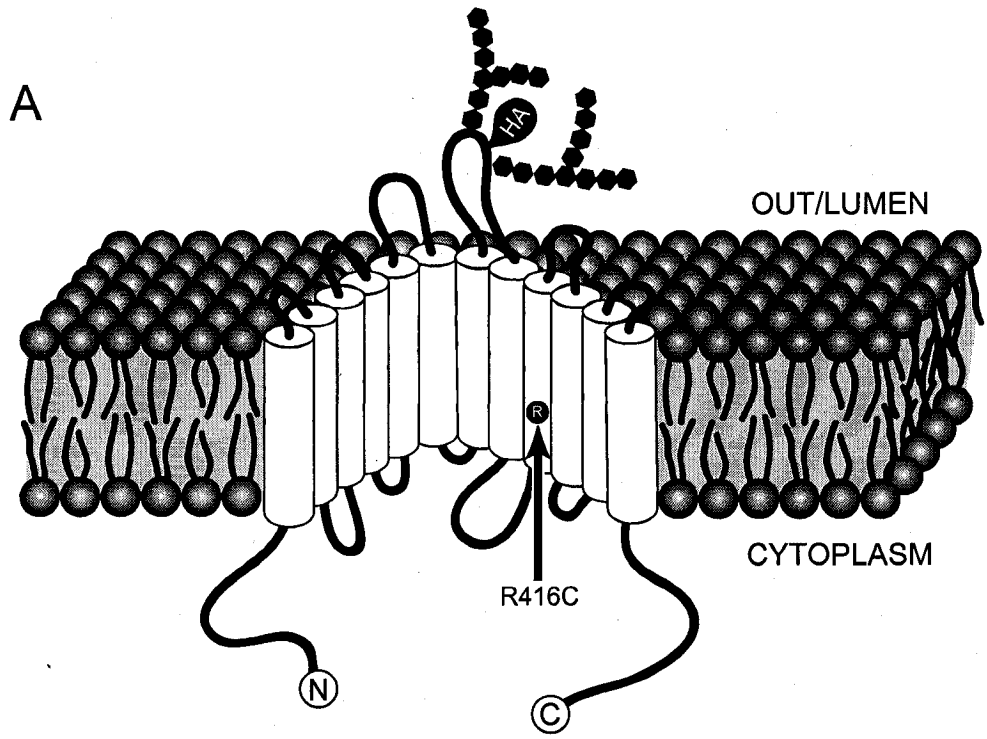

B

```
          Mouse DMT1 LNLKWSRFARVILTRSIAIIPTLLVAVFQDVEHLT
          Human DMT1 LNLKWSRFARVVLTRSIAIIPTLLVAVFQDVEHLT
Zebrafish (Chy) LNLRWSRFARVLLTRSIAIFPTLLVAVFQDVQHLT
    Human Nramp1 LRLRWSRFARVLLTRSCAILPTVLVAVFRDLRDLS
    Mouse Nramp1 LKLRWSRFARVLLTRSCAILPTVLVAVFRDLKDLS
Drosophila (Mvl) LNLQWPRWCRVLVTRCIAIIPTFCLAMFSKMEDLT
   Yeast (Smf1p) INWKLQPWQRRLATRCISIIPCLVISICIGREALS
```

Figure 1. The position and conservation of R416 residue in DMT1. A schematic representation of DMT1-HA showing the position of the R416C mutation in the ninth predicted transmembrane domain (TM) of the protein is shown in (A). A multiple sequence alignment of DMT1 orthologs is shown in (B) for residues neighboring TM9 (grey). The position of R416 is highlighted (black).

RESULTS

The C to T transition at nucleotide 1246 of *DMT1* causes an Arg to Cys substitution (R416C) in the 9th predicted membrane-spanning segment of DMT1 (Figure 1A). Although R416 is positively charged and thermodynamically disfavored in the membrane lipid environment, R416 is invariant among mouse, zebrafish (*cdy*), yeast (*smf1p*), and fly (*mvl*) relatives of human DMT1 (Figure 1B). This suggests an important structural or functional role for R416 in metal transport by DMT1 [1]. To explore the importance of R416 in DMT1 function, we used a mouse *DMT1-HA* isoform II (non-IRE) backbone to create independent mutations at that position: R416C (from *DMT1*^{C1246T} mutation), R416A (loss of charge, smaller side chain), R416K (charge retained), and R416E (negative charge). The effect of these mutations on protein expression, transport activity, subcellular distribution and recycling from the membrane into the endosome compartment were examined in transfected mammalian cells.

DMT1-HA bears an exofacial hemagglutinin (HA) epitope tag that enables us to label cell surface expressed DMT1-HA molecules in intact cells (Figure 1A). We have previously shown that insertion of an HA tag at this position preserves expression, transport activity or subcellular localization of DMT1 [51]. Wild type (WT) and R416 mutant DMT1 variants were transfected into LLC-PK$_1$ porcine kidney cells and cell clones stably expressing individual proteins were selected and expanded for analysis. LLC-PK$_1$ cells were chosen since they are derived from kidney proximal tubule, a site of abundant DMT1 protein expression *in vivo*, and the maturation, targeting and transport function of DMT1 have been extensively characterized in these cells [51;184;184]. Figure 2A shows a typical immunoblot of cell extracts prepared from cells transfected with either WT or mutant DMT1-HA. WT DMT1 was detected as two immunoreactive species, a minor species at ~60 kDa and a major species at ~90 kDa. Previous studies have shown that the minor species corresponds to the precursor "core glycosylated" protein while the major species corresponds to the mature "complex glycosylated" protein [51]. For mutants R416C, R416A and R416E, only expression of the precursor protein was detected (Figure 2A). The slightly slower electrophoretic mobility of the R416A precursor protein reflects the presence of the two additional c-Myc epitope tags inserted at the C terminus of this

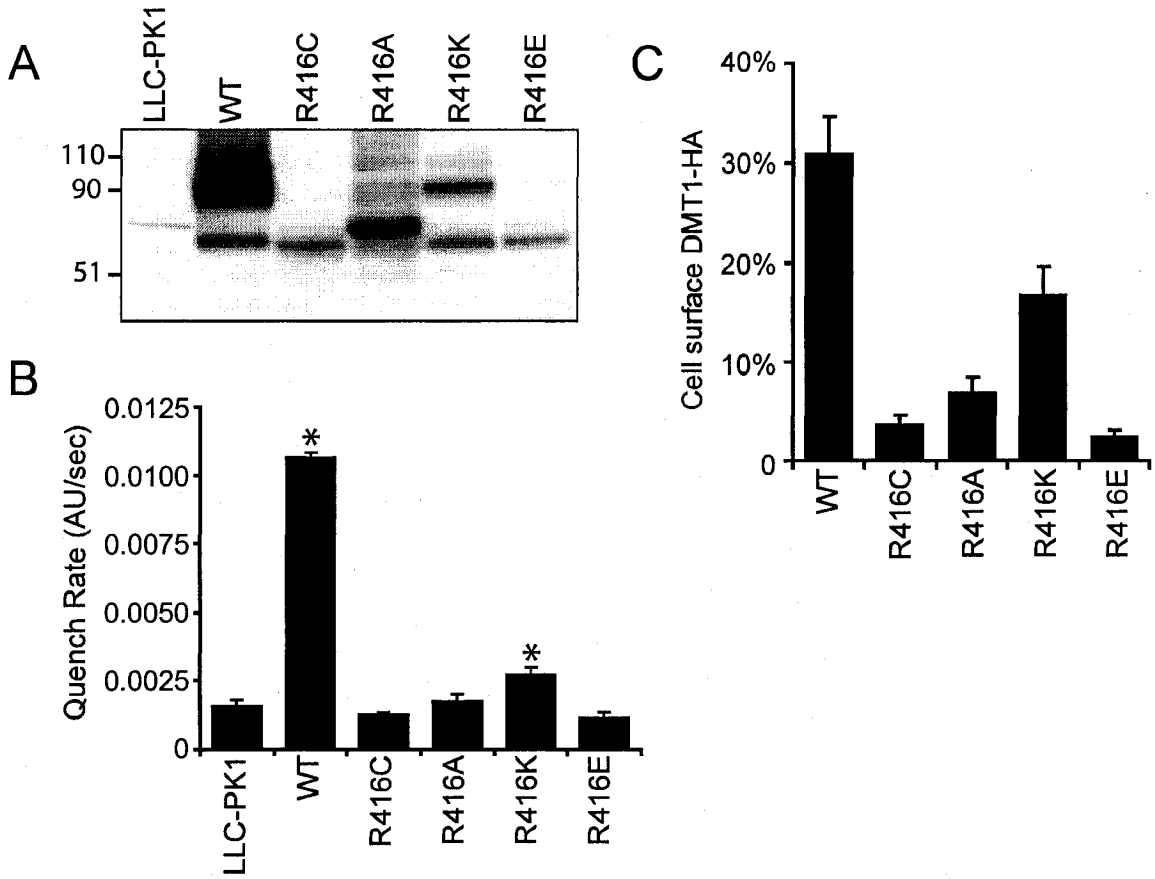

Figure 2. Stable expression and metal transport activity of R416 mutants. Equivalent amounts of total cell extracts from LLC-PK1 cells stably expressing either WT DMT-HA or R416 mutant constructs were separated by SDS-PAGE followed by immunoblotting with an anti-HA monoclonal antibody. A typical immunoblot is shown in (A). The size of molecular weight markers (in kDa) are identified to the left of the blot. Cells loaded with a metal-sensitive fluorescent dye, were incubated with Co2+ in acidic buffer (pH 5.0), and the rate of fluorescence quenching was measured over time. In (B), the results are expressed as initial rates of fluorescence quenching. Error bars represent standard error of the means of three or more independent experiments. Asterixes indicate quench rates that are significantly higher than for untransfected LLC-PK1 cells ($p < 0.001$). In (C), fixed LLC-PK1 cells were incubated with anti-HA primary antibody with or without prior detergent permeabilization as described in Materials and Methods. The amount of bound primary antibody present was determined for both conditions with an HRP-coupled secondary anti-mouse antibody and a colorimetric reaction followed by spectrometry. The amount of DMT1-HA expressed at the cell surface (in non-permeabilized cells) is shown as a fraction (%) of total protein expression (in permeabilized cells).

mutant that are absent in the other variants. These results suggest that mutations at R416 (including R416C) affect proper processing and post-translational modification of DMT1, including maturation to the fully glycosylated polypeptides. Interestingly, only for the most conservative R416K substitution at that position, is mature complex glycosylated protein detected, suggesting that a large positively charge residue at position 416 is required for proper folding/maturation. Maturation of R416K is clearly reduced compared to WT DMT1 (Figure 2A), demonstrating the essential role of R416 in this process.

Earlier studies have shown that conserved charged residues within the membrane-spanning segments of DMT1 are mutation sensitive, and play a critical role in transport activity, cell surface expression, and subcellular targeting.[28] Therefore, we investigated the possible effects of R416 mutations on these parameters. We measured the transport activity of WT and mutant DMT1 variants in live LLC-PK_1 transfectants, using a calcein fluorescence quenching technique where the initial rates of quenching curves are used as an indicator of metal transport into the cell. Mutants R416C, R416A, and R416E demonstrated no significant metal transport activity, displaying transport rates similar to that of untransfected LLC-PK_1 cells (Figure 2B). These results suggest that R416 is not only critical for processing and maturation of DMT1 but is also important for metal transport by this protein. Interestingly, mutant R416K displayed metal transport activity (0.002748 ± 0.00024 AU/sec; mean quench rate ± standard error) that was significantly higher ($p < 0.001$) than that of untransfected LLC-PK_1 cells (0.001472 ± 0.00007 AU/sec) (Figure 2B). Significant activity was also detected for an additional independent transfected cell clone of R416K (data not shown). However, transport activity detected in R416K expressing cells was clearly lower than WT DMT1, which may stem from either reduced transport and/or lower level of expression of R416K compared to WT. Nevertheless, these results suggest that a DMT1 protein with an isoelectric substitution at R416 retains partial metal transport activity.

We used an ELISA-based surface labeling method to determine the amount of WT or mutant DMT1 targeted to the surface of transfected LLC-PK_1 cells. Cells transfected with WT DMT1-HA expressed $30.9 \pm 3.8\%$ of total DMT1-HA at the cell surface (Figure 2C). This result is in agreement with cell surface DMT1 expression

values reported previously for isoform II, which was used as a backbone to construct the mutants [51;184;262]. Mutants R416C (3.6 ± 1.0%), R416A (6.9 ± 1.5%), and R416E (2.5 ± 0.6%) all showed severely reduced cell surface expression (Figure 2C), suggesting that R416 is critical for proper sorting and trafficking of DMT1 to the plasma membrane. These results are consistent with the defective processing and lack of activity observed for these mutants (Figure 2A and 2B). Interestingly, a higher fraction of R416K (16.8 ± 2.9%) was detected at the cell surface compared to the other variants (Figure 2C), consistent with the noted partial maturation/glycosylation and low transport activity of this mutant. This result suggests that a basic, positively charged residue at position 416 is required for cell surface targeting of DMT1.

The subcellular localization of WT DMT1-HA and the R416 variants was next analyzed by double immunofluorescence using a rabbit anti-DMT1 antiserum as well as additional markers of different endomembrane compartments. Co-localization studies show that WT DMT1 isoform II is expressed in syntaxin 13-positive (GFP-Syntaxin 13) recycling endosomes (Figure 3), in agreement with our previous studies [51;184;184;262]. However, mutants R416C, R416A, and R416E were expressed in a peri-nuclear region that showed little overlap with GFP-Syntaxin 13 (Figure 3). Strikingly, R416K was the only variant to show strong co-localization with the recycling endosome marker (Figure 3), suggesting that an isoelectric substitution at R416 does not affect proper subcellular targeting of DMT1. While WT DMT1-HA and variant R416K showed little overlap with the endoplasmic reticulum marker GFP-Sec 61, variants R416C, R416A, and R416E all displayed significant co-localization with this ER marker (Figure 4). These results imply that a large fraction of the variants R416C, R416A, and R416E are mistargeted and are retained in the ER, consistent with the impaired glycosylation, lack of activity, and reduced surface expression observed for these variants.

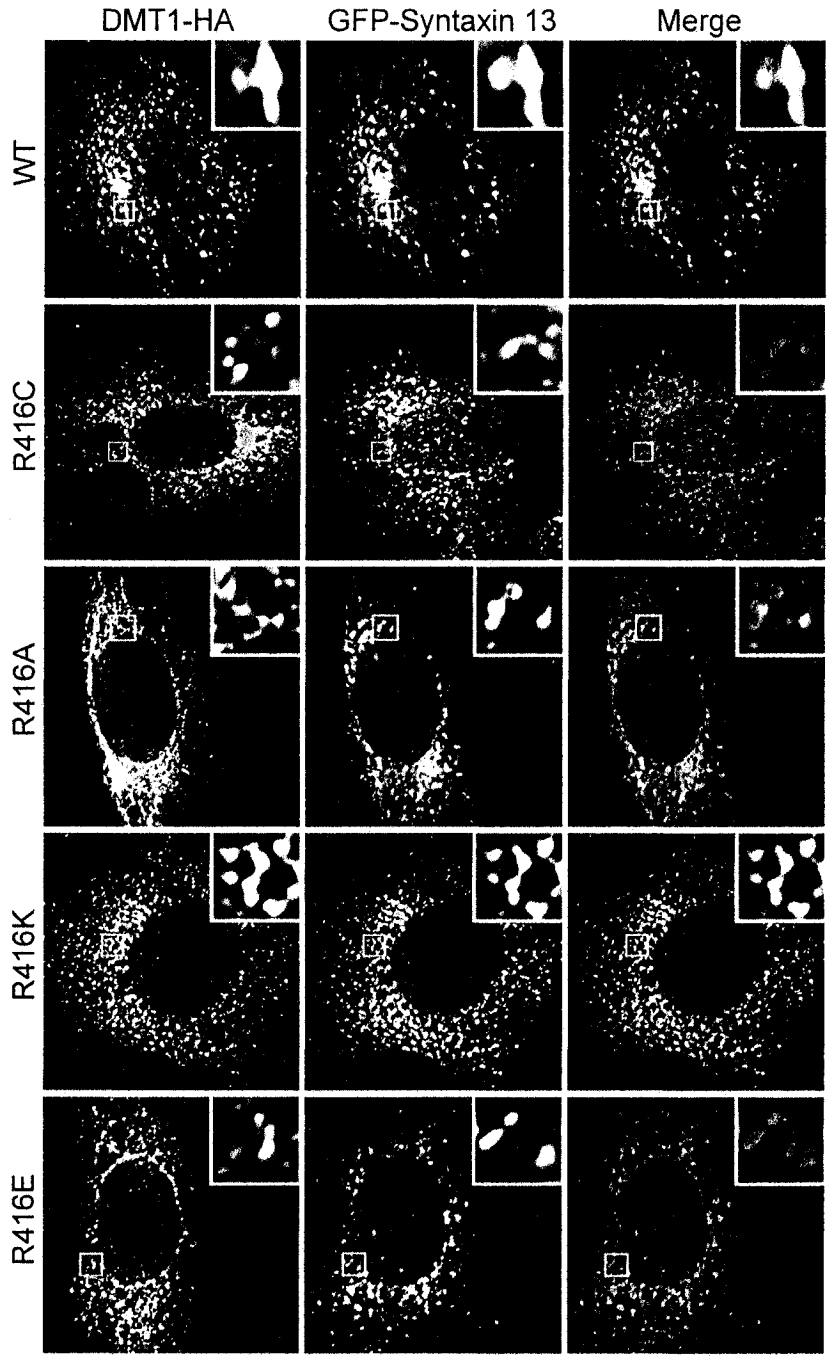

Figure 3. Double immunofluorescence labeling of DMT1-HA and the recycling endosome marker GFP-Syntaxin 13. LLC-PK1 cells stably expressing WT or mutant DMT1-HA were transiently transfected with GFP-syntaxin 13 to label recycling endosomes. The following day, cells were fixed, permeabilized and stained with a polyclonal anti-DMT1 antibody. DMT1 molecules were visualized using a secondary anti-rabbit antibody coupled to fluorescent Cy3. Images were acquired by epifluorescence microscopy. Insets show magnifications of the area boxed in the figure.

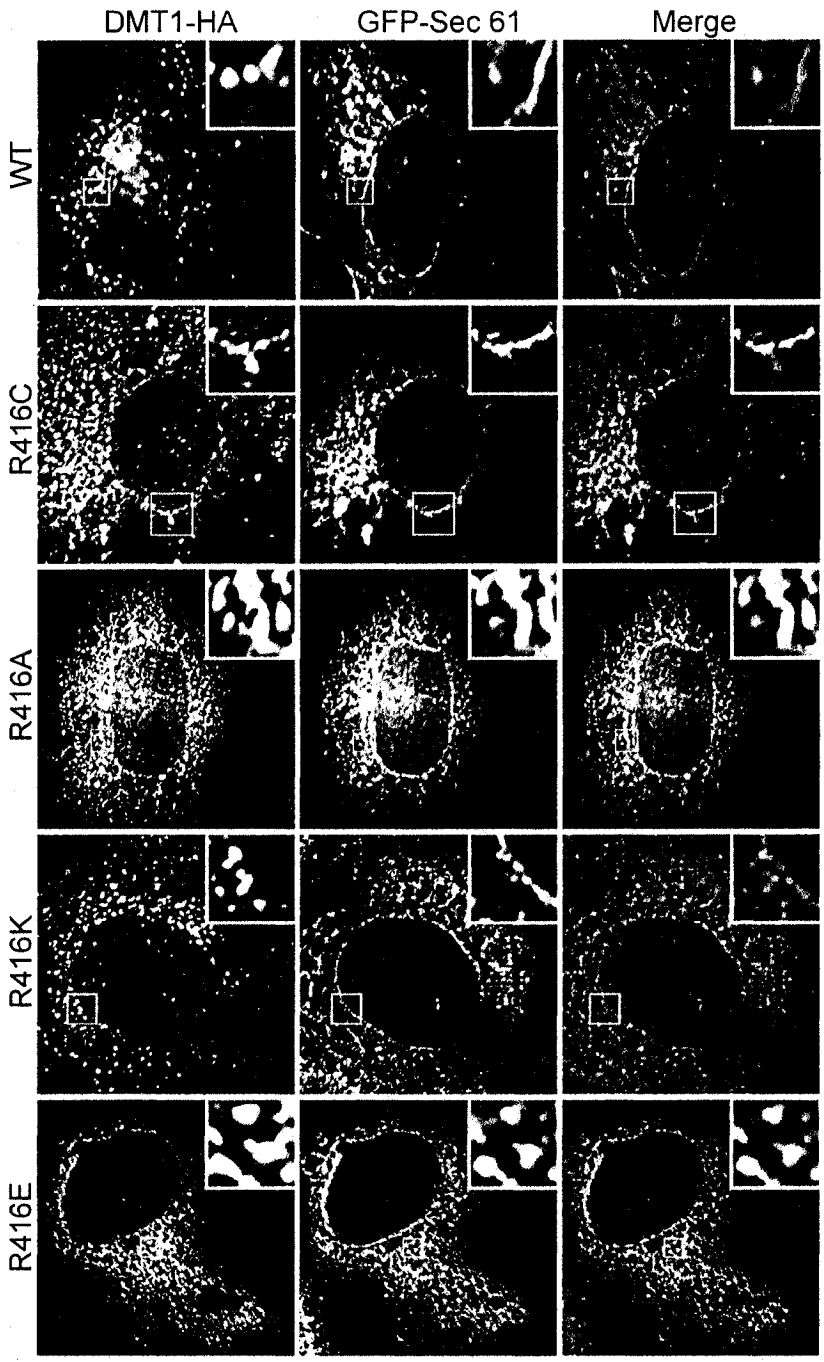

Figure 4. Double immunofluorescence labeling of DMT1-HA and the endoplasmic reticulum marker GFP-Sec 61. LLC-PK1 cells stably expressing WT or mutant DMT1-HA were transiently transfected with GFP-Sec 61 to label the endoplasmic reticulum. DMT1 molecules were visualized as described in the legend of Figure 3. Insets show magnifications of the area boxed in the figure.

DISCUSSION

Taken together, our data strongly suggest that the R416C variant created by the *DMT1*^{C1246T} mutation represents a complete loss-of-function in which the mutant protein is not properly processed and is retained in the ER for degradation. Therefore, we propose that the abrogation of DMT1 function observed in the patient is due to a combination of: a) production of a full length non-functional protein from a null mutation at one allele (R416C) and b) a mutation (*DMT1*^{delCTT}) that partially impairs splicing (exon 5 skipping) in the remaining allele, generating a ΔTM2 truncated non-functional variant, with a small but unknown amount of functional protein produced by residual properly spliced transcript. The resulting overall low level of DMT1 activity in the patient is clearly insufficient to maintain physiological function in the erythroid compartment, and causes microcytic anemia.[263] These results suggest that a low level of DMT1 activity is pathological and is insufficient to support iron metabolism in the erythroid system, yet is sufficient to allow some nutritional iron uptake in the gut, which in the long run leads to iron overload in the liver.

Coincidently, the first reported pathological human mutation in *DMT1* (*DMT1*^{G1285C}) also results in improper splicing of the gene, causing skipping of exon 12 and the creation of a truncated (ΔTM8) non-functional variant [4]. However, the *DMT1*^{G1285C} substitution mutation leading to exon 12 skipping appears to have a more severe effect on splicing than the 3 base pair deletion mutation leading to exon 5 skipping (*DMT1*^{delCTT}).[4;263] Indeed, in the female patient who is homozygote for the *DMT1*^{G1285C} mutation, the remaining small level of proper splicing of exon 12 produces a E399D variant that shows wild type activity. In both patients, disease appears to result from a quantitative reduction in full length functional *DMT1* transcript below a certain minimum threshold, and the similarities in conditions of both patients seem to support this idea. This minimum threshold DMT1 activity appears to be between the low level of activity observed in both *DMT1* mutant patients and the ~50% activity retained in their phenotypically normal heterozygote relatives [4;263]. Finally, a new patient was recently reported with a V114-in frame deletion in transmembrane 2 and a G212V replacement in transmembrane 5. This patient has a phenotype which is very similar to the previously

described subjects [265]. However, the fact that patients with a complete loss-of-function at both *DMT1* alleles have not yet been identified suggests that even a low level of DMT1 activity, while insufficient to maintain normal iron homeostasis, is essential for life.

In addition to providing better insight into the role of DMT1 in iron homeostasis, characterization of the R416C variant produced by the patient has also shed light into the structure and function of the DMT1 protein. Our data shows that the conserved arginine in TM9 of DMT1 (R416) is critical for the proper folding and processing of the transporter. The fact that non-conservative mutations at R416 (R416C, R416A, R416E) are not well tolerated and that an isoelectric substitution (R416K) retains partial function strongly suggests that a positive charge is required by DMT1 at that position, and that loss of that charge rather than the gain of a cysteine at that position is responsible for the loss of function. One possibility is that this positive charge interacts with another negatively charged amino acid elsewhere in the protein to form a salt bridge that aids in the proper folding or tertiary structure assembly of DMT1. Indeed, conserved charged residues residing within the hydrophobic membrane spanning segments of proteins have been shown to be important for the structure of other membrane transporters such as CFTR and the lactose permease [322;323].

Hopefully, the identification of more human mutations in *DMT1* as well as additional data from *in vitro* mutagenesis experiments will help us better understand the role of this transporter in iron homeostasis and lead to novel treatments for iron-related disorders.

Preface to Chapter 5

Whereas the previous three chapters focused on the importance of conserved residues in Nramp2 function, the next two chapters focus on better understanding its subcellular targeting and trafficking. Prior to the work described in Chapters 5 and 6, a number of studies showed that Nramp2 (isoform II) is expressed at the plasma membrane and in transferrin-positive recycling endosomes at steady-state [42]. Studies by Touret *et al* using an exofacially-tagged Nramp2-HA construct showed that Nramp2 (isoform II) molecules present at the cell surface and in recycling endosomes were in dynamic equilibrium, with surface transporters being continuously internalized via a clathrin and dynamin-dependent process. These studies gave further support to the idea that Nramp2 and transferrin receptor are functionally coupled to effect pH-dependent iron uptake across the endosomal membrane. Examination of the sequence of proposed cytoplasmic domains of Nramp2 isoform II revealed the presence of three putative internalization motifs in the amino and carboxyl terminal regions of the transporter. Therefore, we decided to use a site-specific mutagenesis approach to identify cytoplasmic motif(s) responsible for internalization and recycling of the transporter from the plasma membrane. This work is described in Chapter 5.

Chapter 5:

Carboxyl terminus determinants of the iron transporter DMT1/SLC11A2 isoform II (-IRE/1B) mediate internalization from the plasma membrane into recycling endosomes

ABSTRACT

Mutations in *DMT1* (*Nramp2, Slc11a2*) impair iron metabolism and cause microcytic anemia. DMT1 is expressed at the duodenal brush border where it controls uptake of dietary iron, and is present at the plasma membrane and in recycling endosomes of most cells, where it is necessary for acquisition of transferrin-associated iron. The goal of this study was to identify signal(s) in the cytoplasmic segments of DMT1 responsible for its subcellular targeting and internalization from the plasma membrane into recycling endosomes. We introduced mutations in the amino terminus (ΔNT), carboxyl terminus (ΔCT), as well as in $NPAY^{28-31}$, $YSCF^{62-65}$ and $YLLNT^{555-559}$ motifs of a DMT1 construct bearing an exofacial epitope tag, which allowed labeling of the transporter at the cell surface for kinetic studies. Mutants were stably expressed in LLC-PK_1 kidney cells and were studied for transport activity, sub-cellular localization, cell surface and recycling pool distribution, and internalization from the plasma membrane. Kinetic studies showed that carboxyl terminus mutants (ΔCT and ΔYLLNT) had an increased fraction of the "recycling pool" that was expressed at the cell surface due to impaired internalization from the plasma membrane. Further cell surface labeling and immunofluorescence studies in intact cells showed that the ΔYLLNT and ΔCT mutants were targeted to the lysosomal compartment upon internalization. These results suggest that the major signal for internalization and recycling of DMT1 isoform II (-IRE/1B) resides in its carboxyl terminus and that removal of this signal leads to a default lysosomal targeting.

INTRODUCTION

The Divalent Metal Transporter 1 (DMT1, also known as Nramp2, DCT1, Slc11a2) plays a dual role in intestinal iron acquisition and in iron uptake by peripheral tissues. DMT1 is part of a large family of highly conserved metal transporters. It is an integral membrane phosphoglycoprotein consisting of twelve putative trans-membrane (TM) domains, with the predicted amino and carboxyl termini positioned on the intra-cytoplasmic side of the membrane. Studies in *Xenopus* oocytes and transfected mammalian cell lines have demonstrated that DMT1 transports a number of divalent metals (Fe^{2+}, Mn^{2+}, Co^{2+}, Cu^{2+}, Cd^{2+}, Ni^{2+}, Pb^{2+}, Zn^{2+}) in a pH-dependent fashion by a proton co-transport mechanism [26;27;40]. DMT1 is expressed at the brush border of the absorptive epithelium of duodenal villi [161], where it is responsible for the uptake of non-heme dietary iron following reduction from its ferric (Fe^{3+}) to ferrous (Fe^{2+}) state by a ferric reductase. In non-epithelial cells, iron absorption occurs through internalization of transferrin-bound iron via the transferrin receptor pathway. DMT1 is also expressed at the plasma membrane and in transferrin-positive recycling endosomes of most cells and tissues [40;42]. It catalyzes the efflux of iron from acidified endosomes, across the endosomal membrane into the cytosol [324]. Vacuolar ATPase-mediated endosomal acidification simultaneously facilitates release of iron from transferrin and provides the pH gradient required for DMT1 function [51]. Naturally-occurring mutations in *DMT1* cause severe iron deficiency and microcytic anemia in *mk* mice and *Belgrade* rats [136;141]. Both mutants show the same alteration (G185R) in predicted TM4 of DMT1, which abrogates both intestinal iron absorption and endosomal transport of transferrin-iron [137;138;146;155;325]. Finally, DMT1 is also expressed at the brush border of epithelial cells of proximal tubules of the kidney [172], where it may function as a re-uptake system for divalent metals.

The *DMT1* gene produces at least two distinct mRNAs by alternative splicing of two 3' exons encoding different 3' untranslated regions (UTR) and protein products with distinct C-termini [153;154]. *DMT1* isoform I (+IRE) contains an iron-responsive element (IRE) in its 3' UTR. DMT1 isoform I is expressed at the brush border of duodenal enterocytes where its expression is induced by dietary iron depravation [161;253]. DMT1

isoform I is also expressed in the kidney [161;172]. DMT1 isoform II (-IRE) lacks an IRE and encodes a protein which has a different C-terminal 25 amino acid segment. DMT1 isoform II is expressed preferentially in non-epithelial cells, and is very abundant in reticulocytes [169]. Recently, additional isoforms of DMT1 mRNAs have been identified based on alternate promoter usage at *DMT1* exon 1 (exon 1A vs. 1B) [154]. This alternate promoter usage is predicted to produce a DMT1 protein bearing an additional 29 amino acids (exon 1A) upstream of the previously identified start codon of DMT1 isoforms I and II (exon 1B).The role of these additional residues in the expression, function, and targeting of DMT1 has not yet been studied. Touret and colleagues have demonstrated that DMT1 isoform II, when expressed in transfected CHO and LLC-PK_1 cells, is present at the plasma membrane and in an acidic transferrin receptor-positive endomembrane vesicular compartment. Kinetic studies of an exofacially-tagged DMT1 molecule showed similar amounts of protein in endomembrane compartment(s) and at the cell surface. The two components are in dynamic equilibrium: surface transporters being continuously internalized via a clathrin and dynamin-dependent process [51]. Therefore, proper physiological function of DMT1 in iron metabolism involves not only proper targeting to the plasma membrane, but also requires efficient internalization and recycling via recycling endosomes.

Tyrosine-based motifs (NPXY and YXXΦ, where Φ = bulky hydrophobic) have been shown to act as internalization signals for clathrin-mediated endocytosis [183]. The NPXY motif was initially discovered as a mutation (Y807C) in the cytoplasmic domain of the LDL receptor that abolishes internalization of the receptor [326] in a patient with familial hypercholsterolemia. Mutagenesis studies [327] showed that NPXY is an internalization signal for surface proteins such as the LDL receptor-related protein 1 (LRP1) [328], the EGF receptor [329] and megalin [330]. Several proteins, including clathrin, AP-2, and Dab2, appear to function as recognition proteins for NPXY signals.[183] The YXXΦ motif has also been shown to act as a plasma membrane internalization motif for endocytic receptors such as the transferrin receptor and ion transporters such as the cystic fibrosis transmembrane conductance regulator (CFTR) [183]. YXXΦ motifs have also been implicated in targeting membrane proteins such as LAMP-1 and LAMP-2 to lysosomes.

YXXΦ signals interact with the μ subunits of AP-1 and AP-2 complexes, which in turn recruit clathrin molecules [331-333]. Cytoplasmic dileucine based (LL) motifs of membrane proteins (such as GLUT4) have also been shown to act as signals leading to clathrin-mediated endocytosis or targeting to endosomal-lysosomal compartments [183]. Residues neighboring the LL signals appear to dictate whether clathrin recruitment occurs via AP complexes or via ARF-dependent clathrin adaptors.

Examination of the sequence of proposed cytoplasmic domains of DMT1 reveals the presence of three putative internalization motifs: two tyrosine-based motifs of the forms NPXY and YXXΦ (NPAY$^{28-31}$ and YSCF$^{62-65}$) in the amino terminal region, and a di-leucine motif (LL$^{556-557}$) in the carboxyl terminal region. In the present study, we sought to identify the specific signal(s) in the cytoplasmic segments of DMT1 isoform II responsible for internalization and recycling of the transporter from the plasma membrane.

MATERIALS AND METHODS

Materials

Reagent-grade chemicals were purchased from Sigma Chemical (St. Louis, MO). Monoclonal mouse antibody (Ab) HA.11 directed against the influenza hemagglutinin epitope (HA) was purchased from Covance (Princeton, NJ). Cy2- and Cy3-labeled anti-mouse antibodies and HRP-coupled donkey anti-mouse antisera were purchased from Jackson ImmunoResearch Laboratories (West Grove, PA). The plasmid encoding GFP-fusion protein GFP-syntaxin 13 was the kind gift from Dr. D. Williams (Department of Biochemistry, University of Toronto). The GFP-Lamp1 plasmid was a kind gift from Dr. Patrice Boquet (Institut national de la santé et de la recherché médicale, France).

Plasmids and constructs

Full-length murine *DMT1* (*Nramp2, DCT1, Slc11a2,* GenBank accession no. L33415) isoform II (non-IRE, isoform 1B) cDNA was modified by the in-frame addition of an HA epitope at amino acid position 330, as previously described [26]. Deletion and truncation mutations in DMT1-HA were created by site-directed mutagenesis using oligonucleotide primers listed in Table 1 by a recombinant polymerase chain reaction protocol [308]. For ΔNT, a primer was designed to delete the first 67 amino acids of DMT1, up to first membrane-spanning segment, with the addition of an initiator methionine (Table 1). For ΔCT, a primer was designed to remove 34 amino acids from the carboxyl terminus of DMT1, with the insertion of a stop codon after G534 and an *EcoR* I site for subsequent cloning. Mutants were constructed into the mammalian expression vector, pCB6, using restriction enzyme sites *Xho* I and *BstE* II for mutants ΔNPAY, ΔYSCF, ΔNT and sites *Sac* I and *EcoR* I for mutants ΔYLLNT, ΔCT.

Cell culture, transfection, and immunoblotting

LLC-PK_1 cells were grown at 37°C in a 5% CO_2 incubator in Dulbecco's modified Eagle's medium (Invitrogen) supplemented with 10% fetal bovine serum (growth media). LLC-PK_1 cells were transfected with DMT1-HA/pCB6 vectors using a calcium-phosphate co-precipitation method. Selection of stably transfected clones was

Table 1. Oligonucleotides used for mutagenesis.

Primer Name	Nucleotide sequence (5' to 3')
ΔNPAY For	ccttggcgccatcagcaactcatccc
ΔYSCF For	cctgaggaggagagctttcgtaaac
ΔYLLNT For	gctcagcctgaactcgtggatgctgactcag
ΔNT For	ccgctcgaggccacc**atg**ctgaaactctgggcgttcacggggc
ΔCT Rev	cggaattc<u>tta</u>acccaatgcaatcaaacactgc

For indicates forward; Rev, reverse. **Bold type** indicates the inserted initiator methionine codon for ΔNT. The inserted stop codon for ΔCT is <u>underlined</u>.

Table 2. Summary of subcellular localization of WT and mutant DMT1-HA.

	PM	RE	LE/Lys	ER
WT	+	+	–	–
ΔNPAY	+	+	–	–
ΔYSCF	+	+	–	–
ΔYLLNT	+	–	+	–
ΔNT	–	–	–	+
ΔCT	+	–	+	–

PM: Plasma membrane; RE: Recycling endosomes; LE/Lys: Late endosomes/lysosomes; ER : Endoplasmic reticulum.

done using 1.4 mg/mL G418 (Invitrogen) for 10 to 14 days. Individual colonies were then picked and expanded. Total cell lysates were prepared and separated by SDS-PAGE. Clones showing robust DMT1-HA expression were identified by immunoblotting with mouse anti-HA antibody, as previously described [28].

Calcein divalent metal transport assay

Calcein acetoxymethylester (calcein-AM, Molecular Probes) was prepared as a 500 μM stock solution in dimethyl sulfoxide. Fe^{2+} and Co^{2+} solutions were freshly prepared in deionized water as 2 mM stock solutions of ferrous ammonium sulfate and cobalt chloride, respectively. Measurement of Fe^{2+} and Co^{2+} transport in DMT1-HA-transfected LLC-PK_1cells was done using a fluorescence quenching assay, exactly as we have previously described with CHO cells [26]. Initial rates of metal transport were calculated from the fluorescence quenching curves and results for each transfectant were normalized to activity of wild-type DMT1-HA expressing cells.

ELISA

For all ELISA assays, 2.8 x 10^5 cells/well were seeded in 48-well tissue culture plates and grown to confluency (16 to 24 h). Cells were fixed in phosphate buffered saline (PBS) containing 4% paraformaldehyde for 30 min at 20°C. Blocking, permeabilization, and incubations with antibody were carried out at 37°C. A solution of 5% nonfat milk in PBS was used for blocking and dilution of all antibodies unless otherwise noted. Washes were performed three times with PBS containing 1 mM $MgCl_2$ and 0.1 mM $CaCl_2$ (PBS++). After donkey anti-mouse-HRP secondary Ab incubation, peroxidase activity was detected by incubating cells with HRP substrate (0.4 mg/mL o-phenylenediamine dihydrochloride, Sigma *FAST* OPD; 550 μL/well) according to manufacturer instructions. Reactions were stopped with 150 μL of 3M HCl per well and absorbance readings (492 nm) were taken with a spectrometer. For all assays, background absorbance readings from (a) non-specific binding of secondary Ab, and (b) non-specific binding of primary Ab to vector-transfected cells, were subtracted for each sample.

For quantification of cell surface expression of DMT1-HA at steady state, cells were washed with cold PBS++, fixed, blocked, incubated with anti-HA Ab (1:500) for 90 min, washed, and permeabilized 30 min in 0.1% Triton X-100/PBS. Cells were blocked for 30 min, and labeled with secondary Ab (donkey anti-mouse-HRP Ab, 1:4000) for 1 h. For quantification of total DMT1-HA expression, cells were permeabilized prior to incubation with anti-HA Ab. Cell surface readings were normalized to total DMT1-HA values for each cell clone and were expressed as a percentage.

To quantify cell surface DMT1-HA expression as a percentage of the recycling pool, cells were incubated in anti-HA Ab (1:200) diluted in 2% nonfat milk/RPMI for 3 h at 37°C. To measure surface DMT1-HA molecules, cells were washed with PBS, fixed, blocked, and incubated with secondary Ab. To measure recycling pool DMT1-HA, cells were sequentially permeabilized with 0.1% Triton X-100/PBS, blocked, and incubated with secondary Ab. Cell surface values were expressed as a percentage of total recycling DMT1-HA for each clone.

Immunostaining

Cells were fixed with 4% paraformaldehyde diluted in PBS for 15 to 20 min at 20°C, and where indicated, were permeabilized with 0.1% Triton X-100 in PBS for 30 min at room temperature. Cells were blocked for 30 min in 5% nonfat milk in PBS, followed by consecutive incubations with primary antibodies (mouse anti-HA, 1:500; goat anti-EEA1, 1:100; diluted in blocking solution) and secondary antibodies (goat anti-mouse-Cy3, Donkey anti-mouse-alexa Fluor488, donkey anti-goat-alexa Fluor488; all used at 1:2000) each for 1 h at 20°C. For experiments with live cells, the anti-HA antibody was diluted (1:200) in 2% nonfat milk in RPMI and (where indicated) cells were chased by washing twice and incubating the cells in growth media for 90 min at 37°C. For co-localization with GFP-fusion proteins, cells were transfected 24 h prior to fixation using Lipofectamine2000 (Invitrogen) according to the manufacturer's instructions. Cells were visualized using a Leica IRE DR2 microscope using a 100× oil immersion objective. Digital images were acquired with an Orca II ER camera (Hamamatsu)

operated with the Openlab 3 software (Improvision) installed on an Apple G4 computer. Images were cropped, assembled and labeled using Adobe Photoshop software.

Cell surface biotinylation

Cell surface biotinylation was performed based on a similar technique used to study the internalization of CFTR [334]. LLC-PK_1 cells were grown in 100 mm culture dishes one day post-confluency, followed by 2 washes in PBS++ and one with cold borate buffer pH 9.0 (10 mM boric acid, 154 mM NaCl, 7.2 mM KCl, 1.8 mM $CaCl_2$). Cells were biotinylated for 1 h at 4°C in borate buffer containing 0.7 to 1.0 mg/mL sulfo-NHS-SS-biotin (Pierce). After two 5 min washes with cold RPMI, cells were incubated in pre-warmed RPMI for 0, 30, 60, or 90 min at 37°C in 5% CO_2 at which point endocytosis was halted by three washes with cold PBS++. Cell surface associated biotin molecules were removed (3 washes, 30 min each at 4°C) by treating with the membrane impermeable reducing agent 2-mercaptoethanesulfonic acid (MESNA, 100 mM solution with 50 mM Tris-Cl pH 8.6, 1 mM $MgCl_2$, 0.1 mM $CaCl_2$). For quantification of total surface labeling, cells were similarly treated but with final washes in buffer lacking MESNA. Biotinylated cells were collected and solubilized for 30 min on ice in 350 µL of lysis buffer (1% Triton X-100, 0.2% SDS, 50 mM Tris-Cl pH 7.4, 150 mM NaCl, 20% glycerol) supplemented with protease inhibitors (1 mM phenylmethylsulfonyl fluoride, 1 µM pepstatin, 0.3 µM aprotinin, 1 µM leupeptin). Lysates were pre-cleared by centrifugation (20 min, 10,000*g*, 4°C) and proteins in the supernatant were quantified by Bradford assay (BioRad). Biotinylated proteins (250 µg total protein lysate) were isolated by overnight incubation at 4°C of 100 µL ImmunoPure immobilized strepavidin slurry (Pierce) in a final volume of 1 mL in lysis buffer with protease inhibitors. Strepavidin beads were washed 4 times with cold lysis buffer and bound proteins were eluted with 2× Laemmli buffer at room temperature for 30 min. Proteins were separated by SDS-PAGE followed by immunoblotting with anti-HA Ab. Intensity of immunoreactive bands were quantified by densitometry analysis of exposed films using a Fuji LAS-1000. Background intensity readings (after 0 min endocytosis) were subtracted from all readings and results were expressed as a percentage of total surface labeling for each clone.

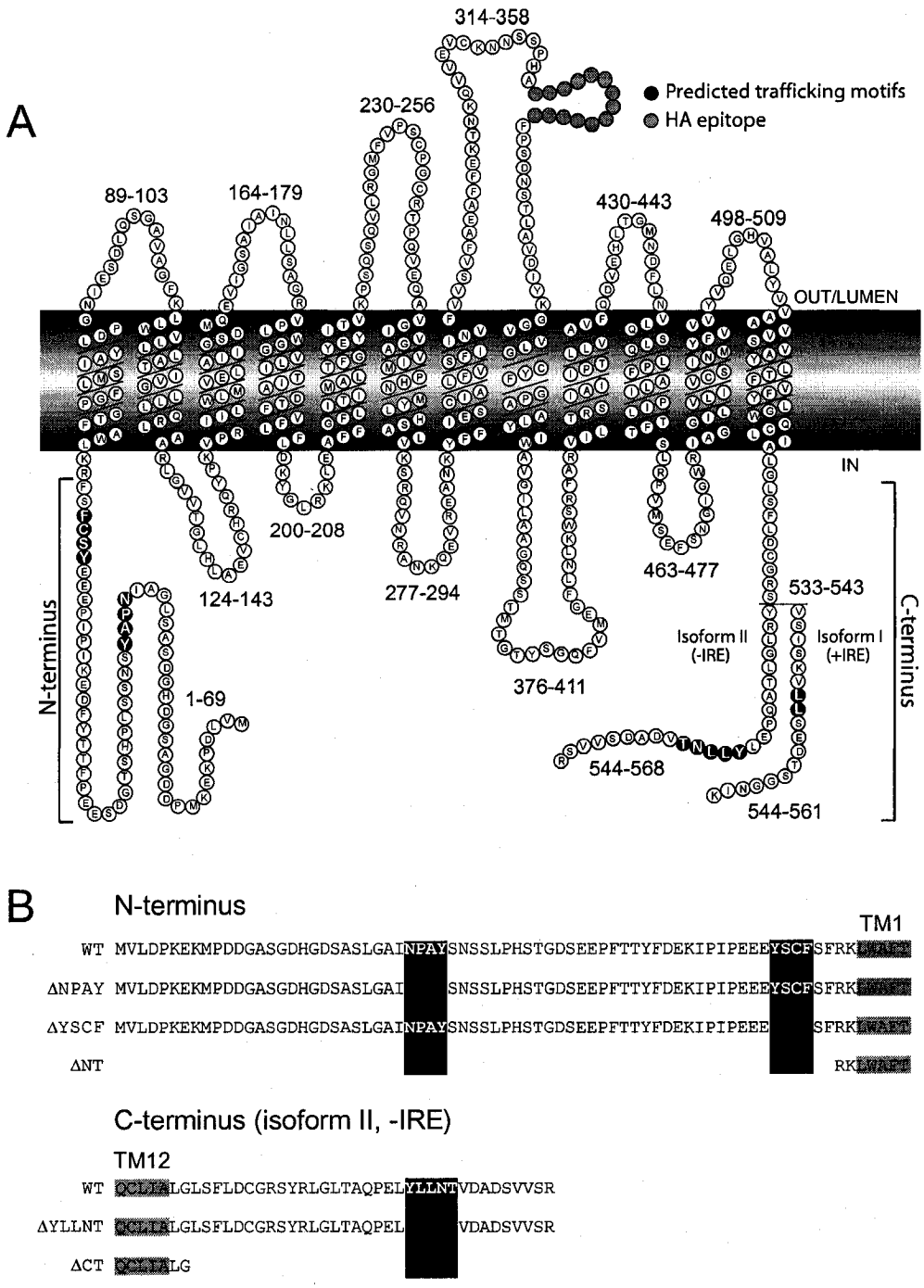

Figure 1. Predicted structural features and membrane topology of DMT1. (A) Schematic representation and membrane topology for mouse DMT1 isoforms I (containing an iron response element; +IRE) and II (-IRE). The amino acid sequence of two isoforms (I and II) is shown. The position and boundaries of the 12 predicted transmembrane (TM) domains and corresponding intra-cytoplasmic and extra-cytoplasmic loops are shown. Highlighted are the positions of the antigenic HA epitope tag inserted between TM7 and TM8 (gray) and the predicted targeting/sorting sequence motifs (black). (B) Schematic representation of mutants harboring deletions of predicted targeting/sorting sequence motifs in the amino (N) and carboxyl (C) termini of mouse DMT1 isoform II tested in this study. Predicted targeting motifs (black) and TM domains 1 and 12 (gray) are highlighted.

RESULTS

Expression and Functional Characterization of DMT1 Mutants

To identify sequences involved in plasma membrane internalization via recycling endosomes, DMT1 isoform II (-IRE, 1B) mutants having independent deletions of the amino terminus (ΔNT), the carboxyl terminus (ΔCT), as well as of NPAY (ΔNPAY), YSCF (ΔYSCF), and YLLNT (ΔYLLNT) signatures were made (Figure 1B). A mouse *DMT1* (isoform II) cDNA backbone was used for mutagenesis, after modification by insertion of an exofacial hemagglutinin (HA) tag into the 4th predicted extracellular loop (delineated by TM7-8; Figure 1A). This enabled recognition of cell surface expressed DMT1 molecules in intact cells. Insertion of an HA tag at this position affects neither expression, transport activity or sub-cellular localization of DMT1 [51]. All *DMT1* mutants were stably transfected in the porcine kidney proximal tubule cell line LLC-PK$_1$, and clones stably expressing individual mutants were isolated. LLC-PK$_1$ cells were chosen since they are derived from the proximal tubule, an abundant site of DMT1 protein expression [172]. These cells are expected to express the necessary machinery and proteins for DMT1 sorting, including recognition of DMT1 targeting and sorting signals. Immunoblot analysis of whole cell extracts (Figure 2A) prepared from wild type (WT) and from the DMT1-HA mutants ΔNPAY, ΔYSCF, and ΔYLLNT displayed 2 immunoreactive bands of ~60 and ~90 kDa, corresponding to the core and complex-glycosylated forms of DMT1, respectively [51]. The C-terminal deletion (ΔCT) was also expressed as 2 immunoreactive variants of slightly faster electrophoretic mobility, consistent with the deletion of the 34 C-terminal residues. Thus, ΔCT, ΔNPAY, ΔYSCF and ΔYLLNT can be expressed and glycosylated in LLC-PK$_1$ cells. The ΔNT construct was expressed as a ~55 kDa variant (Figure 2A), the predicted size of the un-glycosylated truncated species [42;51], suggesting that the N-terminal cytoplasmic domain of DMT1 is essential for proper processing and post-translational modification of the protein.

The ability of the DMT1 variants to transport Fe^{2+} and Co^{2+} at acidic pH (pH 6.0) was tested using a fluorescence-quenching assay [26;28]. LLC-PK$_1$ transfectants were loaded with the metal-sensitive fluorescent dye calcein and the effect of externally added metal on the rate of fluorescence quenching was measured and compared to that of WT DMT1

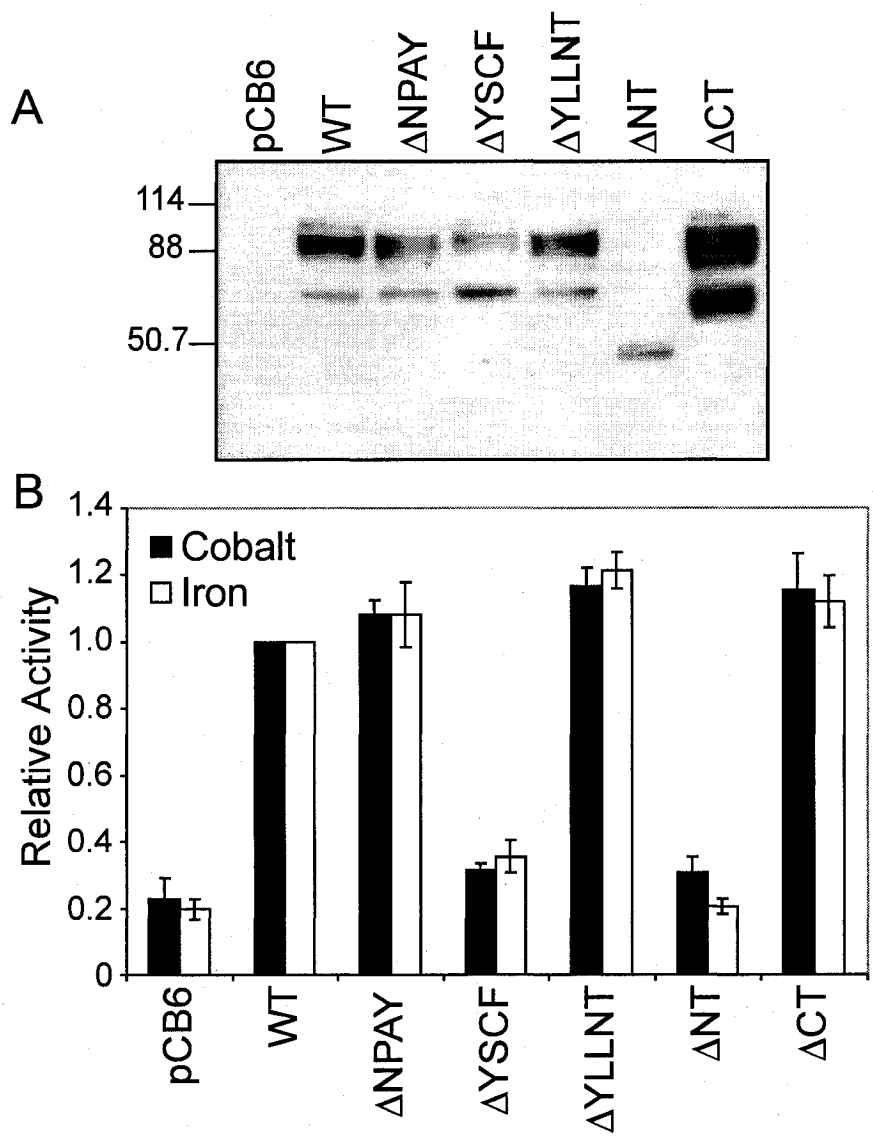

Figure 2. Expression and metal transport activity of DMT1-HA mutants in transfected LLC-PK1 cells. (A) Total cell extracts from LLC-PK1 cells stably transfected with either vector alone (pCB6), wild-type DMT1-HA (WT), or various DMT1-HA deletion mutants were quantified by Bradford protein assay and 25 μg of each lysate was separated by SDS-polyacrylamide gel electrophoresis, followed by immunoblotting with an anti-HA monoclonal antibody. The sizes of the molecular mass markers are indicated. (B) Metal transport activity by WT and mutant DMT1 variants was tested using a fluorescence quenching assay. Cells loaded with a metal-sensitive fluorescent were incubated with Fe2+ or Co2+ in acidic buffer (pH 6.0), and the rate of fluorescence quenching was measured over time. The slopes from initial quenching curves were calculated and transport activity of the mutants was expressed as a percentage of WT activity (relative activity). Error bars = standard error of the means of three or more independent experiments.

(Figure 2B). DMT1 variants ΔNPAY, ΔYLLNT, and ΔCT were fully active for Fe^{2+} and Co^{2+} transport, suggesting that they are expressed at the cell surface and are properly folded in a transport-competent conformation. Cells expressing variants ΔYSCF and ΔNT showed no activity, displaying transport rates similar to cells transfected only with the empty vector (Figure 2B). These results suggest that ΔYSCF and ΔNT are either transport inactive and/or are not efficiently targeted to the proper transport site (plasma membrane and/or recycling endosomes).

Subcellular Localization

To determine whether the mutations we introduced affected DMT1 targeting, the subcellular localization of the different variants was determined by immunoflurescence using an anti-HA monoclonal antibody. In fixed and permeabilized cells, wild type DMT1-HA fluorescence was detected as a punctate and juxtanuclear pattern (Figure 3A) [42;51]. Having previously shown that DMT1-HA isoform II is present and active in syntaxin 13-positive recycling endosomes [51], we examined the effect of the different mutations on targeting to this compartment. Recycling endosomes were labeled by transient transfection of a GFP-syntaxin 13 construct, and DMT1-HA variants were visualized using a secondary antibody coupled to Cy3 (Figure 3A). The ΔNPAY and ΔYSCF variants showed extensive co-localization with syntaxin 13 and shared a pattern similar to that seen for WT DMT1-HA. ΔNPAY and ΔYSCF also showed extensive co-staining with a GFP-transferrin receptor construct (data not shown), confirming that these variants are present in recycling endosomes. These results indicate that the cytoplasmic motifs NPAY and YSCF do not play a major role in targeting DMT1 to early and recycling endosomes. By contrast, the ΔNT variant showed no significant co-localization with GFP-syntaxin 13 and distributed in a more perinuclear pattern possibly corresponding to the endoplasmic reticulum(Figure 3A). The ΔYLLNT and ΔCT variants showed some overlap with GFP-syntaxin 13 (Figure 3A) and with GFP-transferrin receptor (data not shown). However, there was a significant fraction of ΔYLLNT and ΔCT that did not co-localize with the recycling endosome markers.

To determine if any of the mutants were mistargeted to late endosomes and/or lysosomes, we labeled these organelles by transient transfection with a GFP-Lamp1

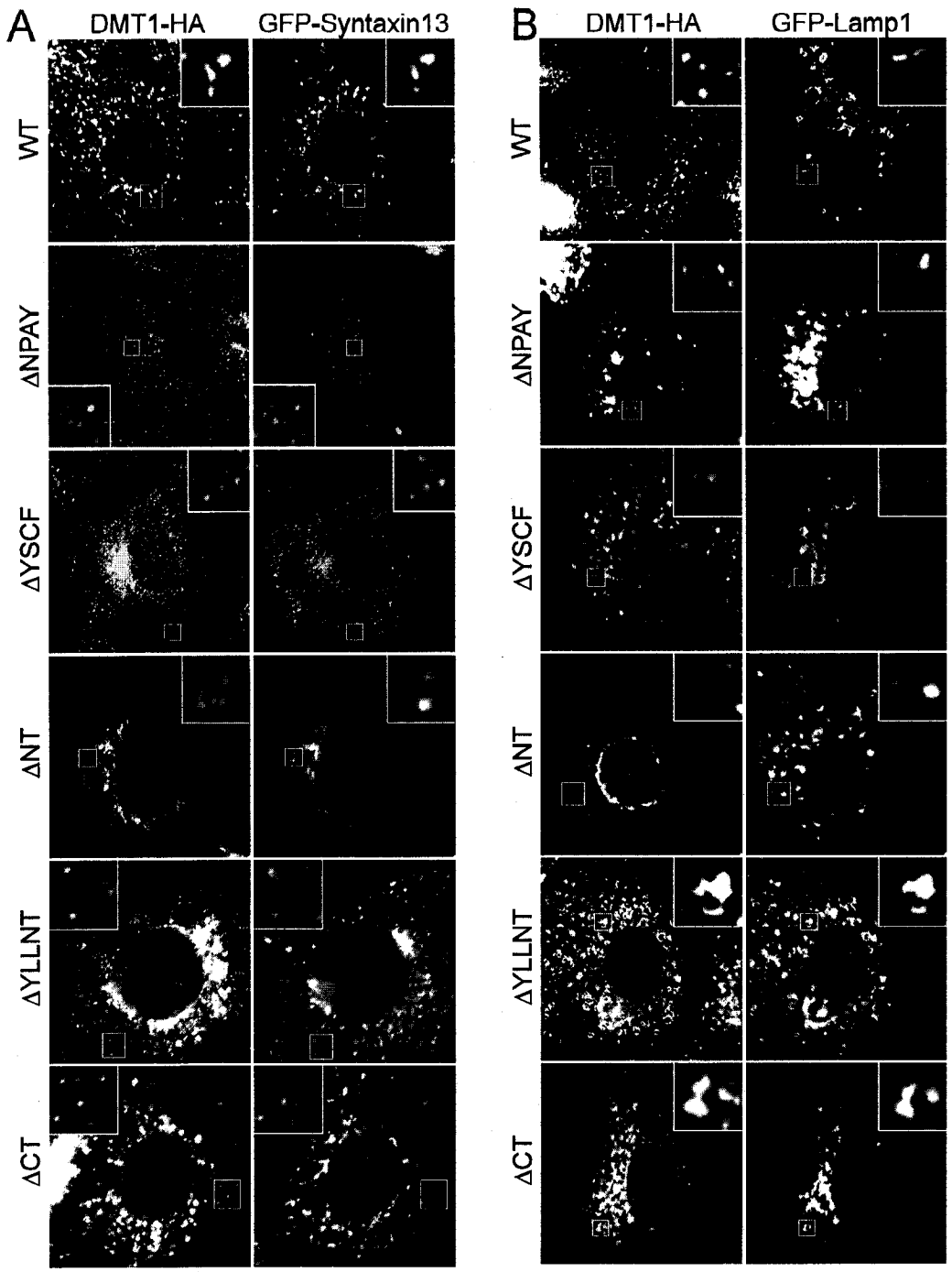

Figure 3. Subcellular distribution of WT and mutant DMT1-HA in endomembrane compartments. LLC-PK1 cells stably expressing WT or mutant DMT1-HA variants (identified) were transiently transfected with either GFP-syntaxin 13 (A) to label recycling endosomes, or GFP-Lamp1 (B) to label lysosomes. 24 hours later, cells were fixed, permeabilized and stained with a monoclonal anti-HA antibody. DMT1-HA molecules were visualized using a secondary anti-mouse Ab coupled to fluorescent Cy3. Images were acquired by epifluorescence microscopy. Insets show magnifications of the area boxed in the figure.

construct. WT DMT1-HA, as well as the ΔNPAY and ΔYSCF variants showed no significant co-staining with GFP-Lamp1. These results are consistent with the extensive co-localization of WT, ΔNPAY and ΔYSCF with recycling endosomes (Figure 3A). The ΔNT variant similarly did not co-localize with GFP-Lamp1 positive lysosomes (Figure 3B). These results suggest that the N-terminus of DMT1 is essential for proper targeting and its deletion results in a protein that is not properly glycosylated (Figure 2A), non-functional (Figure 2B), and is mistargeted to a perinuclear compartment (Figures 3A and 3B). In contrast to the WT and other DMT1-HA variants, ΔYLLNT and ΔCT both displayed significant co-staining with GFP-Lamp1 lysosomes (Figure 3B). These results suggest that the C-terminus of DMT1-HA contains information that is critical for optimal targeting of the transporter to recycling endosomes, and that deletion of this information results in mis-targeting of the protein to late endosomes/lysosomes.

Determinants of Expression at the Cell surface and in the Recycling Compartment

We next examined the effect of the mutations on a) targeting of DMT1 to the cell surface and b) dynamic trafficking through the recycling endosome compartment. The fraction of each DMT1-HA variant present at the cell surface at steady-state was determined by exposing fixed LLC-PK_1 transfectants to anti-HA antibody, with or without prior permeabilization with mild detergent. The amount of bound anti-HA antibody was quantified using a secondary antibody coupled to horse-radish peroxidase. WT DMT1-HA transfectants expressed 29.5 ± 1.4% (mean ± S.E.) of the total DMT1-HA at their cell surface (Figure 4), which is comparable to the fraction we previously determined using radiolabeled antibodies [51]. A significantly higher proportion of variants ΔNPAY and ΔCT was detected at the cell surface (50.1 ± 3.9% and 40.2 ± 2.7%, respectively), while the ΔYSCF and ΔYLLNT variants showed a lower fraction of cell surface expression (17.5 ± 0.2% and 20.5 ±1.2%, respectively). Finally, only a small fraction of the ΔNT variant was expressed at the cell surface (8.8 ± 1.8%). These results suggest that defined sequences in the amino and carboxyl terminal domains of DMT1 play a role in determining the level of DMT1 protein expression at the plasma membrane at steady state.

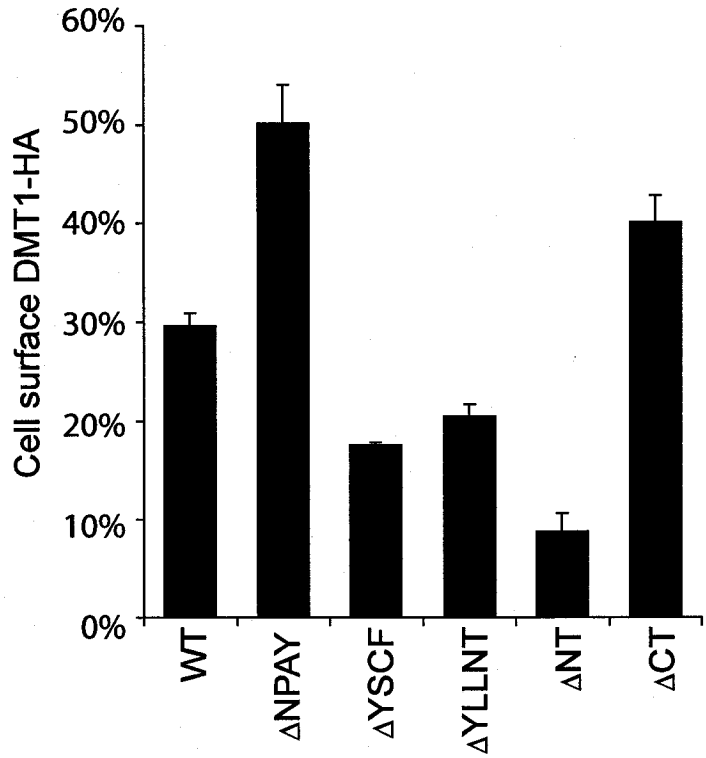

Figure 4. Quantification cell surface DMT1-HA expression at steady-state. LLC-PK1 cells stably expressing individual DMT1-HA variants were fixed and incubated with anti-HA primary antibody with or without prior detergent permeabilization (see Methods). Cells were then incubated with an HRP-coupled secondary anti-mouse antibody, and the amount of bound primary antibody present was determined for both conditions by a colorimetric reaction using o-phenylenediamine dihydrochloride (OPD) followed by spectrometry. The amount of DMT1-HA expressed at the cell surface (in non-permeabilized cells) is shown as a fraction (%) of total protein expression (in permeabilized cells).

Because immunofluorescence studies (Figure 3) indicated that certain variants had a larger fraction of protein associated with either a perinuclear compartment (ΔNT) or with lysosomes (ΔYLLNT, ΔCT), we attempted to visualize the proportion of the recycling pool of WT and variant DMT1-HA that is expressed at the cell surface. For this, live LLC-PK_1 transfectants were incubated with anti-HA antibody (2 h, 37°C), followed by fixation, and incubation with a secondary anti-mouse antibody coupled to a red fluorophore to label DMT1-HA proteins at the cell surface. The same cells were then permeabilized under mild detergent conditions, and total DMT1-HA molecules were labeled with a secondary anti-mouse antibody coupled to a green fluorophore. In these experiments, DMT1-HA molecules at the cell surface are labeled in red while total molecules were labeled in green, with the yellow color in merged images corresponding to the fraction of total labeled DMT1-HA molecules expressed at the cell surface (Figure 5A). This protocol selectively labels only those DMT1-HA molecules that were internalized from the plasma membrane within 2 h, allowing a better determination of the proportion of DMT1-HA at the cell surface *vs.* the intracellular recycling pool. These studies showed that only a small proportion of labeled DMT1-HA is expressed at the cell surface for WT and ΔYSCF, with the majority of protein appearing to be intracellular (Figure 5A). On the contrary, in cells expressing variants ΔNPAY, ΔYLLNT, and ΔCT, a significantly larger proportion of the protein appears to be at the cell surface (yellow staining in Figure 5A). Results for variants ΔNPAY and ΔCT are consistent with the higher expression at the surface detected for these mutants in Figure 4. On the other hand, the high association of ΔYLLNT with the lysosomes noted in Figure 3B may be responsible for the apparent lower surface expression noted in Figure 4. Cells expressing the ΔNT variant showed little if any surface labeling by this method, in agreement with the almost complete association of this mutant with the a perinuclear compartment noted in Figure 3.

The higher proportion of cell surface expression from the total recycling pool detected for variants ΔNPAY, ΔYLLNT, and ΔCT by immunofluorescence (Figure 5B) was further quantified by an ELISA-based assay as described in Materials and Methods. In the case of WT DMT1-HA, 19.3 ± 4.8% of the labeled recycling compartment was

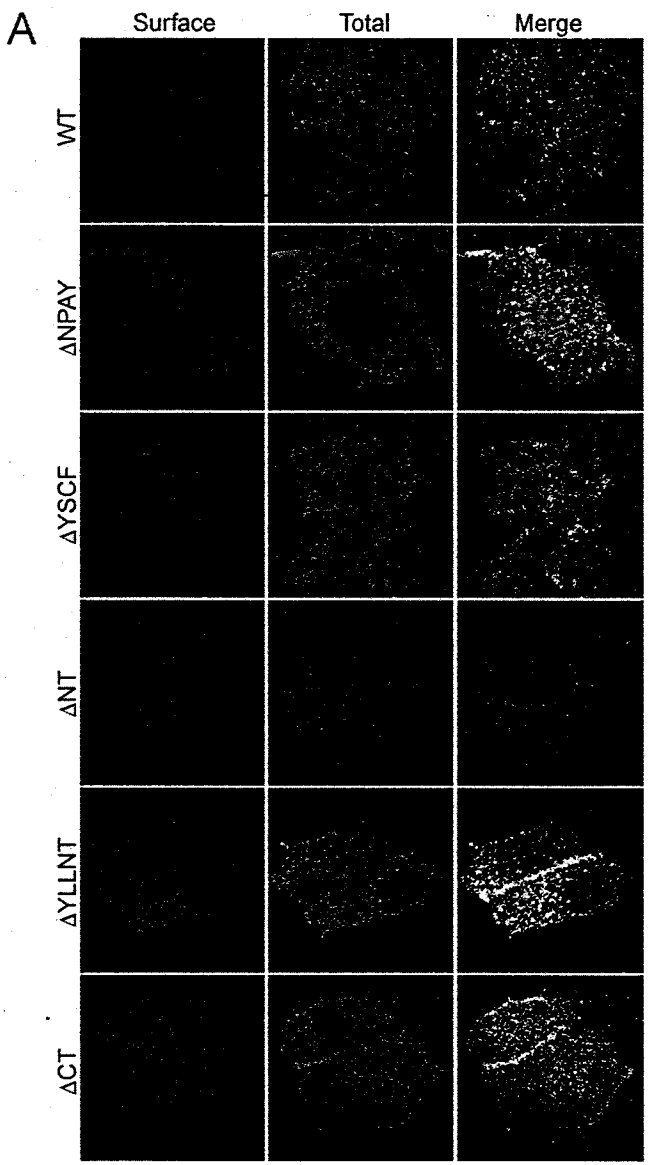

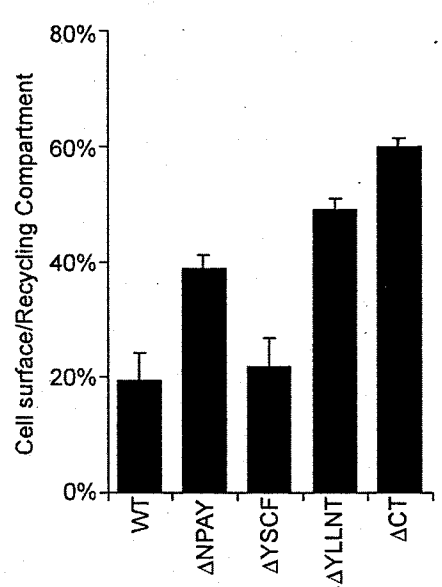

Figure 5. Fraction of the recycling pool expressed at the cell surface for each DMT1-HA variant. (A) Dual labeling of cell surface expressed (Surface; red) and total recycling pool (Total; green) of DMT1-HA variants, with the overlap (Merge; yellow) identifying the fraction of the recycling pool expressed at the cell surface. LLC-PK1 cells stably expressing WT or mutant DMT1-HA were incubated with anti-HA Ab for 2 h at 37°C to label recycling DMT1-HA molecules. Following incubation, cells were fixed and incubated with a secondary anti-mouse antibody coupled to Cy3 (red) to label cell surface DMT1-HA molecules. After washing, cells were permeabilized with detergent and incubated with a secondary anti-mouse antibody coupled to Alexa488 (green) to label total recycling DMT1-HA molecules (plasma membrane plus endosomes). Images were compiled from 0.5 μm confocal microscopy z-plane sections. (B) Quantification of the fraction of the recycling pool of the DMT1-HA variants expressed at the cell surface. The recycling pool, and fraction of the recycling pool expressed at the cell surface for each DMT1-HA variants was labeled as described in (A), except that an HRP-conjugate was used as a secondary antibody for quantification. Results are expressed as the fraction (%) of the total recycling pool of each mutant expressed at the cell surface. Error bars correspond to standard errors on the means from three or more independent experiments.

expressed at the cell surface, and similar results were obtained for the ΔYSCF variant (21.7 ± 5.1%). On the other hand, and in agreement with results in Figure 5A, the ΔNPAY, ΔYLLNT, and ΔCT constructs showed a significantly higher distribution of this recycling pool to the cell surface (38.8 ± 2.4%, 49.0 ± 2.0%, and 60.0 ± 1.6%, respectively). The low level of expression of the ΔNT variant in the recycling pool precluded a similar analysis of this mutant. It is important to note that the extent of surface expression determined for DMT1-HA in intact cells (Figure 5) was somewhat lower than that determined in fixed cells (Figure 4). Therefore, results in Figure 5 may be an underestimate of actual surface expression of DMT1-HA due to incomplete inaccessibility of the HA epitope in native, unfixed cells. However, this does not affect direct comparisons between WT and mutant DMT1-HA expressing cells by either method.

Together, the results in Figures 4 and 5 indicate that the NPAY motif in the amino terminal domain and sequences in the C-terminal domain of DMT1 (including YLLNT), play an important role in directing the traffic of the transporter to and/or from the plasma membrane.

Endocytosis

The noted cell surface accumulation of variants ΔNPAY, ΔYLLNT and ΔCT suggested a potential defect in internalization of these mutants from the PM. To test this possibility, we used a cell surface biotinylation assay to compare the rates of endocytosis of WT and mutant DMT1 variants ΔYLLNT, ΔNPAY, and ΔCT. A similar approach has been previously used to study internalization kinetics of other membrane proteins such as CFTR[334] and the H,K-ATPase [335]. We used cleavable form of biotin (NHS-SS-biotin) to covalently label lysine residues in proteins exposed at the extracellular surface. LLC-PK_1 cell monolayers were biotinylated at 4°C to arrest membrane endocytosis. Following cell surface biotinylation, we raised the temperature of the medium to 37°C for 0 to 90 min to allow internalization of plasma membrane constituents. Biotin molecules remaining at the cell surface were cleaved by washing the cells with the membrane-impermeant reducing agent MESNA. Following cell lysis, biotinylated DMT1-HA molecules were isolated using immobilized streptavidin, followed by SDS-PAGE and immunoblotting with anti-

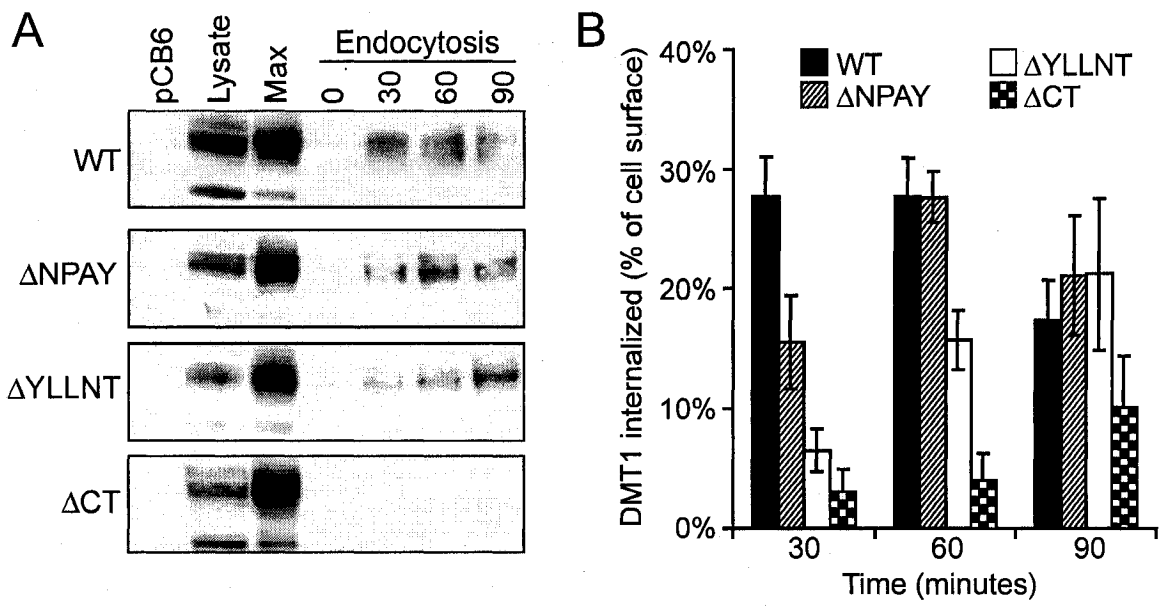

Figure 6. Internalization of DMT1-HA variants from the cell surface. A cell surface biotinylation assay was used to determine the rate of endocytosis of WT and variant DMT1-HA molecules from the plasma membrane. We used a cleavable form of biotin to covalently label all cell surface proteins (see Methods). LLC-PK1 transfectants expressing either WT or ΔNPAY, ΔYLLNT and ΔCT mutant DMT1-HA were labeled with biotin at 4°C to halt endocytosis. After washes, the temperature of the medium was raised to 37°C followed by incubation for 0 to 90 min to allow the internalization of plasma membrane constituents. Biotin molecules remaining at the cell surface were removed with a membrane-impermeant reducing agent. Biotinylated DMT1-HA molecules were isolated from cell lysates with immobilized strepavidin, followed by elution, analysis by SDS-PAGE and immunoblotting with anti-HA Ab. Typical immunoblots from individual experiments are shown in (A). Lysate = 20 μg of unbiotinylated crude cell lysate for each mutant. Max = total surface DMT1-HA expression for each mutant (biotinylated DMT1-HA molecules isolated without prior stripping). (B) Quantification of rates of internalization of DMT1-HA variants from the plasma membrane. Immunoblots were scanned by densitometry, and the amount of DMT1 internalized over time is expressed as a fraction (%) of the total cell surface expression (Max). Error bars correspond to standard errors on the means from three or more independent experiments.

HA antibody. A typical immunoblot is shown in Figure 6A, while quantification from different immunoblots ($n \geq 3$) by densitometry scanning is shown in Figure 6B. In these experiments, controls for equal amounts of labeled lysates introduced in the capture assay (lysate from cells untreated with MESNA), and transferred to membrane (Max) were included for normalization purposes. Using this method, 27.7 ± 3.3% (mean ± S.E.) of surface-labeled DMT1-HA was internalized after 30 min (Figure 6B). Mutant ΔNPAY showed reduced internalization, with 15.7 ± 3.9% after 30 min , but the difference from WT became insignificant after 60 min. On the other hand, mutant ΔYLLNT displayed a more severe deficiency in DMT1-HA internalization (6.5 ± 1.8% internalization after 30 min, 15.7 ± 2.5% after 60 min), while the ΔCT appeared to be completely impaired in this process, with little if any internalization detected (3.0 ± 1.9% after 30 min and 4.0 ± 2.3% after 60 min) (Figure 6B). These results indicate that the C-terminus of DMT1 contains information (including the YLLNT motif) that is essential for rapid endocytosis from the plasma membrane, and consequently mutations in this region lead to accumulation of DMT1 at the cell surface.

The Fate of Internalized DMT1 Molecules

We next investigated whether, once internalized, WT and variant DMT1-HA were targeted to the same endomembrane compartments. To test this, we incubated live LLC-PK1 cells with anti-HA Ab for 2 h at 37°C to label surface and recently internalized DMT1-HA molecules. Following fixation and permeabiliztion, we labeled early endosomes with an antibody against the early endosome marker EEA1. WT DMT1-HA showed significant co-staining EEA1 (Figure 7A), consistent with previous studies with DMT1 isoform II (-IRE, 1B)[51;155]. Interestingly, all variants tested also displayed significant co-staining with EEA1 after 2 h (Figure 7A), with the exception of ΔNT, which showed no co-staining with EEA1 and little anti-HA antibody incorporation. To determine the fate of internalized WT and variant DMT1-HA molecules after a longer incubation period, live LLC-PK1 cells were labeled with anti-HA Ab for 3 h at 37°C. The cells were then washed and chased for an additional 90 min in culture media at 37°C. Lysosomes were labeled by transient transfection with GFP-Lamp1 24 h prior to labeling.

WT DMT1-HA as well as variants ΔNPAY and ΔYSCF showed no significant co-staining with GFP-Lamp1 lysosomes and retained a similar juxtanuclear staining pattern (Figure 7B). These results suggest that WT, ΔNPAY and ΔYSCF proteins are stably recycling from the cell surface and are not targeted to the lysosomes within 90 min of internalization. As expected, ΔNT showed little uptake of anti-HA antibody and no co-staining with GFP-Lamp1 (Figure 7B). Strikingly, however, the ΔYLLNT and ΔCT variants displayed significant co-staining with GFP-Lamp1 lysosomes >90 min after internalization (Figure 7B). These results suggest that the YLLNT motif, and possibly other residues in the C-terminus of DMT1 isoform II, are critical for the recycling of the transporter to the cell surface. Furthermore, this study shows that critical mutations in the C-terminus of DMT1 isoform II result in a transporter that is: (a) internalized with slower kinetics from the cell surface, (b) not efficiently recycled back to the cell surface, and (c) eventually targeted to the lysosomal compartment.

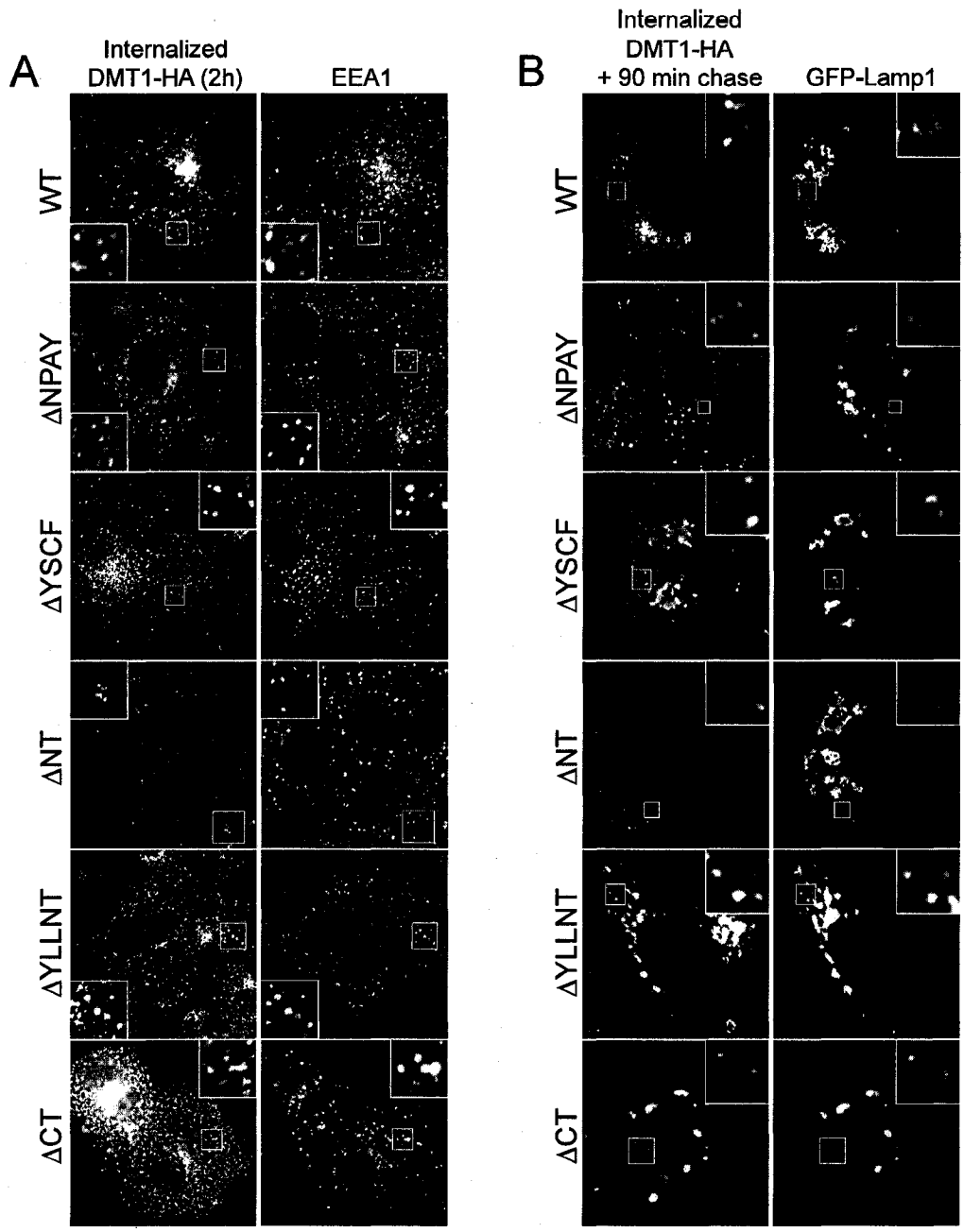

Figure 7. Subcellular localization of internalized DMT1-HA molecules. (A) LLC-PK1 transfectants expressing either WT or mutant DMT1-HA were incubated with anti-HA Ab for 2h to label cell surface and recycling DMT1-HA molecules. Cells were fixed, permeabilized and incubated with an antibody against the early endosomal marker EEA1. (B) LLC-PK1 cells were transiently transfected with the lysosomal marker GFP-Lamp1. 24 h later, surface and recycling DMT1-HA molecules were labeled with anti-HA Ab for 3h, washed and chased by incubation in growth media for 90 min at 37°C. Cells were fixed, permeabilized, and stained with an anti-mouse secondary Ab to visualize DMT1-HA molecules. Images were acquired by epifluorescence microscopy. Insets show magnifications of the area boxed in the figure.

DISCUSSION

In this study, we sought to identify specific signal(s) in cytoplasmic domains of DMT1 responsible for internalization of the transporter from the plasma membrane into recycling endosomes. Truncation of the amino terminal domain of DMT1 (ΔNT) had drastic effects on protein expression and targeting. ΔNT was not properly glycosylated, was transport inactive, and was expressed neither at the plasma membrane, nor in syntaxin 13-positive recycling endosomes or Lamp1-positive lysosomes. ΔNT was found almost exclusively in a perinuclear compartment which was positive for the endoplasmic reticulum marker calnexin (data not shown). These results suggest that an intact amino terminus of DMT1 is essential for processing and stability of the protein.

Deletion of the $NPAY^{28-31}$ motif in the amino terminus of the protein did not have a major effect on either protein function or subcellular targeting. The ΔNPAY variant was transport-competent (Figure 2B) and showed a sub-cellular distribution indistinguishable from that of WT DMT1 (Figure 3). On the other hand, the ΔNPAY mutant showed increased surface expression (Figure 4) and an increased proportion of the recycling pool was present at the cell surface (Figures 4, 5) compared to WT. ΔNPAY showed a somewhat slower rate of internalization (Figure 6B). These results raise the possibility that the NPAY motif may further contribute to internalization of DMT1 in LLC-PK_1 cells. However, this motif appears to be of limited importance when compared to signals in the carboxyl terminus of DMT1 (see below). Finally, we cannot exclude the possibility that the NPAY motif may play additional cell-specific roles in targeting and trafficking of DMT1, which may have gone undetected in LLC-PK_1 kidney cells.

Deletion of the other tyrosine-based motif, $YSCF^{62-65}$, did not have a major effect on the sub-cellular localization of the protein in LLC-PK_1 cells. Like WT DMT1, this mutant was limited to plasma membrane and recycling endosomes (Figure 3). Distribution of the ΔYCSF mutant between the cell surface and endomembranes of the recycling pool was also similar to WT protein. Thus, the YSCF motif appears to be neither critical for DMT1 targeting nor recycling in LLC-PK_1 cells. However, ΔYSCF was clearly transport incompetent (Figure 2B), suggesting that some or all of the residues in $YSCF^{62-65}$ are required for transport. This requirement may involve a direct role for

these residues in the transport process. However, the lower level of expression of this mutant (Figure 2A) may also contribute to the mutant's inactivity.

On the other hand, alterations in the predicted carboxyl terminal intracellular domain of DMT1 had the most dramatic effects on DMT1 targeting and recycling. Truncation of the entire carboxyl terminal domain (ΔCT) or deletion of the YLLNT (ΔYLLNT) motif did not significantly affect either the level of protein expression in LLC-PK_1 transfectants, or their transport properties (Figure 2), suggesting that these regions are not critical for activity or stability. A small fraction of ΔCT and ΔYLLNT was detected in the syntaxin 13-positive recycling endosomes (Figure 3A), suggesting that a part of these variants was properly targeted. However, the C-terminal domain variants showed robust co-localization with Lamp1-positive lysosomes, both at steady state (Figure 3B) and after a transient labeling of internalized DMT1-HA molecules, 90 min after endocytosis (Figure 7B). Interestingly, both ΔCT and ΔYLLNT variants displayed an increased fraction of the "recycling pool" expressed at the cell surface when compared to WT (Figure 5). This increased accumulation at the plasma membrane may be explained by a defect in internalization of these variants that we measured by surface biotinylation (Figure 6). These results implicate the YLLNT sequence of DMT1 as a critical motif for internalization from the plasma membrane. Other carboxyl terminal residues of DMT1 may additionally contribute to internalization since truncation of the entire carboxyl terminus causes a more severe defect than that seen in the YLLNT mutant.

Previous studies have shown that WT DMT1 isoform II is rapidly internalized via a clathrin and dynamin dependent mechanism and is efficiently targeted back the cell surface by means of recycling endosomes [51]. The impaired internalization and accumulation in the lysosomes of the C-terminal domain mutants suggests a model whereby, in the absence of the YLLNT motif, DMT1 is subject to a default lysosomal targeting. In this model (Figure 8), DMT1 recruits specific adaptor proteins required for rapid clathrin-mediated endocytosis through binding to its YLLNT motif. DMT1 is internalized into early endosomes and the recruited adaptor complexes are involved in signaling the recycling of the transporters back to the cell surface via recycling

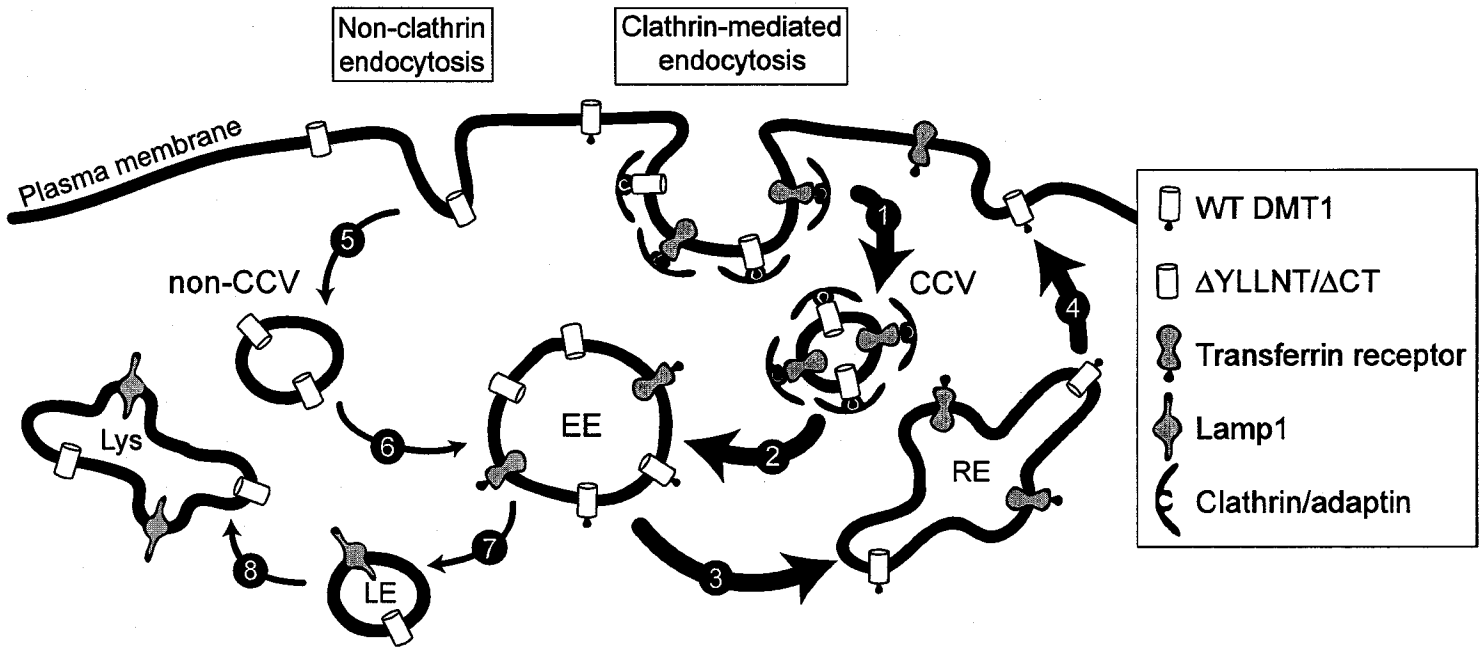

Figure 8. Schematic model for endocytosis of cell surface-expressed WT and C terminus mutant DMT1 molecules. Clathrin molecules interact with cell surface DMT1 molecules via adaptins (Ap-1, Ap-2) that specifically recognize the tyrosine-based motif YLLNT. This causes formation of DMT1 enriched clathrin-coated pits on the cell surface, which are rapidly internalized (step 1) by a dynamin-dependent process into clathrin-coated vesicles (CCV). DMT1-containing CCVs are then sorted to the early endosome compartment (EE, step 2) and eventually recycled back to the cell surface via sorting to the recycling endosome compartment (RE, steps 3 and 4) along with the transferrin receptor. In contrast, DMT1 C-terminus mutants which lack the tyrosine-based sorting motif (ΔYLLNT, ΔCT), are internalized less rapidly by a clathrin-independent mechanism (such as bulk pinocytosis) into non-CCVs (step 5) and are sorted to EE (step 6). The mutant DMT1 proteins are recycled much less efficiently compared to WT and are eventually sorted to the Lamp1-positive late endosome and lysosome compartments (steps 7 and 8).

endosomes (Figure 8). Indeed, proper interaction with clathrin has been previously shown to be critical for internalization and trafficking of certain membrane proteins through recycling endosomes, most notably the transferrin receptor [336;337]. The recruitment of adaptor complexes (Ap1/μ1B) has been shown to be critical for efficient recycling of both the transferrin and LDL-receptors to the basolateral membrane in epithelial cells [338]. In contrast, the C-terminal domain mutants, which lack the YLLNT motif, are unable to recruit clathrin/adaptor complexes and are internalized into early endosomes by a kinetically slower mechanism such as bulk pinocytosis (Figure 8). However, the failure of the C-terminus mutants to recruit specific adaptors disrupts their proper sorting to recycling endosomes and leads to an accumulation in lysosomes. Ultimately, our data does not favour the existence of a true lysosomal targeting motif in DMT1 isoform II, but rather that the lysosome may be the default pathway for the transporter.

Recently, Tabuchi and colleagues observed that in transfected HEp-2 larynx carcinoma cells, the DMT1 isoform I is targeted to the late endosome/lysosome compartment, while isoform II is targeted to the early endosomes of these cells [155]. They demonstrated that the 36 carboxy terminal residues of DMT1 isoform II are important for targeting to early endosomes and alterations in the YXLXX motif (YLLNT) in isoform II impair targeting to early endosomes and cause accumulation of the mutants in Lamp2-positive late endosomes/lysosomes. The authors concluded that the targeting signal for early endosomes dominate over signals for late endosomes/lysosomes in DMT1 isoform II. Our results agree that critical C-terminus mutations in DMT1 isoform II (ΔYLLNT, ΔCT) cause significant colocalization of the transporter with Lamp1/2-positive lysosomes. However, our data suggests that the YLLNT motif is more critical for transporter recycling since, upon internalization of ΔYLLNT/ΔCT from the PM, there was partial co-localization with EEA1-positive early endosomes but not Syntaxin 13-positive recycling endosomes (Figure 7A). Tabuchi and colleagues also showed that the C-terminus of DMT1 isoform II, when fused to a plasma membrane marker (TAC antigen), results in early/recycling endosome targeting [155]. This result is consistent our cell surface biotinylation data (Figure 6) that shows the YLLNT motif is also critical for endocytosis from the plasma membrane.

Cytoplasmic dileucine-based (LL) motifs of membrane proteins have been shown to act as signals leading to clathrin-mediated endocytosis in other transporters such as the glucose transporter GLUT4 [339] and the copper transporter Menkes (MNK) [340-342]. In most proteins, residues preceding the LL signals appear to dictate the method of clathrin recruitment. Dileucine-based signals usually fit the [DE]XXXL[LI] or DXXLL consensus motifs. [DE]XXXL[LI] signals are specifically recognized by AP complexes. Conversely, DXXLL signals are recognized by another family of adaptors known as GGAs, a recently described family of ARF-dependent clathrin adaptors [183]. The residues preceding the dileucine motif in DMT1 isoform II ($ELYLL^{553-557}$) do not correspond to the traditional [DE]XXXL[LI] motif but resemble the DXXLL consensus signature. It has been demonstrated that mutations at either the D or LL residues of the DXXLL cause retention of the mannose-6-phosphate receptor at the cell surface [343], a behavior resembling that of DMT1 mutants ΔCT and ΔYLLNT mutants studied here in LLC-PK_1 cells. This suggests that the $ELYLL^{553-557}$ sequence of DMT1 may function as a DXXLL signal. Although the dileucine motif in DMT1 resembles the DXXLL consensus with a glutamate (E) substituting for aspartate (D), it remains to be determined whether or not they act the same way and whether DMT1 recruits GGAs via this motif. Indeed, previous studies of M6PR mutants have shown that the isoelectric substitution of aspartate in the DXXLL consensus sequence for glutamate is not well tolerated [344]. Furthermore, the aspartate in classical DXXLL motifs is generally found in the context of a cluster of acidic residues, which is not the case for the DMT1 dileucine signal. Thus, the DMT1 dileucine motif $ELYLL^{553-557}$ may be a novel functional variant of DXXLL, or may represent a novel signal for endocytosis of membrane proteins from the cell surface.

Taken together, our results indicate that determinants of the carboxyl terminus cytoplasmic domain of DMT1 play a critical role in internalization of the protein from the plasma membrane and for recirculation in recycling endosomes. Elimination of these signals impairs internalization, and re-directs the internalized DMT1 proteins to the lysosomal compartment, which appears to act as a default pathway for such DMT1 variants.

Preface to Chapter 6

Alternate splicing of *Nramp2* pre-mRNA at 3' exons generates two protein isoforms (I and II) differing only in their carboxyl terminal segments [153]. Although simultaneous expression of both isoforms of *Nramp2* mRNA was detected in some tissues, isoform I is predominantly expressed in epithelial cells while isoform II is predominantly expressed in erythroid cells [40;155;160]. The significance of this tissue-specific expression pattern, including a possible physiological advantage, was unclear and needed to be investigated.

At the subcellular level, it was known that both isoforms are expressed at the plasma membrane but exhibit different steady-state targeting. While isoform II is expressed in early and recycling endosomes, other studies suggested that isoform I is present in late endosomes and lysosomes [42;51;155]. Work by Tabuchi and colleagues showed that a YLLNT motif in the carboxyl terminus of Nramp2 isoform II is responsible for the early endosome targeting of the protein [155]. The work described in the previous chapter showed that the same YLLNT motif in isoform II is responsible for internalization of Nramp2 from the plasma membrane and recycling of the transporter back to the cell surface [184]. In contrast, much less was known about the subcellular distribution, targeting, and dynamic trafficking of Nramp2 isoform I. Therefore, we decided to investigate possible trafficking differences between isoforms I and II by expressing and characterizing exofacially tagged Nramp2-HA proteins in an epithelial cell line. This work is described in the next chapter (Chapter 6).

Chapter 6:

Distinct targeting and recycling properties of two isoforms of the iron transporter DMT1 (NRAMP2, Slc11a2)

ABSTRACT

The metal transporter DMT1 (Slc11a2) plays a vital role in iron metabolism. Alternative splicing of the 3' exon generates two DMT1 isoforms with different C-terminal protein sequences, and 3' untranslated region harboring (isoform I, +IRE) or not (isoform II, -IRE) an iron responsive element. Isoform I is expressed at the plasma membrane of certain epithelial cells, including the duodenum brush border where it is essential for absorption of nutritional iron. Isoform II is expressed in many cells and is essential for acquisiton of transferrin iron from acidified endosomes. The targeting and trafficking properties of DMT1 isoforms I and II were studied in transfected LLC-PK_1 kidney cells, with respect to isoform-specific differences in function, subcellular localization, endocytosis kinetics, and fate upon internalization. Isoform I showed higher surface expression and was internalized from the plasma membrane with slower kinetics than isoform II. As opposed to isoform II, which is efficiently sorted to recycling endosomes upon internalization, isoform I was not efficiently recycled and was targeted to lysosomes. Thus, alternative splicing of *DMT1* critically regulates the subcellular localization and site of Fe^{2+} transport.

INTRODUCTION

Our knowledge and understanding of iron metabolism has increased remarkably in recent years. Much of this knowledge stems from the discovery of proteins that play key roles in iron absorption and regulation, including the identification of membrane iron transporters [251]. One such transporter, the divalent metal transporter 1 (DMT1, also called Nramp2 or Slc11a2), is essential for intestinal iron acquisition and for iron uptake by peripheral tissues. DMT1 is an integral membrane phosphoglycoprotein consisting of twelve predicted trans-membrane segments (TM). DMT1 is part of a large, highly conserved family of metal transporters and has been shown to transport a number of divalent metals (Fe^{2+}, Mn^{2+}, Co^{2+}, Cu^{2+}, Cd^{2+}, Ni^{2+}, Pb^{2+}, Zn^{2+}) in a pH-dependent fashion by a proton co-transport mechanism [26;27;40].

Genetic studies have shown that *DMT1* plays a key role in iron metabolism. A G185R mutation in *DMT1* causes microcytic anemia and iron deficiency in the *mk* mouse and in the *Belgrade* rat, two rodent models of iron deficiency [136-138;141;146;148]. These animals show impaired iron uptake at the duodenal brush border, but are also defective in iron acquisition in peripheral tissues, including erythroid precursors [138;140;143;144]. The G185R mutation likely causes mis-folding of the protein, resulting in altered subcellular localization [147;148;169;172], improper maturation, increased rate of degradation[148], and impairs transport activity. Recently, a human patient suffering from severe congenital hypochromic microcytic anemia and iron overload, was shown to be homozygote for a mutation in *DMT1* ($DMT1^{G1285C}$) [4;259]. The human mutation had two effects: it severely impaired proper splicing of *DMT1* mRNA and introduced an amino acid polymorphism (E399D) in the remaining properly spliced transcript found in the patient. The E399D mutation does not in itself affect expression, function, or targeting of the DMT1 protein [262;345], and thus reduced DMT1 function in this patient is caused by reduced levels of DMT1 expression (improper splicing).

Two major *DMT1* protein isoforms generated by alternative splicing at 3' exons have been identified [153]. Isoform I (+IRE) has an iron responsive element (IRE) in the 3' untranslated region, whereas isoform II (-IRE) lacks the IRE. In addition, the C-terminal 18 amino acids of isoform I are replaced by an alternate 25-amino acid segment in

isoform II. DMT1 isoform I is predominantly expressed in epithelial cells while isoform II is predominantly expressed in erythroid cells. Indeed, isoform I protein is expressed in enterocytes at the duodenal brush border [161] and in epithelial cells lining the kidney proximal tubule [172], while isoform II is expressed abundantly in reticulocytes [169]. However, preferential expression of each isoform is not necessarily mutually exclusive: simultaneous expression of both *DMT1* isoforms I and II mRNAs level has been observed in several tissues including kidney, thymus, and liver [40;155;160]. Recently, additional isoforms of *DMT1* mRNAs have been identified based on alternate promoter usage at *DMT1* exon 1 (exon 1A vs. 1B) [154]. This alternate promoter would produce a predicted DMT1 protein with an additional 29 amino acids (exon 1A) upstream of the previously identified start codon of DMT1 isoforms I and II (exon 1B). However, the role of these additional residues in the expression, function, and targeting of DMT1 has not yet been explored.

Although both DMT1 isoforms are expressed at the plasma membrane, isoforms I and II appear to show different subcellular targeting at steady-state. While in transfected LLC-PK_1, CHO and RAW cells, DMT1 isoform II is expressed in early and recycling endosomes [42;51] studies in transfected HEp-2 cells indicate that isoform I is present in late endosomes and lysosomes [155]. Recent studies using an exofacially-tagged DMT1 molecule have furthered our understanding of isoform II trafficking: isoform II molecules present at the cell surface and in recycling endosomes are in dynamic equilibrium, with surface transporters being continuously internalized via a clathrin and dynamin-dependent process [51]. Tabuchi and colleagues have shown that a $YXLXX^{555\text{-}559}$ motif in the C terminus of DMT1 isoform II is responsible for the early endosome targeting of the protein, with mutations in this motif resulting in lysosomal localization [155]. Recently, we have shown that critical residues in the C terminus of DMT1 isoform II, including the $YXLXX^{555\text{-}559}$ signal, are required for the transporter's internalization from the cell surface and its recycling back to the plasma membrane.[184] Removal of an intact $YXLXX^{555\text{-}559}$ motif appears to cause lysosomal targeting by default.

While DMT1 isoform II trafficking has been well studied, much less is known about the subcellular distribution, targeting and dynamic trafficking of the DMT1

intestinal isoform I. Whereas isoform I lacks the YXLXX signal present in isoform II, close examination of the C terminus of isoform I reveals the presence of a dileucine motif ($LL^{550-551}$). Dileucine-based (LL) motifs present in a number of membrane proteins have been alternately shown to act as signals for clathrin-mediated endocytosis or targeting to various endosomes/lysosomes [183]. In this study, we wanted to investigate possible trafficking differences between isoform I and II of DMT1. We expressed exofacially tagged DMT1-HA proteins in a porcine kidney epithelial cell line and studied differences between expression, function, subcellular localization, internalization kinetics, and fate upon internalization of DMT1 isoforms I and II. We found that DMT1 isoform I is internalized with slower kinetics from the cell surface compared to isoform II. This results in an increased proportion of isoform I expressed at the plasma membrane, perhaps favoring iron transport at this site in epithelial cells.

MATERIALS AND METHODS

Materials and plasmids

All reagent-grade chemicals were purchased from Sigma Chemical (St. Louis, MO). Monoclonal mouse antibody (Ab) HA.11 directed against the influenza hemagglutinin epitope (HA) was purchased from Covance (Princeton, NJ). Cy3-labeled anti-rabbit and anti-mouse Abs and HRP-coupled donkey anti-mouse Ab were purchased from Jackson ImmunoResearch Laboratories (West Grove, PA). Plasmids encoding GFP-fusion proteins were kind gifts from Dr. D. Williams (Department of Biochemistry, University of Toronto; GFP-syntaxin 13) and Dr. Patrice Boquet (Institut national de la santé et de la recherché médicale, France; GFP-lamp1). Full-length murine *DMT1* isoform I (+IRE, isoform 1A) and isoform II (-IRE, isoform 1B) cDNAs were modified by the in-frame addition of an HA epitope in the fourth extracellular loop, as previously described [26].

Cell culture, transfection, and immunoblotting

LLC-PK_1 cells were cultured in a 37°C/5% CO_2 incubator in Dulbecco's modified Eagle's medium (Invitrogen) supplemented with 10% fetal bovine serum (growth media). Cells were transfected with DMT1-HA/pCB6 vectors using Lipofectamine2000 (Invitrogen) according to the manufacturer's instructions. Selection of stably transfected clones was done using 1.4 mg/mL G418 (Invitrogen) for 14 days. Individual colonies were then isolated and expanded. Total cell lysates were prepared and separated by SDS-PAGE. Clones showing robust DMT1-HA expression were identified by immunoblotting with mouse anti-HA antibody, as previously described [28].

Calcein divalent metal transport assay

Calcein acetoxymethylester (calcein-AM, Molecular Probes) was prepared in dimethyl sulfoxide. Fe^{2+} and Co^{2+} solutions were freshly prepared in deionized water as 2 mM stock solutions of ferrous ammonium sulfate and cobalt chloride, respectively. Measurement of metal transport in DMT1-HA-transfected LLC-PK1 cells was done using

a fluorescence quenching assay as we have previously described [262]. Initial rates of metal transport (quench rates) were calculated from the fluorescence quenching curves.

Immunostaining

Cells were fixed with 4% paraformaldehyde/PBS for 20 min and where indicated, were blocked and permeabilized with 0.2% saponin/5% non-fat milk/PBS for 30 min. For co-localization with EEA1 (Fig. 5A), cells were blocked in 5% nonfat milk (30 min) and permeabilized with 0.1% Triton X-100/PBS (30 min) following fixation. All antibody incubations were performed for 1 h at room temperature and diluted in blocking solution unless otherwise indicated. Primary Abs were used at the following dilutions: rabbit anti-DMT1, 1:200; mouse anti-HA 1:100; goat anti-EEA1, 1:200; while corresponding secondary Abs (goat anti-rabbit Cy3, goat anti-mouse Cy3, donkey anti-goat Alexa 488, respectively) were each used at 1:1000. For co-localization with GFP-fusion proteins (Fig. 2 and Fig. 5B), cells were transfected with GFP-syntaxin 13 or GFP-lamp1 plasmids 24 h prior to fixation using Lipofectamine2000. For labeling of cell surface DMT1-HA molecules (Fig. 3A), cells were fixed, blocked in 5% non-fat milk for 30 min, labeled with anti-HA primary Ab and the secondary Ab without permeabilizing the cells with detergent. For experiments with live cells (Fig. 5), anti-HA antibody was diluted (1:200) in RPMI medium and (where indicated) cells were chased by washing twice and incubating the cells in growth media for 90 min at 37°C. Cells were visualized using an Axiovert 200M epi-fluorescence microscope with a 100× oil immersion objective. Digital images were acquired with a Zeiss AxioCam HRm camera operated with AxioVision 4.3. Images were cropped, assembled and labeled using Adobe Photoshop and Illustrator softwares.

Measurement of surface DMT1-HA at steady-state

Quantification of the proportion of DMT1-HA molecules expressed at the cell surface has been previously described [262]. Briefly, LLC-PK_1 cells were grown to confluency in 48-well culture plates and fixed with 4% paraformaldehyde for 30 min. Cells were blocked in 5% non-fat milk in PBS for 30 min, incubated with anti-HA Ab

(1:500) for 90 min, washed and incubated with secondary Ab (donkey anti-mouse-HRP Ab, 1:4000) for 1 h. For quantification of total DMT1-HA expression, cells were permeabilized by incubation with 0.1% Triton X-100/PBS for 30 min prior to incubation with anti-HA Ab. Peroxidase activity was detected by incubating cells with HRP substrate (0.4 mg/mL o-phenylenediamine dihydrochloride, Sigma FAST OPD) according to manufacturer instructions. Reactions were stopped after 30 min with 3M HCl and absorbance readings (492 nm) were taken with a spectrometer. For all assays, background absorbance readings from (a) non-specific binding of secondary Ab, and (b) non-specific binding of primary Ab to vector-transfected cells, were subtracted for each sample. Cell surface readings were normalized to total DMT1-HA values for each cell clone and were expressed as a percentage.

Cell surface biotinylation

Measurement of DMT1 internalization by cell surface biotinylation has been previously described [184]. Briefly, confluent LLC-PK1 monolayers were biotinylated at 4°C in borate buffer pH 9.0 containing 1 mg/mL sulfo-NHS-SS-biotin (Pierce). Cells were washed and incubated in pre-warmed RPMI for 0, 30, 60, or 90 min at 37°C at which point endocytosis was halted by washes with cold PBS. Cell surface associated biotin molecules were removed by 3 cold washes with the membrane impermeable reducing agent 2-mercaptoethanesulfonic acid (MESNA, 100 mM solution). For quantification of total surface labeling, cells were similarly treated but with final washes in buffer lacking MESNA. Biotinylated cells were collected and solubilized in lysis buffer with protease inhibitors. Lysates were pre-cleared by centrifugation and protein yield was quantified. Biotinylated proteins (200 μg total protein lysate) were isolated by overnight incubation at 4°C with 100 μL of ImmunoPure immobilized strepavidin slurry (Pierce) in a final volume of 1 mL in lysis buffer. Strepavidin beads were washed 4 times with cold lysis buffer and bound proteins were eluted with 2× Laemmli buffer at room temperature for 30 min. Proteins were separated by SDS-PAGE followed by immunoblotting with anti-HA Ab. Intensity of immunoreactive bands were quantified by densitometry analysis of exposed films using a Fuji LAS-1000. Background intensity

readings (after 0 min endocytosis) were subtracted from all readings and results were expressed as a percentage of total surface labeling for each clone.

RESULTS

Expression and function of DMT1 isoforms I and II

To investigate the subcellular localization and trafficking properties of the two DMT1 protein isoforms, we modified mouse *DMT1* isoforms I and II cDNAs by insertion of an exofacial hemagglutinin (HA) tag into the extracellular loop of the protein defined by predicted TM7 and 8 (Figure 1A). This exofacial tag enabled us to label and track cell surface expressed DMT1-HA molecules in intact cells. We have previously shown that insertion of an HA tag at this position does not affect expression, transport activity or subcellular localization of DMT1 [51]. We generated stably transfected cells expressing DMT1 isoforms I and II in the porcine kidney cell line LLC-PK_1. LLC-PK_1 cells were chosen since they are derived from the kidney proximal tubule, an abundant site of DMT1 protein expression in normal tissues [172]. Therefore, these cells are likely to express the necessary cellular machinery for proper DMT1 trafficking, including the recognition of sorting and targeting signals. Figure 1C illustrates a representative immunoblot of cell extracts prepared from two independent LLC-PK_1 cell clones expressing different levels of DMT1 isoforms I or II. In each case, a minor species at ~60 kDa and a major species at ~90 kDa were observed. Previous studies from our group have shown that these two populations correspond to core and complex glycosylated species of DMT1, respectively.[51] These observations show that both isoforms of DMT1 are stably expressed and glycosylated to a similar extent in LLC-PK_1 cells. Experiments with the protein translation inhibitor cycloheximide revealed that DMT1 isoforms I and II show similar stability in LLC-PK_1 cells (supplementary data). Finally, we tested the ability of DMT1 isoforms I and II to transport divalent metals (Fe^{2+} and Co^{2+}) at acidic pH by calcein fluorescence quenching. Independent clones from both DMT1 isoforms I and II showed robust transport activity compared to vector-transfected cells (pCB6). No difference in transport rates or ion selectivity between the two isoforms was detected, indicating that both isoforms are expressed at the cell surface and properly folded in a transport-competent manner (Figure 1D).

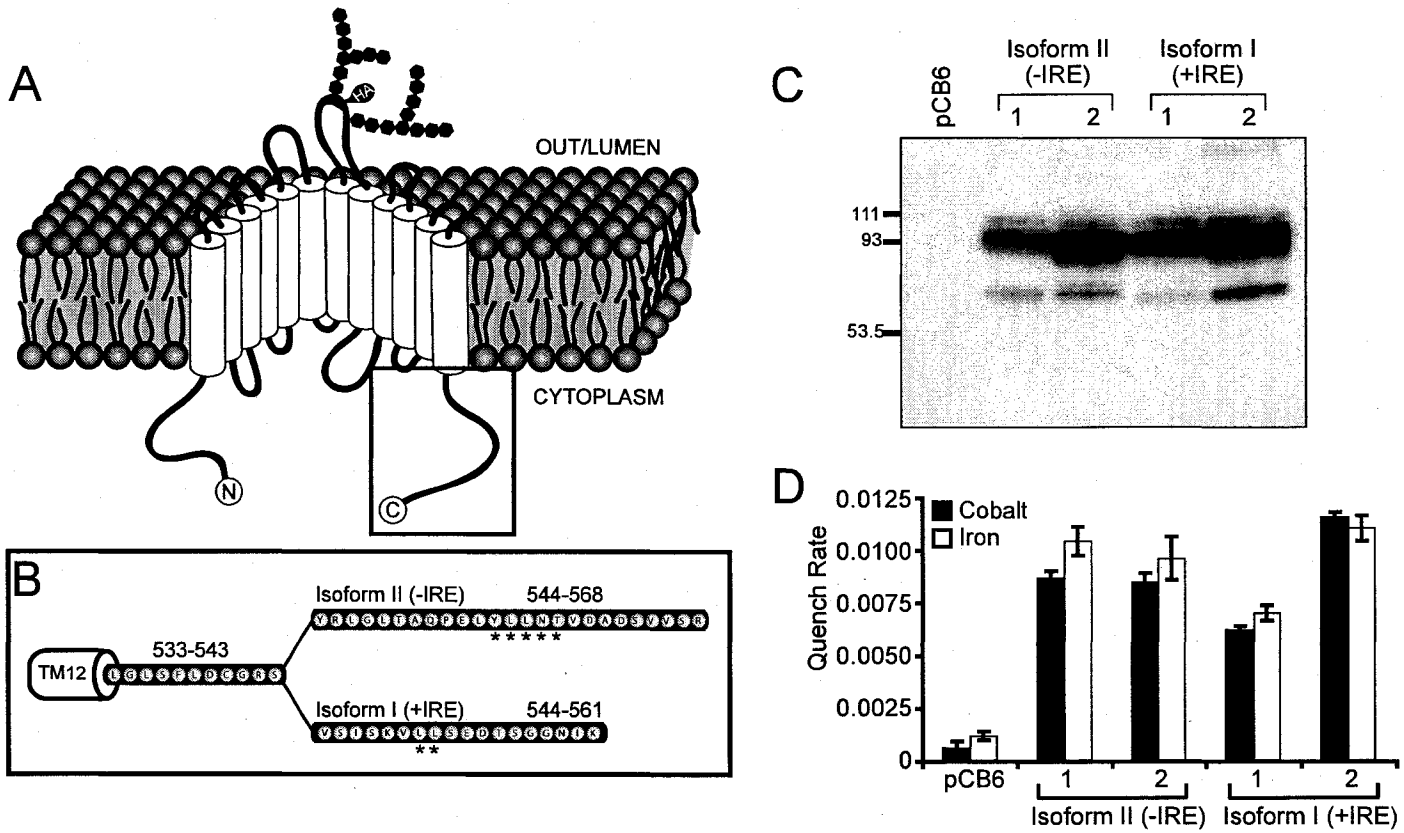

Figure 1. Expression and functional activity of DMT1 isoforms I and II in LLC-PK1 cells. (A) Shows a schematic representation of the DMT1-HA protein, highlighting the positions of the inserted exofacial hemagglutinin (HA) epitope, predicted asparagine-linked glycosylation sites (hexagons), and the carboxyl terminus (boxed). A comparison of the C-terminal sequences of DMT1 isoforms I and II is shown in (B). Asterixes highlight predicted sorting/trafficking signal sequences. We prepared extracts from LLC-PK1 cells transfected with the vector (pCB6) or independent clones (1 and 2) stably-expressing DMT1 isoforms I and II. Equal amounts of each extract was resolved by SDS-PAGE and (C) shows a representative immunoblot performed with an anti-HA Ab. The sizes of molecular weight standards (in kilodaltons) are indicated. (D) Shows the metal transport activity of cells stably transfected with vector only (pCB6) or DMT1 isoforms I and II. Cells loaded with a metal-sensitive fluorescent dye were incubated with Fe2+ or Co2+ in acidic buffer. The results are shown as the initial rates of fluorescence quenching. Error bars represent standard error of the means of three or more independent determinations.

Subcellular localization of DMT1 isoforms I and II

The subcellular localization of DMT1 isoforms I and II was determined by double immunofluorescence with an anti-DMT1 antibody, using fixed and permeabilized cells. As reported earlier, DMT1 isoform II was detected in an endomembrane compartment where it displayed strong co-localization with the recycling endosome marker, GFP-syntaxin 13 (Figure 2A), but showed little overlap with the late endosome and lysosomal marker, GFP-Lamp1 (Figure 2B) [51;184]. Conversely, DMT1 isoform I was detected in endomembrane vesicles of larger size than those positive for isoform II, that showed little co-localization with GFP-syntaxin 13 (Figure 2A) but strong co-localization with GFP-Lamp1 (Figure 2B). These results indicate that the two DMT1 isoforms are differentially targeted at steady-state in LLC-PK_1 cells: isoform II to recycling endosomes and isoform I to late endosomes and lysosomes.

Our transport data in intact cells (Figure 1D) also suggested that both isoforms were present in a functional state at the cell surface. Therefore, we used immunofluorescence microscopy to investigate the cell surface expression of each isoform. Surface-expressed DMT1-HA molecules were visualized by incubating fixed but unpermeabilized LLC-PK_1 transfected cells with anti-HA antibody followed by labeling with a conjugated fluorescent secondary antibody. Interestingly, isoform I displayed much stronger surface expression compared to isoform II (Figure 3A). We quantified this difference in surface expression using a horseradish peroxidase-conjugated secondary antibody and found that a significantly higher proportion of total DMT1 isoform I (clone 1, 44.5 ± 2.8%; clone 2, 45.6 ± 1.5%; mean ± S.E.) was expressed at the plasma membrane compared to isoform II (clone 1, 24.8 ± 2.0%; clone 2, 24.4 ± 1.6%) (Figure 3B). Thus despite similar levels of total DMT1 protein expression in the pair of LLC-PK_1 clones tested, isoform I shows higher cell surface expression than isoform II.

Endocytosis

The different levels of cell surface expression and apparent variations in intracellular localization of isoforms I and II suggested different trafficking properties of

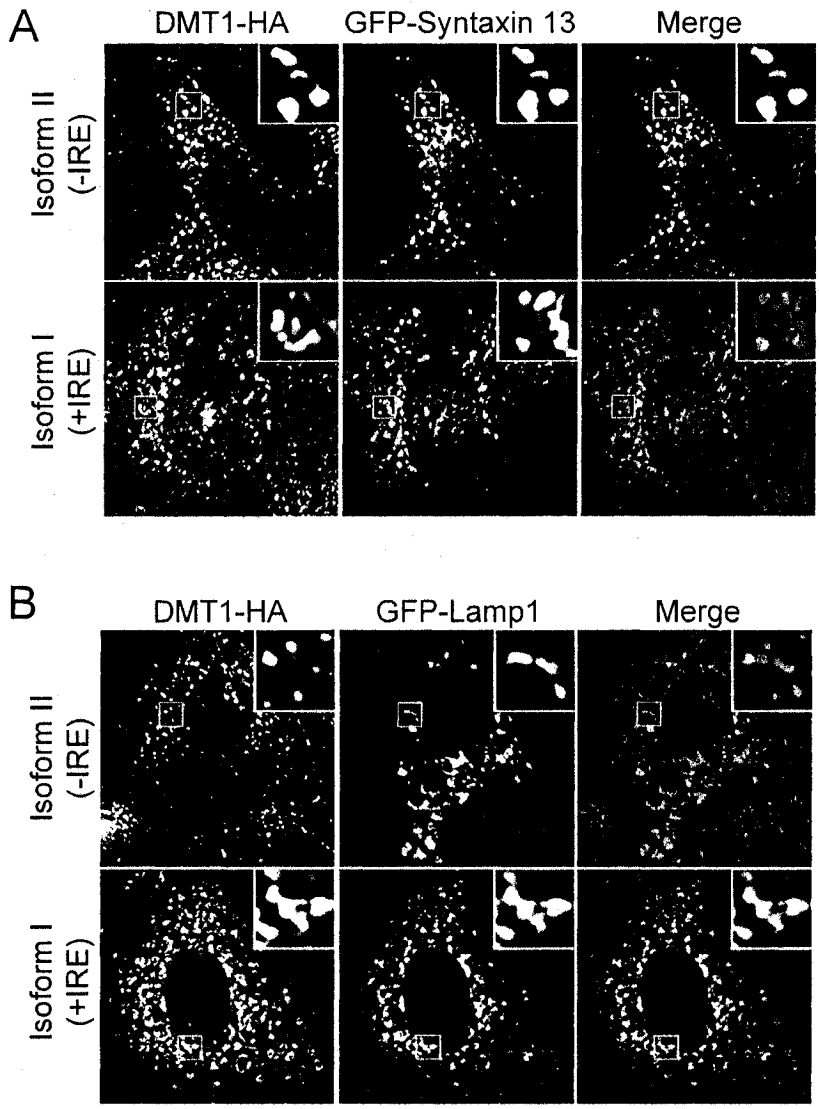

Figure 2. Subcellular localization of DMT1 isoforms I and II in LLC-PK1 cells. LLC-PK1 cells stably expressing DMT1 isoforms I and II were transiently transfected with either GFP-syntaxin 13 (A) to label recycling endosomes or GFP-lamp1 (B) to label late endosomes and lysosomes. 24-hours later, cells were fixed, permeabilized and stained with an anti-DMT1 antibody. DMT1 molecules were visualized using a secondary antibody coupled to fluorescent Cy3. Images were acquired by epifluorescence microscopy. Insets show magnifications of the area boxed in the figure.

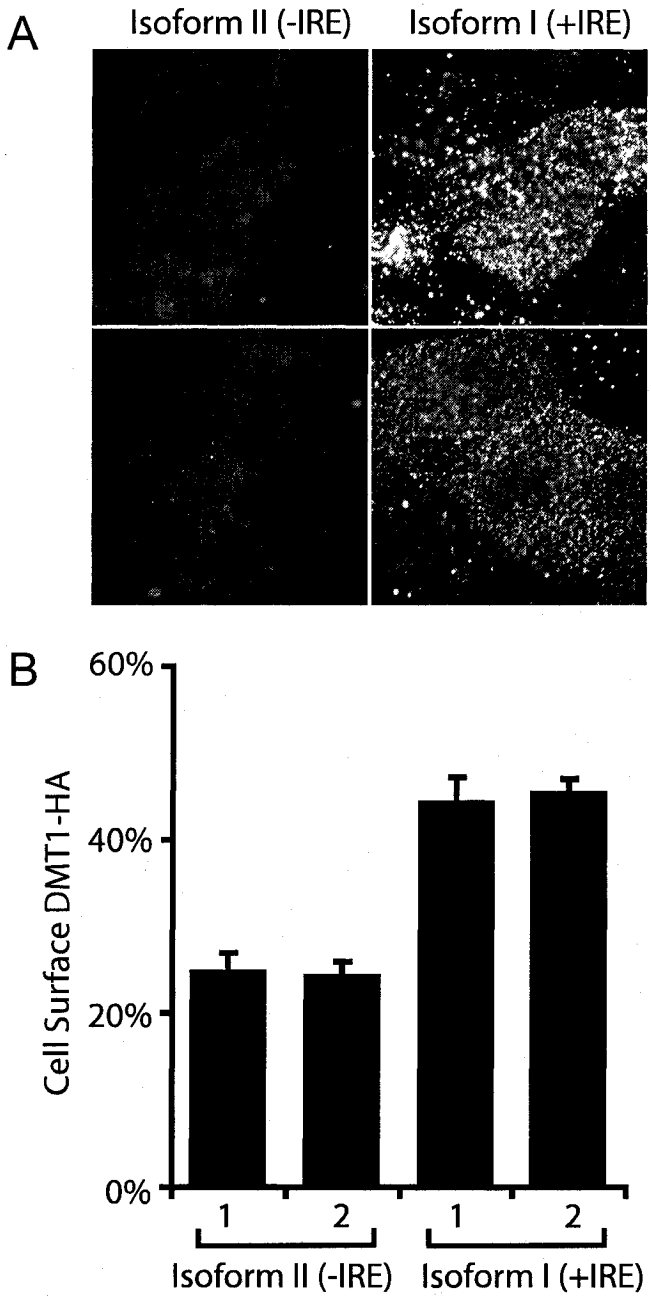

Figure 3. Quantification of cell surface expression of DMT1 isoforms I and II in LLC-PK1 cells. LLC-PK1 cells stably expressing DMT1 isoforms I and II were fixed and surface DMT1 molecules were labeled by incubating the cells with a primary anti-HA antibody without permeabilization, followed by a secondary antibody coupled to Cy3 (A). Images were acquired by epifluorescence microscopy. (B) Shows a quantification of the fraction of DMT1-HA molecules expressed at the cell surface. Cells were fixed and incubated with primary anti-HA antibody with or without prior detergent permeabilization (see Materials and Methods). Cells were then incubated with an HRP-coupled secondary antibody, and the amount of bound primary antibody present was determined for both conditions by a colorimetric reaction using o-phenylenediamine dihydrochloride (OPD) followed by spectrometry. The amount of DMT1-HA expressed at the cell surface (in non-permeabilized cells) is shown as a fraction (%) of total protein expression (in permeabilized cells).

the 2 proteins. Therefore, we measured the rates of endocytosis from the plasma membrane of isoforms I and II using a cell surface biotinylation technique [184]. We used a membrane impermeable, cleavable biotin compound to covalently label all surface-exposed plasma membrane proteins in LLC-PK_1 cells cooled to 4°C to halt endocytosis. Following biotinylation, cells were warmed to 37°C for 0 to 90 min to allow internalization of labeled plasma membrane proteins. Biotin molecules remaining at the cell surface were removed by washing the cells with a membrane-impermeant reducing agent. Cells were solubilized and biotinylated DMT1-HA molecules were isolated using immobilized streptavidin, followed by SDS-PAGE and immunoblotting with anti-HA antibody. Figure 4A illustrates a typical immunoblot, while quantification of 3 different immunoblots by densitometric scanning is shown in Figure 4B. Intracellular accumulation of surface-labeled DMT1-HA molecules after 0 to 90 min was expressed as a percentage of the maximal surface DMT1-HA (without washing with reducing agent) after 0 min (Figure 4B). Strikingly, independent clones of DMT1 isoform II displayed significantly higher internalization at each time point compared to independent clones of DMT1 isoform I. The greatest difference occurred after 60 min with isoform II clones showing 33.6 ± 5.4% and 43.2 ± 11.2% of cell surface DMT1-HA internalized compared to 11.8 ± 2.4% and 13.8 ± 3.9% for isoform I clones. These results demonstrate that the higher plasma membrane expression of isoform I is correlated with a reduced rate of internalization from the cell surface compared to isoform II. Indirectly, these results suggest that the carboxyl terminal cytoplasmic tail of isoform I lacks an endocytosis signal present in the carboxyl tail of isoform II.

Fate of internalized DMT1 molecules

Having shown that DMT1 isoform I is internalized with slower kinetics from the cell surface, we next investigated the fate of internalized isoform I molecules. We labeled surface/internalized DMT1-HA molecules in live LLC-PK_1 cells by incubating the cells with anti-HA antibody at 37°C in culture medium for 2 hours. Cells were fixed, permeabilized, and labeled with an antibody against EEA1, a marker of early endosomes. Both isoforms of DMT1 showed significant co-localization with EEA1 (blue arrowheads

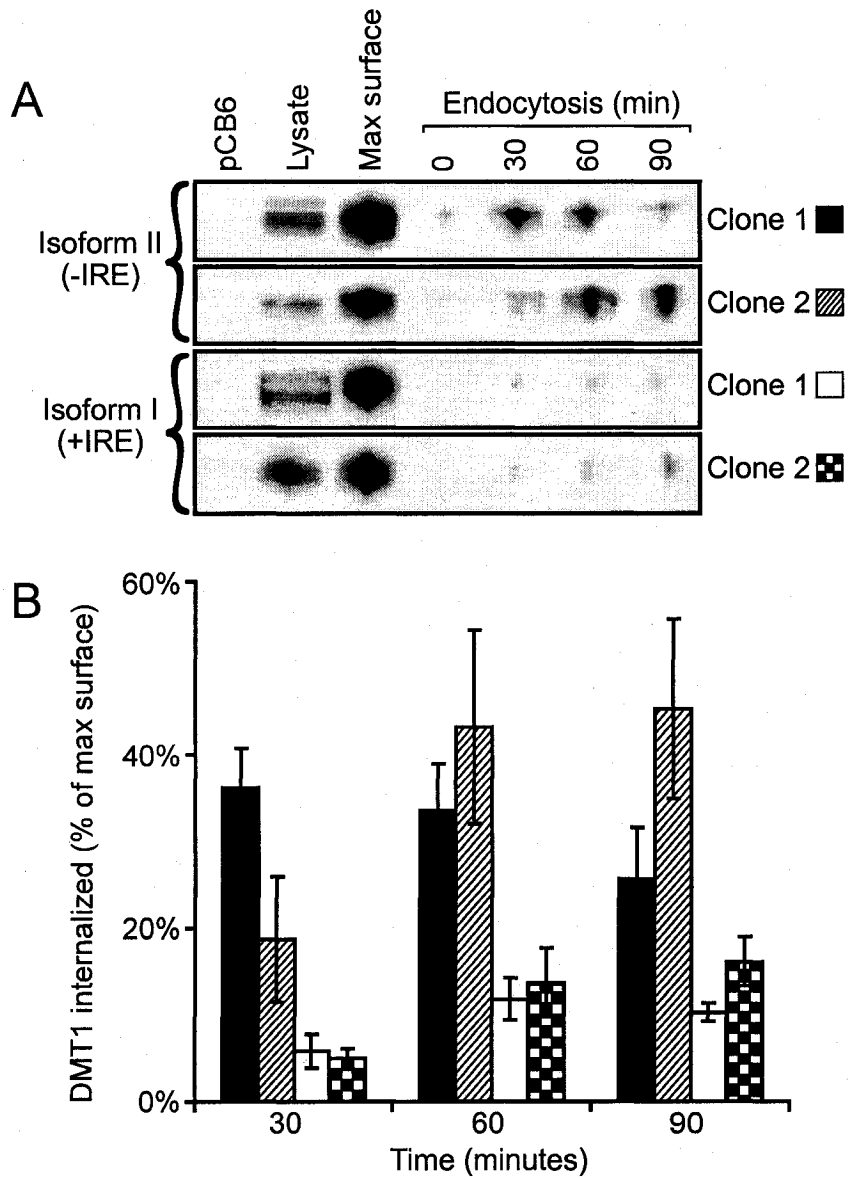

Figure 4. Quantification of the rate of endocytosis of DMT1 isoforms I and II in LLC-PK1 cells. A cell surface biotinylation assay was used to compare internalization rates of DMT1 isoforms I and II from the plasma membrane. We used a membrane impermeable cleavable biotin reagent to label surface proteins, which was performed at 4°C to halt endocytosis. Internalization of surface proteins was allowed to occur at 37°C for 0 to 90 min. After that time, biotin molecules remaining at the surface were removed and biotinylated proteins were isolated from cell lysates with immobilized strepavidin. Proteins were resolved by SDS-PAGE and DMT1 molecules were detected by immunoblotting with anti-HA antibody. Typical immunoblots from individual experiments done on independent clones (1 and 2) are shown in (A). Immunoblots were scanned by densitometry, and the amount of DMT1 internalized over time is expressed as a fraction (%) of the total cell surface expression (Max) in (B). Lysate = 20 μg of unbiotinylated crude cell lysate for each mutant. Max = total surface DMT1-HA expression for each clone (biotinylated DMT1-HA molecules isolated without prior stripping). Error bars correspond to standard errors of the means from three or more independent experiments.

in Figure 5A). To determine the fate of internalized DMT1 molecules after a longer incubation period, the cells were labeled for 3 h, washed and chased in culture media for an additional 90 min. Lysosomes were labeled by transient transfection with GFP-Lamp1 24 h prior to labeling. As expected, isoform II did not show significant co-localization with Lamp1 (Figure 5B), indicating that the protein was efficiently recycled back to the cell surface. Strikingly, in cells labeled for 3 hours, isoform I showed strong co-localization with the lysosomal marker (Figure 5B). These results show that DMT1 isoform I, upon internalization and passage through early endosomes, fails to recycle back to plasma membrane and is targeted to late endosomes and lysosomes. These results suggest that the carboxyl terminus of isoform I not only lacks an endocytosis signal but also a recycling signal present in the carboxyl terminus of isoform II. Slower endocytosis of isoform I from the plasma membrane results in elevated cell surface expression at steady-state (Figure 3).

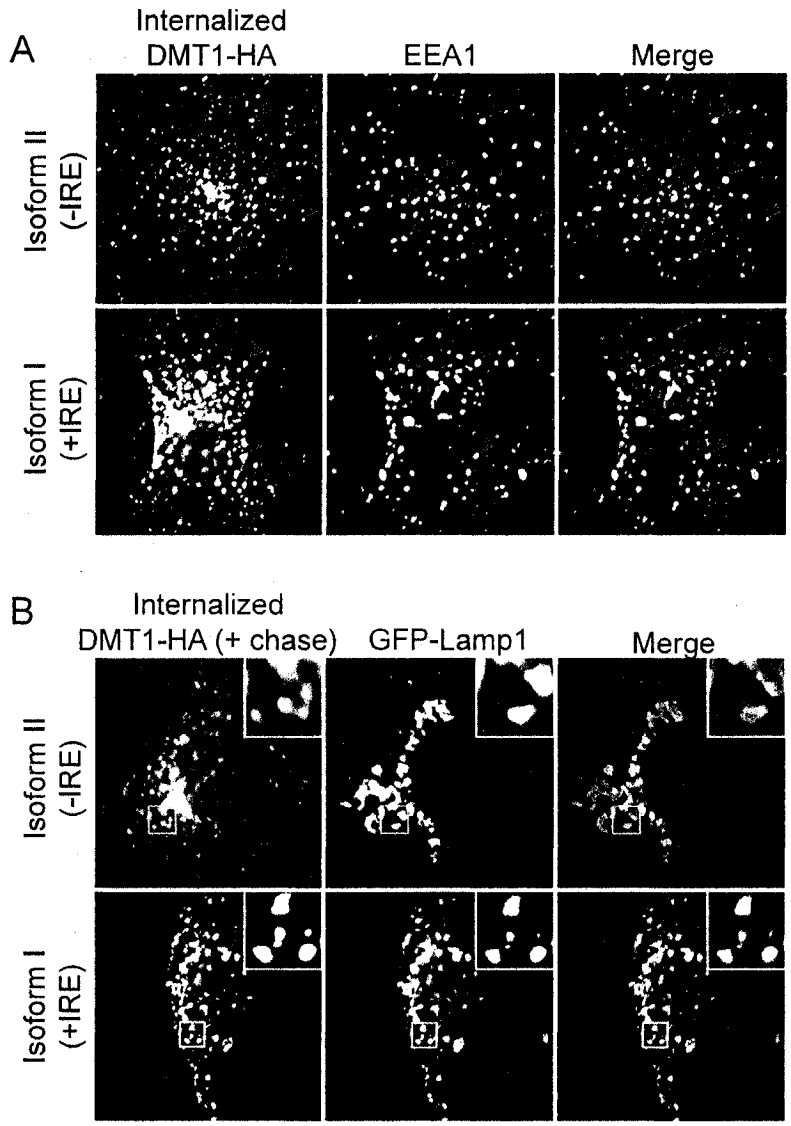

Figure 5. The fate of internalized DMT isoform I and II molecules. In (A), LLC-PK1 cells expressing either DMT1 isoforms I or II were incubated with anti-HA antibody for 2 h to label cell surface and recycling DMT1-HA molecules. To investigate co-localization of internalized DMT1-HA molecules with early endosomes, cells were fixed, permeabilized and incubated with an antibody against the early endosomal marker EEA1. DMT1 molecules were visualized using a fluorescent secondary antibody. Areas showing overlapping staining are highlighted (blue arrow heads). To investigate co-localization of DMT1 isoforms with lysosomes, cells were transiently transfected with the lysosomal marker GFP-lamp1 in (B). 24 hours later, surface and recycling DMT1-HA molecules were labeled with anti-HA Ab for 3h, washed and chased by incubation in growth media for 90 min. Cells were fixed, permeabilized, and stained with an anti-mouse fluorescent secondary Ab to visualize DMT1-HA molecules. Insets show magnifications of the area boxed in the figure. Images were acquired by epifluorescence microscopy.

DISCUSSION

DMT1 isoform II is expressed in many cell types but is particularly abundant in erythroid precursors [169]. Studies in transfected cells *in vitro* have shown that isoform II is rapidly internalized along with the transferrin receptor from the plasma membrane by a clathrin and dynamin dependent process [51]. Endosomal acidification facilitates release of iron from transferrin and provides the proton gradient for DMT1-mediated iron transport across the endosomal membrane. Iron is then stored bound to ferritin or transported into mitochondria for heme synthesis. DMT1 isoform II and transferrin receptor are subsequently recycled back to the cell surface. The critical role of DMT1 in this iron acquisition process is highlighted by the recent report that a patient with a mutation in *DMT1* suffers from erythroid hyperplasia with defective hemoglobinization [4]. In circulation, the majority of iron is bound to transferrin and very little iron exists in its free cationic form. This correlates well our data as well as earlier reports that less than 35% of total DMT1 isoform II is expressed at the cell surface, with the majority of isoform II residing in transferrin receptor-positive recycling endosomes.

Directional or trans-cellular transport is essential in epithelial cells located at sites of absorption or re-absorption of key elements such as iron. Dietary non-heme iron is mainly absorbed at the duodenal brush border. DMT1, expressed at the apical pole of enterocytes lining the intestinal lumen, transports iron across the apical membrane while ferroportin, expressed at the basal pole, transports iron across the basolateral membrane. It is predominantly the isoform I variant of DMT1 that is expressed at the apical membrane of enterocytes [161]. Our finding that cell surface expression of isoform I in LLC-PK_1 cells is higher than isoform II is in agreement with the noted preferential expression of isoform I at the cell surface of different cell types *in vivo* (compared to isoform II), namely the brush border of epithelial cells of the duodenum and of the kidney proximal tubule. We also found that isoform I is not efficiently recycled upon internalization and is ultimately targeted to lysosomes. These findings indicate that iron transported by isoform I (at the duodenal brush border) involves direct transfer of Fe^{2+} from the intestinal lumen into the cytoplasm of enterocytes, in the absence of an active Tf-TfR cycle at the apical pole of these cells. On the other hand, TfR is expressed at the

basolateral membrane and in basal recycling endosomes of intestinal epithelial cells [346;347] and it is possible that DMT1 isoform II may play an additional role in iron acquisition at that site as well [155]. In addition, mutagenesis studies suggested that N-linked glyosylation of DMT1 controls apical vs. basolateral targeting in polarized cells [155]. Thus, it is possible that trafficking differences between DMT1 isoforms I and II in epithelial cells may not only involve differential targeting to the plasma membrane but may also be influenced by different rates of internalization of the transporters from the cell surface, as demonstrated here in transfected LLC-PK_1 cells. In addition, recent work by Johnson and colleagues in Caco-2 cells suggests that isoform I trafficking may be regulated by cellular iron levels. This result emphasizes the importance of isoform-specific trafficking in overall DMT1 function, including coupling to the Tf-TfR cycle [160].

While targeting and dynamic sorting/recycling of DMT1 isoform II has been thoroughly studied by us and others, much less is known about isoform I. The protein sequences of isoforms I and II differ only in their C-terminal segments (Figure 1B). In isoform II, Tabuchi and colleagues have shown that a $YLLNT^{555-559}$ signal in the C terminus of the protein is required for its early endosome targeting in HEp-2 larynx carcinoma cells [155]. We have previously shown that the C terminus of isoform II, along with the YLLNT signal, is vital for the protein's internalization from the cell surface and recycling back to the plasma membrane in LLC-PK_1 epithelial cells [184]. Critical mutations or deletions at YLLNT result in severely impaired internalization, accumulation of the transporter at the cell surface, and failure of the protein to recycle properly resulting in lysosomal targeting. DMT1 isoform I lacks an endogenous YLLNT motif in its carboxyl terminus. Interestingly, the trafficking properties of the isoform II YLLNT mutants (including a C-terminal truncation) virtually mirror the trafficking properties of DMT1 isoform I reported here [184]. These findings together with the results of the present study together demonstrate the critical role of the YLLNT sequence motif as a recycling motif in DMT1. Furthermore, these results argue against the presence of a functional targeting motif in the C-terminal region of DMT1 isoform I.

Examination of the C-terminal sequence of isoform I reveals the presence of a putative dileucine motif ($LL^{550-551}$, Figure 1B). Indeed, cytoplasmic dileucine-based (LL)

motifs of membrane proteins often act as signals leading to clathrin-mediated endocytosis or targeting to endosomal-lysosomal compartments [339-342]. Residues neighboring the LL signals appear to dictate whether clathrin recruitment occurs via AP complexes or via ARF-dependent clathrin adaptors [183]. Dileucine-based signals usually fit either the [DE]XXXL[LI] or DXXLL consensus motifs. [DE]XXXL[LI] signals are specifically recognized by AP complexes while DXXLL signals are recognized by GGAs, a recently described family of ARF-dependent clathrin adaptors. However, the amino acids preceding the dileucine motif in DMT1 isoform I ($SISKV^{545-549}$) do not fit either of these consensus motifs. Therefore, the relevance of this leucine pair ($LL^{550, 551}$) in the targeting and sorting of isoform II remains unclear, and awaits further characterization.

Based on previous work and data reported here, we propose a model for the subcellular trafficking of the two isoforms of DMT1. In this model, DMT1 proteins would be synthesized in the endoplasmic reticulum, post-translationally modified in the Golgi apparatus, and targeted to the plasma membrane. Isoform II molecules are then rapidly internalized from the cell surface by recruiting specific adaptor proteins required for clathrin-mediated endocytosis [51], which we propose interact with the YLLNT motif and possibly other determinants in the C-terminal region of the transporter. Isoform II is internalized into early endosomes and the recruited adaptor complexes are involved in recycling the transporter back to the cell surface via targeting to recycling endosomes (Figure 6). This pathway ensures that the isoform II molecules expressed in erythroid cells can work in conjunction with transferrin receptor in the uptake of transferrin-iron. DMT1 isoform I molecules lack the YLLNT motif would be unable to recruit clathrin/adaptor complexes at the plasma membrane. Consequently, isoform I transporters are internalized into early endosomes by a kinetically slower mechanism such as bulk pinocytosis (Figure 6). The slower rate of endocytosis of isoform I results in a greater fraction of the DMT1 variant expressed at the cell surface at steady-state. However, failure of isoform I molecules to recruit specific recycling adaptor complexes prohibits their sorting to recycling endosomes and leads to an accumulation in the late endosomes and lysosomes. This trafficking pathway ensures a high level of DMT1 isoform I

expression at the plasma membrane of epithelial cells, favoring the absorption/re-absorption of iron.

Overall, our findings highlight the critical role of alternate splicing at the 3' end of the *DMT1* gene for the generation of protein isoforms that transport iron at different subcellular sites in a transferrin-dependent (isoform II), and transferrin-independent (isoform I) manner.

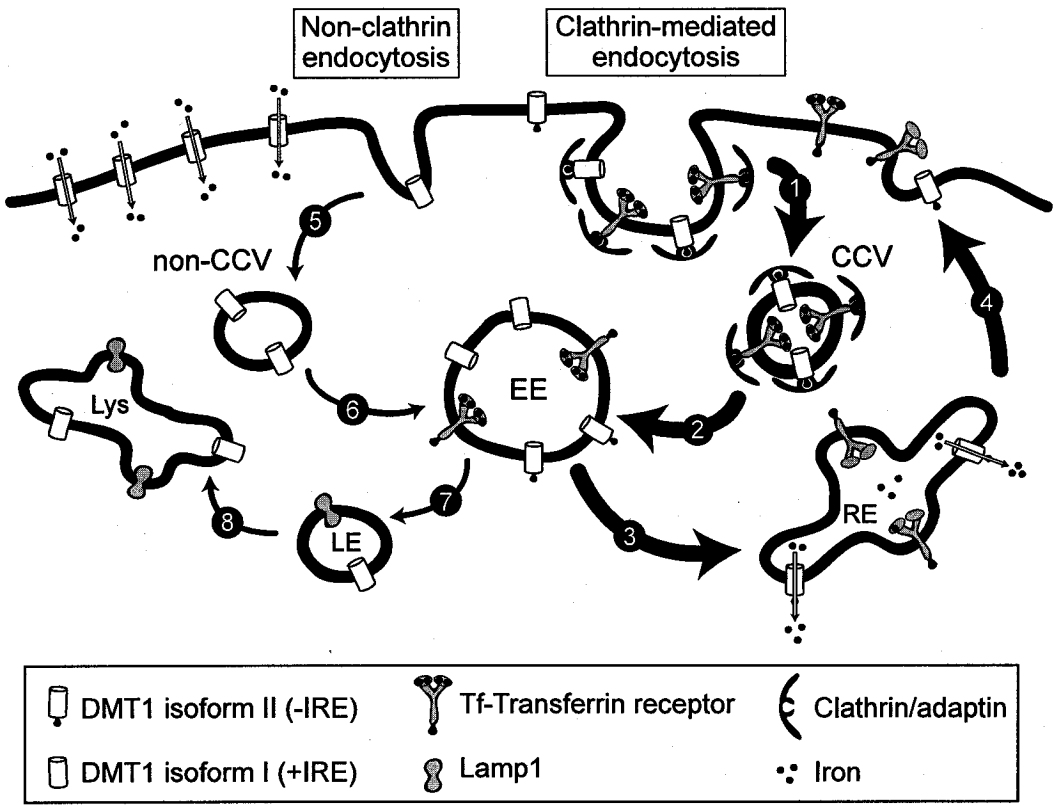

Figure 6. A schematic model for distinct trafficking of DMT1 isoforms I and II. DMT1 molecules are synthesized in the endoplasmic reticulum, post-translationally modified in the Golgi apparatus, and targeted to the plasma membrane by default. Clathrin molecules interact with surface DMT1 isoform II (-IRE) molecules via adaptins that specifically recognize the tyrosine-based motif YLLNT and possibly other residues present in the C terminus of the variant. Isoform II molecules are rapidly internalized (step 1) by a dynamin-dependent process into clathrin-coated vesicles (CCV). DMT1-containing CCVs are sorted first to early endosomes (EE, step 2) followed by recycling endosomes (RE, step 3). The acidic environment of RE favor the release of iron from transferrin and create the proton gradient required for iron transport by DMT1 isoform II. In contrast, surface DMT1 isoform I molecules, which lack the C-terminal tyrosine-based sorting motif, are internalized less rapidly by a clathrin-independent mechanism into non-CCVs (step 5). Isoform I molecules are sorted to EE (step 6) but are not efficiently recycled back the cell surface and are eventually targeted to lamp1-positive late endosomes and lysosomes (steps 7 and 8).

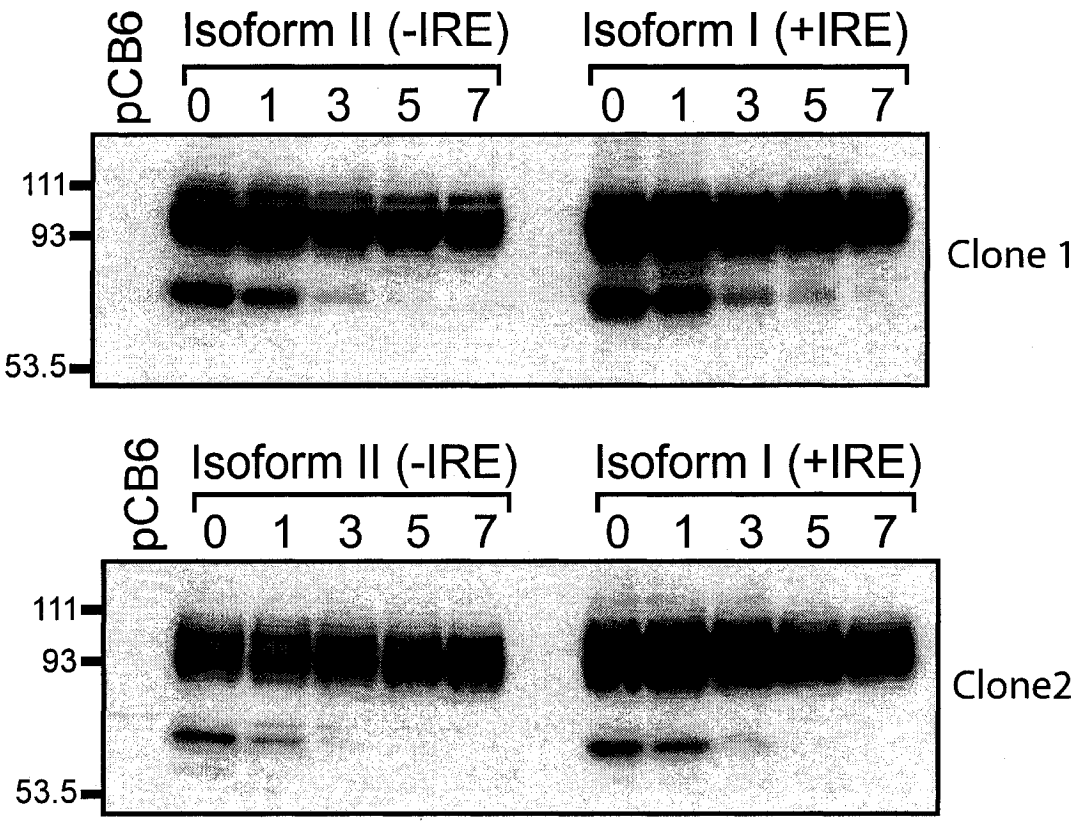

Supplementary figure. The stability of DMT1 isoforms I and II proteins. Independent clones (1 and 2) of LLC-PK1 cells stably expressing DMT1 isoforms I and II were treated with the translation inhibitor cycloheximide (20 μg/mL) for 0, 1, 3, 5, or 7 hours. Following treatment, cell extracts were prepared and equal amounts of total protein were resolved by SDS-PAGE followed by immunoblotting with an anti-HA antibody.

Preface to Chapter 7

The work described in the previous two Chapters of this thesis focused on the subcellular distribution of Nramp2. In these studies, we adapted or developed a number of tools and techniques to study protein stability, steady-state targeting, cell surface expression, endocytosis kinetics, and fate upon internalization of Nramp2. In the next Chapter, we decided to use some of these techniques to characterize the subcellular targeting properties of Nramp1. It was known for some time that Nramp1 is expressed in the lysosomes of phagocytic cells and more recent data support a model whereby Nramp1 restricts the replication of intracellular pathogens by removing divalent metals (Mn^{2+}, Fe^{2+}) from the phagolysosome. However, targeting motifs responsible for the lysosomal localization of Nramp1 were not yet known and needed to be studied. In Chapter 7, the subcellular trafficking properties of Nramp1, including cytoplasmic sequences responsible for targeting to lysosomes, were investigated using Nramp1/Nramp2 chimeric proteins.

Chapter 7:

Identification of a tyrosine-based motif (YGSI) in the amino terminus of Nramp1 (Slc11a1) responsible for lysosomal targeting

ABSTRACT

In macrophages, *Nramp1* (*Slc11a1*) is expressed in lysosomes and restricts replication of intracellular pathogens by removing divalent metals (Mn^{2+}, Fe^{2+}) from the phagolysosome. *Nramp2* (*DMT1*, *Slc11a2*) is expressed both at the duodenal brush border where it mediates uptake of dietary iron, and ubiquitously at the plasma membrane/recycling endosomes of many cell types, where it transports transferrin-associated iron across the endosomal membrane. In Nramp2, a C-terminal cytoplasmic motif ($YLLNT^{555-559}$) is critical for internalization and recycling of the transporter from the plasma membrane. In this report, we have studied the subcellular trafficking properties of Nramp1 and have investigated the *cis*-acting sequences responsible for targeting to lysosomes. For this, we have constructed and studied Nramp1/Nramp2 chimeric proteins where homologous domains of each protein were exchanged. Chimeras exchanging the amino (upstream TM1) and carboxyl terminal (downstream TM12) cytoplasmic segments of both transporters were stably expressed in porcine LLC-PK_1 kidney cells, and were studied with respect to expression, maturation, stability, cell surface targeting, transport activity, and subcellular localization. An Nramp2 isoform II chimera bearing the N terminus of Nramp1 was not expressed at the cell surface but was targeted to lysosomes. This lysosomal targeting was abolished by single alanine substitutions at Y^{15} and I^{18} of a $YGSI^{15-18}$ motif present in the N terminus of Nramp1. These results identify YGSI as a tyrosine-based sorting signal responsible for lysosomal targeting of Nramp1.

INTRODUCTION

Nramp defines a large, highly conserved family of integral membrane proteins that transport divalent metals in a pH-dependent fashion [41]. The first member of this family, *Nramp1* (*Slc11a1*), was identified by positional cloning of a locus (*Bcg/Ity/Lsh*) that regulates susceptibility of mice to infection with a number of unrelated intracellular pathogens [7]. Naturally occurring ($Nramp1^{G169D}$) or experimentally induced ($Nramp1^{-/-}$) loss-of-function mutations at *Nramp1* cause susceptibility to infection with several species of *Mycobacteria*, *Salmonella*, and *Leishmania* [348;349]. Polymorphic variations at human *NRAMP1* have also been linked to increased susceptibility to tuberculosis and leprosy in areas where those diseases are the most prevalent [112;117;350]. Hydropathy profiling and topological studies suggest that Nramp1 is composed of 12 putative transmembrane domains and is expressed primarily in lysosomes of mononuclear phagocytes and in tertiary granules of polymorphonuclear leukocytes [41]. Upon phagocytosis of inert particles or of live pathogens, Nramp1 is rapidly recruited to the membrane of maturing phagosomes [35;37-39]. Recent work has shown that Nramp1 functions as a phagosomal metal efflux pump that transports divalent cations such as Mn^{2+}, Fe^{2+} in a pH-dependent manner down a proton gradient created by the vacuolar H^+-ATPase [27;52;94]. Nramp1-mediated exclusion of essential metals may impair microbial metabolic activity including expression of intracellular survival mechanisms, or may directly enhance the efficacy of bactericidal effector mechanisms, or both.

Nramp2 (also known as *DMT1*, *Slc11a2*) is a close homolog of *Nramp1* [40;131], with 66% amino acid sequence identity and 77% similarity between the 2 proteins [1]. Nramp2 is expressed abundantly and in an iron-regulated fashion at the brush border of the duodenum [161], where it imports dietary iron across the absorptive epithelium. Nramp2 is also expressed in many cell types and is abundant in erythroid precursors [169], where it is required for recruitment of transferrin-associated iron from recycling endosomes into the cytosol [251]. Expression of Nramp2 has also been detected at the brush border of epithelial cells lining the proximal tubules of the kidney, where it may function as a re-uptake system for divalent metals [172]. Two major Nramp2 protein isoforms generated by alternative splicing at 3' exons have been identified. Isoform I (+IRE) has an iron

responsive element (IRE) in the 3' untranslated region, whereas isoform II (-IRE) lacks the IRE. In addition, the C-terminal 18 amino acids of isoform I are replaced by an alternate 25-amino acid segment in isoform II. Nramp2 isoform I is predominantly expressed in epithelial cells while isoform II is predominantly expressed in erythroid cells. Much of our knowledge of the function of Nramp2 *in vivo* comes from studies of rodent models of microcytic anemia and iron deficiency including the *mk* mouse and the *Belgrade* rat, that are both caused by the same mis-sense mutation in predicted TM4 of Nramp2 (G185R) [136;141]. This phenotype is recapitulated in a mouse mutant with targeted inactivation of *Nramp2* (*Nramp2*$^{-/-}$) [258]. Recently, two human patients with severe hypochromic microcytic anemia and hepatic iron overload were shown to harbor mutations in *NRAMP2* [4;263]. In both patients, a quantitative reduction in the expression of functional *Nramp2* has been identified as the cause of disease [260-262].

Although *Nramp1* and *Nramp2* code for functionally undistinguishable pH-dependent divalent metal transporters with similar substrate specificities [27], they differ sharply in their subcellular localizations. Nramp1 is found strictly at the lysosomal compartment of cells with no expression at the cell surface [35;39]. In contrast, Nramp2 is ubiquitously expressed at the plasma membrane as well as in recycling endosomes (isoform II) at steady-state [42;161]. Sequence motifs found in the cytoplasmic terminal regions of membrane proteins often control their subcellular targeting and trafficking [155;184]. The most common motifs are either tyrosine-based signals of the forms NPXY or YXXΦ (where X = any residue, and Φ = large hydrophobic residues) and dileucine-based motifs (LL) [183]. The subcellular trafficking of Nramp1 is not well understood and specific cytoplasmic motifs involved in its lysosomal targeting have not yet been identified. However, we have previously shown that insertion of a hemagglutinin epitope (HA) tag in the fourth extra-cytoplasmic loop of Nramp1 causes the transporter to be mistargeted to the plasma membrane where it displays metal uptake activity [27]. On the other hand, trafficking signals in the amino and carboxyl cytoplasmic regions of Nramp2 have been identified and characterized. We and others have shown that a YLLNT$^{555-559}$ motif in the C terminus of Nramp2 isoform II controls targeting to transferrin-positive recycling endosomes [155;184]. Deletion of this motif or truncation of the entire C terminal

cytoplasmic segment of Nramp2 isoform II results in a mutant protein that is internalized less rapidly from the plasma membrane, is not properly recycled back to the cell surface, and is targeted to late endosomes and lysosomes (32). Mutagenesis experiments have also shown that motifs in the N terminus of Nramp2 (NPAY, YSCF) play an additional but less determinant role in the recycling endosome targeting of Nramp2 [184].

In this study, we have investigated the subcellular targeting and trafficking properties of Nramp1. For this, we have constructed chimeric proteins by exchanging homologous segments of Nramp1 and Nramp2 (isoform II). We expressed the chimeras in stably transfected LLC-PK_1 cells and studied their expression, stability, cell surface expression, metal transport activity, and subcellular localization. We demonstrate that a tyrosine-based sorting signal of the form YXXΦ functions as a lysosomal targeting motif in the amino terminus of Nramp1.

MATERIALS AND METHODS

Materials and antibodies

Reagent-grade chemicals were purchased from Sigma Chemical (St. Louis, MO) unless otherwise indicated. Monoclonal mouse antibody (Ab) HA.11 directed against the influenza hemagglutinin epitope (HA) was purchased from Covance (Princeton, NJ). Cy3-labeled goat anti-rabbit and HRP-coupled donkey anti-mouse Abs were purchased from Jackson ImmunoResearch Laboratories (West Grove, PA). Plasmids encoding GFP-fusion proteins were kind gifts from Dr. D. Williams (Department of Biochemistry, University of Toronto; GFP-syntaxin 13) and Dr. Patrice Boquet (Institut national de la santé et de la recherche médicale, France; GFP-Lamp1). The generation of polyclonal antibodies recognizing the amino terminal segments of murine Nramp1 and Nramp2 proteins has been described [35;42].

Plasmids and constructs

The construction of mammalian expression plasmids containing full-length murine cDNAs for either *Nramp1* (N1/pCB6) or *Nramp2* isoform II (N2/pCB6) were described earlier [26]. Full-length murine *Nramp2* cDNA (N2HA/pCB6) was modified by the in-frame addition of an exofacial hemagglutinin (HA) epitope (YPYDVPDYAS) in the fourth predicted extracellular loop, as previously described [26]. A recombinant polymerase chain reaction (PCR) protocol was used to generate *Nramp2-HA* chimeras bearing the amino (N1N-HA) or carboxyl terminal (N1C-HA) segments of *Nramp1*. Similarly, *Nramp1* chimeras bearing the amino (N2N) or carboxyl terminal (N2C) segments of *Nramp2* were created. For *N1N-HA* and *N2N* constructs, a silent *BstBI* restriction enzyme site was introduced into N2HA/pCB6 and N1/pCB6 plasmids (at nucleotide positions 200 and 155, respectively) immediately preceding the first predicted transmembrane domain of each protein using primers N2-BstBI and N1-BstBI (Table 1). N1N-HA/pCB6 and N2N/pCB6 constructs were then created by exchanging *XhoI-BstBI* fragments of N2HA/pCB6 and N1/pCB6 plasmids. N1C-HA and N2C constructs were created by a recombinant PCR amplification protocol using chimeric oligonucleotides N2HA-N1C and N1-N2C (Table 1), showing complementarity with N1 and N2 at the

Table 1: Oligonucleotides used for mutagenesis.

Primer Name	Nucleotide sequence (5' to 3')
N1-BstBI F	cattcagcctTCgAaagctgtgg
N2-BstBI F	ttagctttcgAaaactctggg
N1-N2CT F	gttgcatcgccTTGGGTCTGTC
N2-N1CT F	gtttgattgcaCACGGAGCCAC
N1 Y15A F	gcaggcccagtGCtggctccatttc
N1 G16A F	gcccagttatgCctccatttccag
N1 S17A F	ccagttatggcGccatttccagc
N1 I18A F	gttatggctccGCttccagcctgcc

F indicates forward. CAPITAL LETTERS indicate nucleotides differing from the template molecule. The *BstBI* restriction site is underlined.

boundaries of regions to be exchanged. The N2HA-N1C amplification product was inserted into N2HA/pCB6 using restriction enzyme sites *SacI* and *EcoRI* to generate N1C/pCB6. The *N1-N2C* amplification product was inserted into N1/pCB6 using restriction sites *AvrII* and *EcoRI* to generate N2C/pCB6. Alanine substitution mutations at the YGSI[15-18] motif of Nramp1 were created using mutagenic primers listed in Table 1. Mutants were introduced into N1N-HA/pCB6 using restriction enzyme sites *XhoI* and *BstBI*. The integrity of all mutant and chimeric cDNAs was verified by DNA sequencing.

Cell culture, transfection, and immunoblotting

LLC-PK$_1$ cells were cultured as previously described [184] and transfected with either N1/pCB6, N2HA/pCB6, or chimeric plasmids using Lipofectamine2000 (Gibco) according to instructions from the manufacturer. Stably transfected cell clones were obtained after 14 days of selection in medium containing G418 (1.4 mg/mL; Invitrogen), and individual colonies were subsequently picked and expanded. Total cell lysates were prepared and resolved by SDS-PAGE. Clones showing robust expression of the transfected constructs were identified by immunoblotting with either a mouse anti-HA Ab (for N2HA/pCB6, N1N-HA/pCB6, and N1C-HA/pCB6), a rabbit anti-Nramp2 NT Ab (N2N/pCB6), or a rabbit anti-Nramp1 NT Ab (N1/pCB6, N2C/pCB6), as previously described [184]. For experiments with cycloheximide (CHX), cells were incubated in growth media supplemented with 20 μg/mL CHX for the indicated time intervals prior to lysis and SDS-PAGE.

Metal transport assay

Measurement of metal transport in transfected LLC-PK$_1$ cells was carried out using a calcein fluorescence quenching assay, as we have previously described [26;28]. Calcein acetoxymethylester (calcein-AM, Molecular Probes) stock solutions were prepared in dimethyl sulfoxide and cells were loaded at a final concentration of 0.25 μM calcein-AM. Co^{2+} solution (cobalt chloride, 2 mM) was prepared fresh in deionized water. Initial rates of metal transport were calculated from the initial fluorescence quenching curves (34;35).

Cell surface biotinylation

LLC-PK_1 cell monolayers were rinsed twice with ice-cold phosphate-buffered saline (PBS) and once with ice-cold borate buffer (10.0 mM boric acid, 154 mM NaCl, 7.2 mM KCl, 1.8 mM CaCl2, pH 9.0), and then incubated (60 minutes, 4°C) in the same buffer containing Sulfo-NHS-SS-biotin (1 mg/mL; Pierce). Unreacted biotin was removed by 3 washes with RPMI medium. Biotinylated cells were collected and solubilized in lysis buffer (1% Triton X-100, 0.2% SDS, 50 mM Tris-HCl pH 7.4, 150 mM NaCl, 20% glycerol) with protease inhibitors. Lysates were pre-cleared by centrifugation (10 000*g*, 30 min at 4°C) and protein yield was quantified by Bradford assay (Bio-Rad). Biotinylated proteins (100 μg total protein lysate) were isolated by overnight incubation at 4°C with 50 μL of ImmunoPure immobilized strepavidin slurry (Pierce) in a final volume of 1 mL in lysis buffer. Strepavidin beads were washed six times with cold lysis buffer and bound proteins were eluted with 2× Laemmli buffer at room temperature for 30 min. Proteins were separated by SDS-PAGE followed by immunoblotting.

Quantification of cell surface expression by ELISA

Quantification of Nramp2-HA molecules expressed at the cell surface by ELISA was as previously described [184]. Briefly, LLC-PK_1 cells were grown to confluency in 48-well culture plates and fixed with 4% paraformaldehyde for 30 min. Cells were blocked in 5% non-fat milk in PBS for 30 min, incubated with anti-HA Ab (1:500) for 90 min, washed and incubated with secondary Ab (donkey anti-mouse-HRP Ab, 1:4000) for 1 h. For quantification of total Nramp2-HA expression, cells were permeabilized by incubation with 0.1% Triton X-100/PBS for 30 min prior to incubation with anti-HA Ab. Peroxidase activity was detected by incubating cells with HRP substrate (0.4 mg/mL o-phenylenediamine dihydrochloride, Sigma FAST OPD) according to the instructions from the manufacturer. Reactions were stopped after 30 min with 3M HCl and absorbance readings (492 nm) were taken with a spectrometer. For all determinations, background absorbance readings from (i) non-specific binding of secondary Ab, and (ii) non-specific binding of primary Ab to vector-transfected cells, were subtracted for each sample. Cell surface readings were normalized to total Nramp2-HA values for each cell clone and were expressed as a percentage.

Immunofluorescence

LLC-PK_1 cells stably expressing Nramp1, Nramp2-HA or chimeric proteins were transiently transfected with GFP-fusion proteins to label recycling endosomes (GFP-syntaxin 13) or late endosomes and lysosomes (GFP-Lamp1). Twenty four hours later, cells were fixed with 4% paraformaldehyde (in PBS) for 20 min and were blocked and permeabilized with a PBS buffer containing 0.2% saponin and 5% non-fat milk (30 min). All antibodies were diluted in blocking solution and incubations were performed for 1h at room temperature. Cells stably expressing N2HA, N2N, and N1C-HA proteins were labeled with anti-Nramp2 NT Ab (1:200), while cells expressing N1, N1N-HA, and N2C proteins were labeled anti-Nramp1 NT Ab (1:400). All cells were subsequently incubated with a goat anti-rabbit secondary Ab coupled to Cy3. Cells were visualized using an Axiovert 200M epi-fluorescence microscope with a 100× oil immersion objective. Digital images were acquired with a Zeiss AxioCam HRm camera operated with AxioVision 4.3. Images were cropped, assembled and labeled using Adobe Photoshop and Illustrator softwares.

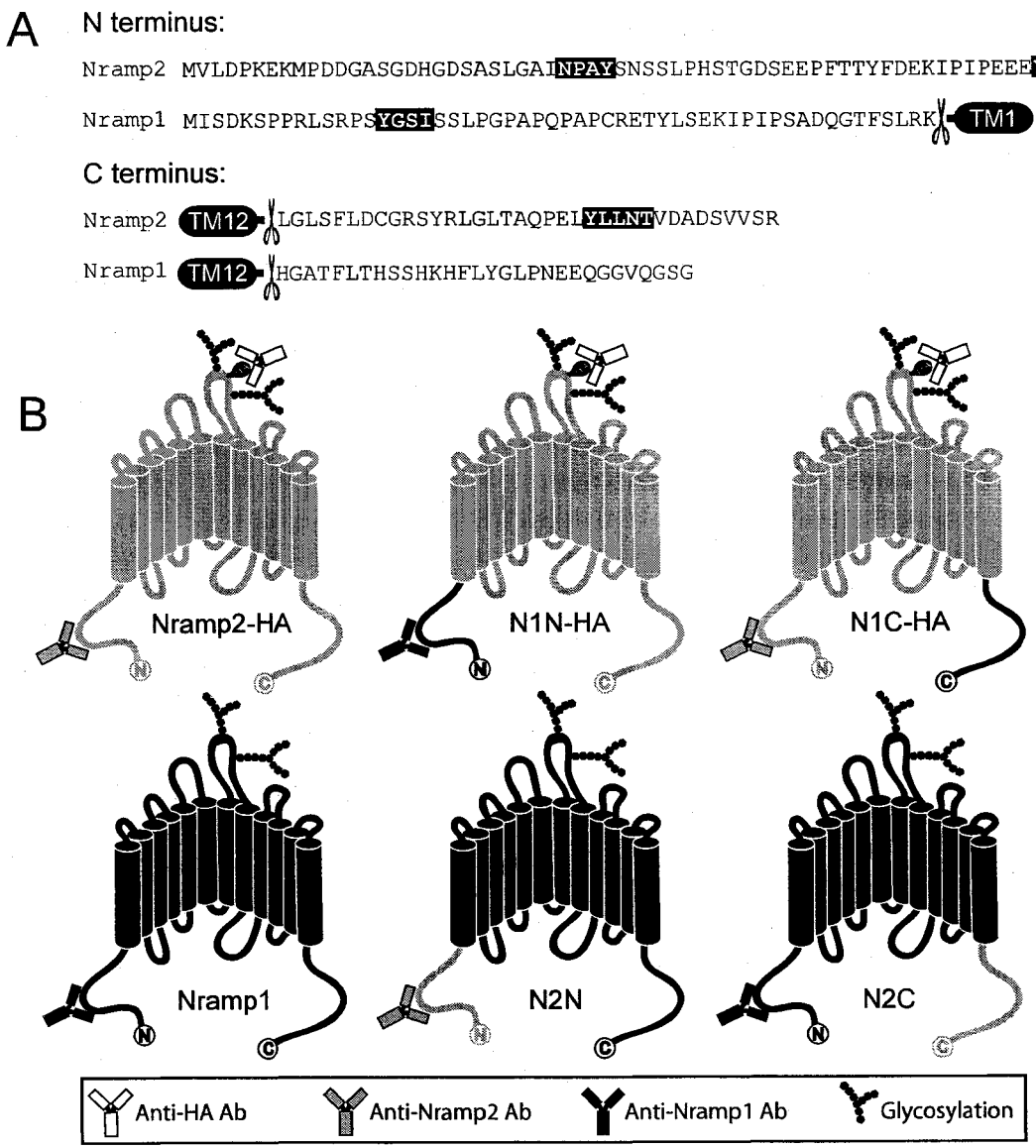

Figure 1. Predicted trafficking motifs and design of Nramp1/Nramp2 chimeric proteins. (A) Sequences of the amino (N) and carboxyl (C) terminal regions of Nramp1 and Nramp2 are shown, including the locations of predicted targeting motifs (highlighted black), transmembrane domains 1 (TM1) and 12 (TM12), and the locations of the sequence boundaries for the chimeras (scissors). In Nramp1, amino acid residues 1-54 and 519-548 were considered as the N and C-terminal regions, respectively. In Nramp2, residues 1-69 and 533-568 were considered as the N and C-terminal regions, respectively. (B) Nramp1/2 chimeras were created by exchanging the amino and carboxyl terminal segments of Nramp1 and Nramp2. Schematic representations are shown of wild-type Nramp2-HA (gray), wild-type Nramp1 (black) as well as the four chimeras created. The positions of antigenic epitopes recognized by the anti-HA, anti-Nramp1 and anti-Nramp2 antibodies as well as the putative N-linked glycosylation sites (Nramp1: N321, N335; Nramp2: N336, N349) are indicated.

RESULTS

Construction and expression of Nramp1 and Nramp2 chimeric proteins

To better understand the trafficking of Nramp proteins, we created chimeric molecules by exchanging the predicted cytosolic amino and carboxyl terminal segments of Nramp1 and Nramp2. Nramp2 chimeras containing either the amino (N1N-HA) or carboxyl (N1C-HA) predicted cytosolic segments of Nramp1 were constructed using the Nramp2 isoform II (non-IRE) backbone bearing an exofacial hemagglutinin (HA) tag that allowed for recognition of cell surface molecules in intact cells (Figure 1B). We have previously shown that insertion of this HA tag in the fourth predicted extra-cytoplasmic loop (EC4) of Nramp2 does not affect its expression, activity, or subcellular localization [51]. Nramp1 chimeras containing either the amino (N2N) or carboxyl (N2C) predicted cytosolic segments of Nramp2 isoform II (non-IRE) were introduced into an unmodified Nramp1 protein backbone (Figure 1B). We have previously shown that an Nramp1 molecule modified by insertion of an HA tag in EC4 is mis-targeted to the plasma membrane of transfected CHO cells [27], precluding the use of that site for epitope tag insertion for the present studies. All Nramp1 and Nramp2 chimeras were introduced into LLC-PK_1 porcine kidney cells and cell clones stably expressing individual variants were selected and expanded for analysis. Figure 2A shows a typical immunoblot of extracts prepared from cells transfected with either *Nramp2*, *Nramp1* or chimeric cDNAs. Immunoblots were probed separately with antibodies against the HA tag, the amino terminus of Nramp2, and the amino terminus of Nramp1. Wild-type (WT) Nramp2 was detected as two immunoreactive species, a minor species at ~60 kDa and major species at ~90-105 kDa (Figure 2A). Previous studies from our group have shown that the minor species corresponds to the precursor "core glycosylated" protein while the major species corresponds to the mature "complex glycosylated" forms of the protein [51]. Interestingly, N1N-HA was detected as two species of faster electrophoreitic mobility than WT Nramp2, indicating a significant difference in the extent of core and complex glycosylation in this chimeric protein (Figure 2A). This result suggests that sequences in the amino terminus of Nramp2 are important for proper glycosylation of the transporter.

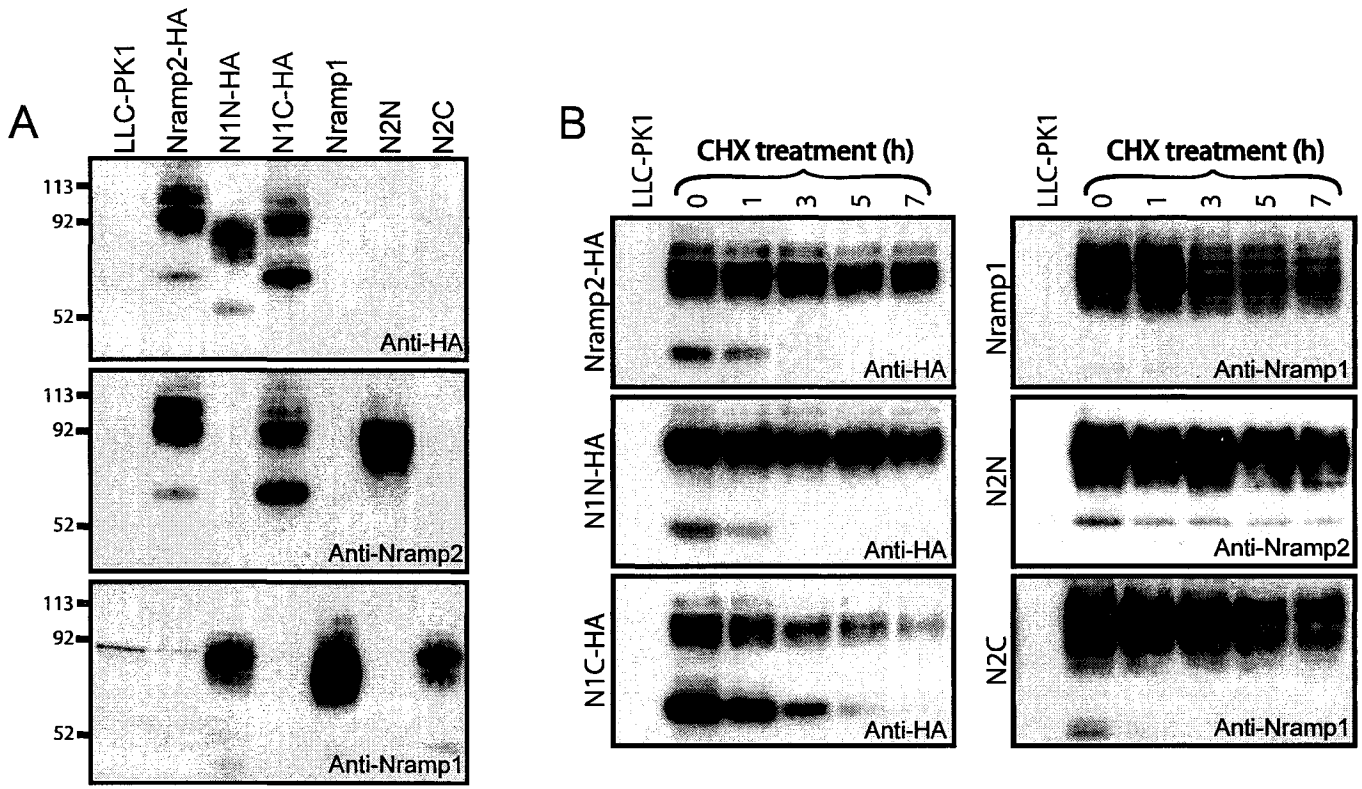

Figure 2. Expression and stability of Nramp1/2 chimeras in transfected LLC-PK1 cells. Total cell extracts from untransfected cells (LLC-PK1) and cell clones stably-expressing wild type Nramp1 (Nramp1), wild type Nramp2 (Nramp2-HA) and the Nramp1/2 chimeras (N1N-HA, N1C-HA, N2N, N2C) were resolved by SDS-PAGE and analyzed by immunoblotting. (A) Immunoblots were incubated with antibodies recognizing either the HA epitope (anti-HA), the amino terminus of Nramp2 (anti-Nramp2), or the amino terminus of Nramp1 (anti-Nramp1). The sizes of molecular mass standards (in kilodaltons) are indicated. In panel (B), transfectants expressing the indicated proteins were treated with the translation inhibitor cycloheximide (20 μg/mL) for 0, 1, 3, 5, or 7 hours. Immunoblotting of total cell lysates was carried out to assess the stability of wild-type and chimeric proteins. Antibodies used for each blot are indicated.

N1C-HA was detected as two immunoreactive species of electrophoretic mobility similar to that of WT Nramp2. However, the proportion of the immature precursor N1C-HA protein (~60 kDa) appeared significantly greater than that found for WT Nramp2, suggesting possible incomplete maturation of this chimera (Figure 2A). WT Nramp1 as well as chimeras N2N and N2C, were detected as single immunoreactive species of ~70-75 kDa (Figure 2A, bottom panel). LLC-PK_1 cells expressing the different WT and chimeric proteins were treated with the translation inhibitor cycloheximide for different periods of time and the fate of core glycosylated and mature protein isoforms was analyzed by immunoblotting (Figure 2B). These experiments showed that WT Nramp2 and Nramp1, as well as the chimeras N1N-HA, N2N, and N2C quickly matured from a core glycosylated precursor to a fully mature form which remained stable for a 7-hour period. Interestingly, the N1C-HA chimera displayed increased persistence of precursor and reduced stability of the mature form compared to controls with little protein detectable at 7 hours (Figure 2B). These results suggest impaired processing of the N1C-HA chimera.

Cell surface expression of chimeric proteins

We used a cell surface biotinylation technique to quantify plasma membrane expression of the Nramp1/2 chimeras at steady-state [184;262]. LLC-PK_1 cells stably expressing either WT or chimeric Nramp constructs were treated with a membrane-impermeable biotin compound to label all cell surface proteins. After solubilization, cell surface proteins were isolated with immobilized strepavidin, followed by separation by SDS-PAGE and visualization by immunoblotting (Figure 3A, *Surface*). Cell surface expression of each protein was then compared to total protein expression for each cell line (Figure 3A, *Total*). WT Nramp2-HA and N1C-HA were detected at robust levels at the plasma membrane while WT Nramp1, N1N-HA, N2N, and N2C displayed little or no cell surface expression (Figure 3A). Clearly, replacing either the amino (N2N) or carboxyl (N2C) termini of Nramp1 with the equivalent segments of Nramp2 did not result in plasma membrane expression. Because Nramp2-HA, N1N-HA, and N1C-HA were constructed with exofacial HA tags in predicted EC4, the fraction of each variant present at the cell surface at steady-state could be determined by exposing fixed LLC-PK_1

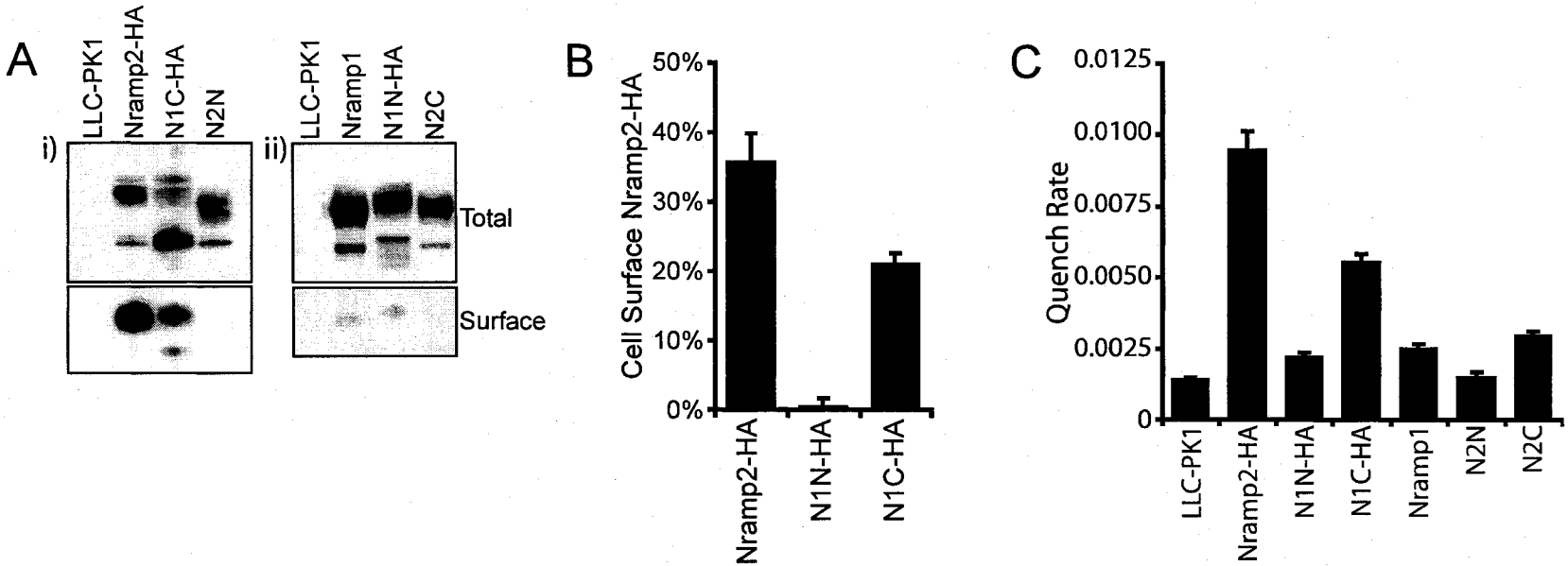

Figure 3. Cell surface expression and metal transport activity of the Nramp1/2 chimeras. (A) Cell surface biotinylation was used to assess plasma membrane expression of wild type Nramp1 (Nramp1), wild type Nramp2 (Nramp2-HA) and the Nramp1/2 chimeras (N1N-HA, N1C-HA, N2N, N2C). Live cells were labeled with a membrane impermeable biotin compound (see "Materials and Methods"). Total cell protein extracts were prepared and biotinylated proteins were isolated by affinity capture with streptavidin-agarose beads. Equivalent amounts of total cell extracts (Total) and captured biotinylated protein (Surface) were resolved by SDS-PAGE followed by immunoblotting with anti-Nramp2 (i) or anti-Nramp1 (ii) polyclonal antibodies. (B) The fraction of Nramp2-HA, N1N-HA, and N1C-HA expressed at the cell surface was quantified using the exofacial HA epitope tag inserted in predicted extra-cytoplasmic loop 4 of those proteins. Briefly, cells were fixed and incubated with primary anti-HA antibody with or without prior detergent permeabilization followed by incubation with an HRP-coupled secondary antibody and quantification by a colorimetric assay. The amount of Nramp proteins expressed at the cell surface (in non-permeabilized cells) is shown as a fraction (%) of total protein expression (in permeabilized cells). In panel (C), metal transport activity of the Nramp1/2 chimeras was determined using a fluorescence quenching assay. Cells loaded with a metal-sensitive fluorescent dye were incubated with Co2+ in acidic buffer. Results are shown as the initial rates of fluorescence quenching. Error bars represent standard error of the means of three or more independent determinations.

transfectants to anti-HA antibody, with (total expression) or without (cell surface) prior permeabilization with detergent. The amount of bound anti-HA antibody was quantified using a secondary antibody coupled to horse-radish peroxidase. We determined that 35.9 ± 3.9% (mean ± S.E.) of WT Nramp2-HA and 21.3 ± 1.3% of N1C-HA were expressed at the cell surface compared to a modest 0.5 ± 1.2% for N1N-HA (Figure 3B). These values are consistent with cell surface biotinylation results (Figure 3A) and suggest that the amino terminus of Nramp1 impairs normal targeting of Nramp2 to the plasma membrane.

Nramp2 isoform II is normally expressed at the plasma membrane and in recycling endosomes in LLC-PK_1 cells. Replacing the carboxyl terminus of Nramp2-HA with the equivalent segment of Nramp1 (N1C-HA) did not have a major effect on the cell surface expression of the transporter (Figure 3A, 3B). Interestingly, despite the impaired processing and reduced stability, N1C-HA retained significant metal transport activity (Figure 3C). This activity likely stems from the significant fraction of mature N1C-HA protein that is expressed at the cell surface. On the other hand, replacing the amino terminus of Nramp2-HA with the equivalent segment from Nramp1 (N1N-HA) drastically reduced surface expression (Figure 3A, 3B) as well as metal transport activity (Figure 3C). This result suggests that the amino terminus of Nramp1 contains targeting information that affects the normal trafficking of Nramp2 to the plasma membrane.

Subcellular localization of chimeric proteins

Immunofluorescence was used to compare the subcellular localization of wild-type and chimeric proteins at steady-state. LLC-PK_1 transfectants were fixed, permeabilized, and chimeric proteins were labeled with polyclonal antibodies recognizing either Nramp1 or Nramp2. Consistent with our previously published data [51;184], Nramp2-HA displayed strong colocalization with GFP-syntaxin 13, while Nramp1 showed little overlap with the recycling endosome marker (Figure 4A). Interestingly, all chimeras showed no significant colocalization with GFP-syntaxin 13 (Figure 4A). These results suggest that substitution of either the amino or carboxyl terminus of Nramp2 by homologous segments of Nramp1 impairs targeting to the recycling endosome compartment.

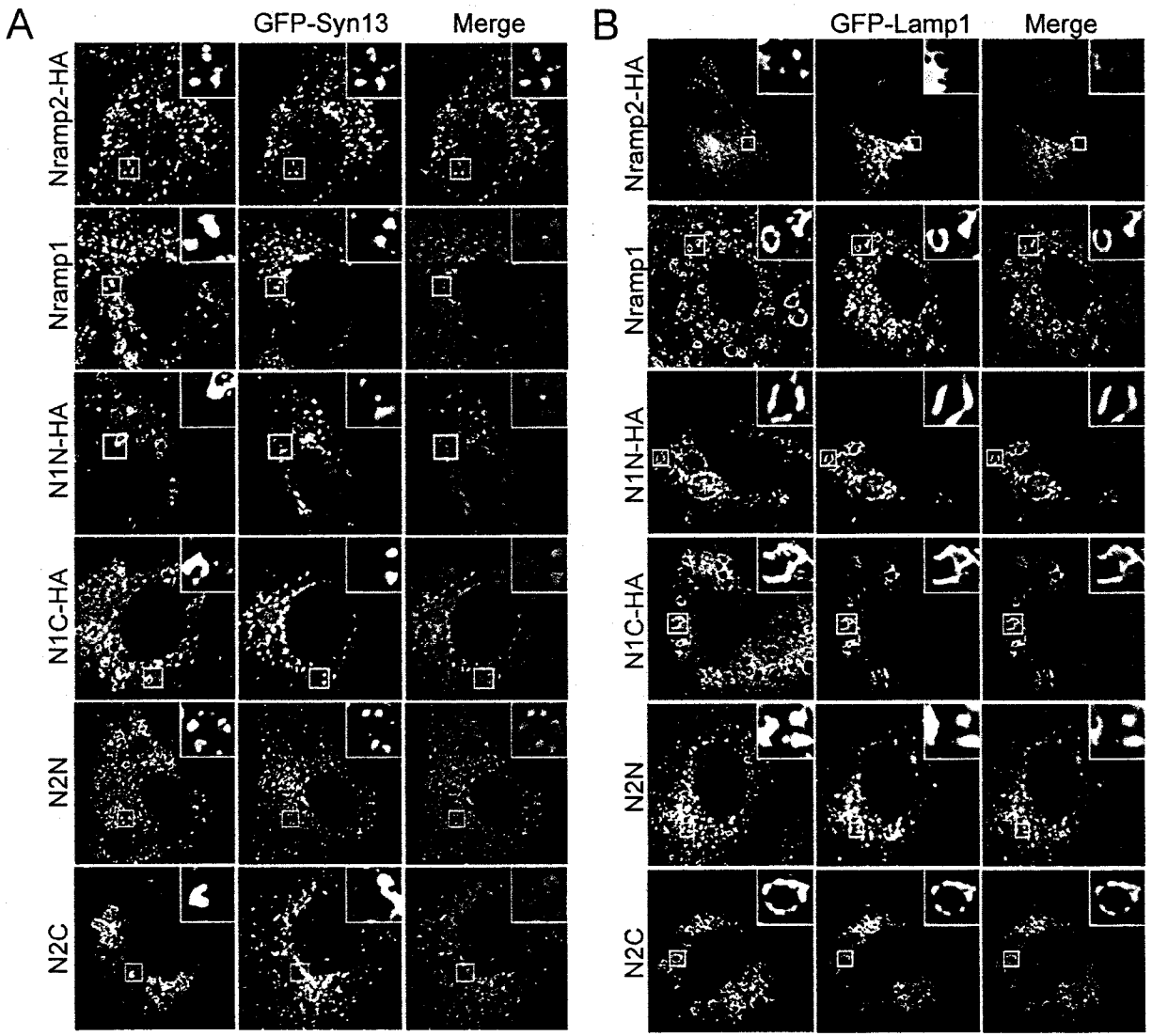

Figure 4. Subcellular localization of Nramp1/2 chimeras. LLC-PK1 cells stably expressing wild type Nramp1 (Nramp1), wild type Nramp2 (Nramp2-HA) and the Nramp1/2 chimeras (N1N-HA, N1C-HA, N2N, N2C) were transiently transfected with either GFP-syntaxin 13 to label recycling endosomes (A) or GFP-Lamp1 to label late endosomes and lysosomes (B). Twenty-four hours later, cells were fixed, permeabilized and stained with either anti-Nramp1 or anti-Nramp2 polyclonal antibodies followed by a secondary antibody coupled to fluorescent Cy3. Images were acquired by epifluorescence microscopy. Insets show magnifications of the area boxed in the figure.

Consistent with previously published data [35], Nramp1 showed strong colocalization with the lysosomal marker GFP-Lamp1 while Nramp2-HA displayed little colocalization with this marker (Figure 4B). These results confirm that Nramp1 is properly targeted to the lysosomal compartment in LLC-PK_1 cells. Remarkably, all chimeras displayed significant colocalization with GFP-Lamp1 (Figure 4B), indicating their presence in late endosomes and lysosomes. Clearly, replacing the amino or carboxyl termini of Nramp1 with the equivalent regions of Nramp2 (N2N, N2C) did not significantly affect the subcellular distribution of Nramp1 at steady-state (Table 2). Previous work by us and others have demonstrated that the C terminus of Nramp2 isoform II contains targeting information (including a YLLNT signal) crucial for endocytosis and recycling of the transporter from the plasma membrane [155;184]. Mutations or deletions in this motif result in a protein that has impaired recycling following internalization from the cell surface and accumulates in the lysosomal compartment [184]. Consistent with these findings, replacing the C terminus of Nramp2 with the equivalent segment from Nramp1 (N1C-HA) resulted in plasma membrane expression (Figure 3) and lysosomal targeting (Figure 4B, Table 2). Therefore, the mistargeting displayed by N1C-HA is probably due to removal of the C terminus of Nramp2 rather than the presence of a dominant targeting signal in the C terminus of Nramp1. A fraction of N1C-HA showed some colocalization with the endoplasmic reticulum marker GFP-Sec61 (data not shown), suggesting that some N1C-HA may be retained in the ER. Finally, substituting the amino terminus of Nramp2 with the equivalent segment from Nramp1 (N1N-HA) yielded the most intriguing result. N1N-HA showed subcellular localization indistinguishable from WT Nramp1, with no significant surface expression (Table 2) but strong lysosomal targeting (Figure 4B). These results suggest that the amino terminus of Nramp1 possesses lysosomal targeting information that can act in a dominant fashion over the recycling endosome signal present in the C terminus of Nramp2 isoform II.

Characterization of the YSGI motif in the N terminus of Nramp1

Closer examination of the predicted cytoplasmic N terminal region of Nramp1 revealed a $YGSI^{15-18}$ motif that fits the YXXΦ consensus signature (Figure 1A). YXXΦ motifs have been implicated in targeting membrane proteins such as LAMP-1 and

Table 2: Subcellular localization of Nramp1/2 chimeras

	PM	RE	LE/Lys	ER
Nramp2-HA	+	+	–	–
N1N-HA	–	–	+	–
N1C-HA	+	–	+	+
Nramp1	–	–	+	–
N2N	–	–	+	–
N2C	–	–	+	–

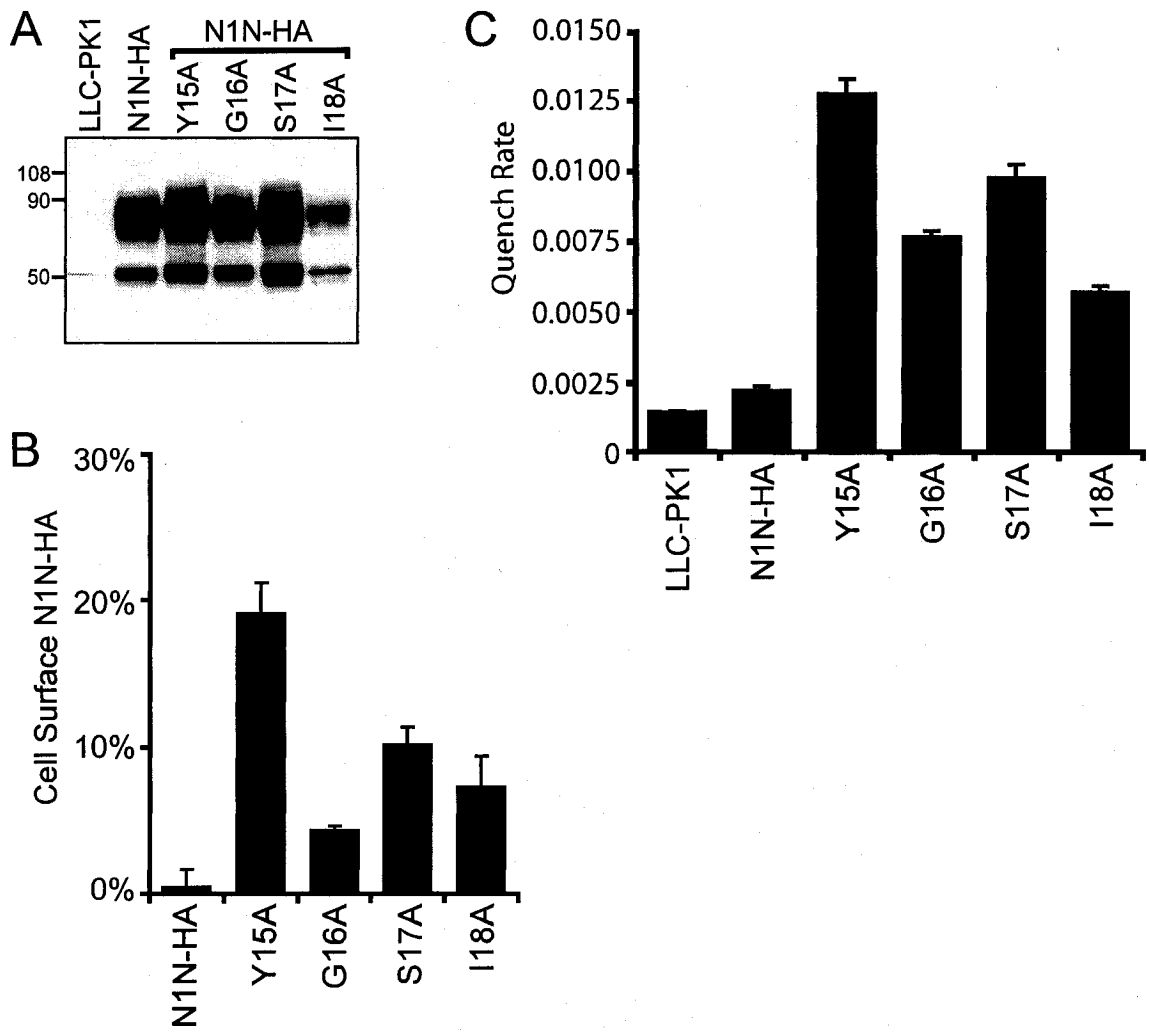

Figure 5. Characterization of N1N-HA targeting motif mutants. (A) Total cell extracts were prepared from transfectants stably-expressing individual mutants (Y15A, G16A, S17A, and I18A) in the putative YGSI lysosomal targeting motif present in the N1N-HA backbone. Equal amounts of cell extract were resolved by SDS-PAGE and analyzed by immunoblotting with anti-HA antibody. The sizes of molecular mass standards (in kilodaltons) are indicated. In panel (B), the fraction of N1N-HA expressed at the cell surface was determined as described in the legend of Figure 3B. (C) Metal transport activity of the N1N-HA targeting motif mutants was measured by quenching of calcein fluorescence, as described in the legend of Figure 3C. Error bars represent standard error of the means of three or more independent determinations.

LAMP-2 to lysosomes by interacting with the μ subunits of AP-1 and AP-2 complexes [183;331;332;351;352]. To determine if the YGSI motif in the N terminus of Nramp1 was responsible for the lysosomal targeting of the N1N-HA chimera, we created alanine substitutions at each position of the YGSI signal within the N1N-HA chimeric construct. The mutants were stably transfected into LLC-PK_1 cells and clones positive for expression were selected for analysis. Immunoblot analysis performed on cell extracts showed stable expression of Y15A, G16A, S17A mutants at levels comparable to N1N-HA, although lower expression was detected for I18A (Figure 5A). We determined the fraction of each N1N-HA expressed at the cell surface. Mutating any of the residues in the YGSI motif to alanine increased the surface expression of the chimera (Figure 5B). Y15A demonstrated the highest surface expression (19.2 ± 2.0%) followed by S17A (10.2 ± 1.2%), I18A (7.4 ± 2.1%), and G16A (4.4 ± 0.3%). This increase in surface expression was concomitant to a commensurate increase in metal transport activity for the mutants (Figure 5C), implying that N1N-HA is indeed properly folded in a transport competent manner at the cell surface.

We determined the subcellular localization of the N1N-HA mutants at steady-state in fixed and permeabilized cells. Mutants G16A and S17A displayed subcellular localization similar to N1N-HA, showing little colocalization with the recycling endosome marker GFP-syntaxin 13 (Figure 6A) but strong colocalization with the lysosomal marker GFP-Lamp1 (Figure 6B). These results suggest that G16 and S17 are not essential for the lysosomal targeting of N1N-HA. Strikingly, mutants Y15A and I18A displayed subcellular localization similar to WT Nramp2, showing strong colocalization with syntaxin 13-positive recycling endosomes (Figure 6A) but little colocalization with Lamp1-positive lysosomes (Figure 6B; summarized in Table 3). These results suggest that Y15 and I18 are critical for the lysosomal targeting of N1N-HA and that the YGSI motif in the N terminus of Nramp1 functions as a YXXΦ lysosomal targeting signal. Furthermore, this YGSI signal appears to dominate the recycling endosome signal present in the C terminus of Nramp2 isoform II.

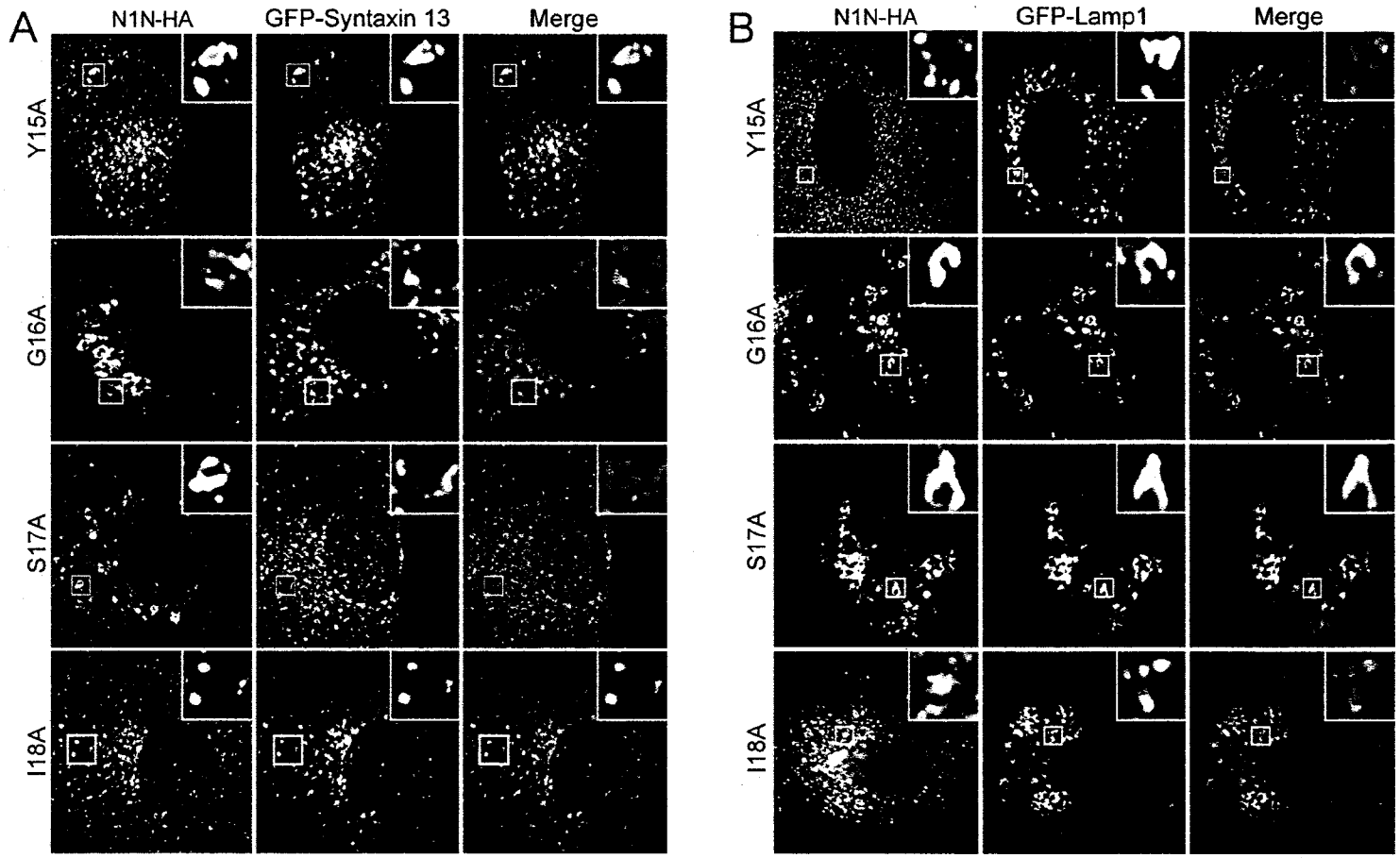

Figure 6. Subcellular localization of N1N-HA mutants. LLC-PK1 cells stably expressing N1N-HA YGSI mutants were transiently transfected with either the recycling endosome marker GFP-syntaxin 13 (A) or the late endosomal and lysosomal marker GFP-Lamp1 (B). Twenty-four hours later, cells were fixed, permeabilized and stained with an anti-Nramp1 polyclonal antibody followed by a secondary antibody coupled to fluorescent Cy3. Images were acquired by epifluorescence microscopy. Insets show magnifications of the area boxed in the figure.

Table 3: Subcellular localization of N1N-HA mutants

	PM	RE	LE/Lys	ER
N1N-HA	–	–	+	–
Y15A	+	+	–	–
G16A	+	–	+	–
S17A	+	–	+	–
I18A	+	+	–	–

DISCUSSION

In this study, we sought to investigate the subcellular targeting and trafficking properties of Nramp1, including the identification of sorting signals responsible for its distinct localization in lysosomes of mononuclear phagocytes. For this, we constructed chimeric proteins in which homologous domains of Nramp1 and the closely-related iron transporter Nramp2 (isoform II) were exchanged. Replacing the amino (N2N) or carboxyl (N2C) terminal cytoplasmic segments of Nramp1 with the equivalent segments from Nramp2 did not drastically affect the expression or subcellular localization of the transporter. Indeed, both N2N and N2C chimeras exhibited little cell surface expression but showed strong lysosomal targeting, typical of WT Nramp1. These results suggested that sorting signals in the amino and carboxyl cytoplasmic termini of Nramp2 are unable to confer cell surface and/or recycling endosome targeting to the Nramp1 backbone. Results with the N2N chimera are supported by our previous work showing that deletion mutations at putative sorting signals in the N terminus of Nramp2 do not significantly affect the cell surface or recycling endosome targeting of the transporter [184]. In contrast, we and other groups have shown that a YLLNT motif in the C terminus of Nramp2 isoform II controls the protein's internalization and recycling from plasma membrane [155;184]. However, results with the N2C chimera suggested that this YLLNT motif was somehow masked or non-functional when placed on the background of Nramp1.

An Nramp2-HA chimera bearing the C terminal cytoplasmic segment of Nramp1 (N1C-HA) was robustly expressed in LLC-PK_1 cells but displayed a higher fraction of a ~60 kDa precursor species and a lower fraction of the ~90 kDa mature protein, suggesting impaired processing of this chimera. N1C-HA also displayed reduced stability. Surface biotinylation experiments revealed that the mature, fully glycosylated N1C-HA was expressed at the cell surface (Figure 2A) and was likely responsible for the residual metal transport activity observed for this construct (Figure 2C). This result suggests that complex glycosylation acquired by the precursor protein in the Golgi apparatus is critical for the plasma membrane targeting of mature Nramp2. Strikingly, the multiple biosynthetic and functional defects of the N1C-HA chimera virtually mirror those observed for the $Nramp2^{G185R}$ mutant protein produced in *mk* mice and *Belgrade* rats [148].

While a small fraction of N1C-HA displayed some colocalization with the ER marker GFP-Sec61 (data not shown), a more significant fraction of the chimera was expressed in late endosomes and lysosomes. We have previously shown that critical mutations at the C terminus of Nramp2 isoform II (including a truncation of the entire C terminal segment) results in a protein that is unable to recycle after internalization from the cell surface and is targeted to the lysosomes by default [184]. Therefore, we reasoned that the lysosomal targeting displayed by N1C-HA is likely the result from the removal of the C terminus of Nramp2 rather than the presence of a dominant targeting signal in the C terminus of Nramp1.

An Nramp2 chimera bearing the N terminus of Nramp1 (N1N-HA) yielded perhaps the most intriguing results. N1N-HA was stably expressed in transfected LLC-PK_1 cells as a protein of lower apparent molecular weight compared to Nramp2-HA (Figure 2A), probably due to altered glycosylation of the chimera. Interestingly, the extent of glycosylation of N1N-HA resembled more closely that of Nramp1 (Figure 2A) and raises the possibility that the N terminus of Nramp2 contains sequence information that affects the extent of glycosylation of the transporter either directly or indirectly by mediating its trafficking and retention to specific subcellular compartments. Strikingly, N1N-HA also displayed subcellular targeting properties similar to Nramp1, with no surface expression yet strong lysosomal targeting (Figures 3 and 4). These results strongly suggested that the N terminal cytoplasmic segment of Nramp1 contained lysosomal targeting information that was able to act in a dominant fashion over a known recycling endosome targeting signal ($YLLNT^{555-559}$) in the C terminus of Nramp2 isoform II present in N1N-HA. The lack of significant transport activity for N1N-HA, as for Nramp1, likely resulted from the lack of expression at the site of transport measurements (plasma membrane) rather than expression of a non-functional protein (Figure 3). Closer examination of the amino acid sequence within the N terminus of Nramp1 revealed a potential tyrosine-based signal of the form YXXΦ ($YGSI^{15-18}$) (Figure 1A). Alanine substitution mutations at Y15 and I18 within the N1N-HA chimera were able to restore cell surface and recycling endosome targeting of the Nramp2 chimera (Figures 5B and 6B). However, alanine mutations at G16 and S17 of N1N-HA retained their lysosomal

targeting (Figure 6B). These results clearly demonstrate that YGSI$^{15-18}$ functions as a lysosomal targeting motif that fits the consensus YXXΦ in the N terminus of Nramp1. YXXΦ signals have been shown to function as lysosomal sorting motifs in membrane proteins such as LAMP-1 (YQTI) [333]. YXXΦ signals are known to bind the μ subunits of AP complexes strictly through their Y and Φ residues, however the X residues and other residues flanking the motif contribute to the strength and specificity of the signals [183].

The identification of an Nramp1 lysosomal targeting signal allows us to propose a model for the role of cytoplasmic motifs in subcellular trafficking of Nramp1 and Nramp2. In this model (Figure 7), Nramp2 isoform II is synthesized in the ER, targeted to the Golgi apparatus for complex glycosylation, and dispatched to the plasma membrane. At the cell surface, Nramp2 recruits specific adaptor proteins required for rapid clathrin-mediated endocytosis through binding to a YLLNT motif present in its C terminus. Nramp2 is then internalized into early endosomes and the recruited adaptor complexes are involved in signaling the recycling of the transporter back to the cell surface via recycling endosomes (Figure 7). This pathway is shared by the transferrin receptor and is of critical importance for iron acquisition from transferrin following acidification of the endosomes and Nramp2-mediated translocation of iron to the cytoplasm. Similar to Nramp2, Nramp1 is targeted from the ER to the Golgi for complex glycosylation. However, the recognition of the YGSI signal by specific adaptor proteins mediate the sorting of Nramp1 directly from the trans-Golgi network to late endosomes and lysosomes (Figure 7). The N1N-HA chimera, which possesses the Nramp1 YGSI signal, is targeted in a similar fashion as WT Nramp1, with the N-terminal lysosomal signal taking precedence over the C-terminal YLLNT recycling signal. N1N-HA$^{Y15A,\ I18A}$ mutants are unable to recruit lysosomal sorting proteins and are targeted to recycling endosomes via the C-terminal YLLNT signal in a similar fashion to WT Nramp2 (Figure 7). On the other hand, while alanine mutations at G16 and S17 of N1N-HA do not drastically affect lysosomal targeting, the mutations may reduce the effectiveness of the YXXΦ signal. This reduced sorting efficiency may result in a higher fraction of N1N-HA$^{G16A,\ S17A}$ mutants being sorted to the cell surface and subsequently targeted to the lysosomal compartment via the endocytic pathway (Figure 7). It has been shown that

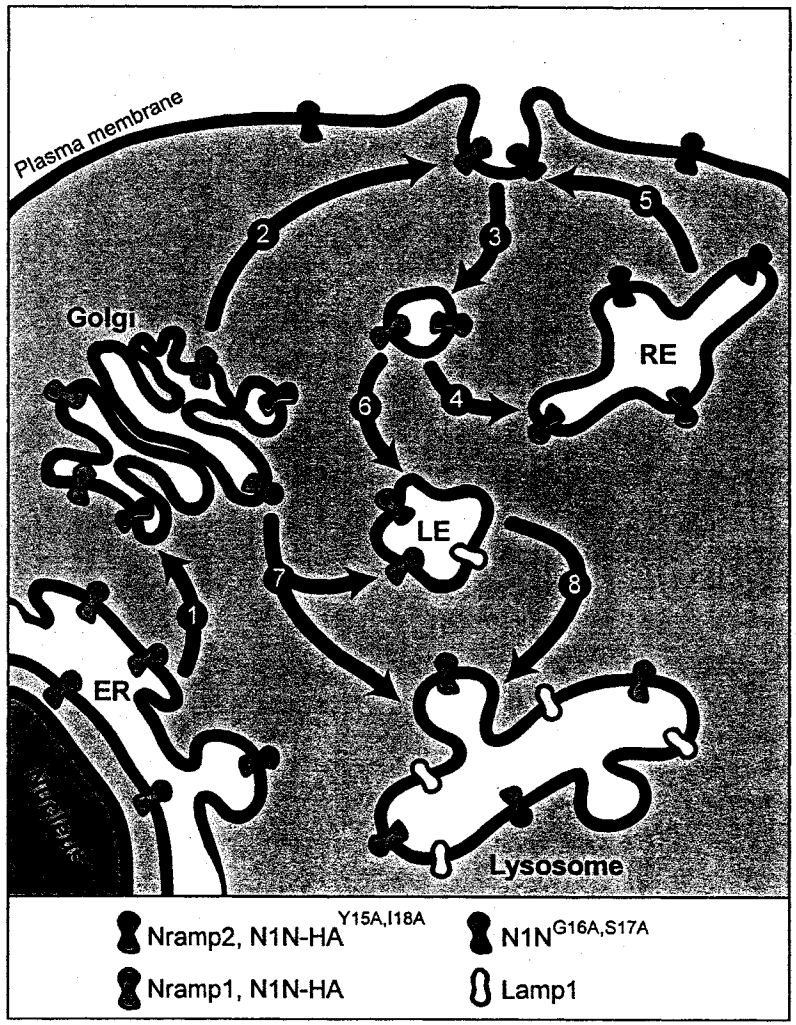

Figure 7. Model for subcellular trafficking of Nramp1 and Nramp2(isoform II). Nramp2 isoform II is synthesized in the ER, targeted to the Golgi apparatus (step 1) for complex glycosylation, and targeted to the plasma membrane (step 2). At the cell surface, Nramp2 is internalized via a clathrin and dynamin dependent process by recruiting adaptor proteins that specifically recognize the C-terminal YLLNT motif (step 3). Nramp2 is then targeted to early endosomes and the interaction of YLLNT with adaptor proteins mediate its recycling back to the cell surface via recycling endosomes (steps 4 and 5). Nramp1 is similarly trafficked to the Golgi after synthesis (step 1). However, recognition of the YGSI signal by lysosomal sorting proteins mediate its targeting from the trans-Golgi network directly to late endosomes and lysosomes (steps 7 and 8). The Nramp2-HA chimera N1N-HA, which possesses the Nramp1 N-terminal YGSI signal, is targeted in a similar fashion as WT Nramp1. N1N-HA(Y15A, I18A) mutants are unable to recruit lysosomal sorting proteins and are targeted to recycling endosomes via the C-terminal YLLNT signal in a similar fashion to WT Nramp2. N1N-HA(G16A, S17A) mutants are sorted less efficiently to lysosomes, leading to some cell surface accumulation. These mutants, however, are not recycled upon internalization and are ultimately targeted to lysosomes via the normal endocytic pathway.

mutations in the X residues or in other residues neighboring the YXXΦ signal can impair lysosomal targeting without significantly disrupting internalization [351;353;354]. An indirect targeting of N1N-HA$^{G16A, S17A}$ mutants to lysosomes via the plasma membrane would explain the increased cell surface expression observed for these mutants (Figure 5B).

Interestingly, the YGSI signal in Nramp1 does not completely conform to the YXXΦ signals found in several other lysosomal proteins, which raises the possibility that YGSI may represent a novel subset of YXXΦ signals. Two common features of YXXΦ signals involved in lysosomal targeting seem to be the presence of a glycine residue preceding the critical tyrosine as well as the prevalence of the motifs in the C terminus of membrane proteins [183]. Nramp1 possesses a serine instead of a glycine upstream of its YGSI signal. Also, the YGSI signal is found in the N terminus of the protein as opposed to the more commonly found C terminus. N-terminal YXXΦ motifs have been identified in proteins such as the transferrin receptor (YTRF) but function typically as endocytic signals. Additional experiments are needed to identify the specific binding partners of YGSI and better understand the molecular machinery involved in the sorting of Nramp1 to late endosomes and lysosomes. Hopefully, the characterization of other tyrosine-based signals in the cytoplasmic domains of lysosomal proteins will clarify whether the YGSI motif in Nramp1 represents a novel subset of YXXΦ motifs.

Clearly, proper lysosomal targeting of Nramp1 is critical for its anti-microbial activity as a metal efflux pump at the phagosomal membrane of macrophages and other phagocytic cells. Upon phagocytosis of a live pathogen, Nramp1-positive lysosomes fuse with the membranes of the pathogen-containing phagosomes and Nramp1 remains associated with the phagosomes through their maturation to fully anti-microbial phagolysosomes [35]. Our discovery that a sequence motif in the amino terminus of Nramp1 is sufficient to target Nramp proteins to the lysosomes suggest a model for functional evolution of Nramp proteins. In this model, Nramp1 and Nramp2 were generated by gene duplication from a common ancestor, followed by subsequent sequence divergence to retain function with respect to mechanism of transport and ion selectivity. Further divergence, including (a) restriction of *Nramp1* transcriptional activity to cells of the mononuclear and polymorphonuclear phagocyte lineages, and (b)

acquisition of a targeting signal in the amino terminus (YGSI) actively directing Nramp1 localization to lysosomes for delivery to pathogen-containing phagosomes, would have ensued to enable metal efflux at the phagosomal membrane. This activity appears to have been extremely beneficial to the host and has been preserved throughout evolution from lower eukaryotes to humans [1].

Chapter 8:

Summary and Future Perspectives

8.1 Summary

The work presented in this thesis examined the structure, function, and subcellular trafficking of Nramp proteins by centering on the two mammalian orthologs, Nramp1 and Nramp2. The first three chapters of this thesis explored structure-function relationships in the Nramp super-family. In Chapter 2, the role of charged amino acids within the membrane-spanning segments of Nramp2 were examined by site-specific mutagenesis followed by functional characterization in both yeast and transfected CHO cells [28]. These studies identified three negatively charged and highly conserved residues in TM1, TM4, and TM7 as essential for metal transport by Nramp2. These studies also identified a pair of invariant histidines in TM6 that play an important role in pH regulation of metal transport by Nramp proteins. In Chapters 3 and 4, the effects of two *NRAMP2* mutations found in human patients suffering from severe congenital hypochromic microcytic anemia and iron overload were characterized. The mutation found in first patient had two effects: it severely impaired proper *NRAMP2* pre-mRNA splicing, and introduced an amino acid polymorphism (E399D) in the protein encoded by the remaining properly spliced transcript [4]. The functional properties the E399D mutation as well as other independent mutants at that position (E399Q, E399A), were studied in transfected LLC-PK_1 kidney cells (Chapter 3) [262]. All mutations at E399 were shown to be fully functional with respect to stability, metal transport activity, and targeting, indicating that the reduced Nramp2 function in the patient was likely caused by a quantitative reduction in *NRAMP2* mRNA levels due to improper splicing. The second patient was found to be compound heterozygote for mutations in *NRAMP2*, including a 3 base pair deletion that partially impairs splicing, and an amino acid substitution (R416C) at a conserved residue in TM9 of the protein [5]. The functional properties and possible contribution to disease of the R416C variant were studied in independent mutants at that position (R416C, R416A, R416K, R416E) expressed in LLC-PK_1 cells (Chapter 4) [264]. Non-conservative substitutions at R416 (C, A, E) caused multiple functional deficiencies concomitant with retention of the transporter in the endoplasmic reticulum. Conversely, a conservative isoelectric substitution (R416K) was less vulnerable, resulting in a functional transporter that was properly processed and targeted to the cell surface and to recycling endosomes.

These results showed that R416C represents a complete loss-of-function and that a quantitative reduction in Nramp2 expression is the cause of the microcytic anemia and iron overload in this patient.

The last three chapters of this thesis were aimed at better understanding the subcellular distribution of Nramp1 and Nramp2. Alternate splicing of *Nramp2* pre-mRNA at 3' exons generates two protein isoforms (I and II) differing only in their carboxyl terminal segments. It had been previously shown that Nramp2 isoform II is expressed at the plasma membrane and in transferrin receptor-positive recycling endosomes at steady-state. The work described in Chapter 5 focused on identifying signal(s) in the cytoplasmic segments of Nramp2 isoform II responsible for its subcellular targeting and internalization from the plasma membrane into recycling endosomes [184]. Deletion mutations were introduced at several predicted tyrosine (NPXY, YXXΦ) and dileucine-based (LL) motifs in the amino and carboxyl terminal segments of Nramp2 isoform II and the mutants were expressed and studied in transfected LLC-PK_1 cells for transport activity, subcellular localization, cell surface and recycling pool distribution, and internalization from the plasma membrane. This work led to the identification of a tyrosine-based motif in the carboxyl terminus of Nramp2 isoform II ($YLLNT^{555-559}$) that is critical for the transporter's internalization from the cell surface and its recycling back to the plasma membrane. Several studies suggested that while isoform II is predominantly expressed in erythroid cells, isoform I is predominantly expressed in epithelial cells [40;155;160]. However, the significance of this tissue-specific expression pattern, including a possible physiological advantage of such a distribution, was unclear and needed to be investigated. Therefore, the targeting and trafficking properties of Nramp2 isoforms I and II were compared in transfected LLC-PK_1 cells, with respect to differences in function, subcellular localization, endocytosis kinetics, and fate upon internalization (Chapter 6) [182]. These studies demonstrated that isoform I possessed higher surface expression and was internalized from the plasma membrane with slower kinetics than isoform II. As opposed to isoform II, which is efficiently sorted to recycling endosomes upon internalization, isoform I was not efficiently recycled and was targeted to lysosomes.

These results suggested a mechanism whereby isoform I would be enriched at the cell surface, favoring Fe^{2+} uptake across the plasma membrane in epithelial cells.

It was known for some time that Nramp1 is expressed in the lysosomes of phagocytic cells and more recent data support a model whereby Nramp1 restricts the replication of intracellular pathogens by removing divalent metals (Mn^{2+}, Fe^{2+}) from the phagolysosome. In Chapter 7, the subcellular trafficking properties of Nramp1, including cytoplasmic sequences responsible for targeting to lysosomes, were investigated. Chimeric Nramp1/Nramp2 proteins were created by exchanging homologous domains of each protein and were characterized in stably transfected LLC-PK_1 cells with respect to expression, maturation, stability, cell surface targeting, transport activity, and subcellular localization. An Nramp2 isoform II chimera bearing the N terminus of Nramp1 was not expressed at the cell surface but was targeted to lysosomes. This lysosomal targeting was abolished by single alanine substitutions at Y15 and I18 of a $YGSI^{15-18}$ motif present in the N terminus of Nramp1. Together, these results identified YGSI as a tyrosine-based sorting signal of the form YXXΦ responsible for the lysosomal targeting of Nramp1 and provided novel insight into the transporter's subcellular trafficking.

8.2 Future Perspectives

8.2.1 Insights into structure/function relationships in Nramp proteins

In the last twenty years, the identification and characterization of Nramp family proteins from a wide range of organisms has greatly furthered our understanding of a number of cellular and physiological processes. In mammals, the most significant advancements have been made in the fields of host resistance to infection and the metabolism of iron, from the characterization of both Nramp1 and Nramp2, respectively. We now know that Nramp1 is expressed in phagocytic cells and counters intracellular pathogen replication by functioning as a pH-dependent divalent metal efflux pump at the phagosomal membrane. On the other hand, Nramp2 is expressed at the duodenal brush border where it controls uptake of dietary iron, and is present at the plasma membrane/recycling endosomes of most cells, where it is necessary for acquisition of

transferrin-associated iron. Because of the high sequence conservation among Nramp proteins, even those from phylogenically distant species, it is likely that all Nramp transporters share a similar transport mechanism. Structure/function studies carried out in various Nramp orthologs have been highly informative and essential to understanding the molecular basis of metal transport and pH dependence. These studies have been difficult to carry out in Nramp1 mostly because of its strict lysosomal localization at steady-state. Conversely, the ubiquitous plasma membrane expression of Nramp2 at steady-state has made it a much more attractive target for mutagenesis studies. Not surprisingly, the amount of data concerning structure/function relationships for Nramp2 significantly exceeds that of Nramp1.

8.2.2 Evidence for a metal binding site or permeation pathway

The work described in Chapter 2 of this thesis examined the functional role of highly conserved charged residues in the TM domains of Nramp2 on substrate transport and pH regulation. This work identified three negatively charged residues in TM1 (D86), TM4 (D192), and TM7 (E299) that are critical for metal transport by Nramp2 [28]. Based on our results, we hypothesized that the negatively charged side chains of these amino acids mediated either direct or indirect interaction with the positively charged divalent cation substrates of Nramp transporters. The negative charges may form part of metal binding pocket or line the walls of a hydrophilic ion transport pathway across the membrane. While this theory seems plausible and would be electrostatically favorable it has not yet been proven. Additional mutagenesis studies at these conserved amino acid residues would help determine the exact importance of these charged residues in Nramp2 function. Charged residues shown to be important for Nramp2 function could be replaced with amino acids that alter some physical properties of the residues while retaining others. For example, aspartate could be replaced with glutamate to conserve charge and alter size, or asparagine to retain size while eliminating charge. A requirement of residues with negatively charged side chains at positions 86, 192, and 299 would support an electrostatic role for these residues in substrate interaction. Interestingly, Su and colleagues have previously characterized the effects of conservative mutations at D192

(D192N, D192E) on Nramp2 function in transiently transfected HEK293T cells [146]. At the time, they postulated that since D192 and G185 resided in close proximity in TM4 from helical wheel projections, the loss-of-function mutation found in *mk* mice and *Belgrade* rats (G185R) could result from a functionally unfavorable novel ionic interaction between D192 and R185. While their mutagenesis data did not ultimately support their hypothesis, they showed that D192N and D192E mutants retained significant metal transport activity, while a D192G mutant was severely impaired. Although exact comparisons between activity of the mutants was not possible since they did not measure protein expression, their results suggested that D192 does not play a major role in substrate interaction. Our observation that D192A results in only a partial but not complete loss of activity supports this idea [28].

Several other studies have pointed to TM4 of Nramp2 as a region critical for metal transport activity. Work by Xu and colleagues has suggested that the mutation causing microcytic anemia in rodents (G185R) in TM4 of Nramp2 exposes a novel calcium channel pathway that may provide some unknown selective advantage to mice born with this mutation [149]. This selective advantage would help explain the spontaneous reoccurrence of the G185R mutation on three separate occasions in rodents. However, the increased calcium permeability would have to function in context with the other biosynthetic and functional defects associated with the G185R. Touret and colleagues clearly demonstrated that Nramp2^{G185R} is less stable than the WT protein, is not properly glycosylated, and is not efficiently targeted to the plasma membrane [148]. Rather, the majority of Nramp2^{G185R} was shown to be retained in the endoplasmic reticulum and degraded by a proteosome-dependent mechanism.

Independent studies by several other groups have supported a role for D86 in substrate interaction. Mutagenesis studies carried out by Chaloupka and colleagues examined the role of D86 in the bacterial Nramp ortholog, MntH [156]. Consistent with our results, they showed that a glycine mutation at D86 (corresponding to D34G in MntH) results in a severe loss of metal uptake (Mn^{2+}, Fe^{2+}, Co^{2+}). While a more conservative asparagine substitution (D34N) did not rescue metal transport, they did not characterize a negative charge-retaining D34E mutant. Such a mutant may indeed retain some activity,

confirming the need for a negative charge at that position and supporting a role for D86 in substrate interaction. Interestingly, D86 resides at the end of TM1 immediately upstream of the first extra-cytoplasmic loop (EC1) and forms part of a four amino acid sequence ($DPGN^{86-89}$) in Nramp2 that is strikingly invariant throughout all members of the Nramp family. In addition, studies by Cohen and colleagues have suggested that certain residues within EC1 of Nramp2 (G88, D93, Q95) are critical for metal ion binding and specificity of transport [159]. They used electrophysiological measurements and radioisotopic metal transport assays to characterize the effects of EC1 mutants expressed in *Xenopus* oocytes. G88A and Q95D mutants resulted in a complete inhibition of metal uptake while a D93A mutant retained partial activity for Fe^{2+} but not Mn^{2+}. The double mutant D93A/Q95D retained partial activity and shifted substrate specificity in favor of Fe^{2+}. However, the triple mutant G88A/D93A/Q95D showed no apparent transport activity. Pre-steady-state current measurements at different pH values for the mutants suggested that EC1 is not only involved in metal binding but is also critical for proton-binding.

Together, these findings suggest a mechanism whereby key residues in EC1 of Nramp proteins work in conjunction with negatively-charged residues in TM1 (D86), TM7 (E299), and possibly TM4 (D192) to bind and translocate divalent metal cations across the membrane. The energy for this translocation is likely derived from a simultaneous proton-coupling mechanism.

8.2.3 A molecular basis for pH dependence and proton-coupling

Early electrophysiological studies by Gunshin and colleagues showed that Nramp2 used a proton-coupled mechanism to transport divalent metals across the membrane [40]. Their initial work suggested a transport stoichiometry of 1:1 (H^+ : divalent metal) at physiological pH ~6, yet an additional proton slip mechanism could proceed uncoupled from divalent metal transport at a more acidic pH (pH < 5.5) [40]. These observations were later supported in studies by Sacher and colleagues, using similar electrophysiological techniques to simultaneously characterize the transport properties of Nramp2 and the yeast ortholog Smf1p [50]. They proposed that this H^+ slip mechanism might be advantageous to the organism and may protect against overloading of metal ions

in the presence of excess acid, for example in the duodenum. At this time, however, a molecular basis for pH dependence and/or proton coupling of metal transport by Nramp2 was still unknown.

The work described in Chapter 2 of this thesis identified two highly conserved histidines (H267, H272) that are critical for pH dependence of metal transport by Nramp2 [28]. Uncharged hydrophobic substitutions (alanine, cysteine) at both histidines, either independently or together, retained little activity at pH 6.5 but showed significant activity at a much lower pH 5.0. Interestingly, substituting both histidines to positive arginine, independently or together, resulted in a completely inactive protein at any pH tested. These results offered one of the first attempts to elucidate the molecular basis of pH-dependence for metal transport by Nramp proteins. Some of our results were later supported in a study by Mackenzie and colleagues, who expressed wild-type and mutant Nramp2 in *Xenopus* oocytes and used electrophysiological techniques to study the mechanism of Nramp2-mediated metal transport [355]. In agreement with our findings, they showed that mutations at H267 and H272 affect optimal activity of Nramp2, and that substitutions at H272 are less tolerated than substitutions at H267. They also found that an arginine mutation at either histidine completely abrogates Nramp2 function. However, the study by Mackenzie *et al* reported some contradictory findings with respect to our study. They reported that H267A displayed properties similar to WT Nramp2 but at a lower level, and that this lower level of activity was simply a reflection of a lower density of transporters present on the membrane. They found more striking effects for H272A, reporting that this mutation actually uncoupled Fe^{2+} and H^+ fluxes, and showed some evidence that metal transport by this variant was independent of extracellular pH [355]. These results clearly contradict our findings that inactive H267 and H272 mutants possess increased pH dependence that could be rescued by lowering the extracellular pH [28]. Still, both our studies evidently show that the conserved histidines in TM6 (particularly H272) play an important role in regulating the pH dependence and/or proton coupling of Nramp2 activity. Since histidine residues can be titratable within the physiological pH range, it is possible that transient protonation of H267 and/or H272 may be a requirement for the H^+ coupling of Nramp2.

The importance of the conserved TM6 histidines in the function of Nramp proteins has been verified in other Nramp orthologs. In a recent publication, Chaloupka and colleagues reported that critical mutations at either H211 or H216 of a bacterial Nramp ortholog (corresponding to H267/H272 of Nramp2), impair metal transport [156]. Consistent with our studies, H211A/H216A mutations displayed significant metal transport at low pH (pH 4.7) while H211R/H272R mutations displayed no significant metal transport activity. Furthermore, mutations at the second histidine (H216) were less tolerated than at the first histidine (H211).

In contrast to the TM6 histidine mutants that appear to uncouple H^+ and divalent metal transport, at least one other mutation in Nramp2 has been shown to have the opposite effect on coupling. In 2004, Nevo and Nelson used yeast complementation assays and electrophysiological measurements on frog oocytes to show that a F196I substitution in Nramp2 (referred to as F227I in this manuscript), results in a 14-fold increase in the ratio between metal to protons transported [158]. In effect, the F196I mutation seems to enhance the coupling of metal ion transport in Nramp2. Interestingly, F196 resides in TM4, which is already known to be critical for Nramp2 activity since a G185R mutation in this region causes microcytic anemia in rodents. Thus, it appears that key residues in TM4 (F196) and TM6 (H267, H272) of Nramp2 play vital roles in maintaining proper proton coupling of the transporter. Hopefully, the identification of additional mutants that affect proton coupling and/or pH dependence will further our understanding of metal transport by Nramp proteins.

8.2.4 Structural determinants of Nramp proteins

Hydropathy plots predict the presence of between ten and twelve membrane-spanning alpha helices for Nramp proteins [1]. The proposed topology has been verified in different regions of different orthologs. The membrane topology of the bacterial Nramp ortholog MntH was studied by Courville and colleagues using genetic fusions with cytoplasmic and periplasmic reporters [356]. Their results were in general agreement with initial computer-assisted predictions, with MntH possessing eleven putative transmembrane domains, an intra-cytoplasmic amino terminus, and an extra-cytoplasmic

carboxyl terminus. The topology of MntH was found to more closely resemble the structure of the yeast orthologs (Smf) than the mammalian proteins. Indeed, epitope accessibility studies with the yeast Nramp ortholog Smf3p also place its C terminus extra-cytoplasmically [357]. However, the membrane topologies of the bacterial and yeast proteins may differ from the mammalian proteins, which possess twelve transmembrane domains compared to eleven. In the mammalian proteins, antibody accessibility studies with Nramp1 and Nramp2 have shown that both the N and C termini of these two proteins face the cytosol and that the sequence between TM7 and TM8 is indeed extra-cytoplasmic [26;27;148]. However, the complete membrane topology of Nramp1 and Nramp2 has not yet been verified experimentally and requires further study. One method to verify the topology of Nramp2 would be to use a systematic mutagenesis approach independently inserting epitope tags within each intra- and extra-cytoplasmic loops of the transporter. Immunofluorescence labeling experiments in fixed intact (non-permeabilized) vs. non-intact (permeabilized) cells could then be used to determine accessibility of the various epitopes to specific antibodies. Epitopes accessible to antibody-labeling in intact cells would confirm the extracellular nature of those regions of the protein. The use of epitope tags such as hemagluttinin (HA) would be favored over the creation of genetic fusions with reporter proteins because of their comparatively smaller size, which would minimize possible disruptions in transporter folding and processing.

Helical wheel projections of the putative transmembrane domains of Nramp proteins reveal strong amphiphilicity for TM3, TM5, and TM9, clearly segregating a polar face made up of charged/polar residues from a non-polar hydrophobic face [1]. The polar faces of these domains likely juxtapose the aqueous solvent while the hydrophobic portions of the domains probably interact with the hydrophobic lipids in the membrane. Interestingly, work described in Chapter 2 revealed that alanine substitutions at two charged residues within amphipathic transmembrane domains TM3 (E154) and TM9 (R416) of Nramp2 resulted in proteins that could not be stably expressed in CHO cells [28]. These results suggested that these two charged residues are important for processing or stability of the transporter. Work in Chapter 4 showed that a conservative amino acid substitution at R416 retaining a positive charge (R416K) was moderately tolerated. One

possibility is that an ionic interaction between E154 and R416 is necessary for inter-helix packing between TM3 and TM9, and that mutating either of these residues to uncharged alanine prevents this interaction and causes decreased stability or mis-folding of the protein. Indeed, conserved charged residues residing within the hydrophobic transmembrane domains of polytopic membrane proteins have been shown to be important for the structure of other transporters such as CFTR and the lactose permease [322;323]. One way to indirectly verify an interaction between E154 and R416 would be to exchange the residues at both positions and attempt to express the mutant protein in transfected cells. Expression of an R154/E416 mutant protein that showed normal processing, stability, and function would support an interaction between both charged residues.

Relating biochemical data to the secondary and tertiary structures of proteins can be difficult in the absence of a high resolution crystal structure. Several attempts have been made by Li and colleagues to determine the structure of a 24 amino acid synthetic peptide corresponding to predicted TM4 of Nramp2 [358-361]. Through the use CD and NMR spectroscopy, they showed evidence that the TM4-corresponding peptide adopts an alpha-helical structure in several membrane-mimicking environments [359]. Furthermore, environmental changes in pH seemed to be associated with structural/conformational changes in the TM4 peptide [360]. From their data, they proposed a model whereby several TM4 helices would self-assemble in the membrane, delineating a hydrophilic channel through which metal ions would be transported. Another study comparing TM4 peptides from WT and G185R mutant Nramp2 proteins suggested that the mutation causing microcytic anemia in rodents alters the self-assembly of the helices and disrupts the quaternary structure of the transporter [361]. Although this is an interesting theory, there has not yet been any biochemical evidence suggesting that Nramp proteins function as multimeric complexes. If, as postulated, the G185R mutation severely disrupted the quaternary structure of the protein, it would likely result in a complete loss of transport activity and not the attenuated functional activity actually displayed by this mutant [28;148]. We must be cautious in interpreting the structural behavior of a single synthetic hydrophobic peptide (TM4) in the absence of the remaining transmembrane domains and

other segments of Nramp2 that are potentially critical for maintaining the transporter's structure. In some cases, the identification of a dominant negative variant of a protein is an indication that the protein functions as a multimeric complex involving interaction of several subunits, where the mutant protein affects the function of the wild-type protein. For example, dominant negative mutants have been identified for ferroportin and some experiments have shown that the iron exporter may oligomerize *in vitro* [295]. The fact that no dominant negative mutations have been identified to date for Nramp2 either *in vitro* or *in vivo*, suggests that the transporter may actually function as a monomer. However, this has not yet been confirmed experimentally. One way to answer this question would be to purify and reconstitute Nramp2 in proteoliposomes under conditions where the transporter is fully functional and then use freeze-fracture electron microscopy to look at the distribution of transporters in the membrane. In addition, the initial rate of metal transport into the proteoliposomes can be compared with the ratio of Nramp2 to phospholipid. A linear relationship would suggest that Nramp2 functions as a monomer while a sigmoidal relationship would indicate the need for oligomerization of the transporter to remain active. Such techniques were used by Costello and colleagues to verify the monomeric nature of the lac permease and cytochrome o oxidase [362].

In the absence of a high resolution crystal structure, several molecular biology approaches can be employed to characterize the secondary structure of membrane proteins. The lactose permease of *Escherichia coli* (LacY) is one of the most well understood membrane protein transporters and several pioneering techniques have been used and developed to study its native structure within the bacterial membrane. Many of the techniques used to characterize LacY can be used to study other membrane proteins with similar characteristics. Like Nramp2, LacY is an integral membrane protein consisting of twelve membrane-spanning alpha helices and functions as a symporter that uses a proton gradient to transport its substrate (galactosides) across the membrane. Several years ago, the group of Kaback and colleagues used a cysteine-scanning mutagenesis approach to: (a) determine residues that played an obligatory role in the function of LacY, and (b) create a library of single Cys mutants for future structure/function studies (reviewed in [363]). The amino acid Cys is average in bulk and

relatively hydrophobic. However, the major advantage of Cys is its sulfhydryl side chain, which is open to highly-specific modification by various chemical groups such as *N*-ethylmaleimide. Furthermore, by introducing single Cys mutants into a functional mutant backbone devoid of endogenous Cys residues, the precise specificity of the chemical modification can be controlled. The group of Kaback and colleagues have used this Cys-scanning mutagenesis approach in conjunction with biochemical and biophysical techniques to elucidate membrane topology [364-366] as well as spatial proximity between transmembrane domains and periplasmic loops of lac permease [367-369]. The latter studies utilized sulfhydryl-specific bifunctional chemical cross-linkers, which have also been used to study the transmembrane domain structure of numerous other polytopic transmembrane proteins such as the Tar [370] and aspartate sensory receptors [371] of *E. coli*. Cys-scanning mutagenesis has also been used to identify hydrophilic pathways formed by membrane transporters. In 1995, Yan and colleagues used Cys-scanning mutagenesis to demonstrate that TM7 of the bacterial membrane transporter UhpT lines a hydrophilic transport pathway for its charged substrate (glucose-6-phosphate) [372]. Beginning with a Cys-less version of UhpT, they introduced Cys residues, one at a time, at each position along TM7 and then probed these single-cysteine variants with *p*-chloromercuribenzosulfonate (PCMBS), a hydrophilic and impermeant sulfhydryl-reactive agent. They found that TM7 of UhpT forms an α-helix whose central portion is highly accessible to PCMBS from both membrane surfaces, and subsequently they concluded that residues within TM7 line a hydrophilic pathway through the transporter. Finally, a Cys-scanning mutagenesis approach can be used to identify specific amino acids that reside in or near a substrate binding site. In some cases, pre-incubation with substrate of a single-cysteine mutant protein is able to protect against chemical modification with a thiol-specific reagent. For example, Wu and colleagues made use of the fluorescent compound MIANS [2-(4'-maleimidylanilino)naphthalene-6-sulfonic acid], whose fluorescence increases dramatically upon reaction with a thiol, to demonstrate that Cys148 of the lac permease is a component of the substrate binding site [373].

In two simultaneous landmark publications in 1995, Voss and colleagues made use of paramagnetic metal-nitroxyl interactions to estimate intramolecular distances within proteins. In the first publication, they validated the technique by measuring distances in T4 lysozyme, a protein of known structure [314]. The calculated distances exhibited strong correspondence to the distances estimated from modeling based on the x-ray structure of the protein. In the second publication, they applied their metal-nitroxide approach to measure distances in the lac permease, a paradigm of polytopic membrane proteins [374]. Site-directed spin labeling (SDSL) is a powerful tool for studying protein structure/dynamics, and has been successfully used to obtain structural data on a number of proteins. However, a thorough description of SDSL technique is beyond the scope of this thesis and has been reviewed elsewhere [375-377]. Briefly, the technique involves introducing a metal-ion binding site (e.g. six contiguous histidine residues) in a fixed region of the protein and a spin-labeled side chain (cysteines) at another region of interest. Of course, other native cysteines must first be replaced. After purification of the protein, the spin-label side chains (Cys) are modified with a specific paramagnetic nitroxide reagent and the electron paramagnetic resonance (EPR) spectra is analyzed in the presence of metal (e.g. Cu^{2+}). Generally, changes in the distance between the metal and nitroxide label reflect changes in the EPR spectra of the spin-labeled protein.

Similar Cys-scanning mutagenesis and spin-labeling approaches may yield valuable information about the transmembrane structure of Nramp proteins. However, these approaches require successful purification and reconstitution of Nramp proteins in a functional state and/or a Cys-less Nramp protein that retains significant metal transport activity. To date, there have been no published reports describing the purification/reconstitution of functional mammalian Nramp1/2, nor reports characterizing the activity of a mammalian Nramp protein devoid of all endogenous cysteines. However, Nramp2 contains ten endogenous cysteine residues, some of which are conserved, and a Cys-less Nramp2 variant may not be stably expressed or retain significant transport activity. An attempt has been made to carry out some of these studies in the mycobacterial ortholog, MntH. In 2002, Reeve and colleagues reported the purification and reconstitution of a cysteine-less variant of MntH from *Mycobacterium leprae*, and

used site-directed spin labeling to gain structural information about the transporter [378]. However, they did not test the functionality of the Cys-less MntH transporter and it is not known whether this variant represented a properly folded protein. Perhaps an ideal candidate for future site-directed spin labeling studies would be the MntH protein from *E. coli*, which does not contain any endogenous cysteines.

8.2.5 Subcellular targeting and trafficking of Nramp proteins

It is clear that proper subcellular targeting is essential for the function of Nramp proteins. The work described in Chapters 5, 6, and 7 of this thesis focused on characterizing the subcellular targeting and trafficking of both Nramp1 and Nramp2. Trafficking differences were identified not only between Nramp1 and Nramp2, but also between two splicing isoforms of Nramp2. In Nramp2, the most critical targeting information appears to reside in the carboxyl terminal segment of the isoform II (B) protein, including a putative YLLNT motif [155;184]. However, the role of the additional 29-31 N-terminal residues of the (A) isoforms of Nramp2 in subcellular targeting are not currently known and need to be further studied. Conversely, one of the signals critical for proper lysosomal sorting of Nramp1 appears to reside in the amino terminal segment of the transporter, most notably a YGSI motif. In the past few years, tremendous progress has been made in the field of transmembrane protein sorting (reviewed in [183]). In particular, numerous cytosolic motifs have now been identified in various functionally unrelated transmembrane proteins and many of their binding partners have also been characterized. An important next step to better understand the subcellular trafficking of Nramp proteins will be to identify the specific adaptor protein complexes that interact with the targeting motifs present in the amino and carboxyl termini of Nramp1 and Nramp2. This can be done several ways. In 1989, Glickman and colleagues used an *in vitro* affinity binding method to study interactions of the cytosolic tail of mannose-6-phosphate receptor (M6PR) with the clathrin-associated plasma membrane adaptor protein AP-2 [379]. They used either intact M6PR or a fusion protein containing the cytoplasmic tail of M6PR for column chromatography experiments to identify adaptor proteins that could bind M6PR. However, the apparent low affinity of the interactions *in*

vitro may preclude the use of this biochemical approach to study other transmembrane proteins. A more sensitive technique might be a yeast two-hybrid screen. In a landmark publication in 1995, Ohno and colleagues successfully used the yeast two-hybrid system to identify proteins that bind to tyrosine-based signals [331]. As "bait", they used a triple repeat of the peptide SDYQRL from the cytoplasmic tail of the integral membrane protein TGN38, which was known to possess characteristics of a YXXΦ motif, mediating internalization and targeting of the protein to the trans-Golgi network (TGN). After screening a mouse spleen cDNA library, they isolated clones corresponding to the medium chain (μ2) of the plasma membrane clathrin-associated protein complex AP-2. The interaction between μ2 and the YXXΦ motif was later confirmed through *in vitro* binding assays. A similar approach could be used to identify proteins involved in trafficking of Nramp1 and Nramp2 proteins, using either the amino or carboxyl terminal segments of each protein as "bait".

Currently, one study has suggested that internalization of Nramp2 isoform II from the cell surface occurs via a clathrin and dynamin dependent mechanism in transfected LLC-PK_1 cells [51]. These observations were made based on some colocalization between Nramp2 and GFP-clathrin, and the apparent lack of internalization of Nramp2 in cells expressing a dominant negative variant (K44A) of dynamin. More studies are needed to verify these results. Traditionally, the requirement of clathrin for the endocytosis of a transmembrane protein has been verified several ways. Over twenty years ago, Larkin and colleagues described a method for inhibiting receptor mediated endocytosis of low density lipoprotein (LDL) receptor [380]. They found that when the level of intracellular potassium was lowered in cultured human fibroblasts below 40% of normal, the internalization of LDL receptor was inhibited. Moreover, under conditions of maximal inhibition, these cells had an 80% reduction in the number of clathrin-coated pits on the cell surface [380]. Inhibition of endocytosis by potassium depletion is reversible and has been found to be surprisingly specific for clathrin-mediated internalization, and therefore has since been used to study endocytosis of a number of membrane proteins [334;380;381]. A reduced rate of internalization and/or an increase in cell surface accumulation of Nramp2 isoform II in potassium depleted cells would support the role of clathrin in the

internalization of Nramp2 from the plasma membrane. Furthermore, Sandvig and colleagues found that when intracellular pH was lowered below pH 6.0, there was a dramatic and specific inhibition of endocytosis through coated pits [382]. Unlike potassium depletion, acidified cells appear to have normal numbers of coated pits but these pits appear to be paralyzed and unable to internalize ligand. Again, reduced internalization and/or increased cell surface accumulation of Nramp2 upon cellular acidification would support a role of clathrin in Nramp2 internalization from the plasma membrane. Intriguingly, since Nramp2 functions through a proton co-transport mechanism, it itself causes cellular acidification as it imports divalent metals. This raises the possibility of a positive-feedback regulation mechanism whereby metal uptake by Nramp2 causes accumulation of the transporter at the cell surface through inhibition of clathrin-mediated internalization via cellular acidification.

Work described in Chapter 7 of this thesis showed that a tyrosine-based motif (YGSI) in the amino terminus of Nramp1 could function as a lysosomal targeting signal when placed on the background of Nramp2. Our results allowed us to propose a model for Nramp1 trafficking whereby recognition of the YGSI signal by specific adaptor proteins mediate the sorting of Nramp1 directly from the trans-Golgi network to late endosomes and lysosomes. However, we could not completely exclude the possibility that Nramp1 is first targeted to the cell surface, then rapidly internalized and targeted to the lysosomes via the endocytic pathway. Therefore, the question remains whether Nramp1 is targeted directly or indirectly to the lysosomal compartment. One way of answering this question would be to treat cells expressing Nramp1 with an inhibitor of endocytosis and look for an accumulation of Nramp1 at the cell surface through cell surface biotinylation. An increase in Nramp1 at the cell surface could indicate an indirect sorting route. Some well-characterized chemical inhibitors of endocytosis are monodansylcadaverine, concanavalin A (conA) and phenylarsine oxide (PAO). Another way to study Nramp1 sorting would be to pulse-label newly synthesized Nramp1 transporters with radiolabeled ^{35}S-methionine and perform subcellular fractionation at different time intervals using differential centrifugation to isolate fractions from various organellar compartments. Nramp1 could be isolated from these fractions by immunoprecipitation and detected by

SDS-electrophoresis and autoradiography. A transient accumulation of Nramp1 in fractions enriched for plasma membrane components would support an indirect sorting route.

8.3 Final Conclusions

Future studies on Nramp proteins are essential for a better understanding of the role of divalent metals in a number of cellular and physiological processes. The numerous studies characterizing *Nramp1* have given insight into the complex nature of host-pathogen interactions and brought to the forefront the importance of divalent metals in the survival/replication of a wide range of intracellular parasites. These and future findings may lead to novel therapeutic approaches for combating the current alarming rise in pathogenic infections. In parallel, the identification and characterization of the iron transporter *Nramp2* has helped spark a recent growth in research in the field of iron metabolism. A better understanding of the function Nramp2 may lead to novel or improved treatments for iron-related disorders such as hereditary hemochromatosis.

REFERENCES

1. Cellier M, Prive G, Belouchi A et al. Nramp defines a family of membrane proteins. Proc.Natl.Acad.Sci.U.S.A 1995;92:10089-10093.

2. Rodrigues V, Cheah PY, Ray K, Chia W. malvolio, the Drosophila homologue of mouse NRAMP-1 (Bcg), is expressed in macrophages and in the nervous system and is required for normal taste behaviour. EMBO J. 1995;14:3007-3020.

3. Fortier A, Min-Oo G, Forbes J, Lam-Yuk-Tseung S, Gros P. Single gene effects in mouse models of host: pathogen interactions. J.Leukoc.Biol. 2005;77:868-877.

4. Mims MP, Guan Y, Pospisilova D et al. Identification of a human mutation of DMT1 in a patient with microcytic anemia and iron overload. Blood 2005;105:1337-1342.

5. Iolascon A, d'Apolito M, Servedio V et al. Microcytic anemia and hepatic iron overload in a child with compound heterozygous mutations in DMT1 (SCL11A2). Blood 2006;107:349-354.

6. Beaumont C, Delaunay J, Hetet G et al. Two new human DMT1 gene mutations in a patient with microcytic anemia, low ferritinemia, and liver iron overload. Blood 2006;107:4168-4170.

7. Vidal SM, Malo D, Vogan K, Skamene E, Gros P. Natural resistance to infection with intracellular parasites: isolation of a candidate for Bcg. Cell 1993;73:469-485.

8. Plant J, Glynn AA. Genetics of resistance to infection with Salmonella typhimurium in mice. J.Infect.Dis. 1976;133:72-78.

9. Bradley DJ. Letter: Genetic control of natural resistance to Leishmania donovani. Nature 1974;250:353-354.

10. Lissner CR, Swanson RN, O'Brien AD. Genetic control of the innate resistance of mice to Salmonella typhimurium: expression of the Ity gene in peritoneal and splenic macrophages isolated in vitro. J.Immunol. 1983;131:3006-3013.

11. Stach JL, Gros P, Forget A, Skamene E. Phenotypic expression of genetically-controlled natural resistance to Mycobacterium bovis (BCG). J.Immunol. 1984;132:888-892.

12. Crocker PR, Blackwell JM, Bradley DJ. Expression of the natural resistance gene Lsh in resident liver macrophages. Infect.Immun. 1984;43:1033-1040.

13. Vidal SM, Pinner E, Lepage P, Gauthier S, Gros P. Natural resistance to intracellular infections: Nramp1 encodes a membrane phosphoglycoprotein absent

in macrophages from susceptible (Nramp1 D169) mouse strains. J.Immunol. 1996;157:3559-3568.

14. White JK, Stewart A, Popoff JF, Wilson S, Blackwell JM. Incomplete glycosylation and defective intracellular targeting of mutant Slc11a1. Biochem.J. 2004;Pt 3:811-819.

15. Vidal S, Tremblay ML, Govoni G et al. The Ity/Lsh/Bcg locus: natural resistance to infection with intracellular parasites is abrogated by disruption of the Nramp1 gene. J.Exp.Med. 1995;182:655-666.

16. Govoni G, Vidal S, Gauthier S et al. The Bcg/Ity/Lsh locus: genetic transfer of resistance to infections in C57BL/6J mice transgenic for the Nramp1 Gly169 allele. Infect.Immun. 1996;64:2923-2929.

17. Govoni G, Vidal S, Cellier M et al. Genomic structure, promoter sequence, and induction of expression of the mouse Nramp1 gene in macrophages. Genomics 1995;27:9-19.

18. Govoni G, Gauthier S, Billia F, Iscove NN, Gros P. Cell-specific and inducible Nramp1 gene expression in mouse macrophages in vitro and in vivo. J.Leukoc.Biol. 1997;62:277-286.

19. Zhong W, Lafuse WP, Zwilling BS. Infection with Mycobacterium avium differentially regulates the expression of iron transport protein mRNA in murine peritoneal macrophages. Infect.Immun. 2001;69:6618-6624.

20. ter-Koltunoff M, Ehrlich S, Dror N et al. Nramp1-mediated innate resistance to intraphagosomal pathogens is regulated by IRF-8, PU.1, and Miz-1. J.Biol.Chem. 2003;278:44025-44032.

21. Bowen H, Biggs TE, Phillips E et al. c-Myc represses and Miz-1 activates the murine natural resistance-associated protein 1 promoter. J.Biol.Chem. 2002;277:34997-35006.

22. Bowen H, Lapham A, Phillips E et al. Characterization of the murine Nramp1 promoter: requirements for transactivation by Miz-1. J.Biol.Chem. 2003;278:36017-36026.

23. Atkinson PG, Blackwell JM, Barton CH. Nramp1 locus encodes a 65 kDa interferon-gamma-inducible protein in murine macrophages. Biochem.J. 1997;325 (Pt 3):779-786.

24. Lafuse WP, Alvarez GR, Zwilling BS. Role of MAP kinase activation in Nramp1 mRNA stability in RAW264.7 macrophages expressing Nramp1(Gly169). Cell Immunol. 2002;215:195-206.

25. Lafuse WP, Alvarez GR, Zwilling BS. Regulation of Nramp1 mRNA stability by oxidants and protein kinase C in RAW264.7 macrophages expressing Nramp1(Gly169). Biochem.J. 2000;351 Pt 3:687-696.

26. Picard V, Govoni G, Jabado N, Gros P. Nramp 2 (DCT1/DMT1) expressed at the plasma membrane transports iron and other divalent cations into a calcein-accessible cytoplasmic pool. J.Biol.Chem. 2000;275:35738-35745.

27. Forbes JR, Gros P. Iron, manganese, and cobalt transport by Nramp1 (Slc11a1) and Nramp2 (Slc11a2) expressed at the plasma membrane. Blood 2003;102:1884-1892.

28. Lam-Yuk-Tseung S, Govoni G, Forbes J, Gros P. Iron transport by Nramp2/DMT1: pH regulation of transport by 2 histidines in transmembrane domain 6. Blood 2003;101:3699-3707.

29. Mackenzie B, Ujwal ML, Chang MH, Romero MF, Hediger MA. Divalent metal-ion transporter DMT1 mediates both H(+) -coupled Fe(2+) transport and uncoupled fluxes. Pflugers Arch. 2005

30. Barton CH, White JK, Roach TI, Blackwell JM. NH2-terminal sequence of macrophage-expressed natural resistance-associated macrophage protein (Nramp) encodes a proline/serine-rich putative Src homology 3-binding domain. J.Exp.Med. 1994;179:1683-1687.

31. Dassa E, Hofnung M. Sequence of gene malG in E. coli K12: homologies between integral membrane components from binding protein-dependent transport systems. EMBO J. 1985;4:2287-2293.

32. Kerppola RE, Ames GF. Topology of the hydrophobic membrane-bound components of the histidine periplasmic permease. Comparison with other members of the family. J.Biol.Chem. 1992;267:2329-2336.

33. Jan LY, Jan YN. Potassium channels and their evolving gates. Nature 1994;371:119-122.

34. Pinner E, Gruenheid S, Raymond M, Gros P. Functional complementation of the yeast divalent cation transporter family SMF by NRAMP2, a member of the mammalian natural resistance-associated macrophage protein family. J.Biol.Chem. 1997;272:28933-28938.

35. Gruenheid S, Pinner E, Desjardins M, Gros P. Natural resistance to infection with intracellular pathogens: the Nramp1 protein is recruited to the membrane of the phagosome. J.Exp.Med. 1997;185:717-730.

36. Canonne-Hergaux F, Calafat J, Richer E et al. Expression and subcellular localization of NRAMP1 in human neutrophil granules. Blood 2002;100:268-275.

37. Cuellar-Mata P, Jabado N, Liu J et al. Nramp1 modifies the fusion of Salmonella typhimurium-containing vacuoles with cellular endomembranes in macrophages. J.Biol.Chem. 2002;277:2258-2265.

38. Govoni G, Canonne-Hergaux F, Pfeifer CG et al. Functional expression of Nramp1 in vitro in the murine macrophage line RAW264.7. Infect.Immun. 1999;67:2225-2232.

39. Searle S, Bright NA, Roach TI et al. Localisation of Nramp1 in macrophages: modulation with activation and infection. J.Cell Sci. 1998;111 (Pt 19):2855-2866.

40. Gunshin H, Mackenzie B, Berger UV et al. Cloning and characterization of a mammalian proton-coupled metal-ion transporter. Nature 1997;388:482-488.

41. Forbes JR, Gros P. Divalent-metal transport by NRAMP proteins at the interface of host-pathogen interactions. Trends Microbiol. 2001;9:397-403.

42. Gruenheid S, Canonne-Hergaux F, Gauthier S et al. The iron transport protein NRAMP2 is an integral membrane glycoprotein that colocalizes with transferrin in recycling endosomes. J.Exp.Med. 1999;189:831-841.

43. Kuhn DE, Lafuse WP, Zwilling BS. Iron transport into mycobacterium avium-containing phagosomes from an Nramp1(Gly169)-transfected RAW264.7 macrophage cell line. J.Leukoc.Biol. 2001;69:43-49.

44. Kuhn DE, Baker BD, Lafuse WP, Zwilling BS. Differential iron transport into phagosomes isolated from the RAW264.7 macrophage cell lines transfected with Nramp1Gly169 or Nramp1Asp169. J.Leukoc.Biol. 1999;66:113-119.

45. Zwilling BS, Kuhn DE, Wikoff L, Brown D, Lafuse W. Role of iron in Nramp1-mediated inhibition of mycobacterial growth. Infect.Immun. 1999;67:1386-1392.

46. Goswami T, Bhattacharjee A, Babal P et al. Natural-resistance-associated macrophage protein 1 is an H+/bivalent cation antiporter. Biochem.J. 2001;354:511-519.

47. Blackwell JM, Goswami T, Evans CA et al. SLC11A1 (formerly NRAMP1) and disease resistance. Cell Microbiol. 2001;3:773-784.

48. Chen XZ, Peng JB, Cohen A et al. Yeast SMF1 mediates H(+)-coupled iron uptake with concomitant uncoupled cation currents. J.Biol.Chem. 1999;274:35089-35094.

49. Kehres DG, Zaharik ML, Finlay BB, Maguire ME. The NRAMP proteins of Salmonella typhimurium and Escherichia coli are selective manganese

transporters involved in the response to reactive oxygen. Mol.Microbiol. 2000;36:1085-1100.

50. Sacher A, Cohen A, Nelson N. Properties of the mammalian and yeast metal-ion transporters DCT1 and Smf1p expressed in Xenopus laevis oocytes. J.Exp.Biol. 2001;204:1053-1061.

51. Touret N, Furuya W, Forbes J, Gros P, Grinstein S. Dynamic traffic through the recycling compartment couples the metal transporter Nramp2 (DMT1) with the transferrin receptor. J.Biol.Chem. 2003;278:25548-25557.

52. Jabado N, Jankowski A, Dougaparsad S et al. Natural resistance to intracellular infections: natural resistance-associated macrophage protein 1 (Nramp1) functions as a pH-dependent manganese transporter at the phagosomal membrane. J.Exp.Med. 2000;192:1237-1248.

53. Skamene E, Gros P, Forget A et al. Genetic regulation of resistance to intracellular pathogens. Nature 1982;297:506-509.

54. Goto Y, Iwakiri A, Shinjo T. [Pathogenicities of Mycobacterium intracellulare and M. avium strains to the mice which were isolated from non-tuberculous mycobactriosis patients]. Kansenshogaku Zasshi 2002;76:425-431.

55. Skamene E, Gros P, Forget A, Patel PJ, Nesbitt MN. Regulation of resistance to leprosy by chromosome 1 locus in the mouse. Immunogenetics 1984;19:117-124.

56. Goto Y, Buschman E, Skamene E. Regulation of host resistance to Mycobacterium intracellulare in vivo and in vitro by the Bcg gene. Immunogenetics 1989;30:218-221.

57. Gautier AV, Lantier I, Lantier F. Mouse susceptibility to infection by the Salmonella abortusovis vaccine strain Rv6 is controlled by the Ity/Nramp 1 gene and influences the antibody but not the complement responses. Microb.Pathog. 1998;24:47-55.

58. Hu J, Bumstead N, Burke D et al. Genetic and physical mapping of the natural resistance-associated macrophage protein 1 (NRAMP1) in chicken. Mamm.Genome 1995;6:809-815.

59. Barthel R, Feng J, Piedrahita JA et al. Stable transfection of the bovine NRAMP1 gene into murine RAW264.7 cells: effect on Brucella abortus survival. Infect.Immun. 2001;69:3110-3119.

60. Chapes SK, Mosier DA, Wright AD, Hart ML. MHCII, Tlr4 and Nramp1 genes control host pulmonary resistance against the opportunistic bacterium Pasteurella pneumotropica. J.Leukoc.Biol. 2001;69:381-386.

61. McLeod R, Buschman E, Arbuckle LD, Skamene E. Immunogenetics in the analysis of resistance to intracellular pathogens. Curr.Opin.Immunol. 1995;7:539-552.

62. Blackwell JM, Roberts CW, Roach TI, Alexander J. Influence of macrophage resistance gene Lsh/Ity/Bcg (candidate Nramp) on Toxoplasma gondii infection in mice. Clin.Exp.Immunol. 1994;97:107-112.

63. Kovarova H, Hernychova L, Hajduch M, Sirova M, Macela A. Influence of the bcg locus on natural resistance to primary infection with the facultative intracellular bacterium Francisella tularensis in mice. Infect.Immun. 2000;68:1480-1484.

64. Kovarova H, Halada P, Man P et al. Proteome study of Francisella tularensis live vaccine strain-containing phagosome in Bcg/Nramp1 congenic macrophages: resistant allele contributes to permissive environment and susceptibility to infection. Proteomics. 2002;2:85-93.

65. Medina E, Rogerson BJ, North RJ. The Nramp1 antimicrobial resistance gene segregates independently of resistance to virulent Mycobacterium tuberculosis. Immunology 1996;88:479-481.

66. Medina E, North RJ. Evidence inconsistent with a role for the Bcg gene (Nramp1) in resistance of mice to infection with virulent Mycobacterium tuberculosis. J.Exp.Med. 1996;183:1045-1051.

67. North RJ, LaCourse R, Ryan L, Gros P. Consequence of Nramp1 deletion to Mycobacterium tuberculosis infection in mice. Infect.Immun. 1999;67:5811-5814.

68. Ma X, Dou S, Wright JA et al. 5' dinucleotide repeat polymorphism of NRAMP1 and susceptibility to tuberculosis among Caucasian patients in Houston, Texas. Int.J.Tuberc.Lung Dis. 2002;6:818-823.

69. Kim JH, Lee SY, Lee SH et al. NRAMP1 genetic polymorphisms as a risk factor of tuberculous pleurisy. Int.J.Tuberc.Lung Dis. 2003;7:370-375.

70. Abe T, Iinuma Y, Ando M et al. NRAMP1 polymorphisms, susceptibility and clinical features of tuberculosis. J.Infect. 2003;46:215-220.

71. Liu W, Cao WC, Zhang CY et al. VDR and NRAMP1 gene polymorphisms in susceptibility to pulmonary tuberculosis among the Chinese Han population: a case-control study. Int.J.Tuberc.Lung Dis. 2004;8:428-434.

72. Fitness J, Floyd S, Warndorff DK et al. Large-scale candidate gene study of tuberculosis susceptibility in the Karonga district of northern Malawi. Am.J.Trop.Med.Hyg. 2004;71:341-349.

73. Hoal EG, Lewis LA, Jamieson SE et al. SLC11A1 (NRAMP1) but not SLC11A2 (NRAMP2) polymorphisms are associated with susceptibility to tuberculosis in a high-incidence community in South Africa. Int.J.Tuberc.Lung Dis. 2004;8:1464-1471.

74. Malik S, Abel L, Tooker H et al. Alleles of the NRAMP1 gene are risk factors for pediatric tuberculosis disease. Proc.Natl.Acad.Sci.U.S.A 2005;102:12183-12188.

75. Clemens DL, Horwitz MA. Characterization of the Mycobacterium tuberculosis phagosome and evidence that phagosomal maturation is inhibited. J.Exp.Med. 1995;181:257-270.

76. Clemens DL, Lee BY, Horwitz MA. Deviant expression of Rab5 on phagosomes containing the intracellular pathogens Mycobacterium tuberculosis and Legionella pneumophila is associated with altered phagosomal fate. Infect.Immun. 2000;68:2671-2684.

77. Clemens DL, Lee BY, Horwitz MA. Mycobacterium tuberculosis and Legionella pneumophila phagosomes exhibit arrested maturation despite acquisition of Rab7. Infect.Immun. 2000;68:5154-5166.

78. Russell DG, Dant J, Sturgill-Koszycki S. Mycobacterium avium- and Mycobacterium tuberculosis-containing vacuoles are dynamic, fusion-competent vesicles that are accessible to glycosphingolipids from the host cell plasmalemma. J.Immunol. 1996;156:4764-4773.

79. Schaible UE, Sturgill-Koszycki S, Schlesinger PH, Russell DG. Cytokine activation leads to acidification and increases maturation of Mycobacterium avium-containing phagosomes in murine macrophages. J.Immunol. 1998;160:1290-1296.

80. Sturgill-Koszycki S, Schlesinger PH, Chakraborty P et al. Lack of acidification in Mycobacterium phagosomes produced by exclusion of the vesicular proton-ATPase. Science 1994;263:678-681.

81. Sturgill-Koszycki S, Schaible UE, Russell DG. Mycobacterium-containing phagosomes are accessible to early endosomes and reflect a transitional state in normal phagosome biogenesis. EMBO J. 1996;15:6960-6968.

82. Frehel C, Canonne-Hergaux F, Gros P, De CC. Effect of Nramp1 on bacterial replication and on maturation of Mycobacterium avium-containing phagosomes in bone marrow-derived mouse macrophages. Cell Microbiol. 2002;4:541-556.

83. Hackam DJ, Rotstein OD, Zhang W et al. Host resistance to intracellular infection: mutation of natural resistance-associated macrophage protein 1 (Nramp1) impairs phagosomal acidification. J.Exp.Med. 1998;188:351-364.

84. Barrera LF, Kramnik I, Skamene E, Radzioch D. Nitrite production by macrophages derived from BCG-resistant and -susceptible congenic mouse strains in response to IFN-gamma and infection with BCG. Immunology 1994;82:457-464.

85. Barton CH, Whitehead SH, Blackwell JM. Nramp transfection transfers Ity/Lsh/Bcg-related pleiotropic effects on macrophage activation: influence on oxidative burst and nitric oxide pathways. Mol.Med. 1995;1:267-279.

86. Fritsche G, Dlaska M, Barton H et al. Nramp1 functionality increases inducible nitric oxide synthase transcription via stimulation of IFN regulatory factor 1 expression. J.Immunol. 2003;171:1994-1998.

87. Wagner D, Maser J, Lai B et al. Elemental analysis of Mycobacterium avium-, Mycobacterium tuberculosis-, and Mycobacterium smegmatis-containing phagosomes indicates pathogen-induced microenvironments within the host cell's endosomal system. J.Immunol. 2005;174:1491-1500.

88. Kelley VA, Schorey JS. Mycobacterium's arrest of phagosome maturation in macrophages requires Rab5 activity and accessibility to iron. Mol.Biol.Cell 2003;14:3366-3377.

89. Schnappinger D, Ehrt S, Voskuil MI et al. Transcriptional Adaptation of Mycobacterium tuberculosis within Macrophages: Insights into the Phagosomal Environment. J.Exp.Med. 2003;198:693-704.

90. Gomes MS, Appelberg R. Evidence for a link between iron metabolism and Nramp1 gene function in innate resistance against Mycobacterium avium. Immunology 1998;95:165-168.

91. Ratledge C. Iron, mycobacteria and tuberculosis. Tuberculosis (Edinb). 2004;84:110-130.

92. Gomes MS, Appelberg R. NRAMP1- or cytokine-induced bacteriostasis of Mycobacterium avium by mouse macrophages is independent of the respiratory burst. Microbiology 2002;148:3155-3160.

93. Knodler LA, Steele-Mortimer O. Taking possession: biogenesis of the Salmonella-containing vacuole. Traffic. 2003;4:587-599.

94. Jabado N, Cuellar-Mata P, Grinstein S, Gros P. Iron chelators modulate the fusogenic properties of Salmonella-containing phagosomes. Proc.Natl.Acad.Sci.U.S.A 2003;100:6127-6132.

95. Kehres DG, Maguire ME. Emerging themes in manganese transport, biochemistry and pathogenesis in bacteria. FEMS Microbiol.Rev. 2003;27:263-290.

96. Kammler M, Schon C, Hantke K. Characterization of the ferrous iron uptake system of Escherichia coli. J.Bacteriol. 1993;175:6212-6219.

97. Kehres DG, Janakiraman A, Slauch JM, Maguire ME. SitABCD is the alkaline Mn(2+) transporter of Salmonella enterica serovar Typhimurium. J.Bacteriol. 2002;184:3159-3166.

98. Tsolis RM, Baumler AJ, Heffron F, Stojiljkovic I. Contribution of TonB- and Feo-mediated iron uptake to growth of Salmonella typhimurium in the mouse. Infect.Immun. 1996;64:4549-4556.

99. Zhou D, Hardt WD, Galan JE. Salmonella typhimurium encodes a putative iron transport system within the centisome 63 pathogenicity island. Infect.Immun. 1999;67:1974-1981.

100. Bearden SW, Perry RD. The Yfe system of Yersinia pestis transports iron and manganese and is required for full virulence of plague. Mol.Microbiol. 1999;32:403-414.

101. Boyer E, Bergevin I, Malo D, Gros P, Cellier MF. Acquisition of Mn(II) in addition to Fe(II) is required for full virulence of Salmonella enterica serovar Typhimurium. Infect.Immun. 2002;70:6032-6042.

102. Janakiraman A, Slauch JM. The putative iron transport system SitABCD encoded on SPI1 is required for full virulence of Salmonella typhimurium. Mol.Microbiol. 2000;35:1146-1155.

103. Zaharik ML, Cullen VL, Fung AM et al. The Salmonella enterica serovar typhimurium divalent cation transport systems MntH and SitABCD are essential for virulence in an Nramp1G169 murine typhoid model. Infect.Immun. 2004;72:5522-5525.

104. Zaharik ML, Vallance BA, Puente JL, Gros P, Finlay BB. Host-pathogen interactions: Host resistance factor Nramp1 up-regulates the expression of Salmonella pathogenicity island-2 virulence genes. Proc.Natl.Acad.Sci.U.S.A 2002;99:15705-15710.

105. Cellier M, Govoni G, Vidal S et al. Human natural resistance-associated macrophage protein: cDNA cloning, chromosomal mapping, genomic organization, and tissue-specific expression. J.Exp.Med. 1994;180:1741-1752.

106. Blackwell JM, Barton CH, White JK et al. Genomic organization and sequence of the human NRAMP gene: identification and mapping of a promoter region polymorphism. Mol.Med. 1995;1:194-205.

107. Kishi F, Tanizawa Y, Nobumoto M. Structural analysis of human natural resistance-associated macrophage protein 1 promoter. Mol.Immunol. 1996;33:265-268.

108. Kishi F, Tabuchi M. Complete nucleotide sequence of human NRAMP2 cDNA. Mol.Immunol. 1997;34:839-842.

109. Newport M, Levin M, Blackwell J et al. Evidence for exclusion of a mutation in NRAMP as the cause of familial disseminated atypical mycobacterial infection in a Maltese kindred. J.Med.Genet. 1995;32:904-906.

110. Blackwell JM. Genetics of host resistance and susceptibility to intramacrophage pathogens: a study of multicase families of tuberculosis, leprosy and leishmaniasis in north-eastern Brazil. Int.J.Parasitol. 1998;28:21-28.

111. Greenwood CM, Fujiwara TM, Boothroyd LJ et al. Linkage of tuberculosis to chromosome 2q35 loci, including NRAMP1, in a large aboriginal Canadian family. Am.J.Hum.Genet. 2000;67:405-416.

112. Bellamy R, Ruwende C, Corrah T et al. Variations in the NRAMP1 gene and susceptibility to tuberculosis in West Africans. N.Engl.J.Med. 1998;338:640-644.

113. Gao PS, Fujishima S, Mao XQ et al. Genetic variants of NRAMP1 and active tuberculosis in Japanese populations. International Tuberculosis Genetics Team. Clin.Genet. 2000;58:74-76.

114. Cervino AC, Lakiss S, Sow O, Hill AV. Allelic association between the NRAMP1 gene and susceptibility to tuberculosis in Guinea-Conakry. Ann.Hum.Genet. 2000;64:507-512.

115. Taype CA, Castro JC, Accinelli RA et al. Association between SLC11A1 polymorphisms and susceptibility to different clinical forms of tuberculosis in the Peruvian population. Infect.Genet.Evol. 2006

116. Li HT, Zhang TT, Zhou YQ, Huang QH, Huang J. SLC11A1 (formerly NRAMP1) gene polymorphisms and tuberculosis susceptibility: a meta-analysis. Int.J.Tuberc.Lung Dis. 2006;10:3-12.

117. Abel L, Sanchez FO, Oberti J et al. Susceptibility to leprosy is linked to the human NRAMP1 gene. J.Infect.Dis. 1998;177:133-145.

118. Alcais A, Sanchez FO, Thuc NV et al. Granulomatous reaction to intradermal injection of lepromin (Mitsuda reaction) is linked to the human NRAMP1 gene in Vietnamese leprosy sibships. J.Infect.Dis. 2000;181:302-308.

119. Meisner SJ, Mucklow S, Warner G et al. Association of NRAMP1 polymorphism with leprosy type but not susceptibility to leprosy per se in west Africans. Am.J.Trop.Med.Hyg. 2001;65:733-735.

120. Koh WJ, Kwon OJ, Kim EJ et al. NRAMP1 gene polymorphism and susceptibility to nontuberculous mycobacterial lung diseases. Chest 2005;128:94-101.

121. Marquet S, Sanchez FO, Arias M et al. Variants of the human NRAMP1 gene and altered human immunodeficiency virus infection susceptibility. J.Infect.Dis. 1999;180:1521-1525.

122. John S, Marlow A, Hajeer A et al. Linkage and association studies of the natural resistance associated macrophage protein 1 (NRAMP1) locus in rheumatoid arthritis. J.Rheumatol. 1997;24:452-457.

123. Shaw MA, Clayton D, Atkinson SE et al. Linkage of rheumatoid arthritis to the candidate gene NRAMP1 on 2q35. J.Med.Genet. 1996;33:672-677.

124. Rodriguez MR, Gonzalez-Escribano MF, Aguilar F et al. Association of NRAMP1 promoter gene polymorphism with the susceptibility and radiological severity of rheumatoid arthritis. Tissue Antigens 2002;59:311-315.

125. Sanjeevi CB, Miller EN, Dabadghao P et al. Polymorphism at NRAMP1 and D2S1471 loci associated with juvenile rheumatoid arthritis. Arthritis Rheum. 2000;43:1397-1404.

126. Hofmeister A, Neibergs HL, Pokorny RM, Galandiuk S. The natural resistance-associated macrophage protein gene is associated with Crohn's disease. Surgery 1997;122:173-178.

127. Kojima Y, Kinouchi Y, Takahashi S et al. Inflammatory bowel disease is associated with a novel promoter polymorphism of natural resistance-associated macrophage protein 1 (NRAMP1) gene. Tissue Antigens 2001;58:379-384.

128. Kotze MJ, de Villiers JN, Rooney RN et al. Analysis of the NRAMP1 gene implicated in iron transport: association with multiple sclerosis and age effects. Blood Cells Mol.Dis. 2001;27:44-53.

129. Bassuny WM, Ihara K, Matsuura N et al. Association study of the NRAMP1 gene promoter polymorphism and early-onset type 1 diabetes. Immunogenetics 2002;54:282-285.

130. Kissler S, Stern P, Takahashi K et al. In vivo RNA interference demonstrates a role for Nramp1 in modifying susceptibility to type 1 diabetes. Nat.Genet. 2006;38:479-483.

131. Gruenheid S, Cellier M, Vidal S, Gros P. Identification and characterization of a second mouse Nramp gene. Genomics 1995;25:514-525.

132. Supek F, Supekova L, Nelson H, Nelson N. A yeast manganese transporter related to the macrophage protein involved in conferring resistance to mycobacteria. Proc.Natl.Acad.Sci.U.S.A 1996;93:5105-5110.

133. Hawlitschek G, Schneider H, Schmidt B et al. Mitochondrial protein import: identification of processing peptidase and of PEP, a processing enhancing protein. Cell 1988;53:795-806.

134. Muir WA, Hopfer U, King M. Iron transport across brush-border membranes from normal and iron-deficient mouse upper small intestine. J.Biol.Chem. 1984;259:4896-4903.

135. Muir A, Hopfer U. Regional specificity of iron uptake by small intestinal brush-border membranes from normal and iron-deficient mice. Am.J.Physiol 1985;248:G376-G379.

136. Fleming MD, Trenor CC, III, Su MA et al. Microcytic anaemia mice have a mutation in Nramp2, a candidate iron transporter gene. Nat.Genet. 1997;16:383-386.

137. Russell ES, Nash DJ, Bernstein SE et al. Characterization and genetic studies of microcytic anemia in house mouse. Blood 1970;35:838-850.

138. Edwards JA, Hoke JE. Defect of intestinal mucosal iron uptake in mice with hereditary microcytic anemia. Proc.Soc.Exp.Biol.Med. 1972;141:81-84.

139. Harrison DE. Marrow transplantation and iron therapy in mouse hereditary microcytic anemia. Blood 1972;40:893-901.

140. Edwards JA, Hoke JE. Red cell iron uptake in hereditary microcytic anemia. Blood 1975;46:381-388.

141. Fleming MD, Romano MA, Su MA et al. Nramp2 is mutated in the anemic Belgrade (b) rat: evidence of a role for Nramp2 in endosomal iron transport. Proc.Natl.Acad.Sci.U.S.A 1998;95:1148-1153.

142. Sladic-Simic D, Martinovitch PN, Zivkovic N et al. A thalassemia-like disorder in Belgrade laboratory rats. Ann.N.Y.Acad.Sci. 1969;165:93-99.

143. Edwards JA, Garrick LM, Hoke JE. Defective iron uptake and globin synthesis by erythroid cells in the anemia of the Belgrade laboratory rat. Blood 1978;51:347-357.

144. Edwards JA, Sullivan AL, Hoke JE. Defective delivery of iron to the developing red cell of the Belgrade laboratory rat. Blood 1980;55:645-648.

145. Garrick MD, Gniecko K, Liu Y, Cohan DS, Garrick LM. Transferrin and the transferrin cycle in Belgrade rat reticulocytes. J.Biol.Chem. 1993;268:14867-14874.

146. Su MA, Trenor CC, Fleming JC, Fleming MD, Andrews NC. The G185R mutation disrupts function of the iron transporter Nramp2. Blood 1998;92:2157-2163.

147. Canonne-Hergaux F, Fleming MD, Levy JE et al. The Nramp2/DMT1 iron transporter is induced in the duodenum of microcytic anemia mk mice but is not properly targeted to the intestinal brush border. Blood 2000;96:3964-3970.

148. Touret N, Martin-Orozco N, Paroutis P et al. Molecular and cellular mechanisms underlying iron transport deficiency in microcytic anemia. Blood 2004;104:1526-1533.

149. Xu H, Jin J, DeFelice LJ, Andrews NC, Clapham DE. A spontaneous, recurrent mutation in divalent metal transporter-1 exposes a calcium entry pathway. PLoS.Biol. 2004;2:E50.

150. Levy JE, Jin O, Fujiwara Y, Kuo F, Andrews NC. Transferrin receptor is necessary for development of erythrocytes and the nervous system. Nat.Genet. 1999;21:396-399.

151. Ci W, Li W, Ke Y, Qian ZM, Shen X. Intracellular Ca(2+) regulates the cellular iron uptake in K562 cells. Cell Calcium 2003;33:257-266.

152. Vidal S, Belouchi AM, Cellier M, Beatty B, Gros P. Cloning and characterization of a second human NRAMP gene on chromosome 12q13. Mamm.Genome 1995;6:224-230.

153. Lee PL, Gelbart T, West C, Halloran C, Beutler E. The human Nramp2 gene: characterization of the gene structure, alternative splicing, promoter region and polymorphisms. Blood Cells Mol.Dis. 1998;24:199-215.

154. Hubert N, Hentze MW. Previously uncharacterized isoforms of divalent metal transporter (DMT)-1: implications for regulation and cellular function. Proc.Natl.Acad.Sci.U.S.A 2002;99:12345-12350.

155. Tabuchi M, Tanaka N, Nishida-Kitayama J, Ohno H, Kishi F. Alternative splicing regulates the subcellular localization of divalent metal transporter 1 isoforms. Mol.Biol.Cell 2002;13:4371-4387.

156. Chaloupka R, Courville P, Veyrier F et al. Identification of functional amino acids in the Nramp family by a combination of evolutionary analysis and biophysical studies of metal and proton cotransport in vivo. Biochemistry 2005;44:726-733.

157. Mackenzie B, Ujwal ML, Chang MH, Romero MF, Hediger MA. Divalent metal-ion transporter DMT1 mediates both H(+) -coupled Fe(2+) transport and uncoupled fluxes. Pflugers Arch. 2005

158. Nevo Y, Nelson N. The mutation F227I increases the coupling of metal ion transport in DCT1. J.Biol.Chem. 2004;279:53056-53061.

159. Cohen A, Nevo Y, Nelson N. The first external loop of the metal ion transporter DCT1 is involved in metal ion binding and specificity. Proc.Natl.Acad.Sci.U.S.A 2003;100:10694-10699.

160. Johnson DM, Yamaji S, Tennant J, Srai SK, Sharp PA. Regulation of divalent metal transporter expression in human intestinal epithelial cells following exposure to non-haem iron. FEBS Lett. 2005;579:1923-1929.

161. Canonne-Hergaux F, Gruenheid S, Ponka P, Gros P. Cellular and subcellular localization of the Nramp2 iron transporter in the intestinal brush border and regulation by dietary iron. Blood 1999;93:4406-4417.

162. Trinder D, Oates PS, Thomas C, Sadleir J, Morgan EH. Localisation of divalent metal transporter 1 (DMT1) to the microvillus membrane of rat duodenal enterocytes in iron deficiency, but to hepatocytes in iron overload. Gut 2000;46:270-276.

163. Griffiths WJ, Kelly AL, Smith SJ, Cox TM. Localization of iron transport and regulatory proteins in human cells. QJM. 2000;93:575-587.

164. Yeh KY, Yeh M, Watkins JA, Rodriguez-Paris J, Glass J. Dietary iron induces rapid changes in rat intestinal divalent metal transporter expression. Am.J.Physiol Gastrointest.Liver Physiol 2000;279:G1070-G1079.

165. Zoller H, Koch RO, Theurl I et al. Expression of the duodenal iron transporters divalent-metal transporter 1 and ferroportin 1 in iron deficiency and iron overload. Gastroenterology 2001;120:1412-1419.

166. Ma Y, Specian RD, Yeh KY et al. The transcytosis of divalent metal transporter 1 and apo-transferrin during iron uptake in intestinal epithelium. Am.J.Physiol Gastrointest.Liver Physiol 2002;283:G965-G974.

167. Sharp P, Tandy S, Yamaji S et al. Rapid regulation of divalent metal transporter (DMT1) protein but not mRNA expression by non-haem iron in human intestinal Caco-2 cells. FEBS Lett. 2002;510:71-76.

168. Tandy S, Williams M, Leggett A et al. Nramp2 expression is associated with pH-dependent iron uptake across the apical membrane of human intestinal Caco-2 cells. J.Biol.Chem. 2000;275:1023-1029.

169. Canonne-Hergaux F, Zhang AS, Ponka P, Gros P. Characterization of the iron transporter DMT1 (NRAMP2/DCT1) in red blood cells of normal and anemic mk/mk mice. Blood 2001;98:3823-3830.

170. Chen L, Boadle RA, Harris DC. Toxicity of holotransferrin but not albumin in proximal tubule cells in primary culture. J.Am.Soc.Nephrol. 1998;9:77-84.

171. Jabado N, Canonne-Hergaux F, Gruenheid S, Picard V, Gros P. Iron transporter Nramp2/DMT-1 is associated with the membrane of phagosomes in macrophages and Sertoli cells. Blood 2002;100:2617-2622.

172. Canonne-Hergaux F, Gros P. Expression of the iron transporter DMT1 in kidney from normal and anemic mk mice. Kidney Int. 2002;62:147-156.

173. Ferguson CJ, Wareing M, Ward DT et al. Cellular localization of divalent metal transporter DMT-1 in rat kidney. Am.J.Physiol Renal Physiol 2001;280:F803-F814.

174. Abouhamed M, Gburek J, Liu W et al. Divalent metal transporter 1 in the kidney proximal tubule is expressed in late endosomes/lysosomal membranes: Implications for renal handling of protein-metal complexes. Am.J.Physiol Renal Physiol 2006

175. Tchernitchko D, Bourgeois M, Martin ME, Beaumont C. Expression of the two mRNA isoforms of the iron transporter Nrmap2/DMTI in mice and function of the iron responsive element. Biochem.J. 2002;363:449-455.

176. Ferguson CJ, Wareing M, Delannoy M et al. Iron handling and gene expression of the divalent metal transporter, DMT1, in the kidney of the anemic Belgrade (b) rat. Kidney Int. 2003;64:1755-1764.

177. Burdo JR, Menzies SL, Simpson IA et al. Distribution of divalent metal transporter 1 and metal transport protein 1 in the normal and Belgrade rat. J.Neurosci.Res. 2001;66:1198-1207.

178. Moos T, Morgan EH. The significance of the mutated divalent metal transporter (DMT1) on iron transport into the Belgrade rat brain. J.Neurochem. 2004;88:233-245.

179. Lis A, Paradkar PN, Singleton S et al. Hypoxia induces changes in expression of isoforms of the divalent metal transporter (DMT1) in rat pheochromocytoma (PC12) cells. Biochem.Pharmacol. 2005;69:1647-1655.

180. Zhang AS, Xiong S, Tsukamoto H, Enns CA. Localization of iron metabolism-related mRNAs in rat liver indicate that HFE is expressed predominantly in hepatocytes. Blood 2004;103:1509-1514.

181. Georgieff MK, Wobken JK, Welle J, Burdo JR, Connor JR. Identification and localization of divalent metal transporter-1 (DMT-1) in term human placenta. Placenta 2000;21:799-804.

182. Lam-Yuk-Tseung S, Gros P. Distinct Targeting and Recycling Properties of Two Isoforms of the Iron Transporter DMT1 (NRAMP2, Slc11A2). Biochemistry 2006;45:2294-2301.

183. Bonifacino JS, Traub LM. Signals for sorting of transmembrane proteins to endosomes and lysosomes. Annu.Rev.Biochem. 2003;72:395-447.

184. Lam-Yuk-Tseung S, Touret N, Grinstein S, Gros P. Carboxyl-Terminus Determinants of the Iron Transporter DMT1/SLC11A2 Isoform II (-IRE/1B) Mediate Internalization from the Plasma Membrane into Recycling Endosomes. Biochemistry 2005;44:12149-12159.

185. Ohgami RS, Campagna DR, Greer EL et al. Identification of a ferrireductase required for efficient transferrin-dependent iron uptake in erythroid cells. Nat.Genet. 2005;37:1264-1269.

186. Ohgami RS, Campagna DR, Antiochos B et al. nm1054: a spontaneous, recessive, hypochromic, microcytic anemia mutation in the mouse. Blood 2005;106:3625-3631.

187. Kawabata H, Yang R, Hirama T et al. Molecular cloning of transferrin receptor 2. A new member of the transferrin receptor-like family. J.Biol.Chem. 1999;274:20826-20832.

188. Camaschella C, Roetto A, Cali A et al. The gene TFR2 is mutated in a new type of haemochromatosis mapping to 7q22. Nat.Genet. 2000;25:14-15.

189. Kozyraki R, Fyfe J, Verroust PJ et al. Megalin-dependent cubilin-mediated endocytosis is a major pathway for the apical uptake of transferrin in polarized epithelia. Proc.Natl.Acad.Sci.U.S.A 2001;98:12491-12496.

190. McKie AT, Barrow D, Latunde-Dada GO et al. An iron-regulated ferric reductase associated with the absorption of dietary iron. Science 2001;291:1755-1759.

191. Gunshin H, Starr CN, Direnzo C et al. Cybrd1 (duodenal cytochrome b) is not necessary for dietary iron absorption in mice. Blood 2005;106:2879-2883.

192. Moos T. Immunohistochemical localization of intraneuronal transferrin receptor immunoreactivity in the adult mouse central nervous system. J.Comp Neurol. 1996;375:675-692.

193. Moos T, Trinder D, Morgan EH. Cellular distribution of ferric iron, ferritin, transferrin and divalent metal transporter 1 (DMT1) in substantia nigra and basal ganglia of normal and beta2-microglobulin deficient mouse brain. Cell Mol.Biol.(Noisy.-le-grand) 2000;46:549-561.

194. Moos T, Morgan EH. Evidence for low molecular weight, non-transferrin-bound iron in rat brain and cerebrospinal fluid. J.Neurosci.Res. 1998;54:486-494.

195. Jeong SY, David S. Glycosylphosphatidylinositol-anchored ceruloplasmin is required for iron efflux from cells in the central nervous system. J.Biol.Chem. 2003;278:27144-27148.

196. Chang YZ, Ke Y, Du JR et al. Increased Divalent Metal Transporter 1 Expression Might Be Associated with the Neurotoxicity of L-DOPA. Mol.Pharmacol. 2006;69:968-974.

197. Moos T, Morgan EH. The metabolism of neuronal iron and its pathogenic role in neurological disease: review. Ann.N.Y.Acad.Sci. 2004;1012:14-26.

198. Wareing M, Ferguson CJ, Delannoy M et al. Altered dietary iron intake is a strong modulator of renal DMT1 expression. Am.J.Physiol Renal Physiol 2003;285:F1050-F1059.

199. Weintraub LR, Conrad ME, Crosby WH. Absorption of hemoglobin iron by the rat. Proc.Soc.Exp.Biol.Med. 1965;120:840-843.

200. Conrad ME, Weintraub LR, Sears DA, Crosby WH. Absorption of hemoglobin iron. Am.J.Physiol 1966;211:1123-1130.

201. Shayeghi M, Latunde-Dada GO, Oakhill JS et al. Identification of an intestinal heme transporter. Cell 2005;122:789-801.

202. Wheby MS, Suttle GE, Ford KT, III. Intestinal absorption of hemoglobin iron. Gastroenterology 1970;58:647-654.

203. Parmley RT, Barton JC, Conrad ME, Austin RL, Holland RM. Ultrastructural cytochemistry and radioautography of hemoglobin--iron absorption. Exp.Mol.Pathol. 1981;34:131-144.

204. Raffin SB, Woo CH, Roost KT, Price DC, Schmid R. Intestinal absorption of hemoglobin iron-heme cleavage by mucosal heme oxygenase. J.Clin.Invest 1974;54:1344-1352.

205. Yang J, Goetz D, Li JY et al. An iron delivery pathway mediated by a lipocalin. Mol.Cell 2002;10:1045-1056.

206. Kaplan J. Mechanisms of cellular iron acquisition: another iron in the fire. Cell 2002;111:603-606.

207. Torti FM, Torti SV. Regulation of ferritin genes and protein. Blood 2002;99:3505-3516.

208. Harrison PM. Ferritin: an iron-storage molecule. Semin.Hematol. 1977;14:55-70.

209. Harrison PM, Arosio P. The ferritins: molecular properties, iron storage function and cellular regulation. Biochim.Biophys.Acta 1996;1275:161-203.

210. Taketani S. Aquisition, mobilization and utilization of cellular iron and heme: endless findings and growing evidence of tight regulation. Tohoku J.Exp.Med. 2005;205:297-318.

211. Zhang AS, Sheftel AD, Ponka P. Intracellular kinetics of iron in reticulocytes: evidence for endosome involvement in iron targeting to mitochondria. Blood 2005;105:368-375.

212. Taketani S, Tokunaga R. Heme transport from rat liver mitochondria to the microsomes in vitro. Biochem.Biophys.Res.Commun. 1980;92:1343-1347.

213. Senjo M, Ishibashi T, Imai Y. Purification and characterization of cytosolic liver protein facilitating heme transport into apocytochrome b5 from mitochondria. Evidence for identifying the heme transfer protein as belonging to a group of glutathione S-transferases. J.Biol.Chem. 1985;260:9191-9196.

214. Johnson DC, Dean DR, Smith AD, Johnson MK. Structure, function, and formation of biological iron-sulfur clusters. Annu.Rev.Biochem. 2005;74:247-281.

215. Muhlenhoff U, Gerber J, Richhardt N, Lill R. Components involved in assembly and dislocation of iron-sulfur clusters on the scaffold protein Isu1p. EMBO J. 2003;22:4815-4825.

216. Chen OS, Hemenway S, Kaplan J. Inhibition of Fe-S cluster biosynthesis decreases mitochondrial iron export: evidence that Yfh1p affects Fe-S cluster synthesis. Proc.Natl.Acad.Sci.U.S.A 2002;99:12321-12326.

217. Adamec J, Rusnak F, Owen WG et al. Iron-dependent self-assembly of recombinant yeast frataxin: implications for Friedreich ataxia. Am.J.Hum.Genet. 2000;67:549-562.

218. Rotig A, de LP, Chretien D et al. Aconitase and mitochondrial iron-sulphur protein deficiency in Friedreich ataxia. Nat.Genet. 1997;17:215-217.

219. Abboud S, Haile DJ. A novel mammalian iron-regulated protein involved in intracellular iron metabolism. J.Biol.Chem. 2000;275:19906-19912.

220. Donovan A, Brownlie A, Zhou Y et al. Positional cloning of zebrafish ferroportin1 identifies a conserved vertebrate iron exporter. Nature 2000;403:776-781.

221. McKie AT, Marciani P, Rolfs A et al. A novel duodenal iron-regulated transporter, IREG1, implicated in the basolateral transfer of iron to the circulation. Mol.Cell 2000;5:299-309.

222. Vulpe CD, Kuo YM, Murphy TL et al. Hephaestin, a ceruloplasmin homologue implicated in intestinal iron transport, is defective in the sla mouse. Nat.Genet. 1999;21:195-199.

223. Harris ZL, Durley AP, Man TK, Gitlin JD. Targeted gene disruption reveals an essential role for ceruloplasmin in cellular iron efflux. Proc.Natl.Acad.Sci.U.S.A 1999;96:10812-10817.

224. Delaby C, Pilard N, Goncalves AS, Beaumont C, Canonne-Hergaux F. Presence of the iron exporter ferroportin at the plasma membrane of macrophages is enhanced by iron loading and down-regulated by hepcidin. Blood 2005;106:3979-3984.

225. Nemeth E, Tuttle MS, Powelson J et al. Hepcidin regulates cellular iron efflux by binding to ferroportin and inducing its internalization. Science 2004;306:2090-2093.

226. Pantopoulos K. Iron metabolism and the IRE/IRP regulatory system: an update. Ann.N.Y.Acad.Sci. 2004;1012:1-13.

227. Hentze MW, Kuhn LC. Molecular control of vertebrate iron metabolism: mRNA-based regulatory circuits operated by iron, nitric oxide, and oxidative stress. Proc.Natl.Acad.Sci.U.S.A 1996;93:8175-8182.

228. Meyron-Holtz EG, Ghosh MC, Rouault TA. Mammalian tissue oxygen levels modulate iron-regulatory protein activities in vivo. Science 2004;306:2087-2090.

229. Wang J, Chen G, Pantopoulos K. Nitric oxide inhibits the degradation of IRP2. Mol.Cell Biol. 2005;25:1347-1353.

230. Cooperman SS, Meyron-Holtz EG, Olivierre-Wilson H et al. Microcytic anemia, erythropoietic protoporphyria, and neurodegeneration in mice with targeted deletion of iron-regulatory protein 2. Blood 2005;106:1084-1091.

231. Meyron-Holtz EG, Ghosh MC, Iwai K et al. Genetic ablations of iron regulatory proteins 1 and 2 reveal why iron regulatory protein 2 dominates iron homeostasis. EMBO J. 2004;23:386-395.

232. Eisenstein RS, Ross KL. Novel roles for iron regulatory proteins in the adaptive response to iron deficiency. J.Nutr. 2003;133:1510S-1516S.

233. Muckenthaler M, Gray NK, Hentze MW. IRP-1 binding to ferritin mRNA prevents the recruitment of the small ribosomal subunit by the cap-binding complex eIF4F. Mol.Cell 1998;2:383-388.

234. Gunshin H, Allerson CR, Polycarpou-Schwarz M et al. Iron-dependent regulation of the divalent metal ion transporter. FEBS Lett. 2001;509:309-316.

235. Ludwiczek S, Aigner E, Theurl I, Weiss G. Cytokine-mediated regulation of iron transport in human monocytic cells. Blood 2003;101:4148-4154.

236. Yang F, Liu XB, Quinones M et al. Regulation of reticuloendothelial iron transporter MTP1 (Slc11a3) by inflammation. J.Biol.Chem. 2002;277:39786-39791.

237. Sayers MH, English G, Finch C. Capacity of the store-regulator in maintaining iron balance. Am.J.Hematol. 1994;47:194-197.

238. Finch C. Regulators of iron balance in humans. Blood 1994;84:1697-1702.

239. Trenor CC, III, Campagna DR, Sellers VM, Andrews NC, Fleming MD. The molecular defect in hypotransferrinemic mice. Blood 2000;96:1113-1118.

240. Levy JE, Montross LK, Cohen DE, Fleming MD, Andrews NC. The C282Y mutation causing hereditary hemochromatosis does not produce a null allele. Blood 1999;94:9-11.

241. Koller BH, Marrack P, Kappler JW, Smithies O. Normal development of mice deficient in beta 2M, MHC class I proteins, and CD8+ T cells. Science 1990;248:1227-1230.

242. Krause A, Neitz S, Magert HJ et al. LEAP-1, a novel highly disulfide-bonded human peptide, exhibits antimicrobial activity. FEBS Lett. 2000;480:147-150.

243. Park CH, Valore EV, Waring AJ, Ganz T. Hepcidin, a urinary antimicrobial peptide synthesized in the liver. J.Biol.Chem. 2001;276:7806-7810.

244. Pigeon C, Ilyin G, Courselaud B et al. A new mouse liver-specific gene, encoding a protein homologous to human antimicrobial peptide hepcidin, is overexpressed during iron overload. J.Biol.Chem. 2001;276:7811-7819.

245. Nicolas G, Bennoun M, Devaux I et al. Lack of hepcidin gene expression and severe tissue iron overload in upstream stimulatory factor 2 (USF2) knockout mice. Proc.Natl.Acad.Sci.U.S.A 2001;98:8780-8785.

246. Nicolas G, Bennoun M, Porteu A et al. Severe iron deficiency anemia in transgenic mice expressing liver hepcidin. Proc.Natl.Acad.Sci.U.S.A 2002;99:4596-4601.

247. Anderson GJ, Frazer DM, Wilkins SJ et al. Relationship between intestinal iron-transporter expression, hepatic hepcidin levels and the control of iron absorption. Biochem.Soc.Trans. 2002;30:724-726.

248. Nicolas G, Chauvet C, Viatte L et al. The gene encoding the iron regulatory peptide hepcidin is regulated by anemia, hypoxia, and inflammation. J.Clin.Invest 2002;110:1037-1044.

249. Shike H, Lauth X, Westerman ME et al. Bass hepcidin is a novel antimicrobial peptide induced by bacterial challenge. Eur.J.Biochem. 2002;269:2232-2237.

250. Yeh KY, Yeh M, Glass J. Hepcidin regulation of ferroportin 1 expression in the liver and intestine of the rat. Am.J.Physiol Gastrointest.Liver Physiol 2004;286:G385-G394.

251. Hentze MW, Muckenthaler MU, Andrews NC. Balancing acts: molecular control of mammalian iron metabolism. Cell 2004;117:285-297.

252. Laftah AH, Ramesh B, Simpson RJ et al. Effect of hepcidin on intestinal iron absorption in mice. Blood 2004;103:3940-3944.

253. Frazer DM, Wilkins SJ, Becker EM et al. Hepcidin expression inversely correlates with the expression of duodenal iron transporters and iron absorption in rats. Gastroenterology 2002;123:835-844.

254. Nemeth E, Valore EV, Territo M et al. Hepcidin, a putative mediator of anemia of inflammation, is a type II acute-phase protein. Blood 2003;101:2461-2463.

255. Gehrke SG, Kulaksiz H, Herrmann T et al. Expression of hepcidin in hereditary hemochromatosis: evidence for a regulation in response to the serum transferrin saturation and to non-transferrin-bound iron. Blood 2003;102:371-376.

256. Oates PS, Thomas C. Augmented internalisation of ferroportin to late endosomes impairs iron uptake by enterocyte-like IEC-6 cells. Pflugers Arch. 2005;450:317-325.

257. Nemeth E, Preza GC, Jung CL et al. The N-terminus of hepcidin is essential for its interaction with ferroportin: structure-function study. Blood 2006;107:328-333.

258. Gunshin H, Fujiwara Y, Custodio AO et al. Slc11a2 is required for intestinal iron absorption and erythropoiesis but dispensable in placenta and liver. J.Clin.Invest 2005;115:1258-1266.

259. Priwitzerova M, Pospisilova D, Prchal JT et al. Severe hypochromic microcytic anemia caused by a congenital defect of the iron transport pathway in erythroid cells. Blood 2004;103:3991-3992.

260. Priwitzerova M, Nie G, Sheftel AD et al. Functional consequences of the human DMT1 (SLC11A2) mutation on protein expression and iron uptake. Blood 2005;106:3985-3987.

261. Gunshin H, Jin J, Fujiwara Y et al. Analysis of the E399D mutation in SLC11A2. Blood 2005;106:2221-2222.

262. Lam-Yuk-Tseung S, Mathieu M, Gros P. Functional characterization of the E399D DMT1/NRAMP2/SLC11A2 protein produced by an exon 12 mutation in a patient with microcytic anemia and iron overload. Blood Cells Mol.Dis. 2005;35:212-216.

263. Iolascon A, d'Apolito M, Servedio V et al. Microcytic anemia and hepatic iron overload in a child with compound heterozygous mutations in DMT1. Blood 2005

264. Lam-Yuk-Tseung S, Camaschella C, Iolascon A, Gros P. A novel R416C mutation in human DMT1 (SLC11A2) displays pleiotropic effects on function and causes microcytic anemia and hepatic iron overload. Blood Cells Mol.Dis. 2006;36:347-354.

265. Beaumont C, Delaunay J, Hetet G et al. Two new human DMT1 mutations in a compound heterozygous patient with mircocytic anemia and low iron stores (Poster). Atlanta, GA, USA. December 10-13, 2005:

266. Pietrangelo A. Hereditary hemochromatosis--a new look at an old disease. N.Engl.J.Med. 2004;350:2383-2397.

267. Feder JN, Gnirke A, Thomas W et al. A novel MHC class I-like gene is mutated in patients with hereditary haemochromatosis. Nat.Genet. 1996;13:399-408.

268. Lebron JA, Bennett MJ, Vaughn DE et al. Crystal structure of the hemochromatosis protein HFE and characterization of its interaction with transferrin receptor. Cell 1998;93:111-123.

269. Drakesmith H, Sweetland E, Schimanski L et al. The hemochromatosis protein HFE inhibits iron export from macrophages. Proc.Natl.Acad.Sci.U.S.A 2002;99:15602-15607.

270. Waheed A, Grubb JH, Zhou XY et al. Regulation of transferrin-mediated iron uptake by HFE, the protein defective in hereditary hemochromatosis. Proc.Natl.Acad.Sci.U.S.A 2002;99:3117-3122.

271. Gross CN, Irrinki A, Feder JN, Enns CA. Co-trafficking of HFE, a nonclassical major histocompatibility complex class I protein, with the transferrin receptor implies a role in intracellular iron regulation. J.Biol.Chem. 1998;273:22068-22074.

272. Parkkila S, Waheed A, Britton RS et al. Association of the transferrin receptor in human placenta with HFE, the protein defective in hereditary hemochromatosis. Proc.Natl.Acad.Sci.U.S.A 1997;94:13198-13202.

273. Bennett MJ, Lebron JA, Bjorkman PJ. Crystal structure of the hereditary haemochromatosis protein HFE complexed with transferrin receptor. Nature 2000;403:46-53.

274. Ahmad KA, Ahmann JR, Migas MC et al. Decreased liver hepcidin expression in the Hfe knockout mouse. Blood Cells Mol.Dis. 2002;29:361-366.

275. Muckenthaler M, Roy CN, Custodio AO et al. Regulatory defects in liver and intestine implicate abnormal hepcidin and Cybrd1 expression in mouse hemochromatosis. Nat.Genet. 2003;34:102-107.

276. Nicolas G, Viatte L, Lou DQ et al. Constitutive hepcidin expression prevents iron overload in a mouse model of hemochromatosis. Nat.Genet. 2003;34:97-101.

277. Hattori A, Wakusawa S, Hayashi H et al. AVAQ 594-597 deletion of the TfR2 gene in a Japanese family with hemochromatosis. Hepatol.Res. 2003;26:154-156.

278. Koyama C, Wakusawa S, Hayashi H et al. Two novel mutations, L490R and V561X, of the transferrin receptor 2 gene in Japanese patients with hemochromatosis. Haematologica 2005;90:302-307.

279. Roetto A, Totaro A, Piperno A et al. New mutations inactivating transferrin receptor 2 in hemochromatosis type 3. Blood 2001;97:2555-2560.

280. Girelli D, Bozzini C, Roetto A et al. Clinical and pathologic findings in hemochromatosis type 3 due to a novel mutation in transferrin receptor 2 gene. Gastroenterology 2002;122:1295-1302.

281. Le GG, Mons F, Jacolot S et al. Early onset hereditary hemochromatosis resulting from a novel TFR2 gene nonsense mutation (R105X) in two siblings of north French descent. Br.J.Haematol. 2004;125:674-678.

282. Piperno A, Roetto A, Mariani R et al. Homozygosity for transferrin receptor-2 Y250X mutation induces early iron overload. Haematologica 2004;89:359-360.

283. De GM, Roetto A, Piperno A et al. Natural history of juvenile haemochromatosis. Br.J.Haematol. 2002;117:973-979.

284. Roetto A, Papanikolaou G, Politou M et al. Mutant antimicrobial peptide hepcidin is associated with severe juvenile hemochromatosis. Nat.Genet. 2003;33:21-22.

285. Camaschella C, Roetto A, De GM. Juvenile hemochromatosis. Semin.Hematol. 2002;39:242-248.

286. Roetto A, Daraio F, Porporato P et al. Screening hepcidin for mutations in juvenile hemochromatosis: identification of a new mutation (C70R). Blood 2004;103:2407-2409.

287. Majore S, Binni F, Pennese A et al. HAMP gene mutation c.208T>C (p.C70R) identified in an Italian patient with severe hereditary hemochromatosis. Hum.Mutat. 2004;23:400.

288. Delatycki MB, Allen KJ, Gow P et al. A homozygous HAMP mutation in a multiply consanguineous family with pseudo-dominant juvenile hemochromatosis. Clin.Genet. 2004;65:378-383.

289. Papanikolaou G, Samuels ME, Ludwig EH et al. Mutations in HFE2 cause iron overload in chromosome 1q-linked juvenile hemochromatosis. Nat.Genet. 2004;36:77-82.

290. Camaschella C. Understanding iron homeostasis through genetic analysis of hemochromatosis and related disorders. Blood 2005;106:3710-3717.

291. Montosi G, Donovan A, Totaro A et al. Autosomal-dominant hemochromatosis is associated with a mutation in the ferroportin (SLC11A3) gene. J.Clin.Invest 2001;108:619-623.

292. Njajou OT, Vaessen N, Joosse M et al. A mutation in SLC11A3 is associated with autosomal dominant hemochromatosis. Nat.Genet. 2001;28:213-214.

293. Schimanski LM, Drakesmith H, Merryweather-Clarke AT et al. In vitro functional analysis of human ferroportin (FPN) and hemochromatosis-associated FPN mutations. Blood 2005;105:4096-4102.

294. Drakesmith H, Schimanski LM, Ormerod E et al. Resistance to hepcidin is conferred by hemochromatosis-associated mutations of ferroportin. Blood 2005;106:1092-1097.

295. De Domenico I, Ward DM, Nemeth E et al. The molecular basis of ferroportin-linked hemochromatosis. Proc.Natl.Acad.Sci.U.S.A 2005;102:8955-8960.

296. Goncalves AS, Muzeau F, Blaybel R et al. Wild type and mutant ferroportins do not form oligomers in transfected cells. Biochem.J. 2006

297. Agranoff D, Monahan IM, Mangan JA, Butcher PD, Krishna S. Mycobacterium tuberculosis expresses a novel pH-dependent divalent cation transporter belonging to the Nramp family. J.Exp.Med. 1999;190:717-724.

298. Belouchi A, Cellier M, Kwan T et al. The macrophage-specific membrane protein Nramp controlling natural resistance to infections in mice has homologues expressed in the root system of plants. Plant Mol.Biol. 1995;29:1181-1196.

299. Haemig HA, Brooker RJ. Importance of conserved acidic residues in mntH, the Nramp homolog of Escherichia coli. J.Membr.Biol. 2004;201:97-107.

300. Mackenzie B, Ujwal ML, Chang MH, Romero MF, Hediger MA. Divalent metal-ion transporter DMT1 mediates both H(+) -coupled Fe(2+) transport and uncoupled fluxes. Pflugers Arch. 2005

301. Tabuchi M, Yoshimori T, Yamaguchi K, Yoshida T, Kishi F. Human NRAMP2/DMT1, which mediates iron transport across endosomal membranes, is localized to late endosomes and lysosomes in HEp-2 cells. J.Biol.Chem. 2000;275:22220-22228.

302. Fleming MD, Andrews NC. Mammalian iron transport: an unexpected link between metal homeostasis and host defense. J.Lab Clin.Med. 1998;132:464-468.

303. Chung J, Wessling-Resnick M. Molecular mechanisms and regulation of iron transport. Crit Rev.Clin.Lab Sci. 2003;40:151-182.

304. Cellier M, Shustik C, Dalton W et al. Expression of the human NRAMP1 gene in professional primary phagocytes: studies in blood cells and in HL-60 promyelocytic leukemia. J.Leukoc.Biol. 1997;61:96-105.

305. Gruenheid S, Gros P. Genetic susceptibility to intracellular infections: Nramp1, macrophage function and divalent cations transport. Curr.Opin.Microbiol. 2000;3:43-48.

306. Supek F, Supekova L, Nelson H, Nelson N. Function of metal-ion homeostasis in the cell division cycle, mitochondrial protein processing, sensitivity to mycobacterial infection and brain function. J.Exp.Biol. 1997;200 (Pt 2):321-330.

307. Orgad S, Nelson H, Segal D, Nelson N. Metal ions suppress the abnormal taste behavior of the Drosophila mutant malvolio. J.Exp.Biol. 1998;201:115-120.

308. Urbatsch IL, Julien M, Carrier I et al. Mutational analysis of conserved carboxylate residues in the nucleotide binding sites of P-glycoprotein. Biochemistry 2000;39:14138-14149.

309. Sherman, F, Fink, G. R., and Hicks, J. B. Methods of Yeast Genetics. 1982. NY, Cold Springs Harbor.
Ref Type: Generic

310. Kwan T, Gros P. Mutational analysis of the P-glycoprotein first intracellular loop and flanking transmembrane domains. Biochemistry 1998;37:3337-3350.

311. Kast C, Canfield V, Levenson R, Gros P. Membrane topology of P-glycoprotein as determined by epitope insertion: transmembrane organization of the N-terminal domain of mdr3. Biochemistry 1995;34:4402-4411.

312. Nakagama H, Heinrich G, Pelletier J, Housman DE. Sequence and structural requirements for high-affinity DNA binding by the WT1 gene product. Mol.Cell Biol. 1995;15:1489-1498.

313. Eng BH, Guerinot ML, Eide D, Saier MH, Jr. Sequence analyses and phylogenetic characterization of the ZIP family of metal ion transport proteins. J.Membr.Biol. 1998;166:1-7.

314. Voss J, Salwinski L, Kaback HR, Hubbell WL. A method for distance determination in proteins using a designed metal ion binding site and site-directed spin labeling: evaluation with T4 lysozyme. Proc.Natl.Acad.Sci.U.S.A 1995;92:12295-12299.

315. Omichinski JG, Trainor C, Evans T et al. A small single-"finger" peptide from the erythroid transcription factor GATA-1 binds specifically to DNA as a zinc or iron complex. Proc.Natl.Acad.Sci.U.S.A 1993;90:1676-1680.

316. Ghazaleh FA, Omburo GA, Colman RW. Evidence for the presence of essential histidine and cysteine residues in platelet cGMP-inhibited phosphodiesterase. Biochem.J. 1996;317 (Pt 2):495-501.

317. Worthington MT, Amann BT, Nathans D, Berg JM. Metal binding properties and secondary structure of the zinc-binding domain of Nup475. Proc.Natl.Acad.Sci.U.S.A 1996;93:13754-13759.

318. Worthington MT, Browne L, Battle EH, Luo RQ. Functional properties of transfected human DMT1 iron transporter. Am.J.Physiol Gastrointest.Liver Physiol 2000;279:G1265-G1273.

319. Kaback HR. The lac permease of Escherichia coli: a prototypic energy-transducing membrane protein. Biochim.Biophys.Acta 1990;1018:160-162.

320. Muller-Berger S, Karbach D, Kang D et al. Roles of histidine 752 and glutamate 699 in the pH dependence of mouse band 3 protein-mediated anion transport. Biochemistry 1995;34:9325-9332.

321. Muller-Berger S, Karbach D, Konig J et al. Inhibition of mouse erythroid band 3-mediated chloride transport by site-directed mutagenesis of histidine residues and its reversal by second site mutation of Lys 558, the locus of covalent H2DIDS binding. Biochemistry 1995;34:9315-9324.

322. Cotten JF, Welsh MJ. Cystic fibrosis-associated mutations at arginine 347 alter the pore architecture of CFTR. Evidence for disruption of a salt bridge. J.Biol.Chem. 1999;274:5429-5435.

323. Guan L, Kaback HR. Lessons from lactose permease. Annu.Rev.Biophys.Biomol.Struct. 2006;35:67-91.

324. Ponka P, Beaumont C, Richardson DR. Function and regulation of transferrin and ferritin. Semin.Hematol. 1998;35:35-54.

325. Touret N, Martin-Orozco N, Paroutis P et al. Molecular and Cellular Mechanisms Underlying Iron Transport Deficiency in Microcytic Anemia. Blood 2004

326. Goldstein JL, Basu SK, Brunschede GY, Brown MS. Release of low density lipoprotein from its cell surface receptor by sulfated glycosaminoglycans. Cell 1976;7:85-95.

327. Chen WJ, Goldstein JL, Brown MS. NPXY, a sequence often found in cytoplasmic tails, is required for coated pit-mediated internalization of the low density lipoprotein receptor. J.Biol.Chem. 1990;265:3116-3123.

328. Pietrzik CU, Busse T, Merriam DE, Weggen S, Koo EH. The cytoplasmic domain of the LDL receptor-related protein regulates multiple steps in APP processing. EMBO J. 2002;21:5691-5700.

329. Prigent SA, Gullick WJ. Identification of c-erbB-3 binding sites for phosphatidylinositol 3'-kinase and SHC using an EGF receptor/c-erbB-3 chimera. EMBO J. 1994;13:2831-2841.

330. Takeda T, Yamazaki H, Farquhar MG. Identification of an apical sorting determinant in the cytoplasmic tail of megalin. Am.J.Physiol Cell Physiol 2003;284:C1105-C1113.

331. Ohno H, Stewart J, Fournier MC et al. Interaction of tyrosine-based sorting signals with clathrin-associated proteins. Science 1995;269:1872-1875.

332. Boll W, Ohno H, Songyang Z et al. Sequence requirements for the recognition of tyrosine-based endocytic signals by clathrin AP-2 complexes. EMBO J. 1996;15:5789-5795.

333. Honing S, Griffith J, Geuze HJ, Hunziker W. The tyrosine-based lysosomal targeting signal in lamp-1 mediates sorting into Golgi-derived clathrin-coated vesicles. EMBO J. 1996;15:5230-5239.

334. Lukacs GL, Segal G, Kartner N, Grinstein S, Zhang F. Constitutive internalization of cystic fibrosis transmembrane conductance regulator occurs via clathrin-dependent endocytosis and is regulated by protein phosphorylation. Biochem.J. 1997;328 (Pt 2):353-361.

335. Duffield A, Kamsteeg EJ, Brown AN, Pagel P, Caplan MJ. The tetraspanin CD63 enhances the internalization of the H,K-ATPase beta-subunit. Proc.Natl.Acad.Sci.U.S.A 2003;100:15560-15565.

336. Nesterov A, Carter RE, Sorkina T, Gill GN, Sorkin A. Inhibition of the receptor-binding function of clathrin adaptor protein AP-2 by dominant-negative mutant mu2 subunit and its effects on endocytosis. EMBO J. 1999;18:2489-2499.

337. van Dam EM, Stoorvogel W. Dynamin-dependent transferrin receptor recycling by endosome-derived clathrin-coated vesicles. Mol.Biol.Cell 2002;13:169-182.

338. Gan Y, McGraw TE, Rodriguez-Boulan E. The epithelial-specific adaptor AP1B mediates post-endocytic recycling to the basolateral membrane. Nat.Cell Biol. 2002;4:605-609.

339. Yeh JI, Verhey KJ, Birnbaum MJ. Kinetic analysis of glucose transporter trafficking in fibroblasts and adipocytes. Biochemistry 1995;34:15523-15531.

340. Petris MJ, Mercer JF. The Menkes protein (ATP7A; MNK) cycles via the plasma membrane both in basal and elevated extracellular copper using a C-terminal di-leucine endocytic signal. Hum.Mol.Genet. 1999;8:2107-2115.

341. Petris MJ, Camakaris J, Greenough M, LaFontaine S, Mercer JF. A C-terminal di-leucine is required for localization of the Menkes protein in the trans-Golgi network. Hum.Mol.Genet. 1998;7:2063-2071.

342. Francis MJ, Jones EE, Levy ER et al. Identification of a di-leucine motif within the C terminus domain of the Menkes disease protein that mediates endocytosis from the plasma membrane. J.Cell Sci. 1999;112 (Pt 11):1721-1732.

343. Johnson KF, Kornfeld S. The cytoplasmic tail of the mannose 6-phosphate/insulin-like growth factor-II receptor has two signals for lysosomal enzyme sorting in the Golgi. J.Cell Biol. 1992;119:249-257.

344. Chen HJ, Yuan J, Lobel P. Systematic mutational analysis of the cation-independent mannose 6-phosphate/insulin-like growth factor II receptor cytoplasmic domain. An acidic cluster containing a key aspartate is important for function in lysosomal enzyme sorting. J.Biol.Chem. 1997;272:7003-7012.

345. Priwitzerova M, Nie G, Sheftel AD et al. Functional consequences of the human DMT1 mutation on protein expression and iron uptake. Blood 2005

346. Banerjee D, Flanagan PR, Cluett J, Valberg LS. Transferrin receptors in the human gastrointestinal tract. Relationship to body iron stores. Gastroenterology 1986;91:861-869.

347. Anderson GJ, Powell LW, Halliday JW. Transferrin receptor distribution and regulation in the rat small intestine. Effect of iron stores and erythropoiesis. Gastroenterology 1990;98:576-585.

348. Malo D, Vogan K, Vidal S et al. Haplotype mapping and sequence analysis of the mouse Nramp gene predict susceptibility to infection with intracellular parasites. Genomics 1994;23:51-61.

349. Vidal S, Gros P, Skamene E. Natural resistance to infection with intracellular parasites: molecular genetics identifies Nramp1 as the Bcg/Ity/Lsh locus. J.Leukoc.Biol. 1995;58:382-390.

350. Awomoyi AA, Marchant A, Howson JM et al. Interleukin-10, polymorphism in SLC11A1 (formerly NRAMP1), and susceptibility to tuberculosis. J.Infect.Dis. 2002;186:1808-1814.

351. Rohrer J, Schweizer A, Russell D, Kornfeld S. The targeting of Lamp1 to lysosomes is dependent on the spacing of its cytoplasmic tail tyrosine sorting motif relative to the membrane. J.Cell Biol. 1996;132:565-576.

352. Guarnieri FG, Arterburn LM, Penno MB, Cha Y, August JT. The motif Tyr-X-X-hydrophobic residue mediates lysosomal membrane targeting of lysosome-associated membrane protein 1. J.Biol.Chem. 1993;268:1941-1946.

353. Ohno H, Fournier MC, Poy G, Bonifacino JS. Structural determinants of interaction of tyrosine-based sorting signals with the adaptor medium chains. J.Biol.Chem. 1996;271:29009-29015.

354. Harter C, Mellman I. Transport of the lysosomal membrane glycoprotein lgp120 (lgp-A) to lysosomes does not require appearance on the plasma membrane. J.Cell Biol. 1992;117:311-325.

355. Mackenzie B, Ujwal ML, Chang MH, Romero MF, Hediger MA. Divalent metal-ion transporter DMT1 mediates both H+ -coupled Fe2+ transport and uncoupled fluxes. Pflugers Arch. 2006;451:544-558.

356. Courville P, Chaloupka R, Veyrier F, Cellier MF. Determination of transmembrane topology of the Escherichia coli natural resistance-associated macrophage protein (Nramp) ortholog. J.Biol.Chem. 2004;279:3318-3326.

357. Portnoy ME, Liu XF, Culotta VC. Saccharomyces cerevisiae expresses three functionally distinct homologues of the nramp family of metal transporters. Mol.Cell Biol. 2000;20:7893-7902.

358. Li H, Li F, Kwan M, He QY, Sun H. NMR structures and orientation of the fourth transmembrane domain of the rat divalent metal transporter (DMT1) with G185D mutation in SDS micelles. Biopolymers 2005;77:173-183.

359. Li H, Li F, Sun H, Qian ZM. Membrane-inserted conformation of transmembrane domain 4 of divalent-metal transporter. Biochem.J. 2003;372:757-766.

360. Li H, Li F, Qian ZM, Sun H. Structure and topology of the transmembrane domain 4 of the divalent metal transporter in membrane-mimetic environments. Eur.J.Biochem. 2004;271:1938-1951.

361. Li F, Li H, Hu L et al. Structure, assembly, and topology of the G185R mutant of the fourth transmembrane domain of divalent metal transporter. J.Am.Chem.Soc. 2005;127:1414-1423.

362. Costello MJ, Escaig J, Matsushita K et al. Purified lac permease and cytochrome o oxidase are functional as monomers. J.Biol.Chem. 1987;262:17072-17082.

363. Frillingos S, Sahin-Toth M, Wu J, Kaback HR. Cys-scanning mutagenesis: a novel approach to structure function relationships in polytopic membrane proteins. FASEB J. 1998;12:1281-1299.

364. Dunten RL, Sahin-Toth M, Kaback HR. Cysteine scanning mutagenesis of putative helix XI in the lactose permease of Escherichia coli. Biochemistry 1993;32:12644-12650.

365. Sun J, Wu J, Carrasco N, Kaback HR. Identification of the epitope for monoclonal antibody 4B1 which uncouples lactose and proton translocation in the lactose permease of Escherichia coli. Biochemistry 1996;35:990-998.

366. Sun J, Li J, Carrasco N, Kaback HR. The last two cytoplasmic loops in the lactose permease of Escherichia coli comprise a discontinuous epitope for a monoclonal antibody. Biochemistry 1997;36:274-280.

367. Wu J, Kaback HR. A general method for determining helix packing in membrane proteins in situ: helices I and II are close to helix VII in the lactose permease of Escherichia coli. Proc.Natl.Acad.Sci.U.S.A 1996;93:14498-14502.

368. Wu J, Kaback HR. Helix proximity and ligand-induced conformational changes in the lactose permease of Escherichia coli determined by site-directed chemical crosslinking. J.Mol.Biol. 1997;270:285-293.

369. Sun J, Kaback HR. Proximity of periplasmic loops in the lactose permease of Escherichia coli determined by site-directed cross-linking. Biochemistry 1997;36:11959-11965.

370. Pakula AA, Simon MI. Determination of transmembrane protein structure by disulfide cross-linking: the Escherichia coli Tar receptor. Proc.Natl.Acad.Sci.U.S.A 1992;89:4144-4148.

371. Lynch BA, Koshland DE, Jr. Disulfide cross-linking studies of the transmembrane regions of the aspartate sensory receptor of Escherichia coli. Proc.Natl.Acad.Sci.U.S.A 1991;88:10402-10406.

372. Yan RT, Maloney PC. Residues in the pathway through a membrane transporter. Proc.Natl.Acad.Sci.U.S.A 1995;92:5973-5976.

373. Wu J, Kaback HR. Cysteine 148 in the lactose permease of Escherichia coli is a component of a substrate binding site. 2. Site-directed fluorescence studies. Biochemistry 1994;33:12166-12171.

374. Voss J, Hubbell WL, Kaback HR. Distance determination in proteins using designed metal ion binding sites and site-directed spin labeling: application to the lactose permease of Escherichia coli. Proc.Natl.Acad.Sci.U.S.A 1995;92:12300-12303.

375. Steinhoff HJ. Inter- and intra-molecular distances determined by EPR spectroscopy and site-directed spin labeling reveal protein-protein and protein-oligonucleotide interaction. Biol.Chem. 2004;385:913-920.

376. Hustedt EJ, Beth AH. Nitroxide spin-spin interactions: applications to protein structure and dynamics. Annu.Rev.Biophys.Biomol.Struct. 1999;28:129-153.

377. Hubbell WL, Gross A, Langen R, Lietzow MA. Recent advances in site-directed spin labeling of proteins. Curr.Opin.Struct.Biol. 1998;8:649-656.

378. Reeve I, Hummel D, Nelson N, Voss J, Hummell D. Overexpression, purification, and site-directed spin labeling of the Nramp metal transporter from Mycobacterium leprae. Proc.Natl.Acad.Sci.U.S.A 2002;99:8608-8613.

379. Glickman JN, Conibear E, Pearse BM. Specificity of binding of clathrin adaptors to signals on the mannose-6-phosphate/insulin-like growth factor II receptor. EMBO J. 1989;8:1041-1047.

380. Larkin JM, Brown MS, Goldstein JL, Anderson RG. Depletion of intracellular potassium arrests coated pit formation and receptor-mediated endocytosis in fibroblasts. Cell 1983;33:273-285.

381. Altankov G, Grinnell F. Depletion of intracellular potassium disrupts coated pits and reversibly inhibits cell polarization during fibroblast spreading. J.Cell Biol. 1993;120:1449-1459.

382. Sandvig K, Olsnes S, Petersen OW, van DB. Acidification of the cytosol inhibits endocytosis from coated pits. J.Cell Biol. 1987;105:679-689.

Original Contributions to Knowledge

1. Identification of five conserved charged residues (D86, E154, D192, E299, R416) residing in the membrane-spanning segments of Nramp2 that are essential for metal transport.
2. Identification and characterization of two invariant histidines in Nramp2 (H267, H272) that are critical for pH-dependence of Nramp2 activity. Proposed a model whereby protonation of these histidines would control pH-dependence of metal transport.
3. Characterization of the functional properties and possible contribution to disease of the first two human *NRAMP2* mutations (E399D, R416C) identified in patients suffering from microcytic anemia and iron overload.
4. Established an ELISA-based technique to be able to quantify the proportion of Nramp2-HA expressed at the cell surface with respect to either total cellular expression at steady-state or the dynamic "recycling pool" expression.
5. Established a cell surface biotinylation technique to measure the rate of internalization of Nramp2 from the cell surface in stably transfected LLC-PK_1 cells.
6. Explored the roles of three putative cytoplasmic motifs in the subcellular targeting and trafficking of Nramp2, and identified a tyrosine-based signal ($YLLNT^{555-559}$) in the carboxyl terminus of Nramp2 responsible for the transporter's internalization from the cell surface and recycling back to the plasma membrane.
7. Demonstrated that two splicing isoforms of Nramp2 (isoform I and II) exhibit distinct targeting and recycling properties in stably transfected LLC-PK_1. Proposed a trafficking model whereby isoform I would become enriched at the cell surface in epithelial cells to facilitate iron uptake across the plasma membrane in these cells.
8. Identification of a tyrosine-based motif of the form YXXΦ in the amino terminus of Nramp1 (YGSI) that functions as a lysosomal targeting signal. Proposed a model for Nramp1 trafficking to late endosomes and lysosomes.